A MULTI-DISCIPLINARY CONCEPTUAL DESIGN METHODOLOGY FOR ASSESSING CONTROL AUTHORITY ON A HYBRID WING BODY CONFIGURATION

A Thesis
Presented to
The Academic Faculty

by

Daniel C. Garmendia

In Partial Fulfillment
of the Requirements for the Degree
Doctor of Philosophy in the
School of Aerospace Engineering

Georgia Institute of Technology
August 2015

A MULTI-DISCIPLINARY CONCEPTUAL DESIGN METHODOLOGY FOR ASSESSING CONTROL AUTHORITY ON A HYBRID WING BODY CONFIGURATION

Approved by:

Regents Professor Dimitri N. Mavris,
Advisor
School of Aerospace Engineering
Georgia Institute of Technology

Professor Mark Costello
School of Aerospace Engineering
Georgia Institute of Technology

Associate Professor Brian J. German
School of Aerospace Engineering
Georgia Institute of Technology

Dr. Frank Gern
Aeronautics Systems Analysis Branch
NASA Langley Research Center

Assistant Professor Graeme J.
Kennedy
School of Aerospace Engineering
Georgia Institute of Technology

Date Approved: 24 July 2015

To my parents, for everything.

ACKNOWLEDGEMENTS

I would like to extend my sincerest gratitude to my advisor Dr. Mavris for his infinite patience and commitment to my professional growth. I am also incredibly thankful to my mentors Frank Gern, Andy Hahn, and Craig Nickol at the NASA Langley Research Center for being so generous with their time, guidance, and support over the last several years.

TABLE OF CONTENTS

LIST OF TABLES

LIST OF FIGURES

SUMMARY

The primary research objective of this dissertation was to develop a methodology to aid in the conceptual design of the Hybrid Wing Body (HWB) configuration. This aircraft lacks a horizontal tail which imposes new requirements on the planform, and consequently requires additional analyses from the stability and control (S&C) disciplines to establish the feasibility of a design. Therefore this methodology includes greater emphasis on S&C than is typical for conceptual design, with the end goal or discovering design trends or heuristics that minimize the additional effort required to properly size this configuration.

The methodology required investigations into three primary areas of research. The first was how to assess control authority for vehicles with redundant multi-axis control surfaces. Once a trim analysis method is selected, the resulting trim solutions (or lack thereof) must be translated into control authority constraints for use in HWB optimization, and a novel metric is proposed for this purpose. A second area of research was to develop a method for designing HWB control surface layouts, a decision typically made early but without adequate justification in the open literature. The final area of research integrated performance and control authority assessments to create a HWB sizing environment, and investigations into how to use it for design space exploration and vehicle optimization completed the overall methodology.

Trim analysis methods were investigated in order to provide control authority constraints for HWB optimization. The control redundancy on the HWB caused the conventional method for finding trim solutions to perform poorly, and alternatives were proposed that would potentially accommodate it better. Two methods from

the control allocation literature were integrated separately into the conventional trim optimization problem, as a way to achieve unique deflections for a given moment demand. Another pair of alternative methods converted the problem from a root finding exercise to a nonlinear constrained minimization of drag and actuation power requirements. These were bench marked against each other in terms of uniqueness of the trim solutions and the number of trials necessary to achieve high confidence in achieving the unique result.

A control authority metric for sets of redundant control surfaces was also proposed and demonstrated in this research. Trim deflection angles relative to deflection limits are a conventional measure of control authority. However, saturation of individual elevons on the HWB is meaningless if adjacent elevons can provide additional moment increments. This led to the creation of a new metric based on the Attainable Moment Subset (AMS) and direct allocation method from control allocation literature. The new metric, named the AMS Margin, is a scalar that compares the moment increment required for trim to the maximum attainable moment increment in the same direction and gives an indication of remaining moment generating capability. An important and useful characteristic of the new metric is that by operating in the moment space ($\mathbb{R}^3$), it is independent of the number of control surfaces. Each off-design flight condition (both longitudinal and lateral-directional) can be assessed with this scalar metric and constrained to be positive during HWB optimization. Methods were also established to quantify AMS Margin when a vehicle has inadequate control authority, making it a continuous and useful constraint for gradient-based optimization of the HWB configuration.

A method is proposed and demonstrated for choosing control surface layouts. These layouts are defined by the types of controls, their positions, amount of redundancy, and allocation of function. The method involves enumerating the alternatives

in a matrix of alternatives, and making selections based on requirements for the vehicle and designer preferences. For the HWB in particular the issue of choosing the appropriate number of elevons on the trailing edge needed to be resolved, and the literature did not provide many insights into this decision. Potential stakeholders are identified as well as disciplinary metrics of interest. These concerns and metrics are synthesized using the Breguet range equation to enable comparison of layout alternatives using mission fuel burn, a system level metric.

The final two chapters of the dissertation bring together the performance models and trim analysis methods to form a HWB sizing environment and complete the methodology. This integrated environment was used to satisfy a research objective to test or discover trends, correlations, and design heuristics to aid in HWB conceptual design. A Monte Carlo Simulation on vehicle design parameters was performed and through data visualization techniques was used to characterize the design space and scrutinize design heuristics from the literature. The final product of the design space exploration study was a small set of vehicles that satisfied all performance and control authority constraints, and would serve as good starting points for HWB optimization experiments.

Finally, an assortment of HWB optimization experiments were performed in order to discover an effective approach for conceptual design. Initial experiments omitted a key tail sizing constraint, and the observed consequence was an exploitation of an unintended elevon yaw effects to minimize the tail size. A ganged or linked elevon control utilization scenario was useful for mitigating this to some degree. Instead it was decided to implement the missing constraints, and best practice was determined to be optimization under the full suite of AMS Margin constraints with independent elevon control utilization assumptions. A tail volume coefficient method was considered as an alternative to the physics-based control authority assessments, but is not recommended without additional research and development. Current roadblocks for

that method include complex interactions between vehicle geometry, speed, and control authority that were not properly accounted for as well as a lack of well established historical data.

CHAPTER I

INTRODUCTION

1.1 Market Forecasts

Global forecasts for air travel and air cargo traffic are predicting significant growth domestically and abroad over the next 20 years. The 2012-2031 market outlook from Boeing expects a world annual growth of 5% for both passenger and cargo air traffic.[3] Figure 1 shows this air traffic growth in terms of Revenue-Passenger-Kilometers, the product of the number of paying passengers and the distance they travel, where it more than doubles from 2011 to 2031. The 2012-2031 forecast from Airbus shows similar trends, with most of the growth occurring in the Asia-Pacific region.[2]

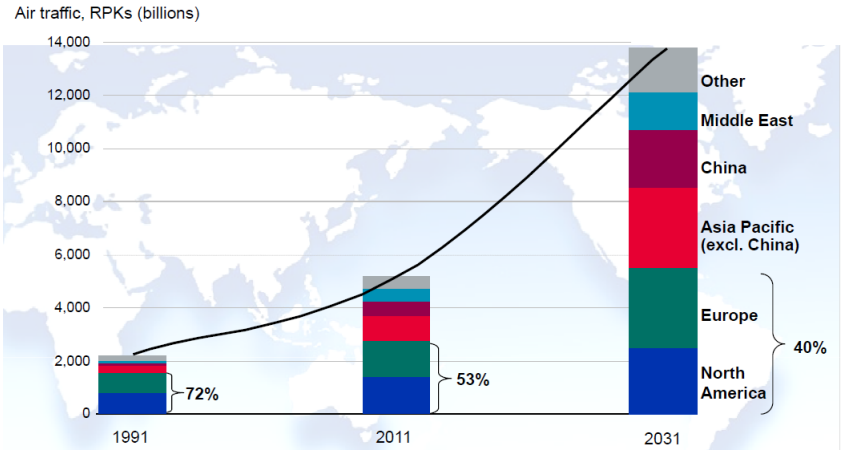

Figure 1: Expected air traffic growth from Boeing.[3]

If left unchecked fleet level fuel burn, noise, and emissions will grow at rates similar to air cargo and passenger traffic.[67] NASA has made this issue a priority and is tackling it in part with the Environmentally Responsible Aviation (ERA) program. The program's purpose is to "Explore and assess new vehicle concepts and enabling technologies through system-level experimentation to simultaneously

v2013.1

TECHNOLOGY BENEFITS*	TECHNOLOGY GENERATIONS (Technology Readiness Level = 4-6)		
	N+1 (2015)	N+2 (2020**)	N+3 (2025)
Noise (cum margin rel. to Stage 4)	-32 dB	-42 dB	-52 dB
LTO NOx Emissions (rel. to CAEP 6)	-60%	-75%	-80%
Cruise NOx Emissions (rel. to 2005 best in class)	-55%	-70%	-80%
Aircraft Fuel/Energy Consumption‡ (rel. to 2005 best in class)	-33%	-50%	-60%

* Projected benefits once technologies are matured and implemented by industry. Benefits vary by vehicle size and mission. N+1 and N+3 values are referenced to a 737-800 with CFM56-7B engines, N+2 values are referenced to a 777-200 with GE90 engines
** ERA's time-phased approach includes advancing "long-pole" technologies to TRL 6 by 2015
‡ CO2 emission benefits dependent on life-cycle CO2e per MJ for fuel and/or energy source used

Figure 2: ERA Metric Goals.[1]

reduce fuel burn, noise, and emissions."[143] Market predictions for the replacement of different classes of aircraft led to ERA goals for three generations of aircraft and technologies, which are summarized in Figure 2. The N+1 (2015) and N+3 (2025) goals are referenced to a single-aisle (Boeing 737) size aircraft and the N+2 (2020) goals are referenced to large twin-aisle (Boeing 777) aircraft. N+1 will likely be satisfied by re-engined or retrofitted single-aisle tube-and-wing (T&W) aircraft. The N+2 goals are more challenging and may require a new configuration in addition to new technologies.

For the N+2 goals an advanced T&W and Hybrid Wing Body (HWB) configuration are being investigated. As will be demonstrated in the next section, the HWB has excellent performance and noise potential compared to advanced T&W designs. Investigating the viability of the HWB concept from a stability and control (S&C) perspective will be the focus of this dissertation.

[1]Courtesy of Craig Nickol, aerospace engineer at the NASA Langley Research Center working on the ERA program.

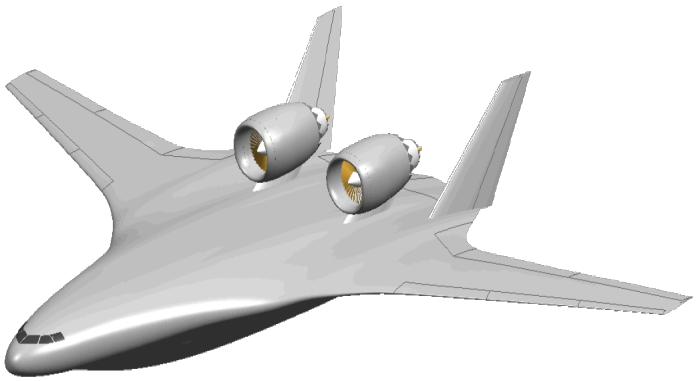

Figure 3: N2A Hybrid Wing Body.[134]

1.1.1 Introducing the Hybrid Wing Body

The HWB concept, also known as the Blended Wing Body (BWB), first appeared in the literature in the early 1990's.[76] The designers of the concept sought to improve aerodynamics by increasing wetted aspect ratio which led to improved cruise L/D.[113] Stated another way, with a configuration like the HWB the internal volume increases faster than the external surface area which results in a lower specific drag.[78] The primary features that characterize the HWB are the single lifting surface, lack of a distinct fuselage, no horizontal tail, and engines integrated in or above the lifting surface (Figure 3). The extended centerbody chord lengths are necessary to accommodate passengers and cargo without excessively thick airfoils. This leads to much greater internal volumes concentrated near the wing root than on flying wing configurations, though they similar in many other respects. The shape of the vehicle requires different cabin layouts and structural concepts than on T&W aircraft. Engine integration over the wing has the potential to provide greater noise shielding than conventional aircraft.

Its features are similar to those of flying wing configurations which have been flown since the 1920's, and consequently it has many of the same S&C problems. Horizontal tails on conventional aircraft provide longitudinal stability, pitch trim, and control

via the elevators. For a given static margin the longer the moment arm, the smaller the tail and elevator area required. Flying wings and HWB aircraft must accomplish these functions with only the wing and its trailing edge controls, which have a much smaller moment arm. This leads to limited control authority or requires very large and powerful control surfaces. No horizontal tail means additional constraints must be met by the wing alone.

One of the new constraints on HWB wing design is to achieve trimmed flight and acceptable static stability throughout the flight envelope. Trim is the balancing of external forces and moments, while static stability refers to restoring moments such as those that provide pitch stiffness. The latter is important so when the vehicle is disturbed from steady flight it has the tendency to return to the equilibrium condition. The degree of static stability needed depends on the design philosophy and the use of stability augmentation with active controls.

A common strategy for achieving trimmed flight and static stability for flying wings has been a combination of wing twist and sweep.[39, 94, 113] This approach can result in an irregular lift distribution with a large induced drag penalty, which diminishes the viability of the flying wing concept. A more recent approach seen on HWB designs reduces the required sweep and tip twist by using reflex airfoils in the centerbody region.[108, 120, 87] These airfoils feature front loading and negative aft camber which produce a nose-up moment. This is the same effect that a horizontal tail or sweep with tip twist would provide, but this approach enables more elliptical lift distributions and lower drag. The reflex airfoils free the wing twist to be used to achieve desired lift distributions or to achieve pitch trim at cruise with faired controls.[86, 97, 87]

The airfoil, sweep, and twist approach for achieving trimmed flight is good for a single cruise design point. At any other speed, center of gravity (CG) location, or altitude the control surfaces are necessary to trim. These off-design conditions are

important for sizing the control surfaces. The static margin and dynamic stability properties may need to be augmented by a flight control system (FCS) at some of these off-design conditions, and additional control authority is needed to do so. The control authority or deflections required for trim and stability augmentation together must be less than or equal to that available from the control surfaces.

1.1.1.1 Potential HWB Benefits

Early studies investigated very large 800 passenger configurations and claimed a 27% fuel burn reduction over a conventional T&W sized for the same mission.[76, 78] This was accomplished by a combination of reduced static stability and a roughly 33% wetted area reduction compared to the T&W. From Roman et al.: "Since the cruise lift-to-drag ratio is linearly related to the square root of the wetted aspect ratio, the configuration offered a substantial improvement in aerodynamic efficiency."[113] Figure 4 shows the relative scale of this BWB design compared to an Airbus A380 (roughly equivalent sizing mission) and a Boeing 747-400.

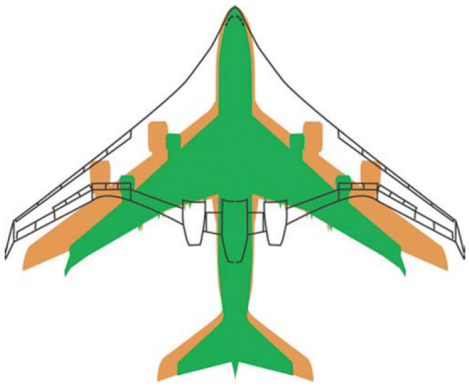

Planform view of an 800-passenger Blended Wing Body compared with an Airbus A380 (orange) and a Boeing B747-400 (green).

Figure 4: Scaled drawing of an 800 PAX BWB, Airbus A380, and Boeing 747.[22]

More recently, Nickol has investigated how these fuel burn reductions change with vehicle scale.[97] Results showed that the HWB has the potential to outperform advanced tube and wing (T&W) configurations for medium to large payloads (200-300+

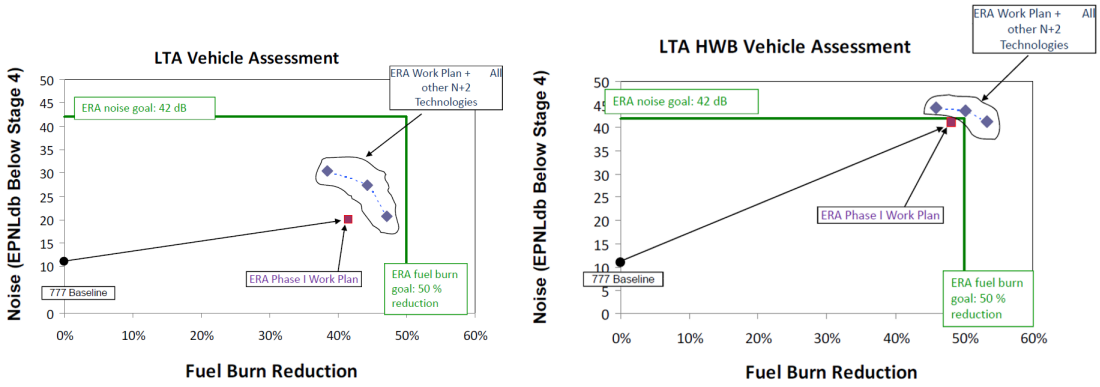

Figure 5: The HWB concept has the potential to meet N+2 goals simultaneously.[95]

PAX) and long range missions. Schutte et al. investigated the effects of ERA N+2 technologies at the system level for large twin-aisle (LTA) class HWB and advanced T&W configurations.[126] They applied over 1,800 technology combinations to both configurations and retained non-dominated solutions on the observed Pareto frontiers, which are shown in Figure 5. This figure indicates that only the HWB with geared turbofans was capable of achieving the ERA N+2 goals simultaneously. Boeing also came to this conclusion in a separate study.[16] The predicted fuel burn benefit over advanced T&W designs is much less than early Boeing designs suggested, observing mostly single digit gains. However the noise margin improvement is much greater, owing to the over-the-wing engine integration with natural noise shielding.

It is the potential simultaneous satisfaction of the ERA N+2 constraints that makes the HWB such an interesting vehicle concept. It has potential but there is still a lot of uncertainty regarding the benefits of the configuration and technologies needed to make it viable. The remainder of this chapter will bring attention to some of the S&C issues and related design challenges for the HWB that motivate this dissertation.

1.2 HWB Design Challenges

Designing a HWB can be broken down into many different disciplines: Structures, packaging, propulsion-airframe integration, thick transonic airfoil design, control surface layout design, planform design / scaling, high lift device integration. Most of those topics have received a great deal of attention in the literature. The following sections will introduce aspects of HWB design that are coupled and are worthy of extra attention.

1.2.1 Control Surface Layouts

A control surface layout shall be defined by the type, number (in the case of redundancy), and positioning of the controls. Regarding the type of controls, sometimes the choices are obvious. For conventional aircraft the primary control surfaces are the aileron for roll, elevator for pitch, and rudder for yaw control. A simple layout would have a pair of ailerons, a single elevator and rudder, and perhaps flaps for high lift (Figure 6). Control surface layouts for modern transports can of course get much more sophisticated with redundant controls, spoilers, leading and trailing edge high lift devices whose use or function may be Mach number dependent (Figure 7).

A survey of the HWB literature shows that about 15 independent control surfaces is typical (excluding leading edge high lift devices). Figure 8 shows some typical control surface layouts. Redundancy, the use of multiple control surfaces that provide similar moment vectors, appears to be a universal design decision made on HWB designs.[18] Redundancy increases complexity but provides fine control over lift distributions and flexibility to help avoid aeroelastic or structural load issues. The elevons in particular are numerous, but the decision processes that led to a specific number were not found in the literature. They also have the property of being multi-axis or coupled controls that generate both pitching and rolling moments.[18] These span the entire wing trailing edge, and this is usually justified by their low individual control

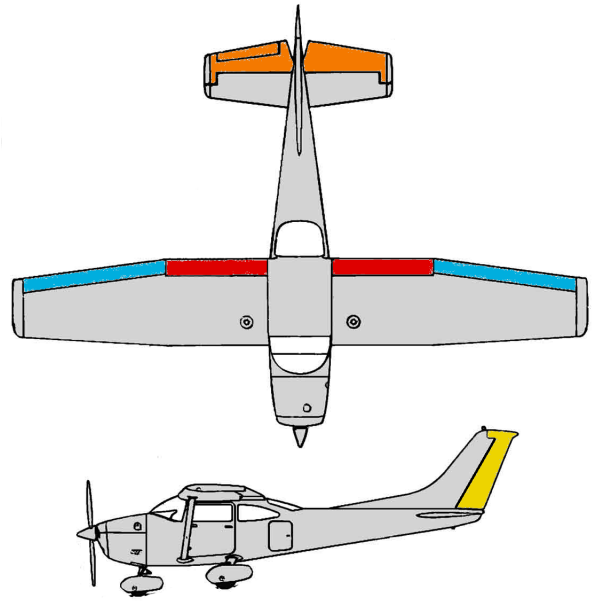

Figure 6: A simple conventional control surface layout.

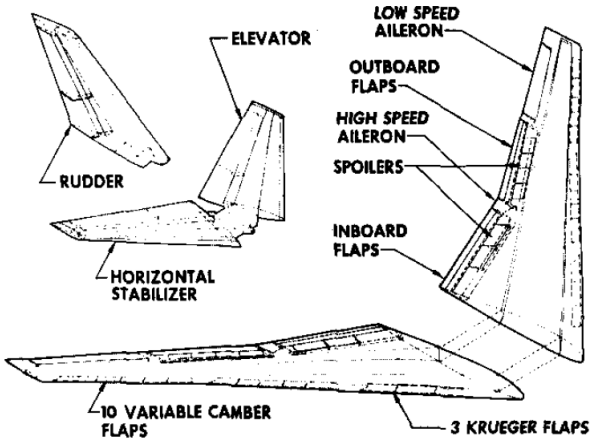

Figure 16. FLIGHT CONTROL SURFACES

Figure 7: Control surface layout on a modern transport.[142]

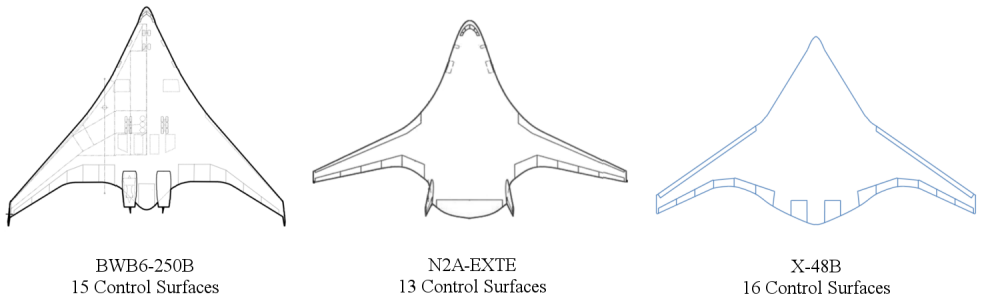

Figure 8: Number of control surfaces on several HWB designs.

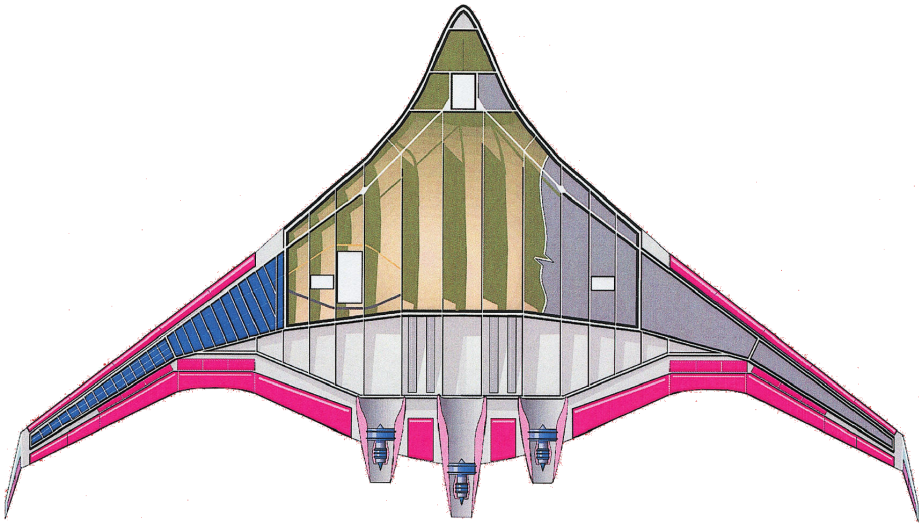

Figure 9: Rear spar segments typically follow the trailing edge.[77]

authority and moment arms.[78] The span-wise spacing of HWB elevons appears to be uniform except where curvature or engine integration makes that impractical. On the outer wing the elevons appear to have constant chord fractions limited by the location of the rear spar. In the transition region between the outer wing and center-body there is a rapid nonlinear change in chord, so constant chord fractions are not used. Instead the hinge lines remain parallel to the rear spar whose segments roughly follow the trailing edge curvature (Figure 9).

The control surface layouts observed in the literature do not feature dedicated trim devices. These devices, such as a variable incidence horizontal stabilizer, have different actuation mechanisms which operate slowly and have no steady state power

requirements. As a consequence, trim must be attained using controls that are powered at all times. All HWB controls can also potentially be used by an FCS that may require rapid deflection rates. These issues combine resulting in high actuation power requirements, which are discussed further in Section 1.2.2.1.

There are control surface layout differences between the HWB designs in the literature. Among the variations that can be observed are vertical tail location, the types of controls used for yaw control, and the types of leading edge high lift devices. Issues that drive decisions regarding some of these choices may come from noise, stability and control, performance and other disciplines. These differences and the reasons for a particular choice are worth investigating and motivate the following research question:

RQ1.1: What control surface type and arrangement options are available and what justifies specific choices made for HWB designs in the literature?

The number of redundant controls can affect drag, weight, and other metrics. Some of these metrics may be competing against each other, leading to trade-offs. The right number of redundant controls may be dependent on designer preferences and the planform shape. However, CS layouts appear to be fixed even in multidisciplinary optimization studies whose planforms can change significantly. Boeing describes their initial design stage as geometry definition where the S&C discipline is sometimes involved.[16] This is likely where their CS layout decisions are made but the methods used are not explained. This potentially important decision is worth exploring and leads to the following observation and research question:

Observation: HWB control surface layouts appear to be an early design decision that remains fixed throughout the design process.

RQ1.2: How should the number of control surfaces be chosen?

The next two sections are necessary to support CS layout decision making. Ensuring sufficient control authority is a coupled control surface and planform design problem. Large actuation power requirements are an issue that may influence the sizing or type of controls used.

1.2.2 Sizing HWB Control Surfaces

The lack of a horizontal tail forces the wing to provide both lift, pitching moment balance, and static stability. At the cruise design point the pitching moment balance and static stability can be accomplished with airfoil selection, sweep, and twist alone. At any other off-design point (speed, mass, CG, altitude) the control surfaces are used to balance the moments. On tailless aircraft the controls must be placed on the wing trailing edge. The adequacy of these control surfaces is determined in part by their size, but also the planform shape.[55] The control authority requirements at multiple off-design points are therefore constraints on wing design.

This coupling of the wing and control authority requires S&C disciplinary analyses to be performed in conceptual design, which is a significant increase in work load compared to conventional T&W conceptual design. The consequence of not evaluating control authority is the risk of having an infeasible design with no simple fixes available. If there are control authority inadequacies, changing the planform may be the best option for relieving those problems. Evaluating control authority in-the-loop during multi-disciplinary optimization (MDO) will produce more realistic designs with reduced risk of expensive redesign in later stages.

Control authority requirements are defined by the moments needed to trim, maneuver, and for a stability augmentation system (SAS) to function. The degree of static stability at the cruise design point is a choice that influences dynamic stability and drag. This design point (as well as many off-design points) may have unsatisfactory handling qualities requiring the use of closed-loop control. Additional control

authority is necessary to do this. Insufficient control authority for a SAS to function will compromise the stability of the aircraft. The total control authority required for trim, maneuvers, and SAS must be less than or equal to the control authority available at each off-design point. These are constraints that will drive the planform design.

There are an infinite number of flight conditions that could be evaluated, but not all of the control authority constraints will be active. For unconventional aircraft it is uncertain which flight conditions are most likely to violate the control authority constraints. The more flight conditions that can be investigated the better, but time constraints force a smaller subset. This motivates the research question below:

RQ1.3: What flight conditions are most likely to result in active control authority constraints for the Hybrid Wing Body?

Evaluating a limited number of flight conditions creates a risk of missing an active control authority constraint, leading to several possible consequences: degraded performance, accidents, expensive redesign and delays, or even program cancellation. In his 2001 dissertation, Chudoba offered the following example of how inadequate control authority led to the crash of a flying wing aircraft:

> "*The fatal accident of the jet-powered Horten Ho 9 FWC illustrates the effects of insufficient control power available. 'During slow flight with the landing gear lowered as well as the landing flaps extended, maintaining direction control for the aircraft with drag rudders only would not be sufficient if one of the turbojets were operating at 100% thrust. It was not enough to keep the aircraft in a straight flight path.'* " [25]

Methods for conducting the trim analyses on the HWB configuration need to be established as well.

Trim analysis methods will need to be investigated for use in the HWB control authority assessments. There are many degrees of freedom (from control redundancy) that complicate the problem, but also potentially grant opportunities to meet secondary objectives besides simply balancing the forces and moments (see the next section). The following research question will help guide the research regarding trim analyses:

RQ1.4: How should the trim analysis be conducted to support HWB design optimization?

1.2.2.1 Actuation Power

Excessive actuation power (also referred to as secondary power) requirements have been noted many times for the HWB configuration.[77, 113, 16] It remains a high risk area that requires attention from a number of disciplines to solve. Power consumption is a function of mechanical power (the product of hinge moment and deflection rate) and resistive power in the case of electric actuators, which incurs losses when holding loads even at zero deflection rates. Both the HWB hinge moments and deflection rates are large and contribute to the problem.

The elevons on the HWB and flying wing configurations are closer to the CG than on tailed vehicles and therefore have shorter moment arms.[132] In order to supply sufficient pitching moments HWB elevons must have large areas, which leads to the apparently universal decision to make them span the entire trailing edge. Roman et al. describe a "square-cube law," also clearly seen in Equation 1, whereby the control surface area increases proportionally to the square of the scale ($\propto L^2$) and the actuating hinge moment grows proportionally to the cube of that scale ($\propto L^3$).[113] The ultimate consequence of not having a horizontal tail is therefore very large hinge moments.

$$M_h = \frac{1}{2}\rho V^2 \underbrace{\underbrace{S_f}_{\propto L^2} c_f}_{\propto L^3} C_h \tag{1}$$

The rate of deflection is driven by the FCS and its stability augmentation role. To respond to gusts and other disturbances the control surfaces must move rapidly. The FCS is designed to meet gain and phase margins and other constraints that are negatively affected by slow actuators. A Boeing report said that they have significant margin on the actuator rates and bandwidth requirements, which are contributing to the excessive actuation power problem.[16] One strategy they will pursue is to perform detailed closed-loop control simulations with the aim of reducing those margins.

Potential aerodynamic solutions include the use of tab surfaces and airfoil redesign with less aft-loading and thicker cross-sections. The tabs would increase the number of moving parts and would have to be integrated into the control law. The airfoil redesign may lead to reduced cruise M(L/D) and reduce the ability of the HWB to achieve N+2 fuel burn goals.[96]

A consequence of the "square/cube law" is that the hinge moment and actuation power problem will get worse at larger aircraft scales. A consequence of ignoring or postponing analysis of actuation power may lead to a situation where the power required exceeds that available from the engines or auxiliary power units.[113] Even if the engine is adequately sized, high actuation power requirements adversely affect specific fuel consumption and reduce the HWBs ability to meet the N+2 fuel burn goals.[16] If the actuation power requirements are not able to be reduced, then Boeing has suggested that it will trade aerodynamic efficiency at cruise for additional static stability.

Control allocation, the mapping of desired moments to redundant controls, is the approach that will be explored in this dissertation. An optimization-based approach will be developed that minimizes actuation power directly. It is anticipated that

this control allocation approach will result in under-utilization of control surfaces with high hinge moments, instead favoring and potentially saturating others. If this behavior is observed, it can be used to refine the type of control surfaces used in the CS layout. The under-utilized controls with high hinge moments can be converted into trim-only devices that use tracks or jack screws, with no steady state power requirements. This control allocation approach will be offered as a complement rather than replacement to the existing approaches being investigated elsewhere.

1.3 Summary and Research Objectives

This chapter introduced the motivation for studying the HWB configuration. Market and pollution projections motivate entities like NASA and its ERA program to investigate new configurations and technologies. The HWB has been shown to have the potential to meet all ERA program goals simultaneously, but its viability still needs to be established.

Several S&C related issues and design challenges were introduced that motivate this dissertation. Research questions regarding the design and sizing of control surfaces were posed. Because the HWB is a tailless aircraft, the disciplines are highly coupled so the control surfaces cannot be designed independently of the rest of the aircraft. In particular they constrain and are constrained by the wing planform. These issues motivate the following research objective for the dissertation:

Primary Research Objective: Develop a control surface layout and sizing methodology for HWB configurations.

HWB design is in general an MDO problem. To accomplish the primary research objective, a set of methods and an MDO implementation will be developed. These will be used to perform design space exploration studies, and will enable the following:

Secondary Research Objective: Use the assembled MDO environment to test or discover trends, correlations, and design heuristics to aid in HWB conceptual design.

CHAPTER II

BENCHMARKING & LITERATURE REVIEW

2.1 Overview

This chapter is a review of the control surface design and HWB MDO literature. The purpose of it is to attempt to find answers to the research questions posed in Chapter 1 which are related to control surface layout design and sizing. The coupling of the planform design and control surface effectiveness was also established, and requires a review of the HWB MDO literature to see how this is treated. By the end of this chapter, useful elements from several different examples in the literature will be identified and retained when developing a new methodology in Chapter 3.

2.2 Control Surface Layout Design

2.2.1 Conventional Control Surface Design Methods for the Conceptual Design Phase

The control surface layouts of conventional aircraft are well established and most of the literature focuses on sizing these assumed layouts. There is usually one set of primary controls for each axis, which can be designed or assumed to have little to no effect in the other axes: ailerons for roll control, elevators for pitch control, and rudders for yaw control. Variations to this may include the presence of high lift devices, control surface redundancy, or the use of control types that combine multiple functions. Secondary controls may include inboard ailerons for use at high speeds, spoilers, etc. Figures 6 and 7 from Chapter 1 show typical layouts on T&W aircraft. The use of these controls is dependent on flight condition and may take into consideration aeroelastic effects, drag, etc.

In the following sections, conceptual sizing methods for tails and primary control

surfaces will be presented which largely rely on historical data. These conceptual sizing methods are useful because they correlate adequate S&C performance with information available in early design phases. They are used as a stand-in for more detailed analyses such as trim and FCS design, which are evaluated farther downstream because of the type and amount of information needed. Higher order physics-based sizing methods do exist but are not presented here. The physics-based methodology steps are covered by the AeroMech methodology from Chudoba presented later.

2.2.1.1 Tail Volume Coefficient

The tail volume coefficient method is commonly used in conceptual design studies. It is a regression of historical data relating horizontal or vertical tail area to either aircraft class or geometry parameters. This regression of historical data is useful because it is based on designs that have gone through preliminary/detailed design, have been certified, have flown, and are similar to the new design being analyzed.

As an example, the Nicolai & Carichner design text provides volume coefficients based on aircraft class which are listed in Table 1.[99] Once a volume coefficient is assumed other information such as wing area, wing span, and wing mean aerodynamic chord must be assembled. The tail area can be estimated using Equations 2 and 3 given an initial guess on the tail moment arms, which are the distances between the quarter chord of the tail mean aerodynamic chord (MAC) and an assumed center of gravity (CG) location. A rule-of-thumb from Raymer allows a 10% reduction in tail areas if a flight control system is used to augment static stability.[111]

$$C_{VT} = \frac{L_{VT} S_{VT}}{b_W S_W} \tag{2}$$

$$C_{HT} = \frac{L_{HT} S_{HT}}{\bar{c}_W S_W} \tag{3}$$

Another method from Morris & Ashford correlates the tail volume coefficient with fuselage parameters as well as wing geometry (Figure 10), instead of vehicle

Table 1: Tail volume coefficients by aircraft class.[99]

Aircraft	C_{HT}	C_{VT}
Sailplane	0.53	0.022
ISR	0.34	0.014
General aviation (one-engine propeller)	0.7	0.032
General aviation (two-engine propeller)	0.76	0.06
Business aircraft (two-engine)	0.91	0.09
Commercial jet transports	1.0	0.083
Military jet trainer	0.6	0.06
Jet fighter (all speeds)	0.5	0.076

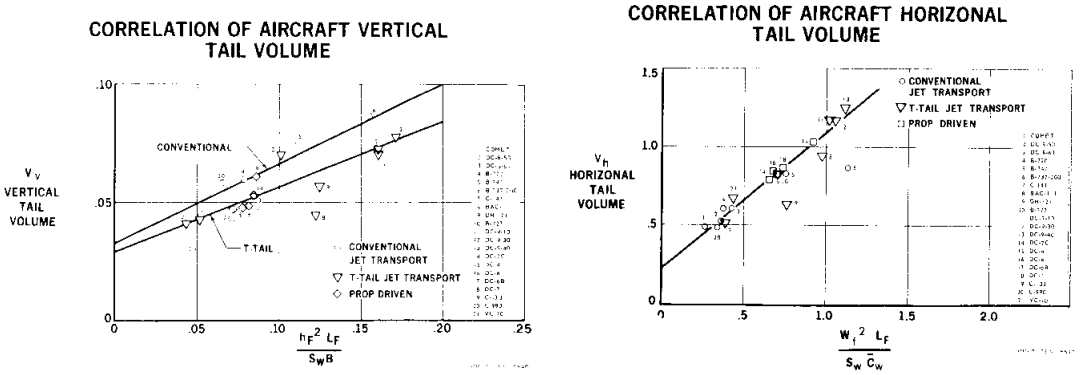

Figure 10: Tail volume coefficients correlated with fuselage and wing parameters.[88]

class alone.[88] Hahn demonstrated that a constant volume coefficient can lead to undersized or optimistic tail areas, and that the Morris & Ashford approach produces more realistic results.[58]

The tail volume coefficient method can be a significant time saver because it is a reliable stand-in for detailed S&C analyses. However, this method is inappropriate for HWB design at this time due to a lack of sufficient historical data for this configuration. As more HWB vehicles are are properly sized, reliable trends for vertical tail volume coefficient may emerge. For example, a Boeing HWB technical report offers X-48C and OREIO configuration vertical tail volumes in the 0.01265 to 0.01304 range.[107]

Observation: Short-cut tail sizing methods such as the tail volume coefficient may not be mature enough to justify skipping S&C analyses during HWB conceptual design. The consequence is that physics-based approaches must be used.

2.2.1.2 Control Surface Historical Trends

Control surface layouts on T&W aircraft are consistent enough that trends regarding the size of ailerons, elevators, and rudders are available. The Raymer design text offers span and chord fraction historical trends for ailerons, elevators, and rudders on several classes of conventional aircraft (Figure 11). The elevator and rudder chord fractions assume full span controls.

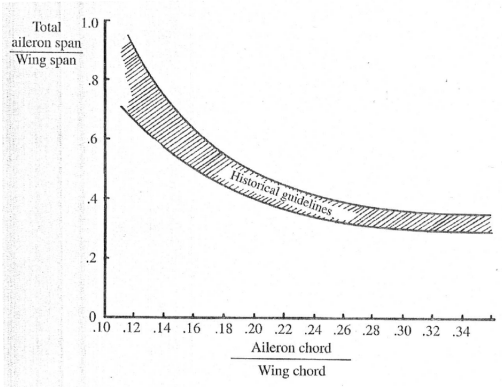

Aircraft	Elevator C_e/C	Rudder C_r/C
Fighter/attack	0.30[a]	0.30
Jet transport	0.25[b]	0.32
Jet trainer	0.35	0.35
Biz jet	0.32[b]	0.30
GA single	0.45	0.40
GA twin	0.36	0.46
Sailplane	0.43	0.40

[a]Supersonic usually all-moving only.
[b]Often all-moving plus elevator.

Figure 11: Historical sizing trends for conventional control surfaces.[111]

Sizing control surfaces is about finding the minimum area required to provide adequate control authority. Sadraey & Colgren offer the following explanation for minimizing area: "Excessive control authority can translate into increased weight and drag, while inadequate control power can result in a failed design."[118] Other reasons to avoid over-sized controls is to leave room for the wing rear spar and actuators.

Higher order physics-based methods for control surface sizing were reviewed by Chudoba and are well represented by the AeroMech sizing methodology presented later.

Observation: Conventional control surface sizing methods do not apply to HWB CS layouts. The sizing methods do not account for redundancy or unconventional CS types. Again, the consequence is that physics-based approaches must be used.

2.2.2 Unconventional Control Surface Design Methods

2.2.2.1 Sadraey and Colgren 2008

Sadraey & Colgren offer a method for designing unconventional control surfaces for UAVs.[118] They agree that assessing control authority is important in conceptual design especially if one wishes to trade relaxed static stability for lower trim drag (explained in Section 2.3). Their design process is shown in Figure 12, and the content of their paper is restricted to the first feedback loop. The initial step chooses the control surface types and the available degrees of freedom for sizing them. Several factors including aircraft mission, cost constraints, and controllability constraints should be taken into account when choosing control surface types. They identify that the choice of a set of unconventional control surfaces must accomplish the same tasks as the conventional set and offer a table with combinations of unconventional control surfaces that do so. The elevon and rudder combination used universally on HWB designs is one of the configurations identified in their table (Figure 13).

Their sizing method assumes a square system (i.e. 3 moment equations and 3 unknown deflection angles) which unfortunately does not address the sizing and allocation of redundant controls. The controls are tested against four trim and maneuver flight conditions and the required deflection angles must be within predetermined limits. These provide a pitching moment constraint, a rolling moment constraint, and two yawing moment constraints. The type of control surface determines which constraints it must satisfy (some may need to satisfy more than one). For vehicles with relaxed static stability they acknowledge that a FCS may impose additional control authority requirements but do not offer a method for assessing them. Their

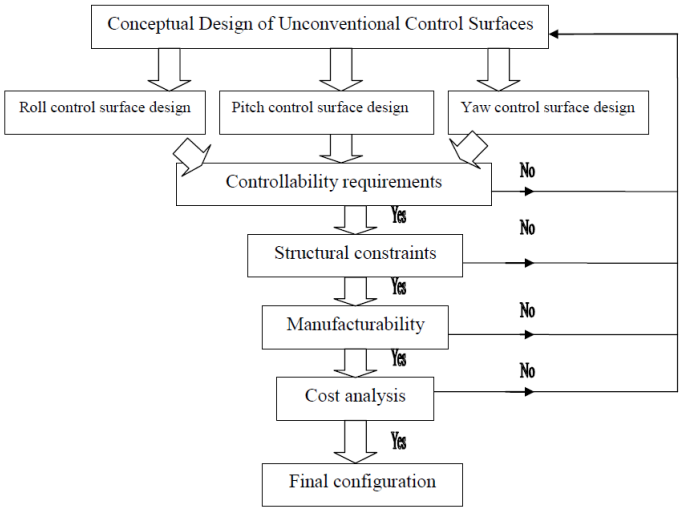

Figure 12: Sadraey and Colgren control surface design process.[118]

No	Control Surface Configuration	Aircraft Configuration
1	Flaperon, Elevator, Rudder	Flap and aileron combined (e.g. X-29)
2	Elevon, Rudder (or equivalent)	Aileron and elevator combined (e.g. Dragon, F-117 Night Hawk, Space Shuttle)
3	Ruddervator, Aileron	V-tail (e.g. Global Hawk and Predator)
4	Drag-Rudder, Elevator, Aileron	No vertical tail (e.g. DarkStar)
5	Canardvator, Aileron	Elevator as part of canard, plus aileron
6	Four Control Surfaces	Cross (+ or ×) tail configuration (e.g. most missiles)
7	Aileron, Elevator (or equivalent), Split Rudder	No vertical tail. Aileron-like surfaces that is split into top and bottom sections (e.g. B-2 Spirit)
8	Spoileron, Elevator, Rudder	Spoiler and aileron combined (e.g. B-52)

Figure 13: Unconventional Control Surface Configuration Options.[118]

method relies on semi-empirical methods to estimate aerodynamic properties. They recommend calculating aerodynamic properties of the controls using DATCOM.

If control authority is inadequate for any of the flight conditions, the corresponding control surface area is increased until the constraints are met. They recognize that in some situations the geometry of the vehicle may need to change to ensure sufficient control authority. This is especially true for tailless configurations like the HWB, and good justification for assessing control authority constraints alongside performance constraints in an MDO environment.

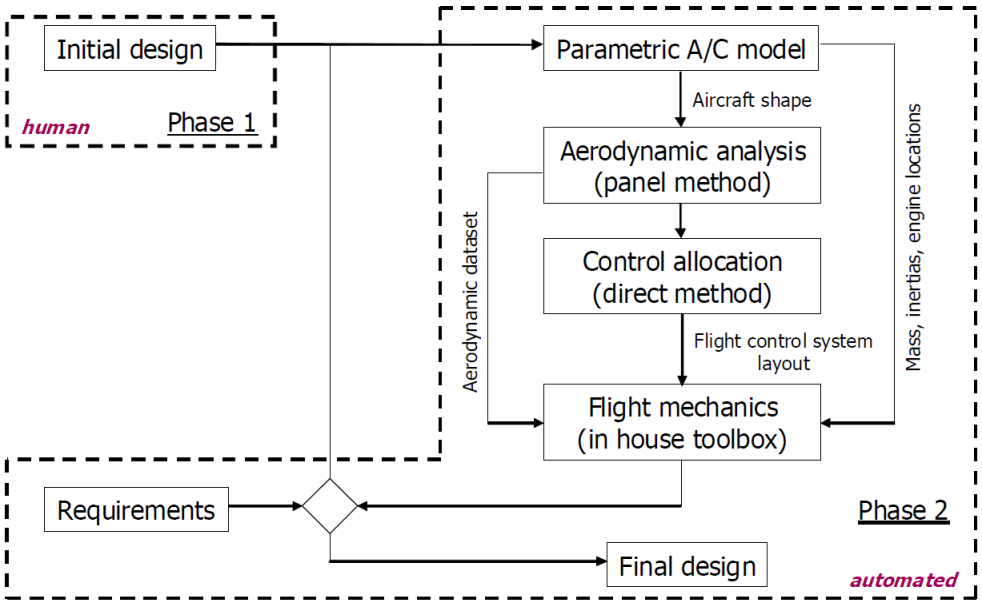

Figure 14: van Ginneken et al. control surface design process.[138]

2.2.2.2 van Ginneken et al. 2010

A paper by van Ginneken et al. describes their methodology for choosing the number, size, and location of control surfaces and is demonstrated on a box wing configuration that they call the Prandtl plane.[138] It is divided into an off-line decision making segment and an automated sizing segment (Figure 14). The off-line segment is an expert driven systems engineering process to decide the type, number, and position of the control surfaces. The design options for achieving roll, pitch, and yaw functions were generated and visualized in an option tree (Figure 15). A Pugh matrix was used to capture designer preferences and choose between competing options based on engineering criteria. The automated sizing segment minimizes the total control surface area subject to deflection constraints at 18 steady state trim and maneuver flight conditions (Figure 16). A smaller control surface area is assumed to imply reduced weight. The trim analysis requires an aerodynamic model which they generate with a 3D panel method, VSAERO.

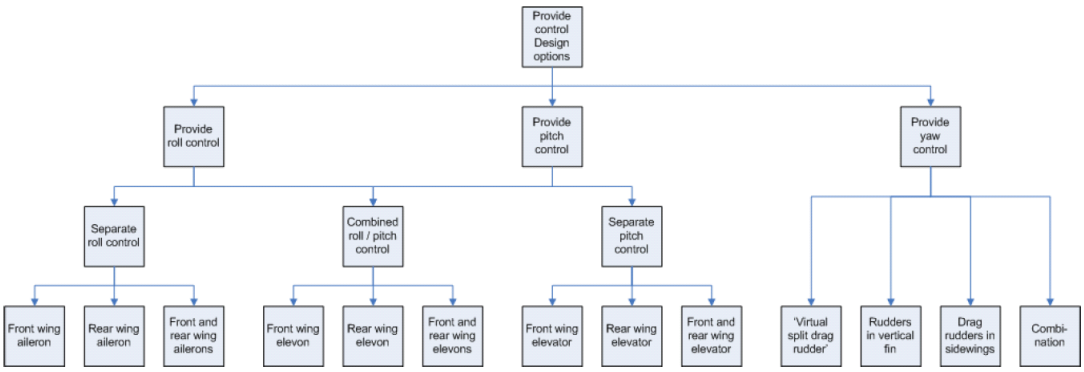

Figure 15: Control surface option tree.[138]

	Take-off rotation speed Sea level		*Approach speed Sea level*		*Cruise speed Cruise altitude (10500 m)*	
Requirement	**No crosswind**	**Crosswind**	**No crosswind**	**Crosswind**	**No crosswind**	**Crosswind**
Aircraft trim	√	√	√	√	√	√
Take-off rotation[8] (7 deg/s^2)	√	√				
Push pull maneuver[9] (0.5 to 2.0 'g')			√	√	√	√
Minimum time to bank[9] (2.3 s to 30 deg)			√		√	
One engine inoperative[9, 10] (trimmed flight)			√	√		
Steady turn			√	√		

Figure 16: van Ginneken control surface sizing conditions.[138]

They recognize redundancy and multi-axis control surfaces as possible design decisions and recommend the use of Direct Allocation to map desired moments to deflections, instead of linking controls together and deflecting them in unison (i.e., ganged controls). Like Sadraey & Colgren they also recognize that if increasing control surface area fails to achieve sufficient control authority the aircraft geometry will need to be modified. The degrees of freedom available to the sizing optimizer were elevator and aileron span fractions, while chord fractions were fixed. It is not clear if rudder dimensions were varied. They characterized their control surface sizing problem as having multiple solutions and local optima, which may be a consequence of using redundant control surfaces. A flight mechanics analysis is described that can perform automated trim and handling quality assessments, but it appears that only trim constraints are included in the control surface sizing optimization.

2.2.2.3 AeroMech (2001)

Chudoba introduced the AeroMech control surface sizing methodology in his 2001 Ph.D. dissertation.[25] Coleman would later implement the method and Omoragbon would extend it to have higher fidelity FCS design.[28, 100] Overall the AeroMech methodology is about evaluating control authority available vs. control authority required for the purpose of sizing in the conceptual design phase (Figure 17). To develop AeroMech over 30 control surface sizing methods were reviewed, many of which were limited to tail-aft T&W configurations, and elements that would enable a generic physics-based method were retained.[27] The methodology goal is to "*... balance control power with inherent airframe stability levels in a performance-optimal way.*"[24] Performance-optimal characteristics include minimum trim drag, smallest control surfaces, light-weight actuation systems, etc. In his publications Chudoba also recognizes the trade-off between good open-loop S&C properties and performance, and advocates for early integration of S&C into the design process.

Chudoba notes that control surfaces are not sized for the cruise design point, but off-design points which require data not typically generated in conceptual studies, and that control surface sizing is an iterative process. Similarly to van Ginneken et al., he calls for control allocation to deal with redundancy. The Linear Optimum Trim Solution (LOTS) method is suggested, which by his description is limited to small degrees of redundancy and only for the longitudinal axis.

The method recognizes that if relaxed static stability is a design decision, additional control authority beyond trim is needed for a stability augmentation system (SAS) to function. "*Although the detailed choice of the controller architecture depends on the particular aircraft type under consideration, the purpose of the tool in the present context is not to design an advanced flight control system for the aircraft, but to emulate only a controller for the estimation of control power requirements.*"[24] This is important because he makes several simplifying assumptions in creating the control law such as neglecting the effect of actuator dynamics. The SAS requires additional control surface deflection (thus additional control authority) to counteract disturbances such as gusts. Also, standard FCS metrics such as bandwidth, gain/phase margins, etc are not evaluated. It is assumed that if enough control authority is available, that the FCS can be designed to have provide adequate handling qualities.

Control authority is evaluated at up to 32 different flight conditions with trim and stability augmentation analyses shown in Tables 2-4. If the deflection required is beyond the limits then AeroMech calls for increasing the control authority by 1) a rebalancing of the vehicle (shifting the center of gravity), or 2) the control effectors need to be larger or moved (increase the moment arm). The critical flight conditions that require the largest CS area define the size of the control surface. The flight conditions whose control authority constraints are active depends on the aircraft configuration.[27] The generic list was generated from A340 and Concorde flight tests,

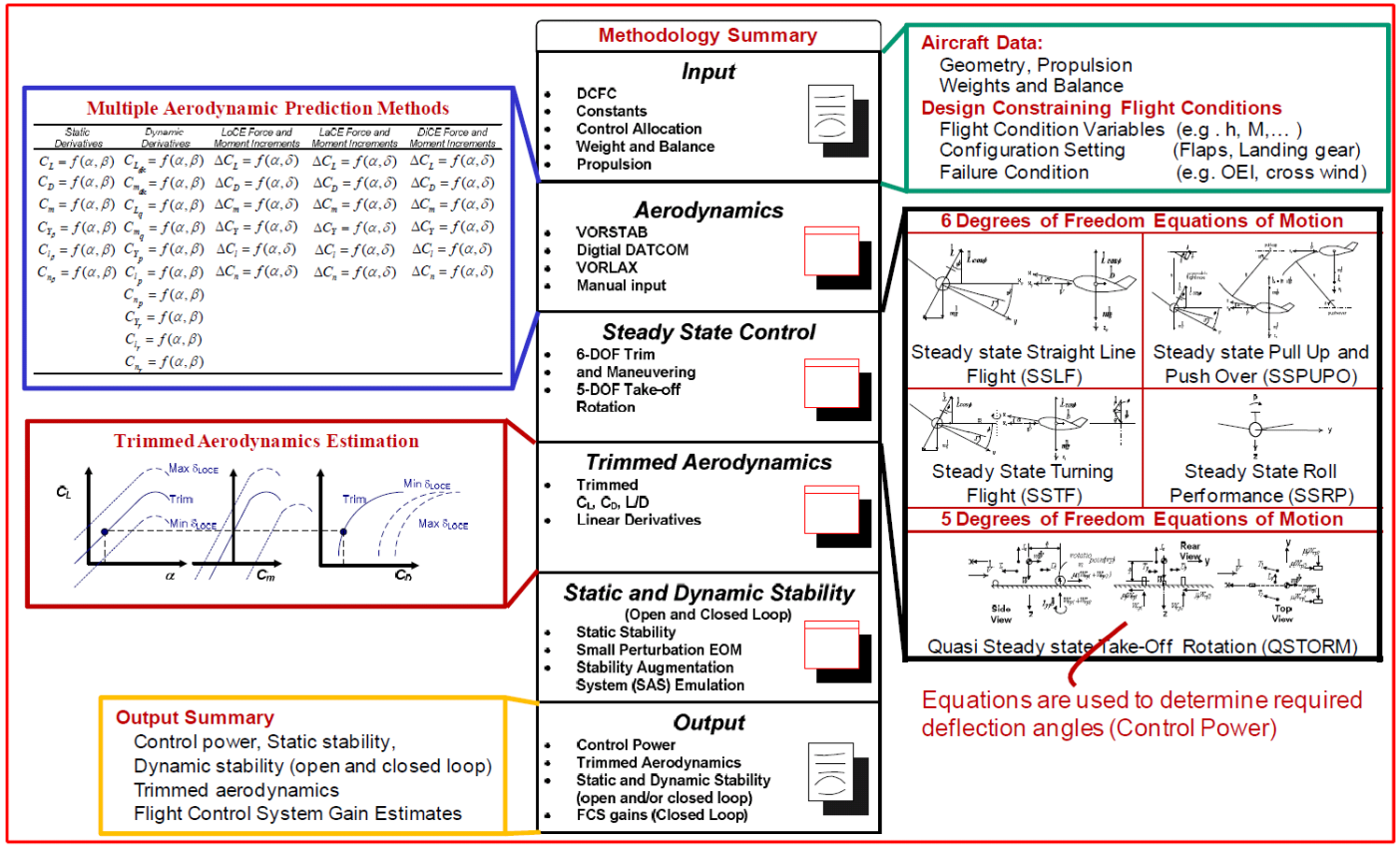

Figure 17: The AeroMech control surface sizing methodology.[100]

Table 2: AeroMech longitudinal flight conditions.[26]

LoCE - DCFC	CS & FCV & FC	Level
	Static	
1 g Trim Stability	Longitudinal Trim	1
	Trim Curves	1
	Aft C.G. Clearance	1
	Double Hydraulic Failure	1
	Approach Trim	1
	Minimum Control Speed, Take-Off Climb (V_{MCA})	1
	Minimum Speed at High Incidence (V_{MIN}, $V_{\alpha,max1g}$)	1
	Go-Around on 4 Engines Without Ground Effect	2
	Cruise with Trim Jam	2
	Trim Tank Failure	2
	C.G. Shifting Speed with Fuel Transfer System	2
	Emergency Descent with Partial Loss of Forward C.G. Transfer Facility	2
	Emergency Descent with Reverse Thrust Operating, Partial Loss of C.G. Transfer Facility	2
	Slats / Flaps Failures	2
	Foreplane Runaway, Failing to a Fixed Position (Control Allocation)	2
	Maneuver	
Rotation Capability	Rotation on Take-off / Nosewheel Lift-of	1
	Rotation on Landing with Ground Effect	1
Load Factor Capability	Dive Recovery / Pull up	2
	Speed Recovery / Push over	1
	Load Factor Capability	1
	Dynamic	
Mode	Short Period Oscillation	2
	Phugoid Oscillation	2
Transient Response	Nose Wheel Load at Break Release	2
	Power Application	2

MIL specs, and JAR/FAR 25 requirements.

The needs of the SAS are expressed in terms of deflection angles by subjecting the closed-loop system to gust induced α and q (pitch rate) disturbances. These SAS required deflection angles are added to the trim deflection angles and compared to the deflection limits. An example of how the trim and SAS deflection requirements change with CG location on the YB-49 is provided by Coleman (Figure 18).[28]

2.2.2.4 Guerreiro & Hubbard 2008

Guerreiro & Hubbard present a methodology for choosing the number and distribution of control surfaces along the trailing edge of a wing.[57] What is particularly useful about this method is that it uses quantitative metrics to choose the number of control surfaces and the decision can be automated. The goal was to match a desired lift distribution, in this case elliptical and thus minimum induced drag. Several other papers have investigated lift distribution control with control surfaces but they used

Table 3: AeroMech directional flight conditions.[26]

DiCE - DCFC	CS & FCV & FC	Level
	Static	
β-Trim Stability	Minimum Control Speed, Approach and Landing, 2 Engines Out (V_{MCL-2})	1
	Engine Failure During Take-off	1
	Trim 2 Engines Inoperative	1
	Demonstration of Max. Crosswind on Landing (One Critical Engine Failed)	1
	Straight Sideslips	1
	Adverse Yaw	1
	Landing from Approach Slope 4° with 2 Critical Engines Failed	2
	Maneuver	
Yaw Control Capability	Directional Control, 2 Engines Inoperative	1
	Time to Yaw	2
	Double Hydraulic Failure	2
	Dynamic	
Mode	Dutch Roll Oscillation	2
	Roll Subsidence	2
	Spiral Divergence	2
Spin Recovery		2
Inertia Coupling	Pitch Due to Velocity Axis Roll	2
	Yaw Due to Loaded Roll	2

Table 4: AeroMech lateral flight conditions.[26]

LaCE - DCFC	CS & FCV & FC	Level
	Static	
β-Trim Stability	Minimum Control Speed, Approach and Landing, 2 Engines Out (V_{MCL-2})	1
	Engine Failure During Take-off	1
	Landing from Approach Slope 4° with 2 Critical Engines Failed	1
	Trim 2 Engines Inoperative	1
	Demonstration of Max. Crosswind on Landing (One Critical Engine Failed)	1
	Straight Sideslips	1
	Demonstration of Max. Crosswind on Landing	2
	Maneuver	
Roll Control Capability	Directional Control, 2 Engines Inoperative	1
	Time to Roll	1
	Double Hydraulic Failure	2
	Dynamic	
Mode	Dutch Roll Oscillation	2
	Roll Subsidence	2
	Spiral Divergence	2
Spin Recovery		2
Inertia Coupling	Pitch Due to Velocity Axis Roll	2
	Yaw Due to Loaded Roll	2

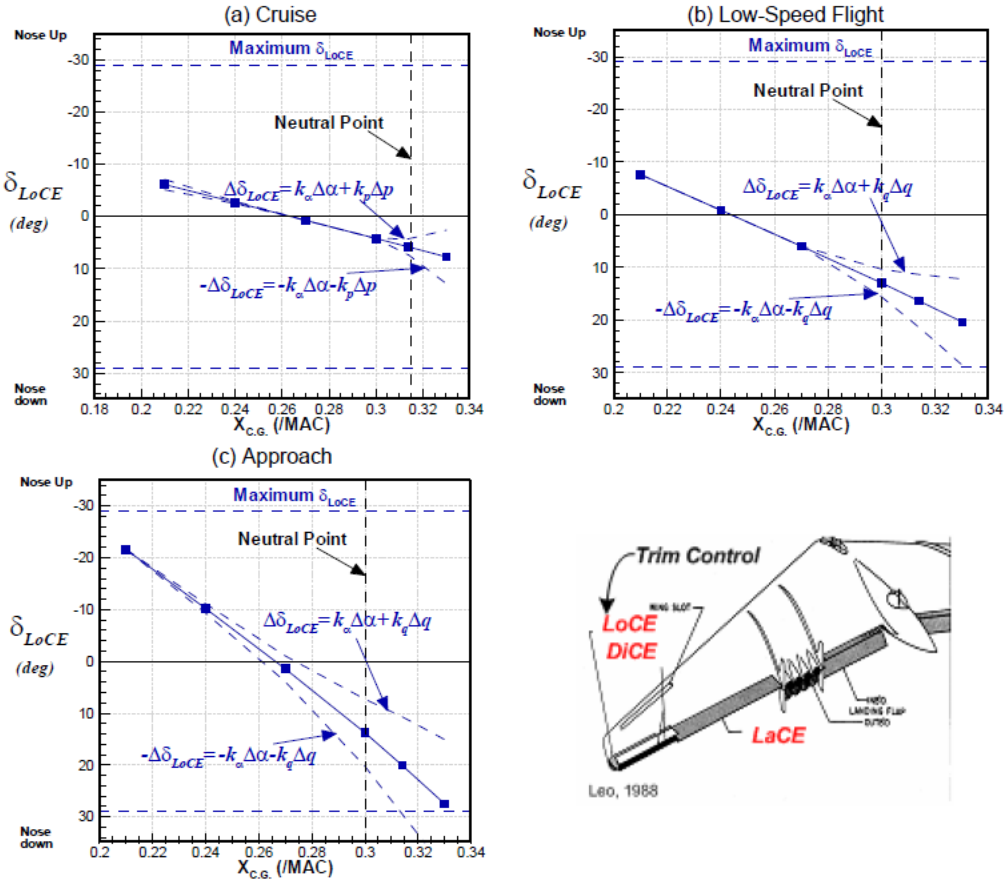

Figure 18: Trim and SAS control authority requirements expressed in deflection angles for a YB-49 model.[28]

a fixed set of uniformly distributed controls.[5, 4, 110, 66, 30] The method from Guerreiro & Hubbard adds the total number of controls and their span-wise distribution as additional degrees of freedom.

For a given number of controls, the span-wise spacing and deflection angles were optimized to generate an elliptical lift distribution. This process was allowed to converge, at which point another pair of controls would be added and the process repeated. What was observed was the error between the desired and achieved lift distribution asymptotically approached zero very rapidly and with diminishing returns as the number of controls was increased (Figure 19). This is equivalent to drag asymptotically approaching a minimum value as the number of controls is increased. The optimal span-wise spacing of the control surfaces resulted in large surfaces near the wing root and smaller ones near the wing tips. This result is reasonable given that the elliptical lift distribution shows little variation at the root and changes rapidly near the tips. The smaller control surfaces near the wing tips allow finer control over the lift distribution.

2.2.3 Control Surface Design Summary

The following elements were deemed useful, and will be retained in the development of a methodology for HWB design:

- There should be a systematic way for choosing the type and initial arrangement of control surfaces.
  - The approaches from Sadraey & Colgren and van Ginneken et al. both accomplish this. Of the methods reviewed, van Ginneken et al. offers a more thorough explanation for how to enumerate the options (decision tree) and how to make a selection (Pugh matrix). The table with unconventional control surface combinations from Sadraey & Colgren also establishes compatibility between the different types.

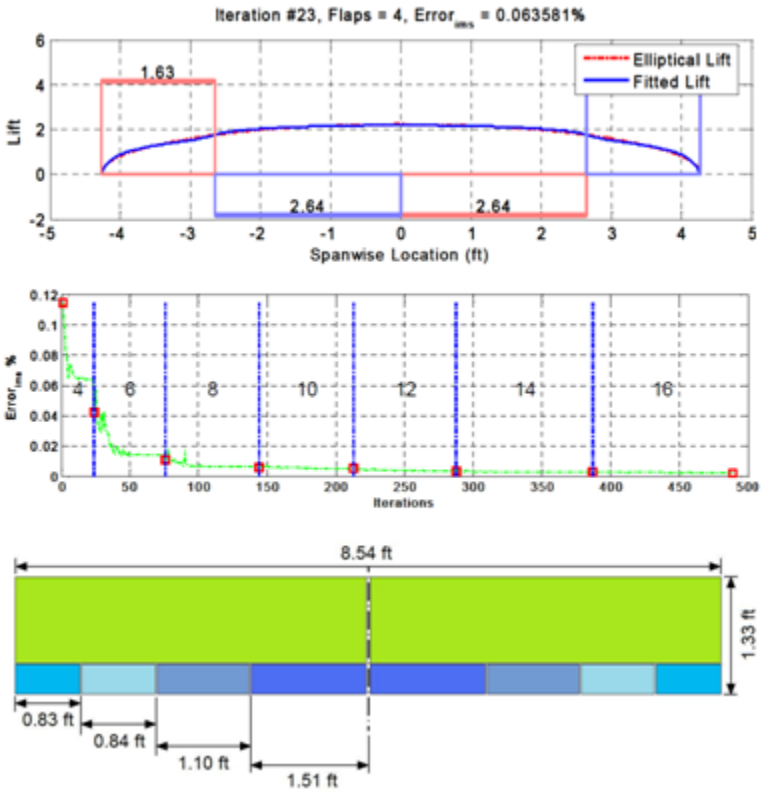

Figure 19: A method for optimal number and spacing of control surfaces on a wing trailing edge.[57]

- The number of redundant control surfaces can be optimized
  - Guerreiro & Hubbard demonstrated that the number of control surfaces in part determines the minimum achievable trim drag.
  - Other metrics for choosing the optimal number of control surfaces should be investigated, and motivates the following research question:

RQ2.1: What disciplinary metrics and design considerations might influence the number of redundant control surfaces?

- Control surface sizing should take into account control authority requirements from trim, maneuvering, and the flight control system.
  - Both the AeroMech and van Ginneken et al. methodologies suggest evaluating control authority requirements at a large number of flight conditions

(32 and 18, respectively). Evaluating a large number of conditions reduces the risk of missing an active constraint, but increases the work load.

  - The AeroMech method measures the control authority requirements of the flight control system in terms of control surface deflections required for it to provide satisfactory handling qualities. These deflections plus the trim deflections define the total control authority required, which must be within the allowable deflection ranges.

- Control allocation can be used to accommodate the extra degrees of freedom from the presence of redundant controls.

  - The method from van Ginneken et al. used Direct Allocation to develop gearing ratios for their unconventional control surfaces, but it could have been used to choose the deflections directly instead.

On T&W aircraft the limits of control authority are indicated by the saturation of the aileron, elevator, or rudder. Control authority can be tracked during each flight condition by comparing those three trim deflections to allowable limits. The HWB on the other hand has several redundant controls. The saturation of a single elevon is not an indicator of the limits of control authority, because other elevons may be able to provide additional moment increments in the desired direction. This issue motivates the following research question:

RQ2.2: Are there more convenient metrics for expressing the control authority available vs. required for a set of redundant controls?

2.3 Design Philosophy: Control Configured Vehicle

The 1970's brought research into Relaxed Static Stability (RSS) which trades inherent static stability for performance gains, enabled by active control technology.[10] One

of the benefits of allowing neutral or negative longitudinal static stability is reduced weight and skin friction drag enabled by reduced horizontal tail area. On T&W aircraft with RSS, smaller elevator deflections are needed to trim which implies reduced trim drag. A consequence of RSS is the need for a flight control system to restore acceptable handling qualities.[10, 62] An aircraft that has made this trade-off and depends on a flight control system is called a Control Configured Vehicle (CCV).

The original application of this design philosophy was in retrofitting existing aircraft.[128] Rynaski & Weingarten argued that to get the most out of RSS it must be integrated early in the design process.[117] Propulsion, aerodynamics, and structures/weights are the primary disciplines involved in the traditional aircraft conceptual design process (Figure 20a). After many iterations and convergence the aircraft design is handed off to stability and control disciplines so they can perform their analyses. However by this point in time the design is largely frozen and only small changes can be made.

MDO is a natural match for a CCV/RSS design philosophy. As shown in Figure 20b, the S&C disciplines are now able to participate in interdisciplinary trades. Their involvement can replace methods that rely on historical trends such as tail volume coefficients and control surface chord and span fractions. For unconventional designs such as the HWB with known S&C challenges, their involvement is critical for finding feasible designs. The challenge comes from the need to generate more detailed models and data than is typical for conceptual design. This includes additional aerodynamic data, mass properties, and the evaluation of control authority available vs. required for trim and stability augmentation. Rynaski & Weingarten argue: "*Stability constraints, such as static margins, have little or no importance if sufficient control effectiveness and power are available to provide for good flying qualities and maneuverability.*"[117] This reveals that static margin constraints are just stand-ins or short-cuts for evaluating whether there is sufficient control authority for

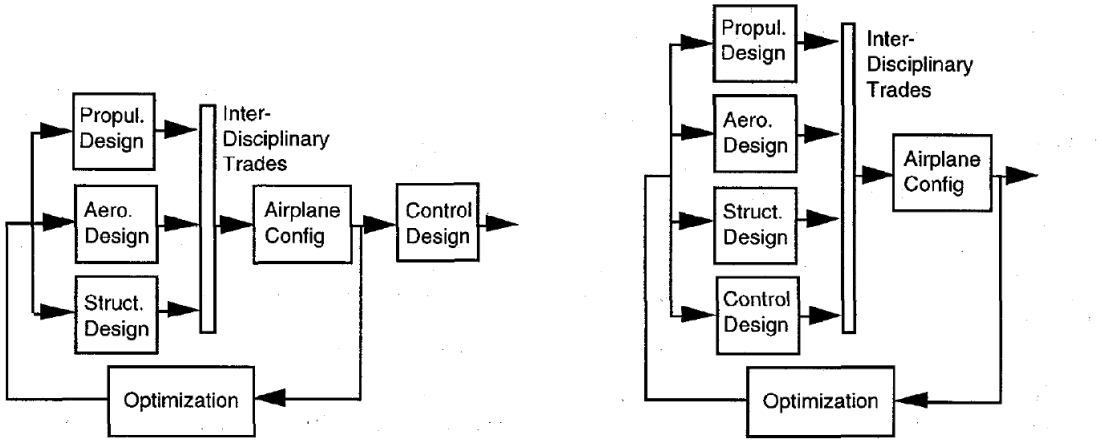

(a) Traditional aircraft design process (b) Control-configured-vehicle design process

Figure 20: The role of S&C disciplines in design.[10]

the FCS to adequately perform its stability augmentation functions.

2.3.1 Examples of CCV / MDO approaches in the literature

An excellent example of CCV design is provided by Perez.[105] This was an MDO study using the Collaborative Optimization technique to optimize a T&W vehicle sized for maximum range with fixed payload and fuel weights. Wing and empennage geometry variables were allowed to vary and constraints on performance, weight, aerodynamic, and S&C metrics at several flight conditions were imposed. Two scenarios were investigated: 1) S&C limited to conventional tail volume coefficients and 2) automated FCS design to ensure closed-loop system stability. The stability augmentation is performed with a proportional feedback controller, whose gains are determined by a lower level optimizer constrained by mode damping/frequency, GCAP, and other constraints.

The results are shown in Figure 21 as a function of the number of passengers. For all passenger classes investigated the FCS integrated approach enables smaller empennage areas and weight, which decreases drag and increases range.

Morris took a CCV design approach to tailless flying wing aircraft and investigated the trade-off between inherent static stability and performance.[89] An overall

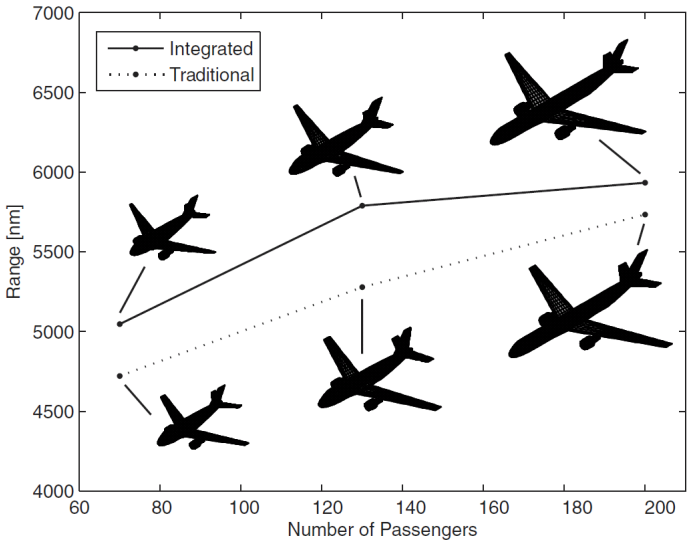

Figure 21: The effect of the Perez et al. CCV methodology on T&W performance.[105]

evaluation criterion (OEC) consisting of handling quality and trim drag metrics at two flight conditions is optimized. The handling quality metric is an integral of the "*square of the error in state vector time histories between the aircraft being designed and a model case chosen for its desirable handling qualities*," and contains a penalty function to minimize control effort. This metric does not indicate whether the handling qualities are good, instead it serves as a way to rank the handling qualities of each design relative to the others. A penalty function enforced design variable side constraints. Span is held constant but 15 other configuration parameters were allowed to vary including planform variables, control surface deflections, and twist at multiple points along the wing span. The optimizer also controlled the gains in a proportional feedback controller.

Figure 22 shows a significant change in wing geometry as the OEC weighting shifts from valuing better handling qualities to valuing low trim drag. It shows that wing sweep drives longitudinal stability much more strongly on tailless configurations than it does on T&W designs. The designs with a stability augmentation system were able to achieve better handling qualities with less sweep and a smaller drag penalty.

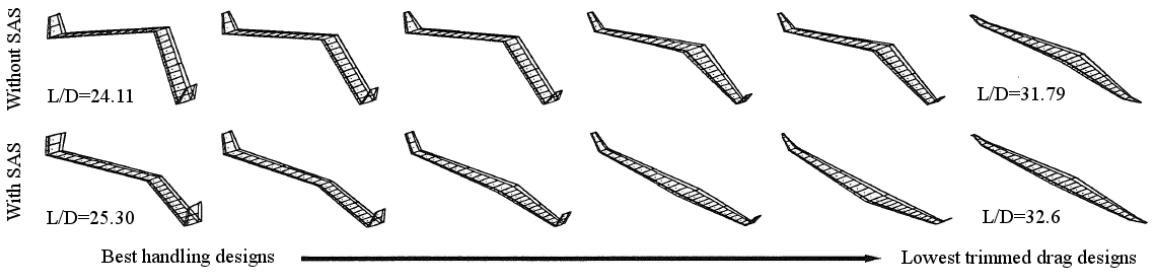

Figure 22: The effect of the drag vs. handling quality trade-off.[89]

2.3.2 HWB MDO

2.3.2.1 WingMOD

Boeing's design code for HWB conceptual design is called Wing Multidisciplinary Optimization Design, or WingMOD. The vehicles were designed by allowing a sequential quadratic programming (SQP) optimizer to drive variables describing the planform, airfoil t/c, structural thicknesses, and internal arrangement of components in order to minimize take-off gross weight (TOGW).[146] The designs were subject to performance, aerodynamic, structural, and S&C constraints. The number of design variables and constraints varies from study to study but are on the order 150+ and 1000+, respectively.[144]

The aerodynamics were estimated using a vortex-lattice method with empirical viscous drag corrections and calibrated using higher order CFD data. Lift and moments from the control surfaces were estimated using DATCOM and corrected with HWB wind tunnel data.[144] A monocoque beam model was used, stress and buckling sizing was performed, and static aeroelastic effects were modeled to size the HWB structure. It also calculated performance metrics, weight and center of gravity, as well as performs trim analyses. The trim analyses were performed for 20-30 flight conditions, but more (especially lateral conditions) were desired.[146] Control authority requirements of stability augmentation systems were not estimated in WingMOD, which used static margin constraints instead.

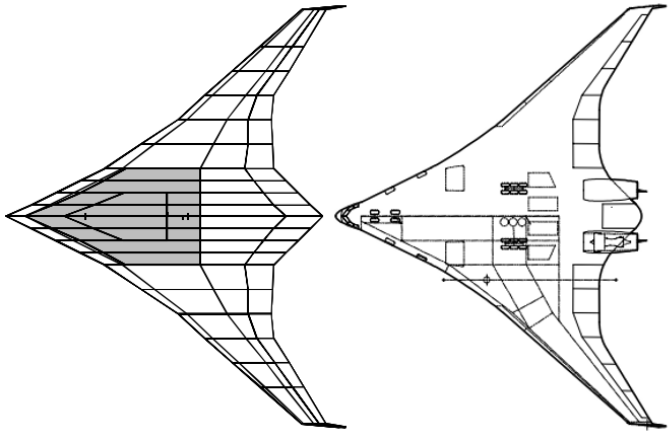

Figure 23: Comparison of the BWB-6-250B and the WingMOD model on which it is based.[53]

A paper from Gilmore et al. offers the clearest view of how control surfaces are treated in WingMOD.[53] Their WingMOD model optimized for a Mach 0.93, 7,500 nm range mission is the basis for the BWB-6-250B configuration. Figure 23 shows that the WingMOD paneling at the trailing edge roughly corresponds with where the control surfaces are located on the BWB-6-250B. It is not clear from this paper or the other WingMOD literature whether the control surfaces were sized during optimization (that is, whether their area is modified directly). The control surfaces appear to have constant chord fractions at the WingMOD panel edges, and that planform modifications were used to resolve balance and control authority issues (Figure 24).

Table 5 summarizes the available WingMOD HWB literature. The published work looks at medium to large payloads and long range missions. This is where Nickol showed that the HWB is competitive with T&W configurations.[97] Several other Boeing design studies exist but they follow a more manual design process or are preliminary design studies.

The WingMOD literature does not describe any study of control surface layout alternatives. All optimization studies appear to use a fixed number and type of control

Table 5: WingMOD HWB MDO methodology body of work.

Author(s)	Year	Summary
Wakayama & Kroo [146]	1998	855 PAX, 7500 nmi, Mach 0.85 starting from a baseline design created using manual design methods
Gilmore et al. [53]	2002	Made geometry and weight trend observations as the cruise Mach number was varied from 0.85 to 0.95 with ranges of 7,500 to 8,900 nmi.
Markish & Willcox [81]	2002	They explore a coupled engineering and financial analysis using WingMOD. A performance model (WingMOD), a cost model, and a revenue model are integrated. Three premade BWB designs of different class size and levels of commonality are evaluated and to show the best combination in terms of their financial metrics.
Liebeck [75]	2002	A 450 PAX BWB starting from a baseline design created using manual design methods. This is primarily a summary paper of BWB history and the WingMOD tool.
Roman et al. [114]	2003	A follow-up to Gilmore et al. 2002. Elaborates on refinements made with a CFD-based inverse design method that resulted in the BWB-6-250B design.
Willcox & Wakayama [148]	2003	This paper investigates the design of a family of BWB aircraft with component commonalities
Markish & Willcox [82]	2003	A journal version of their 2002 paper.
Peoples & Willcox [103]	2004	A financial study that observes profitability of HWB aircraft. Integrates WingMOD in a larger value-based MDO framework.
Liebeck [77]	2004	A journal version of his 2002 paper.
Diedrich et al. [32]	2006	An MIT study using a customized WingMOD. Integrated new acoustics modules and optimized for noise. 215 PAX, 5000 nmi. Early Silent Aircraft Initiative study, precursor to HWBOpt methodology.
Peoples & Willcox [104]	2006	A journal version of their 2004 paper.
Kawai [73]	2008	CESTOL, short take-off and landing study

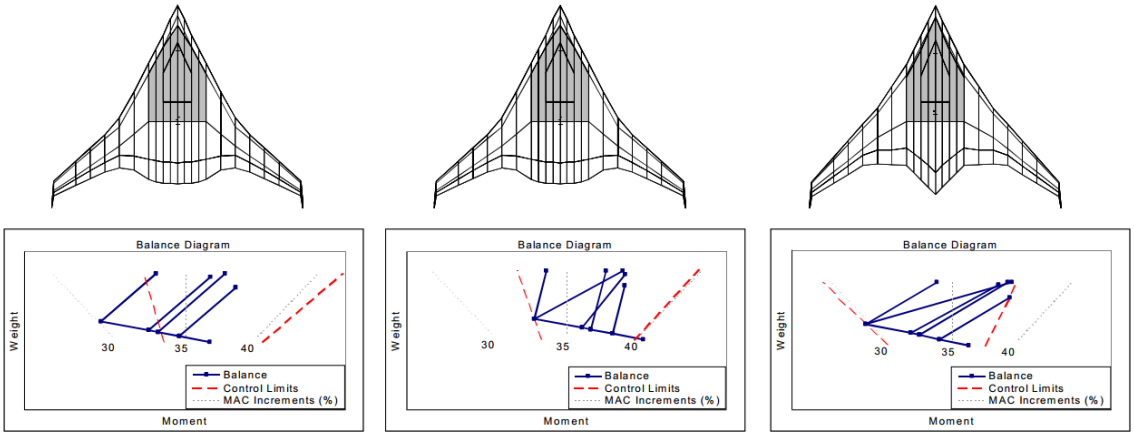

Figure 24: WingMOD Balance Charts.[53]

surfaces. The decision process used to arrive that their initial layouts is absent from the open literature. Also absent from the WingMOD literature are investigations into actuation power issues. No attempts to integrate high lift devices were published.

2.3.2.2 HWBOpt

MIT's HWBOpt methodology has its roots in Boeing's WingMOD. Diedrich et al. used WingMOD for planform optimization but with modified propulsion, aerodynamic, and mission performance analyses.[32] This environment was used to develop the Silent Aircraft eXperiment (SAX) designs. It is not clear whether the WingMOD off-design trim analyses were performed in that study.

In 2006 Hileman et al. introduced a higher fidelity aerodynamic and aeroacoustic design and analysis capability to refine the SAX designs.[60] Mody et al. introduce the HWBOpt methodology (Figure 25), which combines elements from Diedrich et al. and Hileman et al. and updates some of the disciplinary analyses.[86] A surrogate model of the structural weight appears to be the only element of WingMOD that is retained. The HWBOpt methodology is used to develop the H-series HWB designs.

The extensive off-design trim analyses in WingMOD are replaced with only three flight conditions. The wing twist is chosen to ensure a static margin greater than

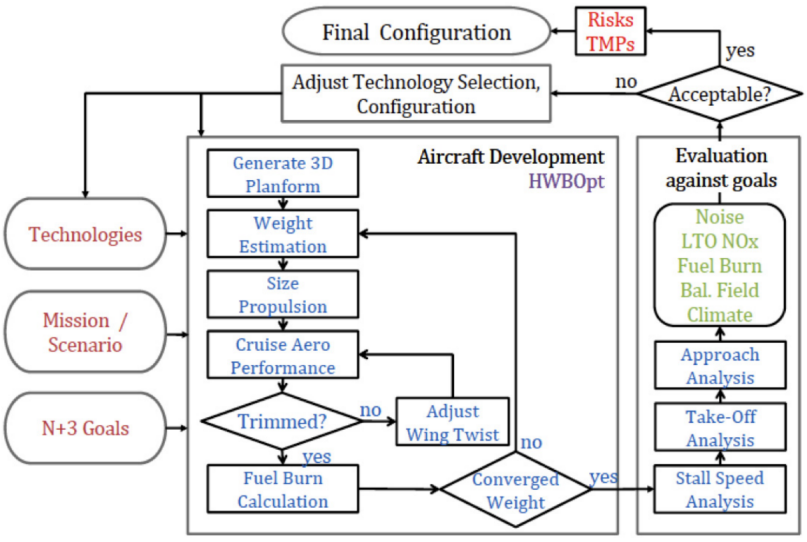

Figure 25: HWBOpt Methodology.[86]

5% and to trim at the start of cruise without control deflections. Thrust vectoring is used to trim for the remainder of the cruise segment. The elevon control authority is evaluated only during an approach trim condition. It is not clear whether a full set of elevons spanning the trailing edge were used, or whether it was a subset. A single deflection angle is reported, implying that all elevons are used as a large pseudo-elevator.

2.3.2.3 NLR and TU Delft

In 2002 Laban et al. of the National Aerospace Laboratory (NLR) in the Netherlands proposed a new metric for incorporating S&C constraints in the MDO problem.[74] The metric is based on the weight and balance envelope (i.e. weight vs. CG location) and evaluates control authority for trim. The "Controllability Margin," labeled CM in Figure 26, is defined as the most critical distance between the actual and allowable CG, and has units of distance. If it is negative, there is insufficient control authority for the vehicle. The Controllability Margin concept is interesting because it combines control authority constraints from an arbitrary number of flight conditions into a single metric. On the other hand, a violation of this constraint does not indicate

Table 6: MIT HWB MDO body of work.

Author(s)	Year	Summary
Diedrich et al. [32]	2006	HWB MDO methodology and framework to study the SAX configurations. MDO environment based on Boeing's WingMOD. New contribution is the inclusion of a noise assessment.
Hileman et al. [60]	2006	Higher fidelity aerodynamic and aeroacoustic analysis and optimization of the final design in Diedrich et al. (2006).
Hileman et al. [61]	2007	Similar to Hileman et al. (2006) but with a more advanced design, the SAX-40, that meets their noise and fuel burn goals.
Jones et al. [68]	2007	An MDO study that minimized a takeoff noise metric as a function of planform, takeoff operations, and outer wing airfoil design.
Hileman et al. [59]	2010	A journal version of Hileman et al. (2007).
Mody et al. [86]	2010	Introduces HWBOpt methodology, which combines elements from Diedrich et al. (2006) and Hileman et al. (2006) and updates some of the disciplinary analyses. Resulted in the H-series HWB designs.
Donaldson et al. [35]	2011	An MDO study with elements similar to HWBOpt for a 10 PAX HWB model.
Sato et al. [121]	2011	Extended the HWBOpt propulsion model to assess alternative propulsion concepts and fuel types on a baseline H3 design.

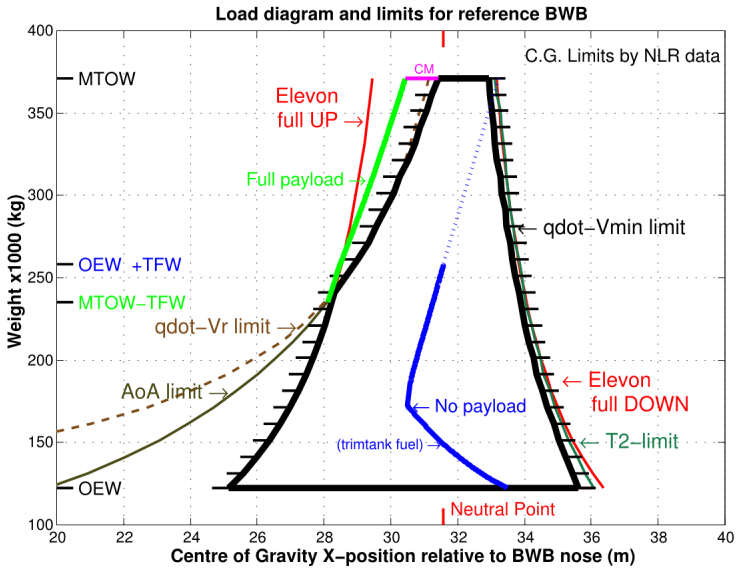

Figure 26: Weight and Balance Envelope.[74]

which control authority constraint was violated. The Controllability Margin also does not indicate whether there is sufficient control authority for a SAS to operate. The MDO environment described in this paper includes an automated FCS design module to assess handling qualities, but it does not appear to contribute any constraints to the optimization problem.

Vos & van Dommelen provide a recent example of HWB MDO at TU Delft.[140] In this paper they maximized range with a constant MTOW and payload. Their S&C constraints include stability derivative constraints, minimum control speed, maximum trim deflection at cruise, and static margin. The trim deflection constraint refers to an elevator which was not depicted. It is unknown whether it was a single control surface, the entire trailing edge, or something in between. The static margin constraint allowed values as low as -10% of the MAC, with the assumption that a flight control system would be able to correct any dynamic stability issues. Implicit in the assumption that the static margin can be traded for lower trim drag is that there is sufficient control authority for the SAS to operate, but this was not verified.

2.3.2.4 Other

In 2012 Nickol followed a manual design process to investigate scaling issues with the HWB, and implemented an interesting design rule.[97] He states that "*Previous Boeing studies have shown that keeping the CG and AC close to 40% MAC results in a design that can be balanced; however, a stability augmentation system will be required in all cases.*" The major components of Nickol's vehicles were positioned with this design rule in mind. If valid, this kind of design rule is incredibly useful for conceptual design because it serves as a short-cut for more detailed S&C analyses and reduces the designer's work load. However, the assumptions and conditions necessary for this simplification to be valid are unclear. The cited Boeing report describes work performed with MDOPT, which uses higher fidelity CFD.[107] The paper lists the design rule as a constraint but does not elaborate on their previous work that led to it. Considering how useful such a design rule could be in conceptual design, an attempt should be made to confirm it.

2.3.3 Summary

The papers summarized here sufficiently characterize the treatment of S&C constraints in the HWB MDO literature. The WingMOD studies have the most thorough investigation of trim control authority constraints, though lateral-directional conditions for sizing the tails are lacking. Most of the HWB MDO literature examines far fewer (if any) trim conditions. No HWB MDO examples in the literature include SAS control authority constraints, though plenty of one-off detailed FCS design studies for HWB are available.

Control authority adequacy for trim is included as a constraint in HWB MDO through trim deflection angle constraints. Dynamic stability and SAS control authority issues are never directly addressed, but instead are treated with constraints on static margin. If the control surface layout is discussed at all, it is fixed and the

control surfaces are not sized during MDO. Many papers refer to an "elevator" or "aileron" but do not clearly define the position, size, and whether multiple trailing edge controls are ganged together as one.

2.4 Literature Review Summary

Methods for making control surface layout choices as well as control surface sizing were presented. The method steps to be retained include a systematic way for choosing the type and arrangement of control surfaces, optimization of the number of redundant controls, and physics-based sizing of the controls. New research questions were posed that sought metrics for deciding the number of redundant controls and more convenient ways to represent control authority constraints for sets of redundant controls. As more HWB designs are scrutinized by rigorous S&C analyses, reliable trends regarding control surface area or vertical tail volume coefficients may emerge that can reduce the analysis burden on the conceptual designer.

The coupling of control authority with planform design required a review of the issue in the HWB MDO literature. The WingMOD method had the most thorough treatment of S&C found in the HWB MDO literature, but still did not evaluate SAS needs. WingMOD and other HWB MDO environments used static margin constraints instead, with the assumption that there would be sufficient control authority for an SAS to function. None of the HWB MDO tools reviewed appeared to perform control surface sizing, instead choosing to modify the planform to solve control authority issues.

Actuation power required for HWB vehicles is known to be very large, potentially exceeding that available from the engines or auxiliary power systems. This is not explored in any of the MDO tools or control surface layout/sizing methods discovered during the literature search. The control surface sizing literature introduced control allocation as a way to accommodate redundancy, and has the potential to be extended

to the actuation power problem. This will be explored and developed in Chapter 4.

CHAPTER III

METHODOLOGY DEVELOPMENT

3.1 Introduction

In this chapter the research questions posed so far will be reevaluated based on the findings in the literature search. Some questions will have been answered sufficiently and can be integrated into a methodology for addressing the research objectives of this dissertation. Other issues remain unresolved and will be identified along with promising avenues of research, which later chapters will explore in greater depth.

3.2 Control Surface Layout Design Method

RQ1.1: What control surface type and arrangement options are available and what justifies specific choices made for HWB designs in the literature?

The choice of type, number, and positions of control surfaces appears to be an early design decision that is carried through the design phases. In the previous chapters it was noted that the literature on HWB control surface layout design was sparse. Some control surface design methods were discovered for other configurations that have useful elements which can be combined to settle this research question.

3.2.1 Control Surface Architecture

Just as in van Ginneken et al. there will be an initial set of decisions made by the designer and subject matter experts prior to any design optimization or detailed analyses.[138] The basic steps in their method include a control surface functional decomposition, enumeration of alternatives, and application of designer preferences and mission requirements to make a selection. These elements will be customized for

the HWB design problem in the coming sections.

3.2.1.1 Matrix of Alternatives

In this section a system decomposition will be performed on the flight controls and options to satisfy those roles will be enumerated. The options will consist of different types of control surfaces as well as thrust vectoring. The method by van Ginneken et al. used "decision trees" for this step, but a more compact method for capturing the available choices is with a matrix of alternatives.[138]

The functions of the control surfaces considered here are straightforward: roll control, pitch control, yaw control, high lift systems, and drag generators. Examples of control surfaces that perform these functions are shown in Table 7. This is not an exhaustive list, but demonstrates that there are options beyond the aileron-elevator-rudder layouts of conventional T&W aircraft. If a control surface layout is constrained to one selection per row, then there are a potential 7,200 combinations represented in the matrix of alternatives. The selection of hybrid controls (e.g., elevon) in one row warrants their selection in others (e.g, roll *and* pitch). Some choices such as the inclusion of trailing edge flap high lift devices may be infeasible due to the configuration's sensitivity to the large pitching moments they generate.[113] Other combinations may be incompatible, such as using rudders for yaw control when there are no vertical tails.

3.2.1.2 Making a Selection

Several factors should be considered when choosing the control surface architecture. These may include the aircraft configuration, the design mission, and design legacy or experience. In addition, the architecture must ensure satisfaction of all control functions. In Chapter 2, Figure 13 from Sadraey & Colgren provides combinations of control surface types that accomplish this.

For competing options, Quality Function Deployment or similar methods can be used to make a decision. The van Ginneken et al. method used "trade-off" matrices

Table 7: HWB control surface matrix of alternatives.

		Alternative					
		1	2	3	4	5	6
Control Function	Roll	Aileron	Flaperon	Spoiler	Elevon		
	Pitch	Elevator	Belly flap	Elevon	Thrust vectoring	Ruddervator	Rotating tail
	Yaw	Rudder	Clamshell	Thrust vectoring	Ruddervator	Rotating tail	
	VT placement	Wingtip	Ctrbody	No VT			
	High lift	TE flaps	Flaperon	Krueger flaps	LE droop	LE slats	
	Drag	None	Belly flap	Clamshell	Spoiler		

= N2A-EXTE, = X-48B

(i.e. Pugh matrices) with criteria such as complexity, unintended control influence, remaining space for high lift devices and other relevant factors.[138] A 1-3-9 scale is recommended over their 1-2-3 scale in order to better distinguish between competing options. Their matrices are analogous to the "competitive assessment" or "rating of alternatives" room in the house of quality.[33]

The choices made by the X-48B and N2A-EXTE designers are highlighted in Table 7. What is common to them and to other HWB designs is the rudder and redundant elevon combination which provides control in all three axes of rotation. The X-48B designers may have also chosen clamshell elevons because the vehicle was designed to serve as a testbed for investigating S&C issues. The N2A-EXTE was designed with noise reduction as a priority. High lift devices are among the largest sources of noise during approach, which justified their selection of a drooped leading edge over leading edge slats.[61] The control surface layout used by the N2A-EXTE will be the baseline for the HWB configurations developed and analyzed in subsequent chapters. This is an initial assumption that may be subject to change later as more information is learned about a given design.

3.2.1.3 Degrees of Freedom for Sizing

Following the selection of the types of controls, decisions regarding the other degrees of freedom for the control surface layout need to be settled. The HWB optimization studies reviewed in Chapter 2 appeared to fix elevon chord fractions, relying on planform changes to resolve control authority issues. If the elevons were originally undersized, then suboptimal planforms may result. On a well balanced planform, the elevons may not need to have the largest allowable chord fraction. Allowing smaller elevons will reduce hinge moments, actuation power requirements, and weight. Chord fractions are an important degree of freedom and for the HWB optimization studies to follow in later chapters, sufficient control authority will be assured through a combination of planform and chord fraction variation. Rather than individual control surface chord fractions a single one will be used for the outer wing elevons which share a rear spar. Another chord fraction will be used for the centerbody elevon which has its own distinct rear spar. In addition the elevons will span the entire trailing edge with uniform spacing where trailing edge curvature allows.

The rudders will be full span except for a small offset to avoid interference with the elevons, and their chord fraction will be fixed at 25% from the trailing edge. Yaw control authority issues will be resolved by changing vertical tail scale. The drooped leading edge will be full-span on the outer wing and have a fixed chord fraction of 12.5% from the leading edge, matching measurements from a scaled drawing of the baseline N2A-EXTE configuration.

3.2.2 Unresolved Issues

RQ1.2: How should the number of control surfaces be chosen?

RQ2.1: What disciplinary metrics and design considerations might influence the number of redundant control surfaces?

Elevons have been chosen to provide roll and pitching moment control, and the

questions regarding how to design redundancy remain. An observation was made in Chapter 2 that HWB designs in the literature appear to have uniform spacing of elevons where trailing edge curvature or engine integration allow. No reason was found to suggest that a uniform spacing or a particular number of elevons are preferable to alternatives. In the literature search a study was found that varied the number, spacing, and deflection of elevons on a simple flying wing planform in an effort to minimize drag. Aerodynamics was the sole criteria used in that study, but it prompted the second research question listed above.

This is likely a strongly coupled multidisciplinary design problem, and the relevant stakeholders need to be identified. Metrics or figures of merit important to those stakeholders also need to be established. Finally these disciplinary concerns need to be synthesized into a system level metric that can be used to compare alternatives layouts and make decisions. This will be explored in Chapter 6 using the N2A-EXTE configuration as the baseline.

3.2.3 Summary

The basic elements of the proposed control surface layout design method are shown in Figure 27. The top-down design decision support process is a useful tool for framing design problems.[125] Section 3.2.1 explained the steps needed to define the control surface architecture and that feeds into defining the problem and assumptions. Next the issue of designing redundancy needs to be considered. A method which takes into account all relevant disciplines should be used, and this will need to be established.

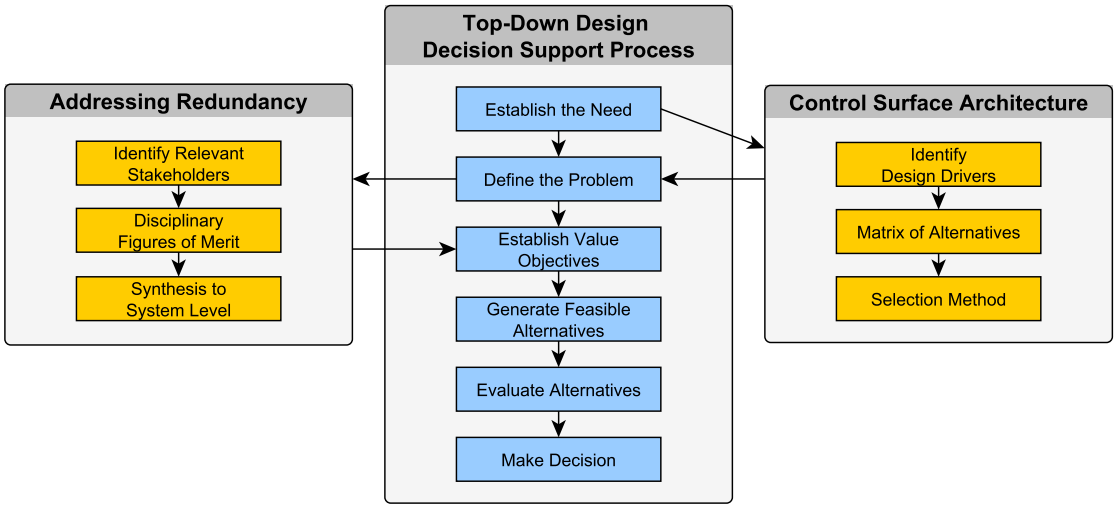

Figure 27: Control surface layout design method elements integrated into the Top-Down Design Decision Support Process.

3.3 HWB Multidisciplinary Optimization

Primary Research Objective: Develop a control surface layout and sizing methodology for HWB configurations.

Secondary Research Objective: Use the assembled MDO environment to test or discover trends, correlations, and design heuristics to aid in HWB conceptual design.

The latter half of the primary research objective from Chapter 1 still needs to be addressed. It is known from the literature survey on design and sizing of unconventional control surfaces that there are no rapid sizing methods based on historical data, especially for unconventional aircraft configurations. As a result, physics-based methods are necessary to investigate this problem. The control sizing flight conditions and trim analysis issues related to redundant multi-axis controls are discussed in Section 3.4. First, however, the MDO environment necessary for generating inputs to the trim analysis will be described.

3.3.1 HWB Modeling Environment Requirements

The basic required modeling environment elements for the HWB are not dramatically different from those needed in conventional aircraft sizing. Parametric geometry models are needed for the cabin, planform, vertical tails, estimating available fuel volume, and landing gear & engine positioning. A performance or mission analysis with mass estimating relationships will be needed to estimate takeoff gross weight and fuel burn for a design mission. Drag polars linked to the geometry and an engine model are needed to support the performance analysis as well. Mass properties including center of gravity (CG) and moments of inertia under various loading scenarios will be necessary to support the trim analyses. One important feedback loop for tailless aircraft configurations is a twisting of the wing to trim at a cruise design point. This requires knowledge of the weight (i.e. design C_L) and CG location at the design point, and will require an update to the aerodynamic model used in the performance analysis. Finally, control authority assessments are needed at several off-design flight conditions to size the elevons and vertical tails. It is important to include these in-the-loop, because control authority deficiencies may frequently require significant planform modifications. These basic elements are depicted in Figure 28, and are developed further in Chapter 7. The control authority assessment capability is developed in Chapters 4 and 5. Once the analysis capability has been generated, methods for their utilization in design space exploration and optimization will need to be established. The motivates the following research question:

RQ3.1: How should HWB sizing be conducted?

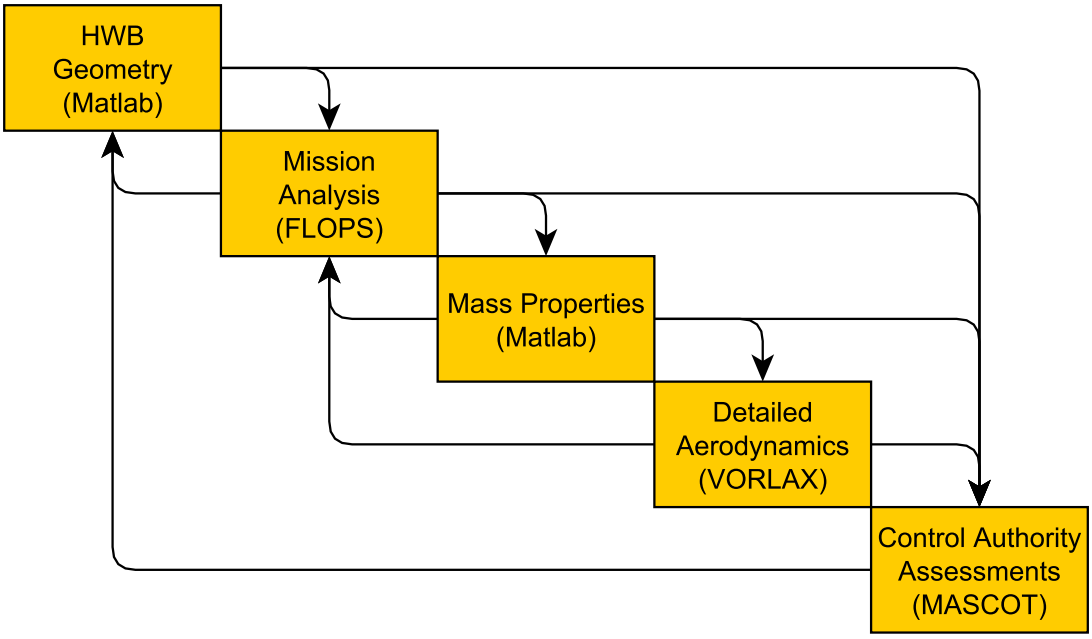

Figure 28: Basic elements of the HWB MDO environment to be developed in later chapters.

3.4 Control Authority Assessments

A control authority assessment capability for the HWB with redundant multi-axis controls is a complex issue that required several chapters to explore, conduct experiments, and finally settle on recommended methods for use in HWB MDO. However, certain aspects of the control authority assessment method can be discussed here. First, a list of off-design flight conditions for control sizing are recommended based on the findings of the literature search. Second, the use of redundant elevons that have strong effects in multiple axes confounds conventional control authority metrics (i.e. deflection angles and control derivatives). The saturation of a single control surface is no longer a good indicator of when the control authority limits have been reached, when the other redundant elevons may still be able to contribute useful moment increments. A new metric that can accommodate this added complexity in an intuitive way is proposed in Section 3.4.2.

3.4.1 Recommended Flight Conditions

RQ1.3: What flight conditions are most likely to result in active control authority constraints for the Hybrid Wing Body?

Early MDO work by Boeing evaluated 20-30 longitudinal flight conditions in the WingMOD tool.[146] Control authority constraints (defined in terms of maximum deflection angles) were checked for most of them, but the primary purpose may have been to establish operational CG limits. Wakayama included cruise and landing phase roll maneuvers in WingMOD analyses as well, but no flight conditions that would size the vertical tails (such as engine out or crosswind landing) were included.[145, 144] A more recent Boeing report from a detailed design study offers a more definitive list of flight conditions (including additional lateral-directional ones) that should be used to test the limits of HWB control authority in the early design phases.[16] These longitudinal and lateral-directional flight conditions and maneuvers from Bonet, et al. are summarized in Tables 23 and 24, respectively.

Table 8: Boeing flight conditions used to determine flight CG limits. Quoted text from Bonet, et al. [16]

No.	Flight Condition / Maneuver
1	"Takeoff nose wheel liftoff at 3.0 deg/s^2 pitch acceleration (nose-up longitudinal control authority)." Forward CG.
2	"Trim at Landing Reference Speed (V_{REF}) and maneuver to stall ($V_S = V_{REF}/1.23$) (nose-up longitudinal control authority)." Forward CG.
3	"Trim at Landing Reference Speed (V_{REF}) and go-around at 6.0 deg/s^2 pitch acceleration (nose-up longitudinal control authority)." Forward CG.
4	"Landing nose wheel hold-off down to stall speed (nose-up longitudinal control authority)." Forward CG.
5	"Stall recovery at -4.0 deg/s^2 pitch acceleration (nose-down longitudinal control authority)." Aft CG.

This set of flight conditions is not as comprehensive as that recommended by Chudoba in Chapter 2. However, Boeing's list is more authoritative due to their experience with the HWB configuration and will be assumed to be the most likely

Table 9: Boeing lateral-directional flight conditions for testing control authority. Quoted text from Bonet, et al. [16]

No.	Flight Condition / Maneuver
1	Engine-Out Minimum Control Speed: "Balance engine-out on ground with no sideslip and no nose wheel steering (yaw control authority at V_{MCG})"
2	Engine-Out Minimum Control Speed: "Balance engine-out in air with no sideslip and less than 5 degrees bank angle (yaw control authority at V_{MCA})"
3	Crosswind Landing Trim: "Trim in 35 knot crosswind with no crab angle at slowest approach speed (lightest weight)"
4	Crosswind Landing Maneuver: "A 6 degree heading (sideslip) change in 2 seconds at maximum wing fuel landing weight (yaw control authority). Future work with 6 Degree-Of-Freedom (6 DOF) simulation will be required to determine requirements for yaw acceleration and steady state yaw rate."
5	Landing Roll Maneuver: "A 30 degree bank angle change in 2.5 seconds at maximum wing fuel landing weight (roll control power). This requirement equates to 20 deg/s^2 roll acceleration and 20 deg/s steady state roll rate."

control sizing conditions. It will serve as the basis for generating control authority constraints in the HWB optimization experiments to follow, and inclusion of the four tail sizing conditions will be the first known implementation in a HWB MDO setting.

3.4.2 Control Authority Metric for Redundant Control Surface Layouts

RQ2.2: Are there more convenient metrics for expressing the control authority available vs. required for a set of redundant controls?

The WingMOD and other HWB optimization environments frequently only assessed control authority for longitudinal flight conditions. In doing so, a simplification could be made in how the elevon redundancy was utilized. Linking or "ganging" the elevons together to behave as a pseudo-elevator requires only one deflection angle to be determined during trim analyses. Pitching moment control authority is then simple to measure as the difference between the required and maximum allowable deflection angle. Flight conditions that test lateral-directional control authority are problematic because the designer must allocate control function (e.g., roll vs. pitch) to the elevons and control authority must be assessed in all three axes.

If a simplified "ganging" approach is used to allocate roll and pitching moment functions to the redundant elevons then the conventional aileron, elevator, and rudder deflection angles could be used to assess control authority for the HWB configuration. However if a more continuous or overlapping allocation of control function is used, these conventional deflection limit metrics begin to lose their meaning as measures of control authority.

The literature search revealed that control allocation methods are useful tools for utilizing redundant multi-axis controls. Direct allocation is one such method and for linear control moments is guaranteed to return deflections that maximize moment increments in any direction.[37] At the heart of the method is a concept known as the attainable moment subset (AMS) which describes the effects of the controls relative to a reference vehicle state. The state S^* in Equation 4 is defined as the state vector consisting of Mach, α, β, and deflections that trim the vehicle (i.e. balance the forces and moments), and is the product of a trim analysis. Vehicle state S_{ref} in Equation 5 is identical to the trimmed vehicle state with the exception that the controls are not deflected.

$$\mathbf{S}^* = \{\text{Mach}^*, \alpha^*, \beta^*, \delta_1^*, \ldots, \delta_N^*\} \tag{4}$$

$$\mathbf{S}_{ref} = \{\text{Mach}^*, \alpha^*, \beta^*, \delta_1^* = 0, \ldots, \delta_N^* = 0\} \tag{5}$$

A basic 2D linear AMS is plotted in Figure 29 for a swept wing with two control surfaces. The axes in this figure are incremental rolling and pitching moments and the origin is defined by $textbf{S}_{ref}$. As the control surfaces are deflected an incremental moment vector can be traced in this space. Also plotted in this figure are the deflection combinations for the flying wing example that generate the largest moment increments (nose up/down, roll left/right). All moments that are possible with these controls are either on or within the AMS boundary (the solid lines connecting the dots).

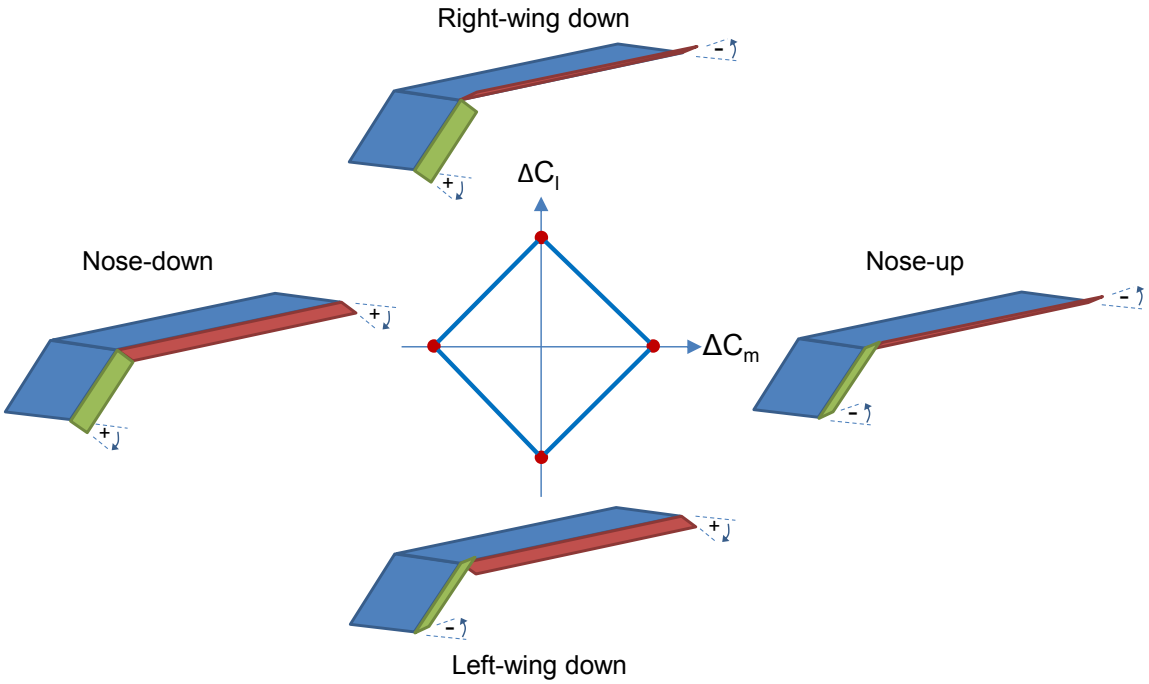

Figure 29: Construction of a 2D AMS (rolling moment vs. pitching moment) for a flying wing example.

In the deflection space ($\mathbb{R}^m$), there are 2^m vertices, where m is the number of control surfaces. This is essentially a full factorial design of experiments of controls at their min or max deflection angle. There are $2^{m-1}\binom{m}{1}$ edges, which represent a single control surface being swept from one extreme to the other. Finally there are $2^{m-2}\binom{m}{2}$ faces which are 2D planes in which two control surfaces are swept simultaneously. In the moment-space ($\mathbb{R}^3$) these vertices, edges, and faces can lie on the AMS boundary, within it, and coincident with each other. Only those on the AMS boundary are important, and the others can be filtered out using convex hull methods.

The AMS boundary is equivalent to a multi-dimensional Pareto frontier in the moment-space ($\mathbb{R}^3$) and it shows the trade-offs that exist between the maximum moments that can be achieved by the control surfaces. In Figure 29 it is clear that this swept wing model with two elevons cannot achieve maximum pitching moment and maximum rolling moment simultaneously. A more formal definition of the AMS is provided by Durham and is paraphrased below [36]:

Consider an m-dimensional control space $\boldsymbol{u} \in \mathbb{R}^m$. The controls are constrained to minimum and maximum values, defined by the subset Ω

$$\Omega = \{\boldsymbol{u} \in \mathbb{R}^m | u_{i\min} \leq u_i \leq u_{i\max}\} \subset \mathbb{R}^m \tag{6}$$

The subset of controls that lie on the boundary of Ω, $\partial(\Omega)$, are denoted by $\boldsymbol{u^*}$.

$$\boldsymbol{u^*} \in \partial(\Omega) \tag{7}$$

These controls generate moments through a mapping B onto the n-dimensional moment space:

$$B : \mathbb{R}^m \rightarrow \mathbb{R}^n \tag{8}$$

$$\mathbf{M} = B\mathbf{u} \tag{9}$$

where $m > n$. B is the control effectiveness matrix and contains the linear control derivatives. The image of Ω in $\mathbb{R}^n$ is denoted Φ and represents all of the moments that are attainable within the constraints of the controls.

$$\Phi = B\mathbf{u} \subset \mathbb{R}^n \tag{10}$$

The AMS boundary or surface (Figure 29) is denoted $\partial(\Phi)$ and represents the set of maximum attainable moment increments relative to the reference vehicle state. Desired moments within the AMS surface ($\mathbf{m} \in \Phi$) can potentially be achieved by multiple deflection combinations, but desired moments on the surface ($\boldsymbol{m^*} \in \partial(\Phi)$)

have unique deflections. Desired moments outside the surface cannot be achieved by the control surfaces.

In the swept flying wing example, as the trailing edge is divided into more control surfaces the number of vertices, edges, and faces will increase. Finer control over the lift distribution will also be possible and will lessen the severe tradeoff between rolling and pitching moments. In other words, for a given desired pitching moment the maximum rolling moment that can be achieved simultaneously may increase.

3.4.2.1 New Control Authority Metric: AMS Margin

A HWB design can be said to have sufficient control authority if the control moment increments required for trim lie within the AMS at all flight conditions of interest (Equation 11). $\mathbf{M}_{max}$ in Equation 12 is the maximum attainable moment increment in the direction of $\mathbf{M}_{req}$. A new metric, the AMS Margin, is proposed for assessing control authority for redundant multi-axis control surface layouts, and for serving as a constraint during optimization of control configured vehicles.

$$\mathbf{M}_{req} = \underbrace{\begin{bmatrix} C_{l_{\delta_1}} & \dots & C_{l_{\delta_N}} \\ C_{m_{\delta_1}} & \dots & C_{m_{\delta_N}} \\ C_{n_{\delta_1}} & \dots & C_{n_{\delta_N}} \end{bmatrix}}_{\text{Control Effectiveness Matrix},B} \begin{bmatrix} \delta_1^* \\ \vdots \\ \delta_N^* \end{bmatrix} \in \Phi \tag{11}$$

$$\mathbf{M}_{max} = a\mathbf{M}_{req} \tag{12}$$

$$\text{AMS Margin} = 1 - \frac{\|\mathbf{M}_{req}\|}{\|\mathbf{M}_{max}\|} \tag{13}$$

The term $\mathbf{M}_{max}$ is calculated using direct allocation algorithm, defined below. In this linear programming problem $\mathbf{u}$ is the Nx1 deflection vector and if $a > 1$ then $\mathbf{u}$ is set to $\mathbf{u} = \mathbf{u}/a$. An AMS Margin greater than zero indicates more than adequate control authority, a value of zero indicates the controls are at their limits, and a

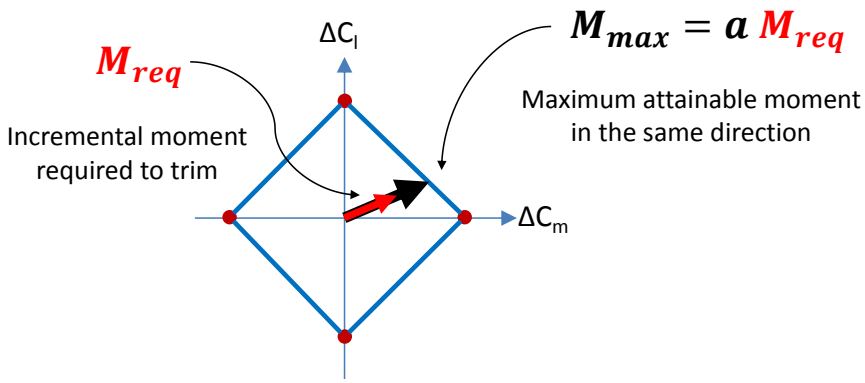

Figure 30: Example trim solution ($\mathbf{M}_{req}$) with positive AMS Margin.

negative value indicates that the controls are unable to provide the required moment increments. Figure 30 visualizes the first of these scenarios, where $\mathbf{M}_{req}$ is shown as a red vector and $\mathbf{M}_{max}$ as a black vector.

$$\begin{aligned} \max_{a,u} \quad & a \\ \text{subject to} \quad & B\mathbf{u} = a\mathbf{M}_{req} \\ & \mathbf{u}_{min} \leq \mathbf{u} \leq \mathbf{u}_{max} \end{aligned}$$

During vehicle optimization, one AMS Margin metric is required per flight condition investigated. This new metric is an intuitive measure of *remaining* control authority, and takes the place of m deflection angle constraints for each flight condition. The saturation of an individual control surface no longer defines the limits of control authority if the remaining controls can increase the moment increment magnitude in the desired direction. This metric, which is continuous and independent of the number of controls, is a novel contribution to the literature and answers the research question that opened Section 3.4.2.

3.4.3 Unresolved Issues

The AMS Margin control authority metric proposed in the previous section is a function of the outputs from a trim analysis. The conventional methods used to balance the forces and moments acting on aircraft will be described and demonstrated

in Chapter 4. Complications caused by control redundancy will also be identified, and methods will be proposed for relieving or circumventing those problems. Once the trim analysis methods have been established the advantages and conveniences of the new AMS Margin metric can be demonstrated, and the full HWB MDO environment can be assembled.

3.5 Hybrid Wing Body - Control Authority Testbed (HWB-CAT) Methodology

The HWB is an unconventional configuration lacking in historical databases and design knowledge that enables the conceptual design phase for other configurations like the T&W. In the absence of historical data a physics-based method must bridge the gaps to generate new knowledge, data, and insights to enable design. The highly integrated nature of the HWB causes a strong coupling between aircraft performance and control authority that requires a S&C disciplinary perspective at the earliest stages in design. This dissertation seeks to explore this coupling and bridge the gap with a methodology covering three primary areas of research: 1) a control authority assessment method, 2) a control surface layout design method, and 3) the synthesis of methods and tools to enable HWB design and optimization. Given the heavy emphasis on controls and flight mechanics, it has been named the Hybrid Wing Body - Control Authority Testbed (HWB-CAT) methodology. A basic road map of three component methods and outstanding issues to be resolved in each is shown in Figure 31. Below, the basic steps of the methodology are defined:

Step 1: Establish the control authority assessment method The first component of the methodology that must be established is the control authority assessment method. The other two methods are dependent on the research conducted in this area. The redundant control surface layouts on the HWB create interesting challenges and opportunities for the trim analysis.

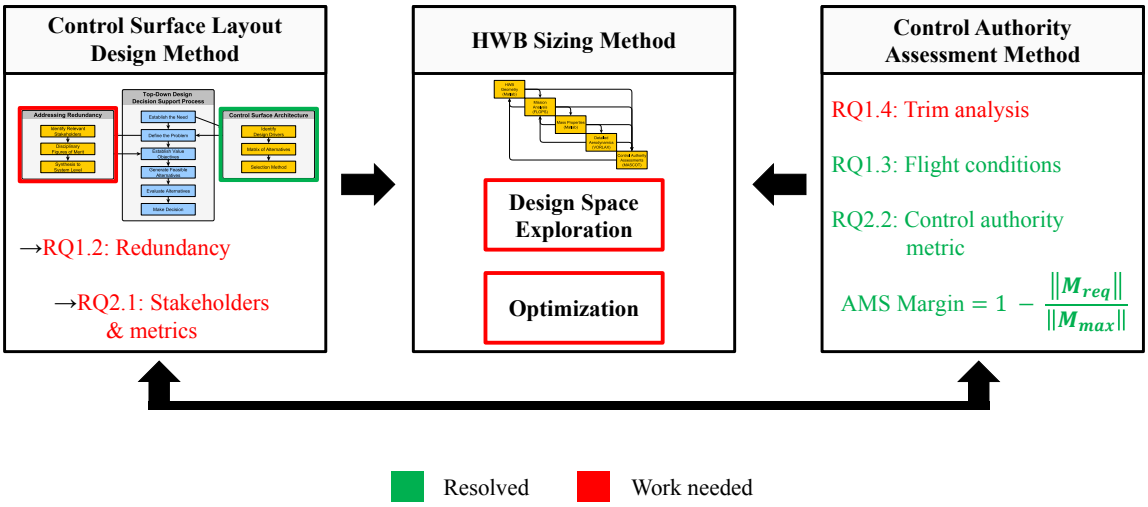

Figure 31: Road map to the Hybrid Wing Body - Control Authority Testbed (HWB-CAT) methodology.

1. The existing methods for balancing the forces and moments of flight must be evaluated and if found to be inadequate, alternatives will have to be proposed and demonstrated. These trim analysis methods are being developed with the intent to integrate them into an MDO, from which certain requirements can be derived. This is the primary outstanding issue that will be developed in the next two chapters.

2. Once a trim analysis method is established, the resulting trim solutions (or lack thereof) must be translated into control authority constraints for use in HWB optimization. A potential solution was described in Section 3.4.2.

3. Finally, deciding which flight conditions and maneuvers to evaluate for unconventional configurations in the early design phases is the final component of the method that must be established. The flight conditions relevant assessing control authority in conceptual design were defined in Section 3.4.1.

Step 2: Establish the control surface layout design method A method to bring clarity and perspective to the HWB control surface layout design problem was needed. Decision rationale for the observed variety in the HWB literature was sparse

and was the primary motivation for this step of the methodology

1. Section 3.2.1 established the series of steps necessary to define a control surface architecture, the output of which are the types of controls and the functions they will perform.

2. Control redundancy is a key issue in the HWB control surface layout design problem, and one with the least insights available from the HWB literature. This step of the method seeks to answer the what the right number of elevons may be and what stakeholders may be involved. A multi-disciplinary method will be required resolve competing interests among stakeholders, and is the subject of Chapter 6.

Step 3: Establish HWB sizing methods and models This component of the methodology is where the new control authority assessment method must be integrated with the traditional conceptual design phase methods and tools

1. Methods and models for the traditional sizing disciplines must be assembled and customized for the HWB design problem.

2. These must then be implemented to conduct HWB design space exploration. The existence and location of the feasible design space may not be known, and a method for discovering it will be established in Chapter 8.

3. Finally, the last element of the HWB sizing method will be to establish best practices for optimization. These methods are developed in Chapter 9.

3.6 Conclusion

The large amount of variability in the number of control surfaces among HWB designs in the literature and insufficient explanation of design rationale was the main motivation behind research question 1.1. Design drivers for control surface layout

options were collected including the need to influence each moment axis, the need to fit controls on the available aerodynamic surfaces, and other considerations driven by mission requirements. Alternatives for the types of control surfaces were identified, stored in a matrix of alternatives, and decision making methods were suggested when the choices were not obvious. The control surface layout chosen for this dissertation was based on the N2A-EXTE configuration. The work covered in this chapter settles research question 1.1 in its entirety.

The literature survey did not find adequate answers regarding how to design control redundancy on the HWB or other configurations. This required a new method to be developed and motivated the creation of research questions 1.2 and 2.1. The basic steps required to settle these questions were identified in this chapter, but are fully resolved in Chapter 6.

The time and resources available to designers during the conceptual design phase are limited, and the evaluation of off-design flight conditions must be prioritized. As Chapter 1 noted, evaluating a limited number of flight conditions creates a risk of missing an active control authority constraint. Consequences to this may include degraded vehicle performance, accidents, or late phase redesign which can be costly. Fortunately, Boeing offered a reduced set of more likely flight conditions based on approximately 25 years of experience with the HWB configuration. This list of flight conditions for control authority assessments was sufficient to settle research question 1.3. The trim analyses for these flight conditions are formally defined in Chapter 5.

One of the novel contributions of this chapter was the introduction of a metric for assessing the control authority of a set of redundant multi-axis control surfaces. The AMS Margin metric is based on the attainable moment subset concept from the control allocation literature, and converts an N-dimensional trim deflection vector into a scalar measure of remaining control authority. The chapters to come demonstrate the behavior of the metric and establish methods for calculating it when a lack of

control authority prevents the discovery of a trim solution.

CHAPTER IV

ALTERNATIVE TRIM ANALYSIS FORMULATIONS FOR VEHICLES WITH REDUNDANT MULTI-AXIS CONTROL SURFACES

4.1 Introduction

RQ1.4: How should the trim analysis be conducted to support HWB design optimization?

A method for assessing control authority of a set of redundant multi-axis controls will need to be established for use in HWB vehicle optimization. This will require trim analyses, involving the balancing of the forces and moments acting on a vehicle at various flight conditions and maneuvers. Research question 1.4 from Chapter 1 was regarding how the trim analysis should be set up for the HWB. Immediate follow-up questions to help guide the research include: 1) How are the trim analyses typically performed today? and 2) Are existing methods adequate? The rigid body nonlinear equations of motion will be presented as well as the conventional method for solving them for trim or equilibrium solutions.

Control redundancy on the HWB configuration is expected to cause several challenges for the conventional trim analysis method. They will be described and alternative trim analysis methods will be proposed for dealing with these problems. Experiments will be conducted to verify whether the predicted issues exist, and to determine if any of the proposed trim analysis methods are viable alternatives.

Ultimately the purpose of the trim analysis is to provide control authority constraints for HWB vehicle optimization. This suggests a few requirements that the

chosen method must satisfy. The selected method shall be automatable and provide consistent and repeatable results. The method shall also be required to produce trim solutions with reasonable angles of attack and deflections when possible. In other words extreme solutions should not be returned if more moderate ones exist, especially given the limitations of the VORLAX aerodynamic models.

The trim analysis experiments will be conducted using a VORLAX model of the N2A-EXTE HWB configuration. A landing approach flight condition in symmetric and crosswind conditions will be used to assess the alternative trim analysis methods. The symmetric condition is meant as a simple test case to set up and debug the various trim analysis methods. The crosswind condition will serve as a stress-case that is intended to push the control authority limits for each of the methods. Metrics that will be tracked are the optimization trial success rate, consistency and uniqueness of the results, and engineering judgment on the reasonableness of the trim deflections.

4.2 The Nonlinear Rigid Body Equations of Motion

The trim analysis requires solving the rigid body steady state nonlinear equations of motion (EOMs) for equilibrium points by manipulation of the state vector. The state vector includes the Euler angles, velocity components, control surface deflections, angular velocity components, thrust (magnitude and direction for each engine), main gear contact forces, and quasi-static terms (Equation 14). Many of these terms are constants set by the flight condition and others will be free to vary within side constraints. The EOMs are first-order nonlinear ordinary differential equations with time as the independent variable. In general, there is no analytical solution and an optimizer must be used to manipulate the state vector in order to find the equilibrium or quasi-equilibrium solutions.

$$\mathbf{S} = \left\{ \psi, \theta, \phi, V, \alpha, \beta, \delta's, p, q, r, (\text{prop. settings}), (\text{main gear contact forces}), \dot{u}, \ddot{\theta} \right\} \tag{14}$$

The equations of motion introduced below are used under several standard assumptions. Rigid body motion is assumed, meaning aeroelastic effects will be unaccounted for. A flat Earth (stationary plane in inertial space) is assumed, so the rotation and curvature of the Earth are neglected. This is valid for the subsonic speeds in the HWB mission profile. Other assumptions include an atmosphere at rest, symmetric aircraft (i.e. $I_{yz} = I_{xy} = 0$), and constant mass.

The number and form of the equations of motion in the literature vary between the problems being solved and trim analysis implementations. Here the navigation, force, and moment equations form the set of nonlinear equations to be solved.

The navigation equations, which ensure the vehicle is traveling at the desired speed in the desired direction:

$$\begin{aligned} \mathbf{v}_{cg}^{\mathcal{E}} &= L^{\mathcal{EB}} \mathbf{v}_{cg}^{\mathcal{B}} \\ &= L_z(-\sigma) L_y(-\gamma) \begin{bmatrix} V & 0 & 0 \end{bmatrix}^T \end{aligned}$$

where σ is the target course angle, γ is the target climb angle, V is the speed, $\mathcal{E}$ is the Earth frame, and $\mathcal{B}$ is the body frame. This equation can be rearranged to provide the following scalar navigation equations:

$$\sigma = \tan^{-1} \left(\frac{\mathbf{v}_{cg}^{\mathcal{E}}(2)}{\mathbf{v}_{cg}^{\mathcal{E}}(1)} \right) \tag{15}$$

$$\gamma = \tan^{-1} \left(\frac{-\mathbf{v}_{cg}^{\mathcal{E}}(3)}{\sqrt{\mathbf{v}_{cg}^{\mathcal{E}}(1)^2 + \mathbf{v}_{cg}^{\mathcal{E}}(2)^2}} \right) \tag{16}$$

$$\| \mathbf{v}_{cg}^{\mathcal{E}} \| = V \tag{17}$$

The force equations in the body frame:

$$X - mg\sin(\theta) = m\left(\dot{u} + qw - rv\right) \tag{18}$$

$$Y + mg\cos(\theta)\sin(\phi) = m\left(\dot{v} + ru - pw\right) \tag{19}$$

$$Z + mg\cos(\theta)\cos(\phi) = m\left(\dot{w} + pv - qu\right) \tag{20}$$

The moment equations in the body frame:

$$L = I_x\dot{p} - I_{xz}\left(\dot{r} + pq\right) + qr\left(I_z - I_y\right) \tag{21}$$

$$M = I_y\dot{q} - I_{xz}\left(r^2 - p^2\right) + rp\left(I_x - I_z\right) \tag{22}$$

$$N = I_z\dot{r} - I_{xz}\left(\dot{p} - qr\right) + pq\left(I_y - I_x\right) \tag{23}$$

The X,Y,Z,L,M,N terms contain the aerodynamic, thrust, landing gear, and other external forces and moments. The terms p, q, and r are the rotation rates about the body axes. The Euler angles ϕ, θ, and ψ define the relationship between the Body and Earth-fixed reference frames. This formulation of the EOMs is used in the Matlab Stability and Control Toolbox (MASCOT) trim analysis code, which was available for use and modification. It was developed by NASA Langley Research Center and the National Institute of Aerospace, and has been used to study the High Speed Civil Transport and other multidisciplinary optimization problems.[91, 90, 6, 7]

4.2.1 Finding Trim Solutions with a Conventional Problem Formulation

These nine equations form a nonlinear system of equations whose roots are the equilibrium or trim solutions. The residual equations (e.g. Equation 24 for the first force equation) are obtained by moving all terms to one side,and can be thought of as a measure of error:

$$residual_X = X - mg\sin(\theta) - m(\dot{u} + qw - rv) = 0 \tag{24}$$

The aircraft is trimmed when all of the residual equations are zero simultaneously. This is done by minimizing the sum of squares of the residual equations (0 at its smallest), and is equivalent to driving translational and rotational accelerations to zero (or to target values) simultaneously. This is the general approach taken in the Stevens and Lewis text and the MASCOT, AeroMech, and CEASIOM trim analysis codes.[131, 29, 112, 28] The optimization problem statement is shown below:

$$\begin{aligned} \underset{S}{\text{minimize}} \quad & \sum_{i=1}^{9} residual_i^2 \\ \text{subject to} \quad & S_i = a_i,\ i = 1, \ldots, l. && \text{Flight/Operating conditions} \\ & b_i \leq S_i \leq c_i,\ i = l+1, \ldots, m. && \text{State variable side constraints} \end{aligned}$$

Some of the state variables are fixed by the particular flight and operating condition of interest (e.g. Mach number, altitude, climb angle, etc). Others such as thrust, angle of attack, and control surface deflections are free to change subject only to side constraints. Each residual is desired to be within 10^{-5} of zero and therefore the tolerance for the sum of squares must be $9 \cdot 10^{-10}$. A failure to find a trim solution can happen due to insufficient control authority, poor initial guesses, or tolerances that are too strict.

4.2.2 Anticipated Issues with Conventional Trim Problem Formulation

4.2.2.1 Complications Caused by Redundant Controls

For conventional aircraft with three control surface deflections in the state vector, it is possible to have under-determined, determined, and over-determined systems of nonlinear equations depending on the number of constraints imposed by the flight condition being investigated.[29] A determined system has an equal number of unknown parameters and equations. An over-determined system has more equations

than unknowns. However because the equations are nonlinear, this property of the system and its parameters is insufficient for determining how many solutions there will be.[1] There can in general be between zero and infinitely many solutions. For a HWB configuration with redundant control surfaces this system of equations will be consistently under-determined because there will be more unknowns than equations, and is expected to have more than one trim solution if there is sufficient control authority. This situation is also known as a non-square or rectangular system. Formally, the problem is to find a point $x^* \in \mathbb{R}^m$ such that:

$$F(x^*) = 0, F : \mathbb{R}^m \to \mathbb{R}^n \text{ with } m > n \tag{25}$$

This has implications for which algorithms can be used to seek out trim solutions. Many methods such as the least-squares algorithms Levenberg-Marquardt and Gauss-Newton are restricted to N equations and N unknowns.[83, 11] There are modified Newton methods that use generalized inverses to invert non-square Jacobians and enable the solution of under and over-determined systems.[127] Matlab's fgoalattain algorithm is the default within the MASCOT trim analysis tool for solving non-square systems. This optimizer is based on the sequential quadratic programming (SQP) method and will be used to demonstrate the conventional trim optimization for the N2A-EXTE.

The ultimate consequence of control redundancy is that for a given desired moment there may be multiple control surface deflection combinations that can achieve it. It will be shown that when there is sufficient control authority to trim, the HWB will potentially have infinitely many trim solutions (i.e. roots to the EOMs). Conversely when there is insufficient control authority, no trim solutions will exist. For borderline cases there may be a unique solution. If an analyst is only interested in whether the

[1] Take for example the equation $x^2 - 1 = 0$. There is 1 unknown and 1 equation, but two solutions at $x = -1$ and $x = 1$. Or $\sin\theta = 0$ with infinitely many solutions.

vehicle can trim, then any feasible solution may be acceptable. Otherwise, a value system will have to be established in order to choose from the feasible solutions or a simplification that results in unique solutions will have to be imposed.

4.2.2.2 Complications Caused by the Conventional Objective Function

De Marco et al. offer a useful definition for objective functions used in the discovery of trim solutions: "The cost function is, by definition, always non negative and evaluates to zero when the aircraft is in a steady-state flight."[31] The sum of squares of residual equations used by default in MASCOT satisfies this definition, but is less restrictive because it allows for accelerating flight. Trim optimization problems that use it and other objective functions in this category shall be referred to as conventional trim optimization problem formulations.

The conventional trim optimization problem by definition values all trim solutions equally. By using this formulation the optimizer seeks trim solutions closest to the initial condition, and upon finding it terminates. To gain an understanding into how many trim solutions there are (i.e. none, one, or infinitely many), the trim optimization must be executed from many randomly generated initial conditions. A manual post-processing to see if any solutions are reasonable is useful for generating insights into the problem, but will not satisfy the method requirements for use in MDO laid out in the beginning of the chapter. In the next section, the aerodynamic modeling method used throughout this dissertation will be discussed and validated using the N2A-EXTE configuration. Then, the conventional trim method will be demonstrated using the N2A-EXTE model.

4.3 N2A-EXTE Aerodynamic Model

The N2A-EXTE is a non-proprietary HWB design that was modeled and used to demonstrate trim analysis methods. It features 11 redundant elevons along the trailing edge of the wing, two centerbody mounted vertical tails with rudders, and a

drooped leading edge high lift device. This configuration was tested at NASA Langley's 14x22 wind tunnel at low speeds, but a full stability and control database was not generated.[49] The available data was used to validate and correct an aerodynamic model generated with the VORLAX vortex-lattice method. The model (Figure 32) uses separate panels for the controls which enabled more precise definition of the hinge lines. This generated more accurate results than camber line modification on a combined wing-elevon panel.

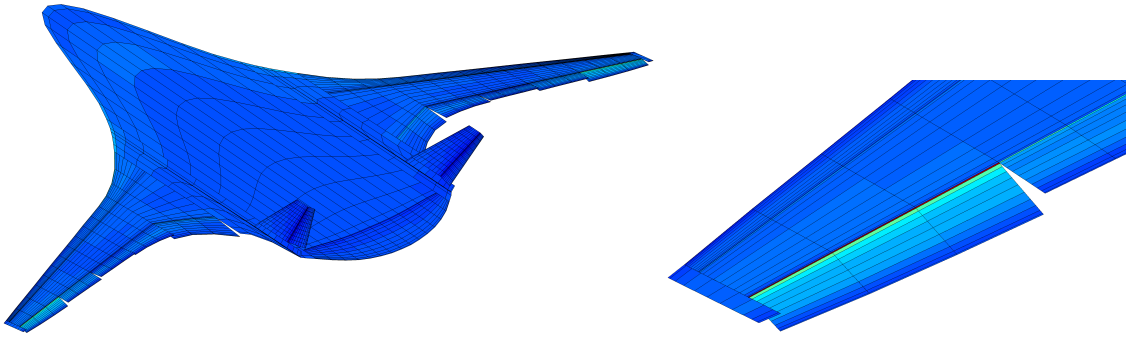

Figure 32: C_p visualization for the N2A-EXTE VORLAX model.

At moderate angles of attack and deflections the VORLAX model was shown to have good agreement with the wind tunnel data (Figure 33). A limitation of the model is that flow separation at large deflection angles is not modeled and therefore VORLAX over-predicts control effectiveness there. A viscous drag correction was necessary, and the wind tunnel drag polar was used to anchor the VORLAX drag model.

Surrogate models were generated for each force and moment coefficient as a function of α, β, and the deflection angles. A third-order response surface equation constructed with stepwise regression was found to have sufficient accuracy. The surrogates were trained with data from a Latin Hypercube design augmented with a fractional factorial design to cover the corners. A positive deflection for the elevons is defined to be trailing edge down which produces a negative (nose-down) pitching moment. For the rudders a positive deflection is defined to be trailing edge left and

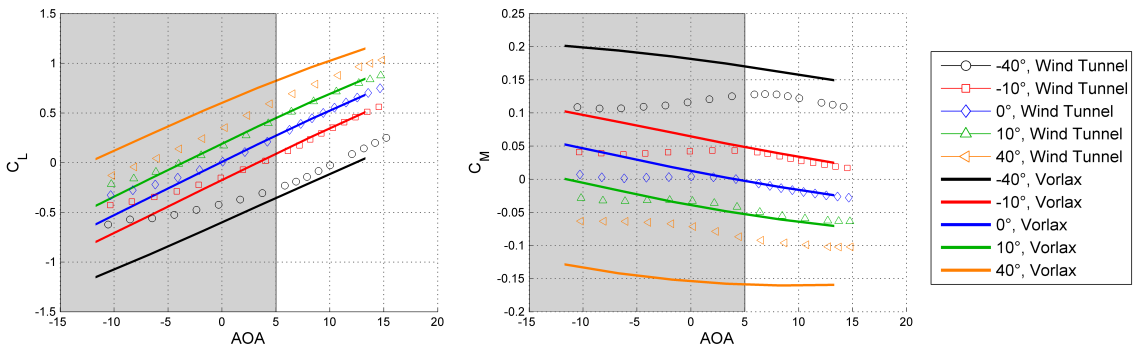

Figure 33: VORLAX and wind tunnel data for the N2A-EXTE in high lift configuration at Mach 0.2.

produces a positive side force and a negative (nose-left) yawing moment.

The approach flight condition explored in this study was flown at $1.3V_{stall}$ as suggested by Anderson.[8] With a C_{Lmax} of 1 and take-off wing loading of 47.2 lbs/ft^2 the stall speed was estimated using Equation 54 to be 118.2 knots.[72] The trim analyses were therefore conducted at a speed of 153.7 knots.

$$V_{stall} = \sqrt{\frac{2}{\rho_\infty}\frac{W}{S}\frac{1}{C_{Lmax}}} \tag{26}$$

4.4 Evaluation of the Conventional Method in an Approach Flight Condition

4.4.1 Experiment Assumptions

The approach flight condition for the N2A-EXTE will be investigated using the conventional trim optimization problem formulation. A high lift configuration defined by a leading edge droop of 30 degrees will be used. The primary characteristics of this flight condition will be zero crosswind, traveling due north, a standard climb angle of -3 degrees, a forward center of gravity, and symmetric deflections. The elevons on the right wing will mirror the left wing and the rudders will not be deflected. A subset of the state vector is fixed, taking values defined in Table 10. The remaining state vector variables are bounded (Table 11) and manipulated by the optimizer to drive

the residual equations to zero. As mentioned previously, each residual is desired to be within 1e-5 of zero and therefore the tolerance for the sum of squares must be 9e-10. The variable θ has a known relationship with other variables ($\theta = \alpha + \gamma$) but because MASCOT does not allow this kind of constraint it is treated as a free variable.

Table 10: Symmetric approach fixed variables for the conventional method.

	Variable	Value	Units
1	V_{app}	$1.3V_{stall}$	
		0.23	Mach
		153.7	knots
2	γ (climb angle)	-3	degrees
3	ψ (heading)	90	degrees
4	ϕ (roll)	0	degrees
5	β	0	degrees
6	Altitude	0	ft
7	Weight	343,660	lbs
8	Fwd CG	36.1	% MAC
9	$\delta_{rudders}$	0	degrees
10	$\delta_{LEdroop}$	30	degrees

Table 11: Symmetric approach free variables for the conventional method.

	Variable	Min	Max	Units
1	α	5	20	degrees
2	θ (pitch angle)	2	17	degrees
3-8	$\delta_1 \ldots \delta_6$	-30	30	degrees
	(symm. elevons)			
9	$T_{\text{per engine}}$	0	76,733	lbs

4.4.2 Experimental Results and Observations

One hundred trials of the trim optimization were run with randomly generated initial conditions for the free state variables. Of those trials, 68% of the cases successfully converged to trim solutions within the tolerance specified. Each point in Figure 34 is a converged solution, with identical objective function values (all residuals zero within the tolerance), but they have widely varying characteristics in terms of drag, thrust, and deflections.

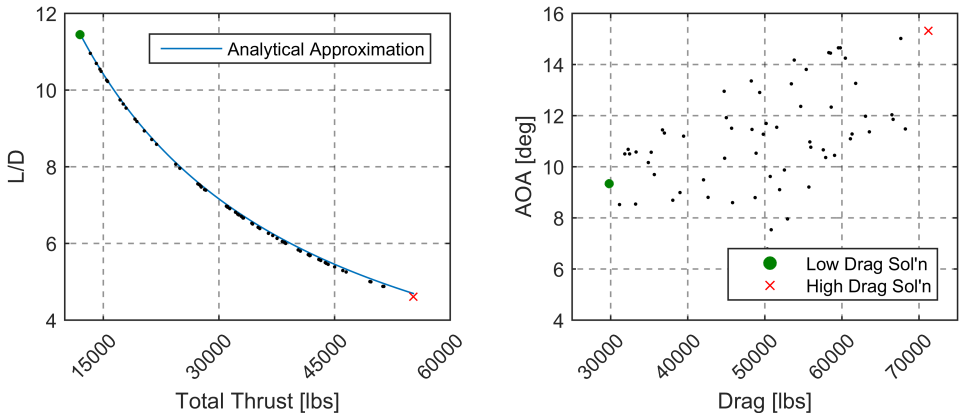

Figure 34: Symmetric approach trim solutions found by the conventional method.

In Figure 34 it can be observed that the trim solutions are evenly spread across a wide range of angles of attack, drag, and required thrust values. The highest drag solution seen in this set requires more than twice the thrust of the lowest drag solution. A nearly full throttle setting during approach cannot be justified, and therefore these solutions have excessive drag. These results support the prediction that there could be infinitely many trim solutions where there is sufficient control authority, and that the conventional objective function is not useful for distinguishing between them. Numerous randomly generated trials would have to be evaluated and post-processed in this example to know the limits of achievable drag and thrust.

The left hand plot within Figure 34 shows a strong correlation between L/D and total thrust. This can be explained by an inspection of a simplified rate of climb equation (Equation 27), which assumes steady (unaccelerated) climbing flight and the thrust line in the direction of flight. This can be rearranged to estimate an analytical relationship between L/D and thrust (Equation 28), which has good agreement with the observed data. It shows that for a given instantaneous thrust-to-weight ratio there is a corresponding L/D that must be achieved for the chosen climb angle.

$$\frac{R}{C} = V \sin\gamma = V\frac{T-D}{W} \tag{27}$$

$$L/D = \frac{1}{T/W - \sin\gamma} \tag{28}$$

The deflections for all of the converged trim solutions are visualized together in Figure 35. The elevon deflections are plotted from left wing to right, with negative deflections indicating trailing edge up positions. Every individual elevon has been completely saturated in at least one trim solution. The red solid line has the highest observed drag and saturates nearly every elevon simultaneously. The VORLAX aerodynamic model does not capture separation effects likely to be seen with such deflections, so this solution and others like it (a majority) should be discarded. The green dashed line achieved trimmed flight with the lowest observed drag of the set and more modest deflections. This trim solution shows that many of the others have unnecessary saturation of the controls, and avoiding this result was one of the requirements for the trim method.

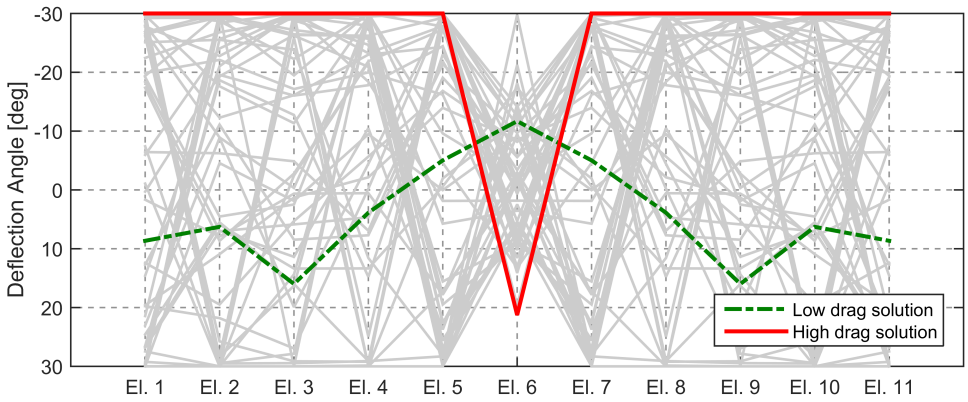

Figure 35: Symmetric approach trim deflections found by the conventional method.

4.4.3 Regularization Techniques

The predicted complications from control redundancy and the objective function treating all solutions equally have been confirmed. These results indicate that the conventional trim analysis method does not satisfy the requirements set at the start

of the chapter and is not well suited for configurations like the HWB with redundant multi-axis controls. There exist methods of modifying the optimization problem to achieve improved results. One approach that can potentially improve the convergence rate of the conventional method is to rescale the residual equations. The force equations have units of lbs, the moment equations have units of ft-lbs, and the navigation equations have units of ft/s and radians. The scales of these equations differ by orders of magnitude and can cause gradient methods to perform poorly. An alternative objective function below can be used to rescale the residual equations:

$$f(\mathbf{S}) = \varepsilon^T \mathbf{A} \varepsilon \tag{29}$$

where ε is a 9x1 vector of the residuals and $\mathbf{A}$ is a diagonal matrix. The diagonal elements, $A_{i,i}$, can be chosen to bring the residual equations within an order of magnitude of each other by dividing each residual by its initial value (Equation 30).

$$A_{i,i} = \frac{1}{\text{residual}_{i,0}} \tag{30}$$

The rescaling technique could help improve the rate of converged initial conditions but it will not resolve issues caused by redundancy. There will still be many solutions with wildly varying characteristics using this type of objective function. Ridge regression is another technique with similar looking objective functions for solving underdetermined linear systems. This type of objective function (Equation 31) introduces an additional term to try and improve solution characteristics, where λ is called the ridge parameter. For the trim problem one possible term $\mathbf{S}_d$ is a subset (just the deflection angles) of the state vector $\mathbf{S}$, which would have the effect of minimizing trim deflection magnitudes.

$$f(\mathbf{S}) = \varepsilon^T \mathbf{A} \varepsilon + \lambda \mathbf{S}_d^T \mathbf{S}_d \tag{31}$$

The issue with the objective function above is that a trim solution must by definition achieve zeroed residual equations simultaneously. If that is not accomplished then the trim optimization is a failure. If it is accomplished, then only the second term remains and the ridge parameter λ no longer serves a purpose. In addition, despite the appearance of the objective function the problem is not necessarily convex because the residual equations are nonlinear. New trim analysis experiments were run with the $\mathbf{S}_d^T\mathbf{S}_d$ objective function and they were found to consistently favor the centerbody elevon because its large control derivative required the smallest deflection angle to trim. The global optimum deflected the centerbody elevon exclusively, and was found for 85 of the 100 randomly generated initial conditions (Figure 36). Unfortunately, this elevon will also be a very strong driver of other metrics like drag and actuation power (the latter due to it having the largest hinge moment derivative). This dissertation will explore optimization of these metrics directly and in isolation. After methods for optimizing these metrics have been established, an interesting future avenue of research would be to develop cost functions that explored different weightings of power, drag, and other metrics of interest in an effort to find a favorable combination of these properties.

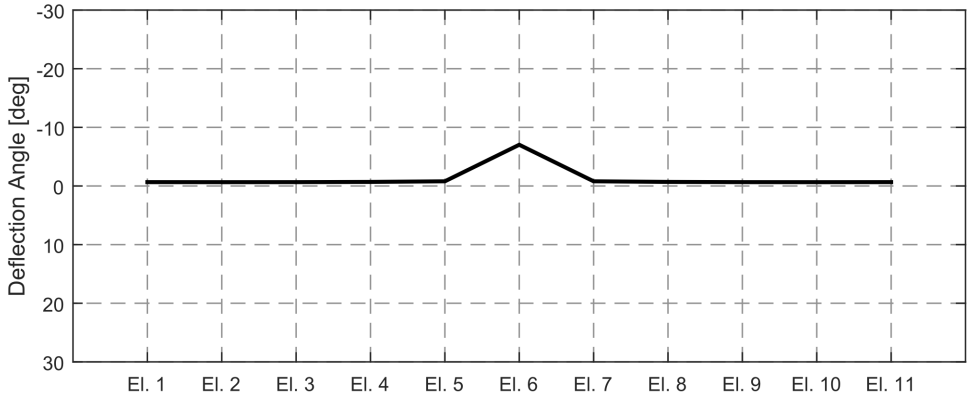

Figure 36: Symmetric approach trim deflections found by the conventional method with regularizing objective function.

4.5 Evaluation of Alternative Methods in an Approach Flight Condition

Several alternatives trim analysis methods are proposed to tackle the problems faced by the conventional method. The first alternative is to allow control allocation (CA) methods discovered during the initial literature review to choose the control surface deflections instead of the trim optimizer. This is meant to sidestep redundancy by reducing the number of variables and provide unique deflections for commanded moments. A primer on control allocation and a more focused literature review will be given, and a pair of representative methods will be chosen for evaluation. Other proposed trim analysis method alternatives are designed to utilize redundancy to minimize a secondary metric in addition to trimming the vehicle. Drag is an obvious metric to try to minimize and actuation system power is particularly relevant to the HWB configuration.

4.5.1 Control Allocation Methods

An alternative to the conventional method is to separate the control surface deflection state variables into a sub-optimization or sub-routine. This will allow the use of methods from the extensive control allocation literature. These methods are typically used in the context of a flight control system guiding vehicle motion over time. Several times a second the aircraft state is assessed, compared to the desired state, and a control law issues moment commands. When the set of controls are not uniquely associated with a given axis of rotation (e.g. aileron/elevator/rudder and roll/pitch/yaw), control allocation methods are used to map the control law moment commands to the set of redundant control surfaces. For control allocation methods, the aircraft state and control law moment commands are taken as fixed and the deflections are the degrees of freedom.

In this study the trim optimizer will choose an aircraft state and commanded

moments, then delegate the deflection positions to the control allocator. This process will iterate and the aircraft state, commanded moments, and control allocation chosen deflections will change simultaneously until the residual equations are satisfied (i.e. the vehicle is trimmed). The main appeal of this approach is that it will reduce the number of optimization variables by removing control deflections from the state vector and replacing them with fewer moment commands. The unique mapping between required moments and deflections may also reduce the number of local optima.

The control allocation problem can be defined as the need to optimally schedule, blend, or allocate the deflection of redundant control surfaces subject to constraints.[38, 17] The function f maps the deflection space $\mathbb{R}^N$ to moment space $\mathbb{R}^3$:

$$\mathbf{m}_{desired} = f(\mathbf{u}) \tag{32}$$

where $\mathbf{m}_{desired}$ is the desired moment vector and $\mathbf{u}$ is the vector of control deflection angles. If the moments are linear in the deflections, then the mapping function can be represented by a 3-by-N control effectiveness matrix, B.

$$\mathbf{m}_{desired} = B\mathbf{u} = \begin{bmatrix} \frac{\partial C_l}{\partial \delta_1} & \frac{\partial C_l}{\partial \delta_2} & \dots & \frac{\partial C_l}{\partial \delta_N} \\ \frac{\partial C_m}{\partial \delta_1} & \frac{\partial C_m}{\partial \delta_2} & \dots & \frac{\partial C_m}{\partial \delta_N} \\ \frac{\partial C_n}{\partial \delta_1} & \frac{\partial C_n}{\partial \delta_2} & \dots & \frac{\partial C_n}{\partial \delta_N} \end{bmatrix} \begin{pmatrix} \delta_1 \\ \delta_2 \\ \dots \\ \delta_N \end{pmatrix} \tag{33}$$

The control allocation problem is to define the inverse mapping, f^{-1}, from moment space to deflection space. A simple control allocation problem to solve is for an aileron-elevator-rudder arrangement that has a 3X3 full-rank B matrix, whose solution is a simple matrix inversion: $\mathbf{u} = B^{-1}\mathbf{m}_{desired}$. With redundant controls the B matrix will be neither square nor full rank. A linear algebra method for inverting non-square matrices called the Moore-Penrose pseudo-inverse can solve this problem and

is popular in the literature.[141] However, it sacrifices some of the available control authority and prevents the achievement of maximum moments in all directions.[101]

Techniques like ganging and daisy chaining are strategies for reducing the complexity of the CA problem. Oppenheimer et al. say that ganging is often used when it is obvious how to combine redundant controls.[101] At its simplest this method creates a square B matrix by grouping control surfaces together, one group for each axis. Goldthorpe et al. describe a more sophisticated ganging and axis prioritization arrangement used on the X-48B BWB aircraft.[54] Daisy chaining, which has been used previously in the HWB literature, divides control surfaces into several groups.[70, 63] As a moment demand increases the first group is deflected until saturated, at which point the next group is used.

The direct allocation method is based on the attainable moment subset (AMS) concept and with linear control derivatives is guaranteed to generate the maximum attainable moments in arbitrary directions.[36] An example AMS for the N2A-EXTE is shown in Figure 37. The intersection of the desired moment vector with the AMS surface identifies faces, edges, and vertices associated with known deflection combinations. A desired moment vector that intersects a face will be a linear combination of three of the deflection vectors that define that face. Linear programming formulations of direct allocation exist that avoid the need to generate the entire AMS at every FCS cycle.[106, 12] Should the moments be nonlinear functions of the control deflections, a piecewise linear programming approach can be used.[13]

The vortex-lattice aerodynamic model used in this study produces forces and moments that are linear functions of the control deflections. The direct allocation method is therefore an appropriate method and was used to demonstrate control allocation integrated trim optimization. A Matlab implementation was readily available in the Quadratic Programming Control Allocation Toolbox (QCAT) by Ola Härkegård.[64] This implementation solves the linear programming problem:

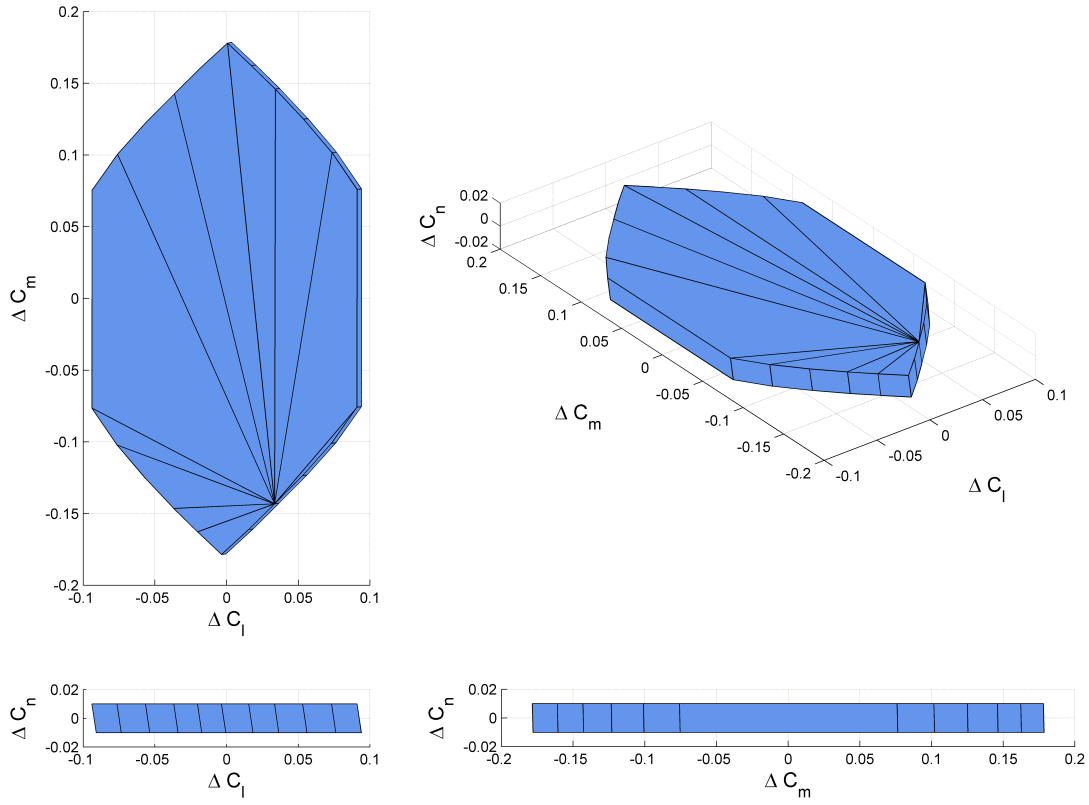

Figure 37: The attainable moment subset for the N2A-EXTE in the symmetric approach flight condition.

$$\begin{aligned} \max_{a,u} \quad & a \\ \text{subject to} \quad & \mathbf{Bu} = a\mathbf{v} \\ & \mathbf{u}_{min} \leq \mathbf{u} \leq \mathbf{u}_{max} \end{aligned}$$

where $\mathbf{v}$ is the 3x1 commanded moment vector, and $\mathbf{u}$ is the Nx1 deflection vector. If $a > 1$, set $\mathbf{u} = \mathbf{u}/a$.

The linking or ganging of elevons will also be explored using the conventional trim optimization method. This will reduce the number of independent variables, potentially resulting in unique solutions. This approach has been used by Boeing for early design phase control authority assessments, as well as on the operational X-48B.[16]

It is a simplification that sidesteps the redundancy issue, and any benefits or penalties that come as a consequence will be noted and compared to the other methods investigated in this chapter. The predictions made regarding the use of control allocation methods is formalized below:

Hypothesis: Integrating control allocation methods into the conventional trim optimization method will result in unique and repeatable trim solutions.

4.5.2 Conventional Method with Direct Allocation

4.5.2.1 Integrating the Direct Allocation Method

The trim optimizer interacts with this CA method by manipulating "desired moments from the controls" in the state vector instead of individual control deflection angles. The CA method then tries to achieve those moments, subject to available control authority defined by control derivatives and deflection limits. Figure 38 visualizes how the optimizer, equations of motion, and control allocator interact. Matlab's fgoalattain algorithm and the conventional objective function were used again to demonstrate the CA-integrated technique. The combined approach is referred to in this dissertation as the conventional method with direct allocation, or the direct allocation results for short.

The optimization statement remained unchanged with the exception of the modified state vector. For the symmetric approach flight condition the deflection angles were swapped for a single new variable controlling "demanded pitching moment" in the body axis system. As shown in Table 12, this reduced the number of free variables from nine to four. The moments that can be commanded are technically bounded by the attainable moment subset, which is a function of angle of attack and other state variables. The commanded moments of successfully converged solutions always had positive moment commands, so the lower bound can be set to zero. The upper bound can be chosen by testing all elevons trailing edge up for maximum nose-up moment,

plus a 20% margin.

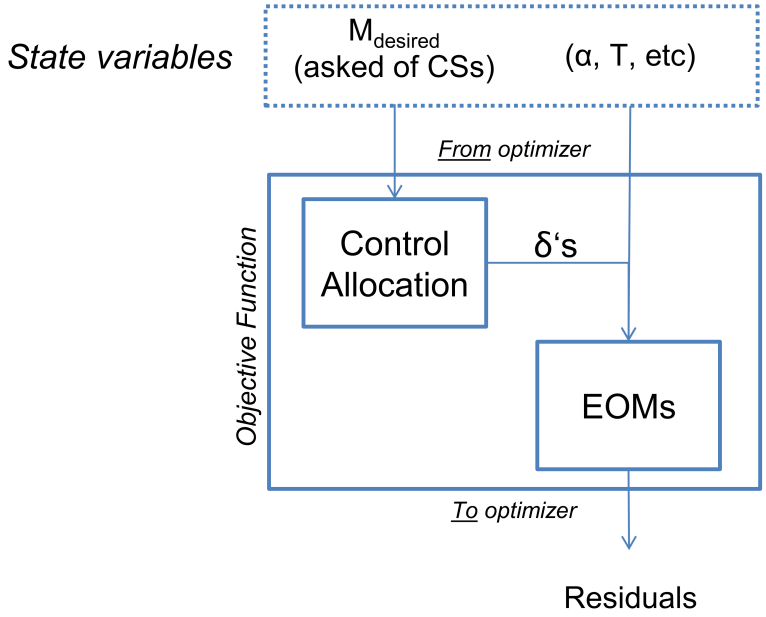

Figure 38: Integrating control allocation into the trim optimization process.

Table 12: Symmetric approach free variables for the conventional method with direct allocation.

	Variable	Min	Max	Units
1	α	5	20	degrees
2	θ (pitch angle)	2	17	degrees
3	$\left[M^B_{pitch}\right]_{des.}$	0	1.61e7	ft-lb
4	$T_{\text{per engine}}$	0	76,733	lbs

The B matrix is constructed from dimensional control derivatives in the body axes using a forward finite difference method. At each iteration the optimizer defines the state of the vehicle (e.g. α, β) and all control surfaces are in faired positions (zero degree deflections). Each control available to the direct allocation algorithm is then perturbed by one degree to generate the linear control derivatives.

4.5.2.2 Experimental Results and Observations

The conventional method with direct allocation was tested with 100 randomly generated initial conditions for variables 1,3, and 4 in Table 12. The second variable was

given an initial condition $\theta = \alpha + \gamma$. The method successfully converged 92% of the time, much better than the conventional method's 68%, and they all converged to identical trim solutions (Figure 39). As predicted by using direct allocation to reduce the number of variables in the search space gave the optimization problem a unique solution, which supports the hypothesis made earlier.

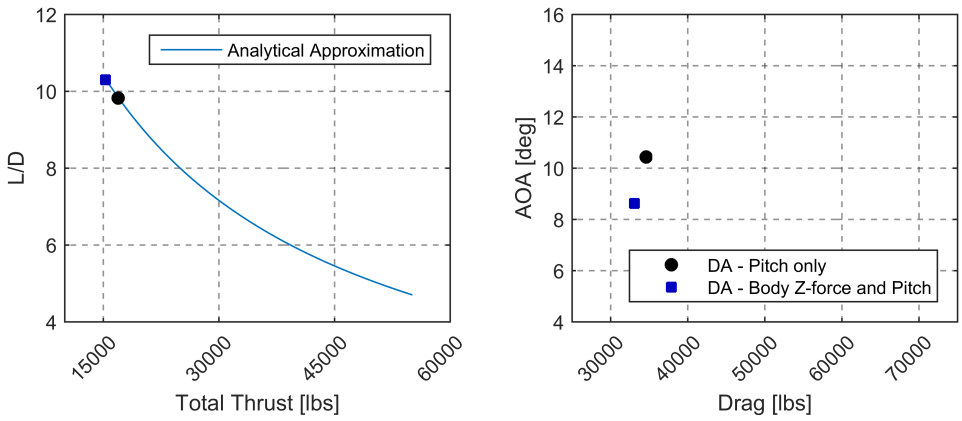

Figure 39: Symmetric approach trim solutions found by the conventional method with direct allocation.

The unique trim deflections discovered using direct allocation are an improvement over most of the previously discovered solutions because there is no unnecessary elevon saturation. As seen in Figure 40 these deflections are curiously uniform across the trailing edge. This can be explained in the following manner: The desired moment for the symmetric approach flight condition was a strictly nose-up command. That intersects the attainable moment subset surface at a point representing a set of deflections that has all elevons at -30 degrees. To achieve the desired moment magnitude, direct allocation scales this deflection linearly between all elevons at -30 and all 0 degrees. This behavior is equivalent to using the elevons as a large elevator. There is an excess of control authority for this flight condition so this "pseudo-elevator" needs only be deflected -3 degrees to trim the vehicle.

Something to consider is that on the HWB configuration the elevons do not influence the moments in isolation. For instance, a pitch up maneuver (trailing edge up

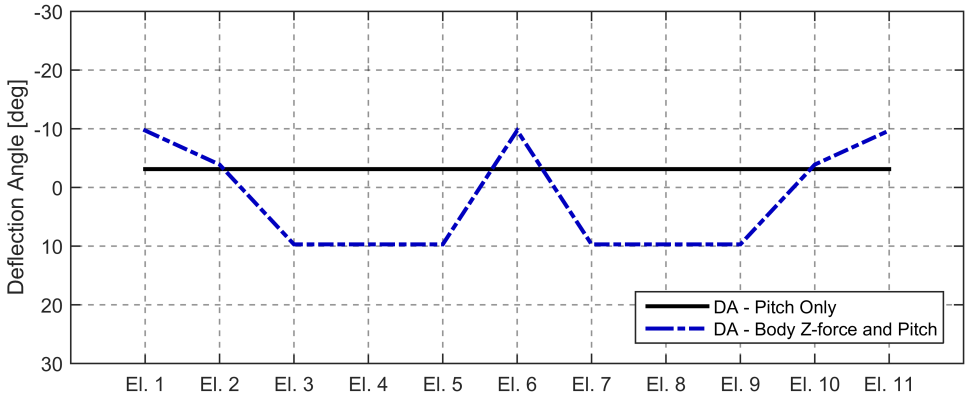

Figure 40: Symmetric approach trim deflections found by the conventional method with direct allocation.

deflections) will also result in a loss of lift. This has been referred to as a plunging behavior that results in an unwanted sagging of the flight path.[130] Direct allocation can be set up to avoid this problem by incorporating an additional "demanded lift" command. This plunging effect will not be present in steady state trim analyses investigated here, where forces are always balanced, but allowing the trim optimizer to command lift and pitching moment simultaneously may result in other interesting trim solutions.

For the next experiment, a desired body-axis Z-force (F_3^B) was added to the trim optimization state vector (Table 13), and an additional row of body Z-force derivatives were added to the B matrix. Early experiments indicated that successful trim solutions only commanded positive body Z-forces, which corresponds to decreased lift. The set of deflections that bounded the pitching moment (all elevons trailing edge up) was also used to determine the minimum body Z-force. Another 100 randomly generated initial conditions were run and all successfully converged to the same unique solution. The deflections are no longer uniform and now resemble the low drag deflections discovered with the conventional method but with smaller deflection magnitudes.

Table 13: Alternative symmetric approach free variables for fgoalattain and direct allocation.

	Variable	Min	Max	Units
1	α	5	20	degrees
2	θ (pitch angle)	2	17	degrees
3	$\left[M^B_{pitch}\right]_{des.}$	0	1.61e7	ft-lb
4	$\left[F^B_3\right]_{des.}$	0	6e5	lbs
5	$T_{\text{per engine}}$	0	76,733	lbs

4.5.2.3 Imposing a Throttle Constraint

The throttle settings for the direct allocation solutions are on the order of 10-11%. The flight idle throttle settings are likely to be higher than that in order to make it possible to reduce spool-up delays and comply with the steady gradient of climb requirements in FAR 25.119.[2] A sensitivity study was performed to observe how the trim solutions changed with increasing throttle equality constraints. This was done with direct allocation commanding both body Z-force and pitching moment. Drag cannot be commanded directly when making the large deflections necessary here, because a linear control derivative would poorly approximate the quadratic behavior. The body Z-force, on the other hand, is linear with deflection, and will give direct allocation the opportunity to influence lift-induced drag.

Throttle equality constraints were imposed at 11%, 15%, 20% and 30% with the assumption of a $T_{max,SL}$ of 76,733 lbs per engine. A very interesting trend can be seen in the deflections in Figure 41. To trim with increasing drag, the centerbody elevon deflects increasingly downward and the remaining elevons deflect increasingly upward. The elevons are therefore behaving similarly to clamshell elevons. This unexpected discovery could potentially be programmed into flight control systems as a simple way to control speed during approach. The angles of attack for these solutions can be observed in Figure 42. Compared to the conventional results or the minimum drag

[2]Mentors at NASA Langley Research Center recommended that flight idle throttle should be no lower than 20%.

results in the next section, these angles of attack are on the higher end of the solution space.

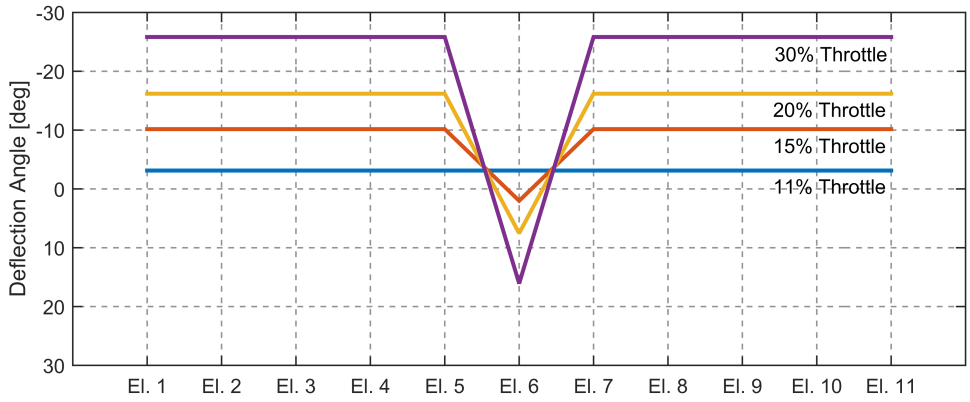

Figure 41: Sensitivity of the direct allocation deflections to the throttle constraint.

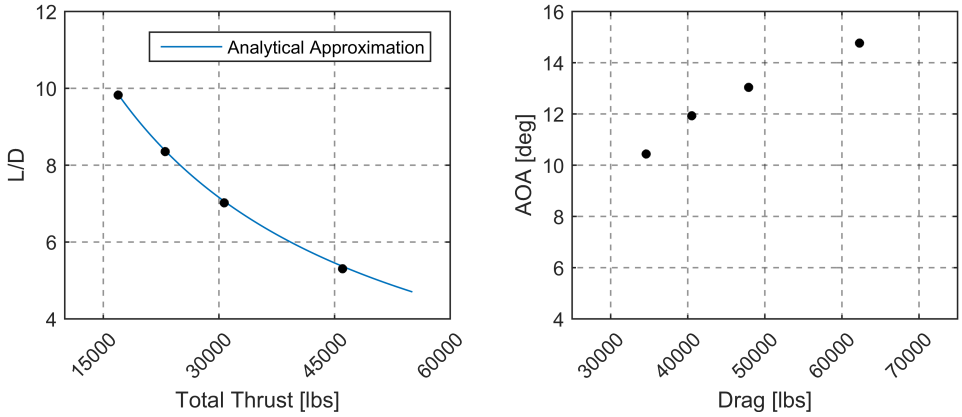

Figure 42: Throttle constrained direct allocation trim solutions.

4.5.3 Conventional Method with Ganging

A reduction of redundancy through ganging was also investigated as a way to achieve consistent and unique results. The ganging layout shown in Figure 43 was created based on control surface groupings that seemed natural. Others are possible but this will serve as the baseline ganging layout. The four most outboard elevons were each ganged together to act as "pseudo-ailerons." These pseudo-ailerons were operated as independent control surfaces. The centerbody elevon and the elevon pair just

outboard of it were also ganged together into a "pseudo-elevator." The rudders were linked to move together as before, but in this symmetric flight condition were not deflected. In total there are four independent controls, so the vehicle is still overactuated. Linking the pseudo-ailerons to move in opposite directions by default might prevent the vehicle from generating the additional drag needed to achieve a 20% throttle.

Table 14: Symmetric approach free variables for the conventional method with ganged elevons.

	Variable	Min	Max	Units
1	α	5	20	degrees
2	θ (pitch angle)	2	17	degrees
3	$\delta_{1,2,3,4}$ (symm. elevons)	-30	30	degrees
4	$\delta_{5,6}$ (symm. elevons)	-30	30	degrees
5	$T_{\text{per engine}}$	0	76,733	lbs

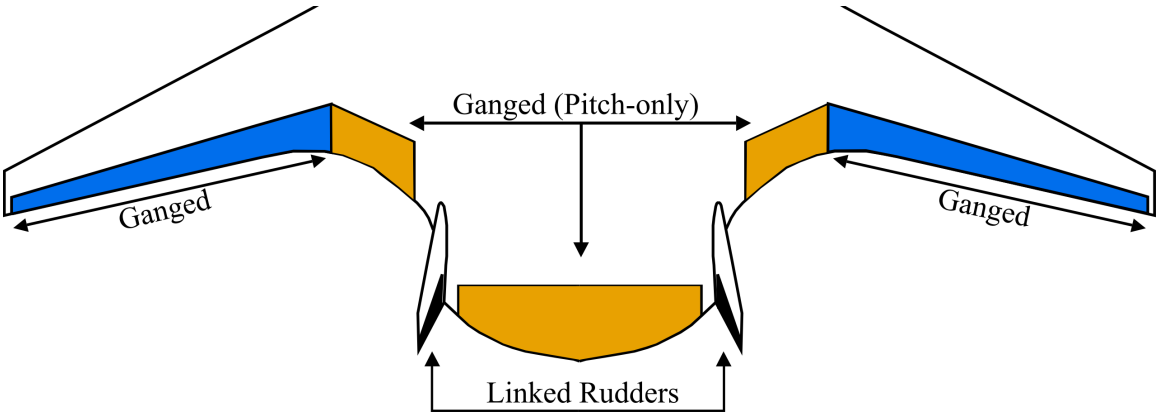

Figure 43: Ganged layout for reduced redundancy

The loss of control authority caused by ganging the controls together in this manner can be visualized with the attainable moment subset. Figure 44 compares the AMS for the original layout and the new ganged one. It shows that the maximum attainable pitching moments are unchanged, and that is because the pseudo-ailerons can still be used for that purpose. The pair of elevons ganged to the centerbody elevon

(5 & 7 in the original layout) can no longer be used to generate rolling moments, and this can be seen as a reduction in the maximum attainable rolling moment.

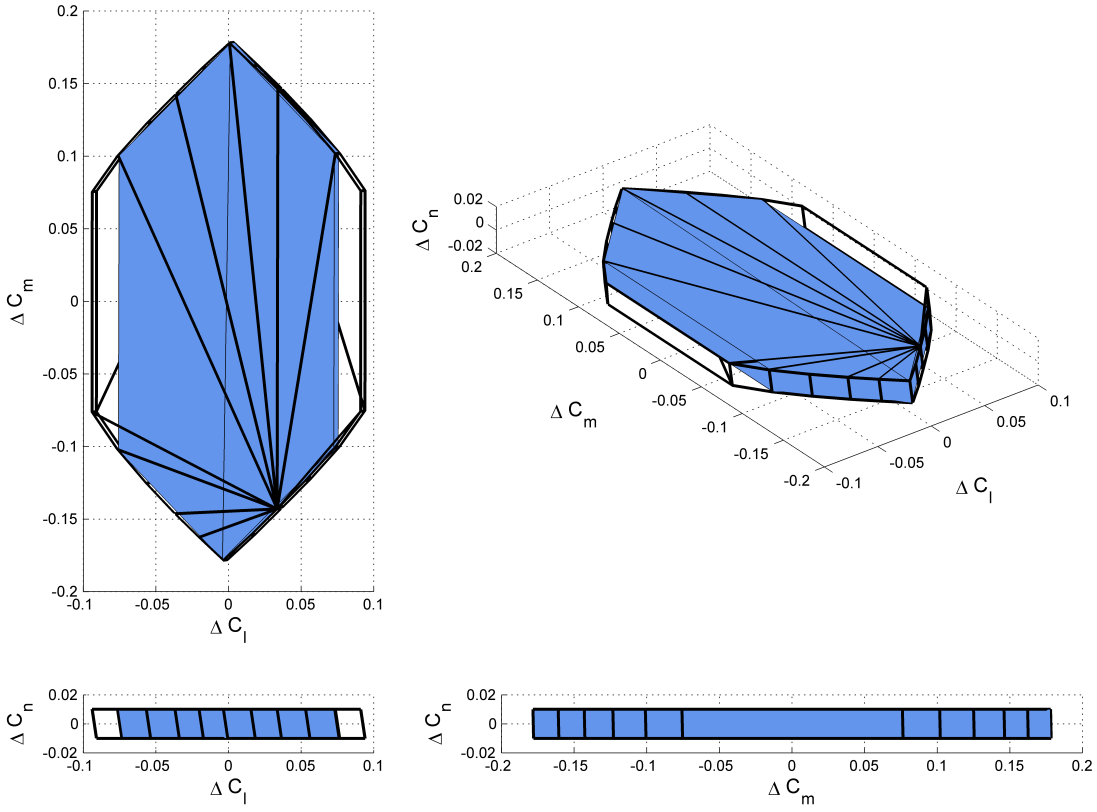

Figure 44: A comparison of attainable moment subsets for the original layout (black wire mesh) and the ganged layout (solid blue).

4.5.3.1 Experimental Results and Observations

A throttle sensitivity study was conducted for the conventional method with ganged elevons, and the results are shown in Figure 45. Overall they have a strong resemblence to the trim deflections from the direct allocation method (commanding pitch and lift). Three of the four throttle settings have unique solutions, but with a 15% throttle there were two solutions. The second solution for the 15% throttle (blue in the figure) does not follow the trend, instead occurring at a lower angle of attack as seen in Figure 46. It requires maximum trailing edge down deflection of the outer

wing elevons to generate sufficient lift, and is not a realistic solution due to the limitations of the VORLAX model. This type of solution is not possible at the higher throttle settings due to the elevon deflection limits, which means the other solutions are unique. The ganging method overall produces similar results as direct allocation in symmetric conditions but is much simpler to implement. The results show that whether conventional trim methods with control allocation integrated will have unique trim solutions depends on the particular control allocation method chosen, or that other factors (e.g., minimum throttle setting) will also be important.

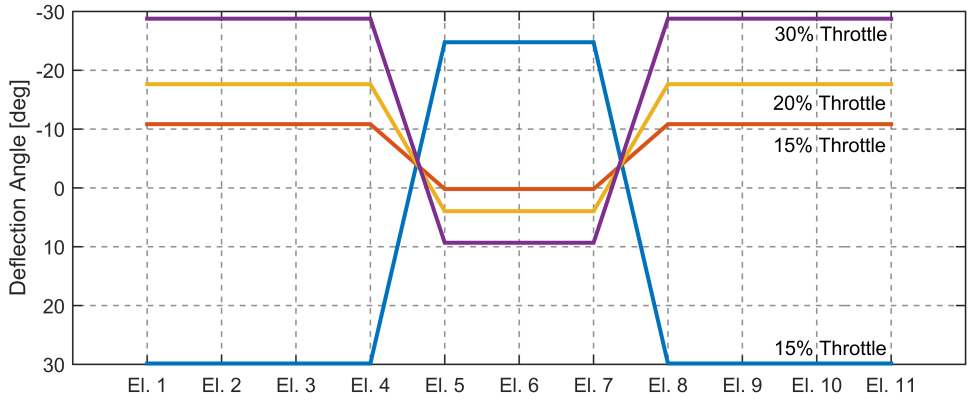

Figure 45: Sensitivity of ganged elevon trim deflections to the throttle constraint.

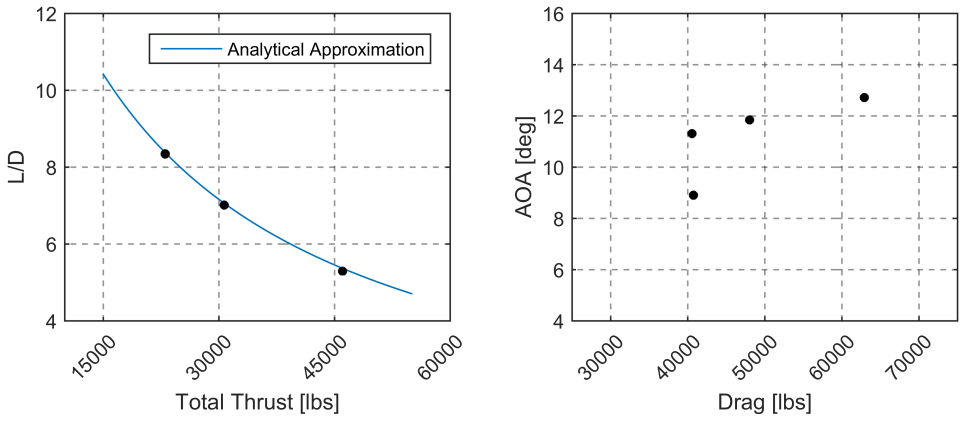

Figure 46: Throttle constrained ganged trim solutions.

4.5.4 Minimization of Secondary Metrics

The conventional method minimized the sum of squares of the residual equations. As a consequence optimization stopped at the first feasible solution whose qualities could vary widely. When integrated with direct allocation or simplified with ganging, the problem changed and there was typically only one feasible solution. The following two sections reformulate the trim optimization statement from root finding to minimization of secondary metric in order to take advantage of the control redundancy. For the solutions to be valid the residual equations must still be driven to zero simultaneously. This will be accomplished by imposing them as nine nonlinear equality constraints. The new trim optimization statement is shown below:

$$
\begin{array}{lll}
\underset{S}{\text{minimize}} & f(\mathbf{S}) & \\
\text{subject to} & S_i = a_i,\ i = 1, \ldots, l. & \text{Flight/Operating conditions} \\
& b_i \leq S_i \leq c_i,\ i = l+1, \ldots, m. & \text{State variable side constraints} \\
& residual_j = 0,\ j = 1, \ldots, 9 & \text{EOM residual constraints}
\end{array}
$$

4.5.5 Minimum Drag Trim Optimization

The minimum drag trim optimization method will optimize the function in Equation 34. The optimizer will be attempting to minimize the induced drag through a combination of angle of attack and elevon deflections. The same variables and ranges used for the conventional method were used in these experiments (Tables 10 and 11).

$$
f(\mathbf{S}) = \text{Drag}(\mathbf{S}) = \frac{1}{2}\rho V^2 S C_D\left(\alpha, \beta, \delta' s\right) \tag{34}
$$

4.5.5.1 Experimental Results and Observations

Matlab's fmincon was used to investigate this constrained nonlinear optimization problem, because the previous algorithm (fgoalattain) was set up for root finding and

multi-objective optimization problems only. Several algorithms available within fmincon were tested on this problem, each with 100 randomly generated initial conditions. The best solutions from each algorithm (SQP vs. Active-Set vs. Interior Point) were practically identical. The deciding factor was in how many initial conditions need to be tried in order to be confident that the global optimum solution had been found.

Minimizing drag with SQP and Interior-Point resulted in a spread of solutions similar to the conventional method, meaning that they were susceptible to local minima. The rates of successful convergence were 44% and 15%, respectively. Most of the trim solutions were not near the global minimum drag solution, and overall SQP and Interior-Point are not recommended for this problem.

With a 96% rate of successful convergence, Active-Set was the preferred fmincon algorithm. Of the converged solutions, the majority (84%) were within 1% of the global minimum drag which is shown as the green square in Figure 47. Based on this sample, just three random trials are sufficient to have a 99% chance of finding the global minimum drag solution shown in Figure 48. The lift distribution for this trim solution is shown in Figure 49, which also has for comparison an elliptical distribution with equivalent total C_L. The trim solution is obviously not elliptical, but has the least induced drag given the constraint of balanced pitching moments. It has a modest angle of attack with no saturated elevons and the solution can be consistently repeated making it essentially unique.

4.5.5.2 Sensitivity of the Results to a Throttle Constraint

The minimum drag trim solution had a unique set of deflections but a throttle setting of 7.6%, which is also lower than the expected flight idle settings. Sensitivity to the throttle constraint was again investigated as a series of thrust equality constraints. One hundred randomly generated initial conditions were run for throttles of 10% to 30%, in 5% increments. The control surface layout would need the addition of speed

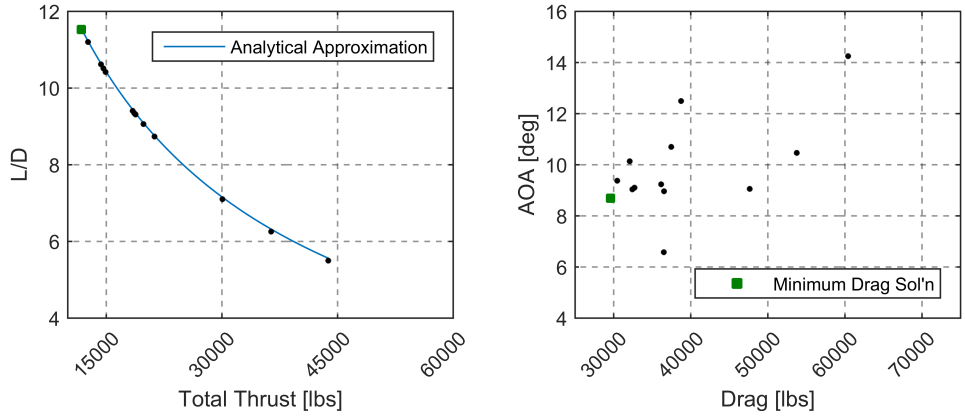

Figure 47: Symmetric approach trim solutions for minimum drag with fmincon and Active-Set algorithm.

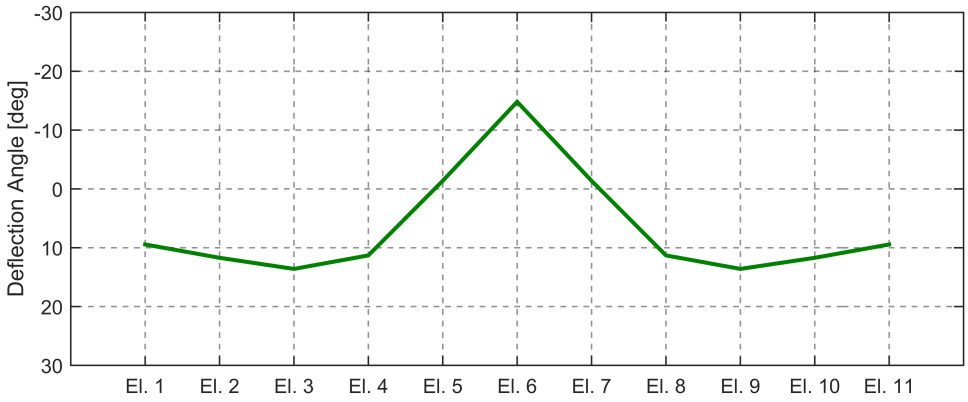

Figure 48: Global minimum drag trim deflections.

brakes if greater throttle settings than about 36% are desired.

The successfully converged trim solutions are visualized in Figure 50, which shows that the throttle constrained solutions exist at a wide range of angles of attack. The introduction of the throttle constraint has resulted in nonunique solutions, many of which have one or more pairs of saturated elevons. The throttle constrained direct allocation solutions prove that this saturation is unnecessary. Each band of points in the right half of the figure corresponds to solutions with identical L/D and throttle settings. At the highest throttle settings, trim solutions were only available at higher angles of attack. The ultimate take-away is that under minimum throttle constraints,

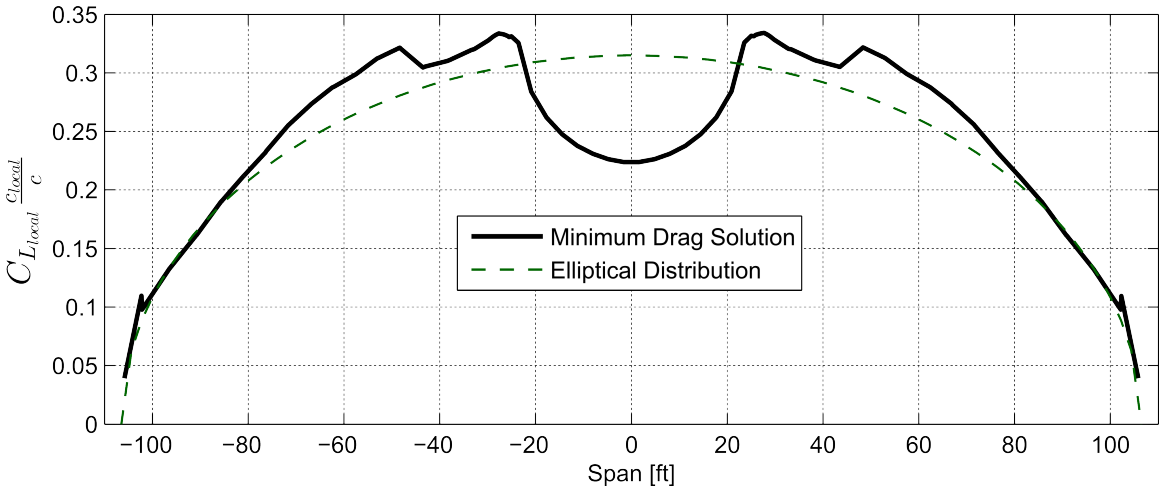

Figure 49: The lift distribution of the global minimum drag trim solution.

drag is not a useful objective function to minimize.

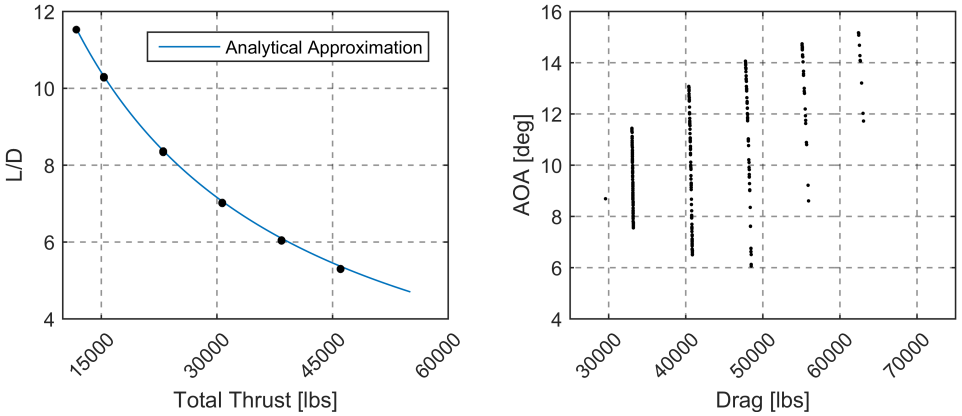

Figure 50: Sensitivity of minimum drag trim solutions to throttle constraints.

4.5.6 Minimum Power Trim Optimization

This section investigates the possibility of taking advantage of control redundancy to minimize actuation subsystem power requirements. The challenge in this comes from the level of effort, disciplinary expertise, and design knowledge needed to evaluate power directly. A metric based on the control surface hinge moments is developed in the next section and argued that it is a good stand-in for steady state power under certain assumptions.

Lessons learned from the previous optimization methods are employed here and a 20% throttle is imposed from the start. Otherwise, the state variables and their ranges match those in the conventional method and minimum drag (Tables 10 and 11).

4.5.6.1 Development of an Actuation Power Metric

Excessive actuation power requirements have been noted several times in the literature for the HWB configuration.[77, 113, 16] They are driven by hinge moments and deflection rates, both of which are expected to be large for this configuration. HWB elevons have shorter moment arms as they are closer to the aircraft center of gravity (CG) than elevators are on conventional aft-tail configurations.[132] Therefore in order to obtain sufficient pitch control authority a large total elevon planform area is required, and in most concepts the elevons span the entire trailing edge. Following the "square-cube law", as the control surface area increases proportional to the square of the vehicle scale ($\propto [L]^2$), the actuation load rises rapidly proportional to the cube of that scale ($\propto [L]^3$).[113] At the other extreme of the load-speed envelope, the potentially lower static margins of HWB designs may require control surface rates considerably higher than those found in automatic flight control systems of conventional aft-tail designs ($\approx$ 60 deg/s), with rates of 100 deg/s considered in some works.[23, 147, 47]

The convention for actuation of control surfaces in commercial transport aircraft has been to use a centralized hydraulic system. Replacing the hydraulic system with electric actuators has been an active field of research with the potential for weight savings.[40, 133, 93, 65] The weight savings (over a triple redundant hydraulic system) coupled with the quickly improving power-to-weight ratio of electric actuator technologies and Boeing's projected use of the technology are sufficient reasons to reasonably expect their use in HWB vehicles.[43, 16]

The actuation subsystem power requirements for electric actuators are known to

be driven primarily by high hinge moments, rather than deflection rates.[42, 65, 21] Electric actuators must be powered at all times to maintain a control surface in place against a steady state hinge moment. Therefore trim deflections with reduced hinge moments will also result in reduced power requirements. The advantage of evaluating hinge moments as a stand-in for power is the availability of this information from simple aerodynamic analyses, which can be performed during the early stages of the design process. Evaluating actuation power directly requires significantly more effort and disciplinary expertise.[42]

A metric based on hinge moments, named H_{sum} in Equation 35, is proposed for use in selecting trim solutions with low steady state actuation power requirements. A similar metric has been used in other HWB studies to select deflections for a 2.5g pull-up maneuver.[52] It aggregates hinge moments from the full set of elevons into a single metric:

$$H_{sum} = \sum_{i=1}^{11} |H_i| = \sum_{i=1}^{11} \frac{1}{2} \rho V^2 S \bar{c} |C_{h_i}| \tag{35}$$

where H_i is the dimensional hinge moment, S is gross planform area, and $\bar{c}$ is the mean aerodynamic chord (MAC). Hinge moments were calculated from the C_p distribution by converting VORLAX panel C_p values to normal forces, multiplying by the panel centroid's orthogonal distance from the hinge line, and summing the individual panel contributions. These were non-dimensionalized by the vehicle reference area (gross planform) and vehicle reference length (MAC). It should be noted that Equation 35 is non-differentiable and may cause gradient optimizers to perform poorly. This will be discussed in further detail in Section 4.5.6.4.

4.5.6.2 Aerodynamic Hinge Moment Model

Surrogate models of the aerodynamic hinge moments were generated for rapid assessment of the hinge moment metric during trim optimization. A data set was generated using a face-centered central composite design augmented by a 300 case Latin hypercube design for seven design variables (angle of attack and symmetric elevon deflections). A 2nd order response surface equation provided an excellent fit to the data, and is usable as a one-to-one replacement for VORLAX in this study.

The statistical analysis program JMP was used to generate the surrogate models and it provided Pareto plots for each response (Figure 51). This analysis ranks the input parameters in terms of how much of the variability of the response they explain within the ranges tested. The surrogates reveal that elevon deflection angle has the strongest influence over the hinge moment, typically followed by angle of attack. What is interesting is that adjacent elevons affect the hinge moment at comparable levels to angle of attack. The Pareto principle states that in many situations, 80% of the variation in a response can be explained just 20% of the input factors.[71] This is roughly observed here with AOA, elevon 1, elevon 2, and elevon 3 explaining 80% of the variation in elevon 2 hinge moment. Only the hinge moment for elevon 6 did not show any significant influence from adjacent elevons.

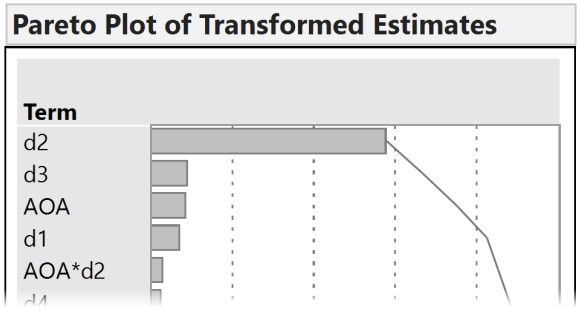

Figure 51: Pareto plot for elevon 2 hinge moment.

These models do not include hinge moments caused by gravity which is expected to be small, and roughly constant for modest deflections. It can be neglected since

constant terms in an objective function will not affect the location of optimal solutions. Hinge moment contributions from elevon inertia can be neglected as well, since these are steady state trim solutions. Effects due to sideslip were also found to be negligible and are not included in the crosswind approach experiments of Section 4.6.4, which allows models for left wing elevons to be used on the right wing as well. The VORLAX code from which the hinge moment models are generated does not take into account separation effects at high deflections. This would change the pressure distribution downstream of the hinge, resulting in higher hinge moments than are currently predicted. A more accurate hinge moment model would likely result in smaller elevon deflection magnitudes than those presented here.

The modified trim optimization statement is shown below:

$$
\begin{aligned}
\underset{S}{\text{minimize}} \quad & H_{sum}(\mathbf{S}) & \\
\text{subject to} \quad & S_i = a_i,\ i = 1, \ldots, l. & \text{Flight/Operating conditions} \\
& b_i \leq S_i \leq c_i,\ i = l+1, \ldots, m. & \text{State variable side constraints} \\
& residual_j = 0,\ j = 1, \ldots, 9 & \text{EOM residual constraints}
\end{aligned}
$$

4.5.6.3 Experimental Results and Observations

Matlab's fmincon with the Active-Set algorithm was used to perform this optimization, based on past success in minimizing the drag objective function. A set of 500 randomly generated initial conditions were run and the 329 (66%) that converged are shown in Figure 52(a). A clear Pareto frontier is visible between H_{sum} and angle of attack, with a global optimum near 10.5 degrees. Very few of the converged solutions (just 13) were within 5% of the minimum H_{sum} solution. However, if an increase in H_{sum} of roughly 15% above the minimum can be tolerated, a flat region or "bucket" exists across several angles of attack.

Similarly to the conventional method and minimum drag results under throttle constraints, many of the trim solutions still saturate or nearly saturate one or more

pairs of elevons. In an effort to avoid stall or separated flow, another 500 randomly generated initial conditions were run with reduced elevon deflection ranges ($\pm 20°$ vs. $\pm 30°$). These results are shown adjacent to the full deflection range results in Figure 52(b). It had the effect of increasing the minimum H_{sum} angle of attack slightly, as well as increasing the minimum H_{sum} value by about 23%. For comparison, the direct allocation trim solution with 20% throttle had an H_{sum} about 82% higher.

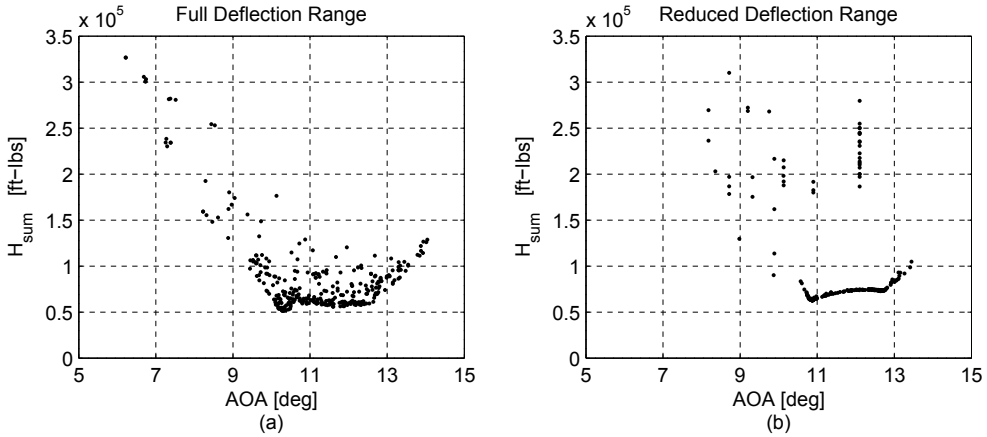

Figure 52: H_{sum} vs. AOA for (a) full deflections allowed and (b) reduced deflections.

The minimum H_{sum} solutions from the full and reduced deflection optimizations are shown in Figure 53. They are very similar to one another, and both are able to trim the vehicle with enough drag to meet the throttle constraint and simultaneously keep the steady state power requirements low. There is only a small penalty to H_{sum} and small changes to the trim solution when reduced elevon deflections are imposed. An important feature of these solutions is that the centerbody elevon (with the largest hinge moments) is hardly deflected at all.

An inspection of the individual hinge moments reveals why these deflections minimize the H_{sum} metric. The dimensional hinge moments are plotted against elevon deflection angles in Figure 54. These deflection sweeps are conducted for each elevon in isolation with the remaining elevons held fixed in their trim position. These figures indicate that primarily elevon pair 5/7 are powered and the others are free floating.

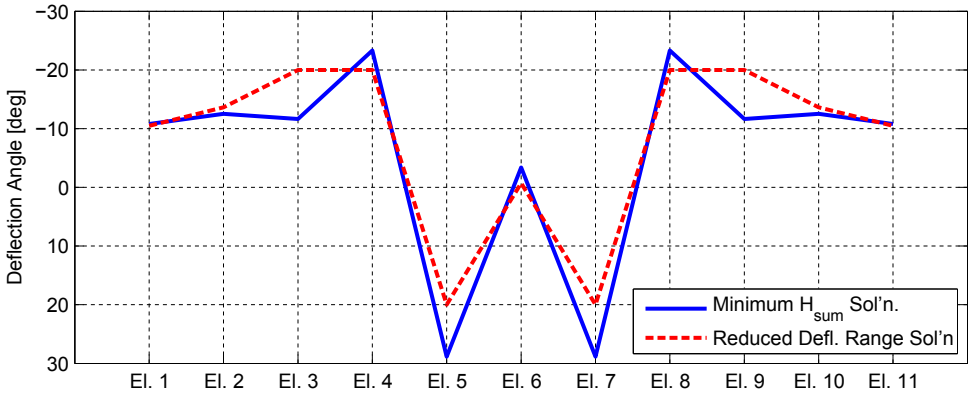

Figure 53: Minimum H_{sum} deflections.

One drawback to this solution is that elevon pair 5/7, the elevons just outboard of the centerbody elevon, are fully saturated. Their extremely large deflection angles would likely cause separation, making the aerodynamic and hinge moment model inaccurate. The hinge moments were also inspected for the reduced deflection range trim solution that minimized H_{sum}, and the primary difference was that fewer elevons were free floating. The compromise is that flow separation may be avoided at the cost of slight deflections away from the minimum hinge moment positions.

Overall, the variability of the trim solution using the minimum power method makes it a poor match for HWB MDO. Given enough trials of the trim analysis the minimum power solutions can be found, but this comes at the expense of time and computational resources. This trim optimization method is better suited for detailed analysis of vehicles. Additional scenarios were investigated, such as using the centerbody elevon as a trim-only device. These studies produced useful insights regarding control surface layout decisions and are available in Appendix B and have been published at AIAA SciTech 2015.[44]

4.5.6.4 Techniques for Minimizing Non-Differentiable Objective Functions

The $Hsum$ metric was non-differentiable due to the absolute value function within it (an L_1-norm). Gradient methods are designed to minimize twice continuously

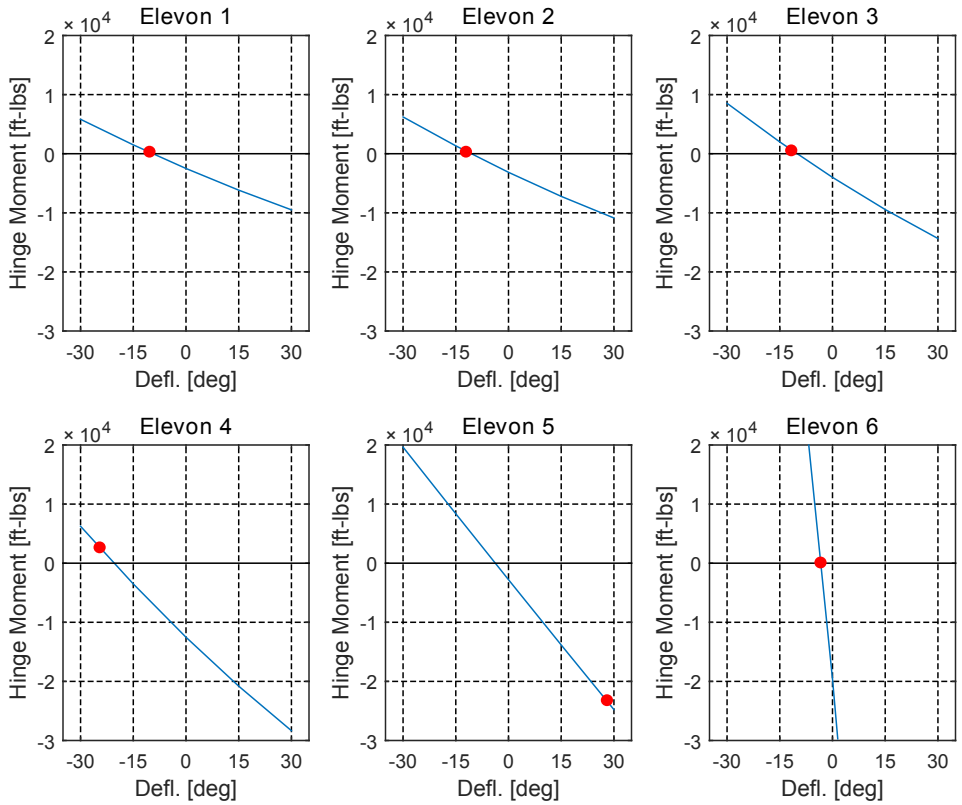

Figure 54: Hinge moment plots for each elevon indicate that many are free floating.

differentiable functions, and therefore it is no surprise that they were not very effective at minimizing H_{sum}. Global search algorithms or pattern search methods are generally recommended for this type of objective function, but have difficulty meeting the nonlinear constraints (i.e. the residual equations and throttle constraint) and can take a long time to evaluate.

Smoothing functions are differentiable approximations that can be substituted for H_{sum} and potentially improve optimizer performance. Several such approximations exist for the L_1-norm such as Equations 36-38.[69, 109] As the smoothing parameter μ approaches zero the smoothing function more closely approximates H_{sum}. New optimization experiments were conducted for each smoothing function and with several values of μ. None were found to improve the ability of gradient optimizers to find the global minimum power solution. Finally the L_2-norm of the hinge moment

vector, which is differentiable, was also tried but failed to improve convergence rates or the optimizer's ability to find a global minimum solution. The issue preventing better optimizer performance is likely the nonlinear 20% throttle constraint and the nonlinear residual constraints.

$$\widetilde{H_{sum}}(x) = \sum_{i=1}^{11} s_i\left(x,\mu\right) = \sum_{i=1}^{11} \mu \log\left[\exp\left(\frac{H_i(x)}{\mu}\right) + \exp\left(-\frac{H_i(x)}{\mu}\right)\right] \tag{36}$$

$$\widetilde{H_{sum}}(x) = \sum_{i=1}^{11} s_i\left(x,\mu\right) = \sum_{i=1}^{11} \sqrt{H_i(x)^2 + \mu} \tag{37}$$

$$\widetilde{H_{sum}}(x) = \sum_{i=1}^{11} s_i\left(x,\mu\right) = \sum_{i=1}^{11} \frac{H_i(x)^2}{\sqrt{H_i(x)^2 + \mu}} \tag{38}$$

4.5.7 Summary

The four trim analysis methods produced a variety of solutions for the symmetric approach flight condition. The 20% throttle constraint made finding unique solutions more of a challenge for some, however. The direct allocation method commanding body Z-force and pitching moment resulted in a unique and consistent solution. Using ganged elevons with the conventional method is simpler to implement and resulted in similar unique deflections. The minimum drag method reliably produced a unique globally minimum drag solution when there was no throttle constraint, but nonunique solutions with unnecessary control saturation under a 20% throttle constraint. The minimum power method was plagued by local optima despite attempts to employ smoothing functions and would require an excessive number of cases to find the global minimum power trim solution. In the next section, these methods will be tested on a crosswind landing approach flight condition.

4.6 Evaluation of Alternative Methods in a Crosswind Approach Flight Condition

A crosswind approach flight condition was also investigated as a stress-case for the proposed alternative trim analysis methods. A crosswind magnitude of 35 knots was suggested by Boeing as a sizing condition for HWB control surfaces.[16] This crosswind magnitude exceeds that required by FAR 25.237, but is in line with demonstrated crosswind capability for modern commercial transports.[137] Trim solutions at this crosswind magnitude (if they exist for the N2A-EXTE) should be close to the limits of control authority. The sensitivity of the trim solutions to crosswind magnitude will be investigated for each of the analysis methods.

The orientation of the relevant axis systems, Euler angles, and velocity components are depicted in Figure 55. The MASCOT Earth frame x-axis points in the west direction, the y-axis points north, and the z-axis points down. The desired velocity vector is defined relative to the vehicle carried Earth frame by Euler angles σ and γ. The angle σ, the target course angle, is the first rotation about z_E, and is set at 90 degree (north). The angle γ, the target angle of climb, is the second rotation about the intermediate frame's y-axis (which in this case points east) and is set to -3 degrees for a standard approach. The crosswind velocity is defined to be westward, perpendicular to the desired direction of travel. The vehicle Euler angles ψ, θ, ϕ (3-2-1) define the body axis system relative to the vehicle carried Earth frame. The vehicle will not be flown crabbed into the crosswind so the Euler angle ψ is also required to be 90 degrees, and results in a constant positive sideslip. This orientation will require positive (trailing edge left) rudder deflections and a positive roll (right wing down). The roll angle during this crosswind approach flight condition was required to be less than 5 degrees. The set of fixed state variables that define this flight condition are collected in Table 15. The Euler angle ψ required a little "wiggle" room to enable convergence, so it is given a margin of half a degree in either direction. The other

free variables available to the trim optimizer depend on the trim method at hand.

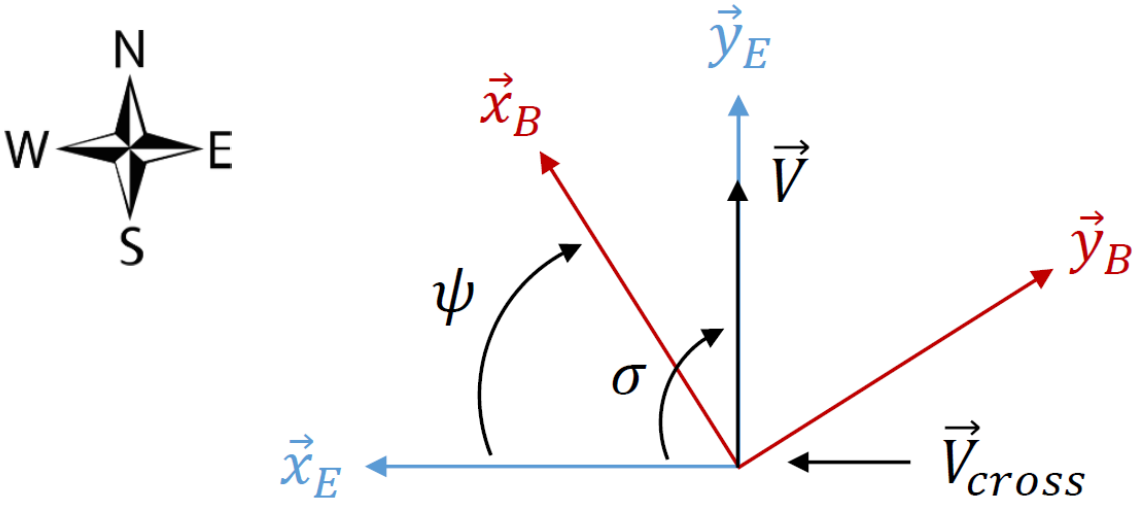

Figure 55: Orientation of vehicle carried Earth frame and body frame in crosswind conditions.

Table 15: Crosswind approach fixed variables.

	Variable	Value	Units
1	V_{app}	$1.3V_{stall}$	
		0.23	Mach
		153.7	knots
2	γ (climb angle)	-3	degrees
3	V_{cross}	various up to 35	knots
4	β	$\arctan\left(\frac{V_{cross}}{V_{app}}\right)\frac{180}{\pi}$	degrees
5	Altitude	0	ft
6	Weight	343,660	lbs
7	Fwd CG	36.1	% MAC
8	$\delta_{LEdroop}$	30	degrees
9	$T_{\text{per engine}}$	15,347 (20%)	lbs

4.6.1 Conventional Method with Direct Allocation

These experiments were again performed with fgoalattain, the sum of squares residual objective function, and direct allocation choosing the deflections. The body Z-force and all three moments are commanded by the trim optimizer in lieu of the 11 elevons and two rudders. Rudders are operated together and the resulting 4x12 B matrix

is constructed the same way as described in Section 4.5.2.1. The full list of free variables and their ranges is shown in Table 16. Due to the low throttle settings seen in the symmetric approach condition, throttle was fixed at a more reasonable 20%. The number of variables that the trim optimizer must control has grown from five in symmetric conditions to eight despite fixing the throttle constraint. Again, the variable θ has an algebraic relationship with angle of attack and sideslip, but MASCOT does not allow this type of constraint.

The bounds for the commanded forces and moments were established in part by inspecting successful trim solutions (originally run with unbounded commands). One side of the ranges could be bounded at zero based on the sign of the feasible commands and physics of the problem. The commands of the converged solutions had positive body Z-force, rolling moment, and pitching moment. The body yawing moment required to trim is negative. The other side of the bounds were determined from a set of maneuver deflections. The largest positive (nose-up) moment and positive Z-force (z-axis points downward) are achieved when all elevons are deflected -30 degrees trailing edge up. The largest positive rolling moment is achieved with all left wing elevons +30 degrees trailing edge down, right wing elevons -30 degrees trailing edge up, and with positive rudder deflections trailing edge left. The most negative yawing moment was approximated with both rudders +30 degrees trailing edge left. These deflections were commanded for a grid of α's and β's, and the largest observed change from the undeflected state plus a margin of 20% were used as the other bounds for commandable forces and moments.

Additional experiments were conducted regarding the initial conditions for the commanded forces and moments. At first the commands were always initialized at zero, and the rate of successful convergence was tolerable. Next, random values within the new bounds were tried, but this resulted in far fewer successful trials. The third and best option was to calculate the residual forces and moments for the given initial

Table 16: Crosswind approach free variables for the conventional method with direct allocation.

	Variable	Min	Max	Units
1	α	5	20	degrees
2	$\left[M^B_{roll}\right]_{des.}$	0	2.06e7	ft-lbs
3	$\left[M^B_{pitch}\right]_{des.}$	0	1.61e7	ft-lbs
4	$\left[M^B_{yaw}\right]_{des.}$	-2.06e6	0	ft-lbs
5	$\left[F^B_3\right]_{des.}$	0	6.01e5	lbs
6	ψ (heading)	89.5	90.5	degrees
7	θ (pitch angle)	2	17	degrees
8	ϕ (roll)	0	5	degrees

condition. Setting the initial commanded force and moments to the opposite of these residuals resulted in the highest rates of convergence. The results using this method of initializing the commanded forces and moments are shown in this section.

One hundred randomly generated initial conditions (force/moment commands initialized with the residuals) were run for each crosswind magnitude under the 20% throttle equality constraint, and their rates of successful convergence are shown in Table 17. This is a fairly steep drop in convergence rates from the symmetric condition, but all successfully converged trim solutions are identical for each level of crosswind (Figure 56). Therefore, despite the low convergence rates the trim optimization need only be repeated until the first feasible solution is found.

Table 17: Direct allocation method results for crosswind approach under 20% throttle constraint.

Crosswind Mag.	Successful Conv. Rate
11.7 kts	35%
23.3 kts	45%
35 kts	24%

The force and moments commanded by the trim optimizer as a function of crosswind magnitude are shown in Figure 57. The yawing moment demanded from the controls changes linearly and by the full 35 knot crosswind is nearly at the lower limit allowed in Table 16. The rudder deflections commanded by direct allocation

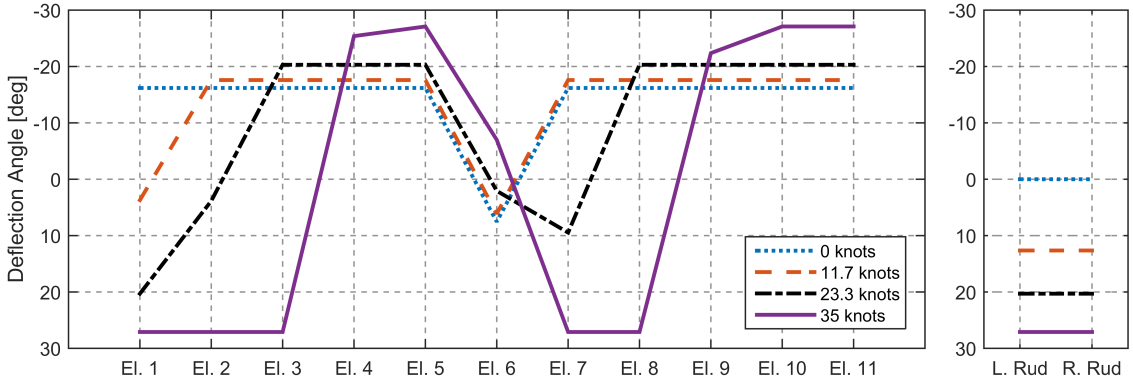

Figure 56: Direct allocation deflections in crosswind approach conditions.

are consequently also near their limits. This flight condition is therefore useful as a vertical tail and rudder sizing condition. The body Z-force, rolling moment, and pitching moment commanded by the trim optimizer are not near their limits. The roll angle, ϕ, is plotted as a function of crosswind in Figure 58 and is well within the five degree limit.

4.6.2 Conventional Method with Ganging

The free variables used for optimization with ganged elevons in crosswind conditions are shown in Table 18. The large pseudo-ailerons are independent of each other and the rudders are linked. One hundred randomly generated initial conditions were run for each crosswind magnitude, using the fgoalattain algorithm and conventional objective function. The results were not as good as the direct allocation method, due to lower rates of convergence (Table 19) and loss of control authority caused by ganging. No trim solutions were found at the full 35 knot crosswind.

The solutions that did converge are unique and are shown in Figure 59. The trends for α, β, and ϕ (Figure 60) are the same as the direct allocation solutions. None of the elevons are close to being saturated in any of the solutions. The limiting factor for the ganged layout is the rudder control authority, which becomes saturated prior to the full crosswind magnitude. The other trim optimization methods were

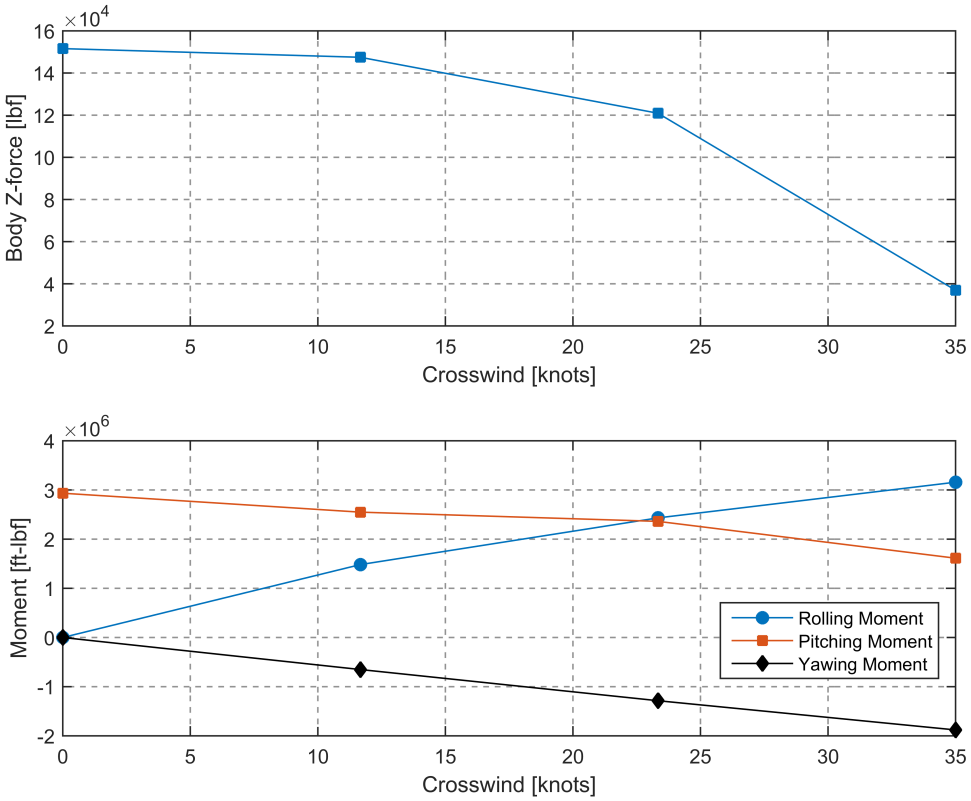

Figure 57: Direct allocation commanded forces and moments as a function of crosswind magnitude.

able to use the elevons to generate asymmetric drag to augment the rudders, but this was an unintended utilization of the elevons. The loss of yawing moment control authority caused by ganging the control surfaces was enough to prevent convergence at full crosswind. The consequence for design is that any HWB whose controls are sized with this trim analysis method will need a larger vertical tail. This is formalized below, and experiments in Chapter 9 will be performed to test the hypothesis:

Hypothesis: The reduction in control authority caused by simplifying the redundancy with elevon ganging will cause over-sized tails and increased TOGW during HWB MDO.

The moments achievable by the vehicle as well as the moments necessary to trim are changing as the crosswind magnitude increases. These changes can be observed

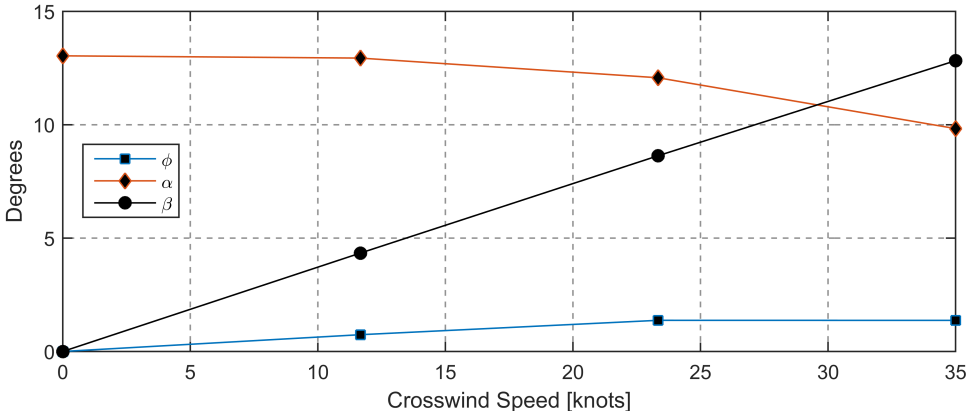

Figure 58: Angle of attack, sideslip, and roll angle for the direct allocation solutions in crosswind approach conditions.

Table 18: Crosswind approach free variables for the conventional method with ganged elevons.

	Variable	Min	Max	Units
1	α	5	20	degrees
2	$\delta_{1,2,3,4}$	-30	30	degrees
3	$\delta_{5,6,7}$	-30	30	degrees
4	$\delta_{8,9,10,11}$	-30	30	degrees
5	δ_{rud}	-30	30	degrees
6	ψ (heading)	89.5	90.5	degrees
7	θ (pitch angle)	2	17	degrees
8	ϕ (roll)	0	5	degrees

in Figures 61 and 62. The bounds in Figure 61 show that the tradeoff between rolling and pitching moments becomes skewed as the crosswind magnitude increases. The black arrow depicts the moment vector required to trim the vehicle, which is calculated based on the converged trim solution. The red dashed line, which depicts the available moments, extends along the same direction until intersecting the AMS surface. The ratio of the L_2-norms of those two vectors defines the AMS Margin. When there is sufficient control authority, the red line is always longer than the black one.

The AMS Margin for the 23.3 knot crosswind is only around 5%, meaning the available control authority is nearly exhausted. Neither pitching moment nor rolling

Table 19: Ganged method results for crosswind approach under 20% throttle constraint.

Crosswind Mag.	Successful Conv. Rate
11.7 kts	44%
23.3 kts	25%
35 kts	0%

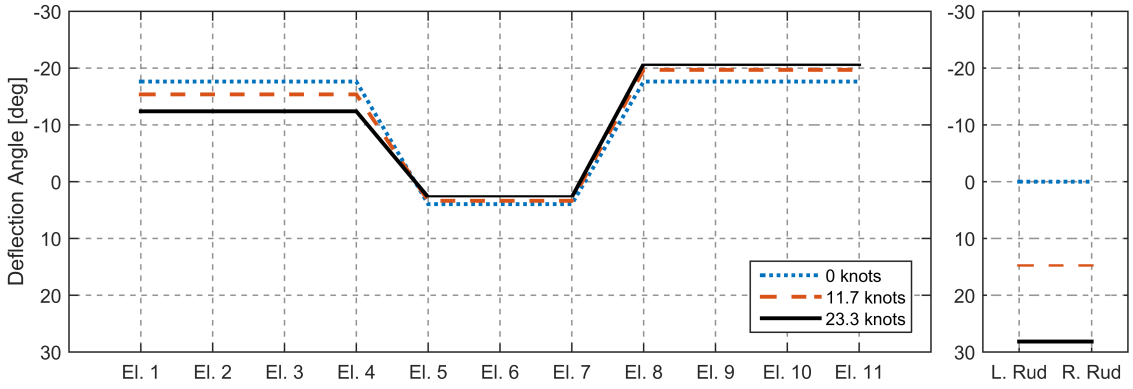

Figure 59: Angle of attack, sideslip, and roll angle for the ganged solutions in crosswind approach conditions.

moment are the limiting factor for this flight condition. Figure 62 shows another angle on the same AMS plots, confirming that the available yawing moment is the limiting factor.

The trim analyses with the original layout had the benefit of generating asymmetric drag using the elevons to augment the rudders. The ganged layout also has this ability but to a lesser extent. The effect is quadratic with deflection, and cannot be depicted accurately with AMS plots generated using a linear control derivative matrix as is done here. The effects are small, but for the original layout they are just large enough to help trim at the full crosswind magnitude.

4.6.3 Minimum Drag Trim Optimization

In the symmetric approach flight condition, the throttle constraint had the effect of making the minimum drag method perform poorly. The throttle constraint resulted in nonunique solutions with equivalent L/D and thrust but widely varying angle of

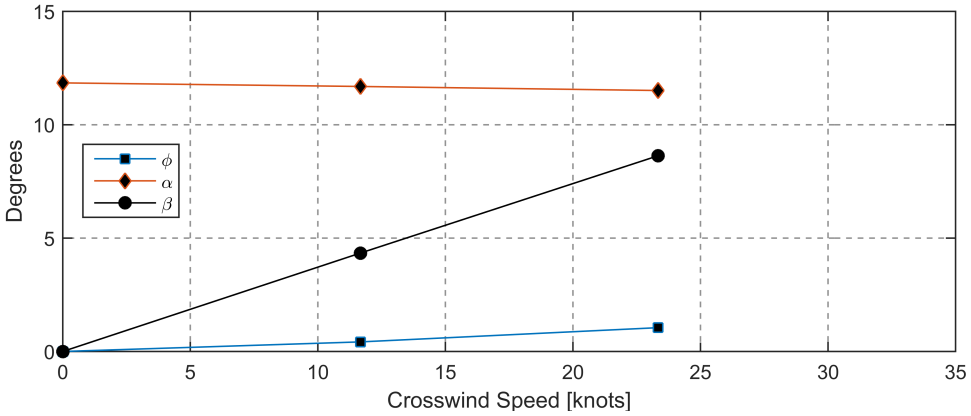

Figure 60: Angle of attack, sideslip, and roll angle for the ganged solutions in crosswind approach conditions.

attack, deflections, and unnecessary saturation of elevons. The minimum drag method retained these problems in crosswind conditions as well. The results presented in this section relax the throttle constraint to demonstrate the type of results and method performance that can be expected if used on a vehicle without throttle issues or one equipped with speed brakes to generate sufficient drag.

The variables controlled by the trim optimizer (Table 20) are quite numerous due to the number of control surfaces and loss of symmetric deflections. Each elevon can be deflected independently of the others and the rudders are again linked. The engines will again generate symmetric thrust and will not be used to augment rudder control authority.

Table 20: Crosswind approach free variables for minimum drag optimization

	Variable	Min	Max	Units
1	α	5	20	degrees
2-13	$\delta_1 \ldots \delta_{11}, \delta_{rud}$	-30	30	degrees
14	ψ (heading)	89.5	90.5	degrees
15	θ (pitch angle)	2	17	degrees
16	ϕ (roll)	0	5	degrees
17	$T_{\text{per engine}}$	0	76,733	lbs

When the throttle constraint was enforced, the minimum drag trim optimization convergence rates were extremely low (less than 10%). However, with that constraint

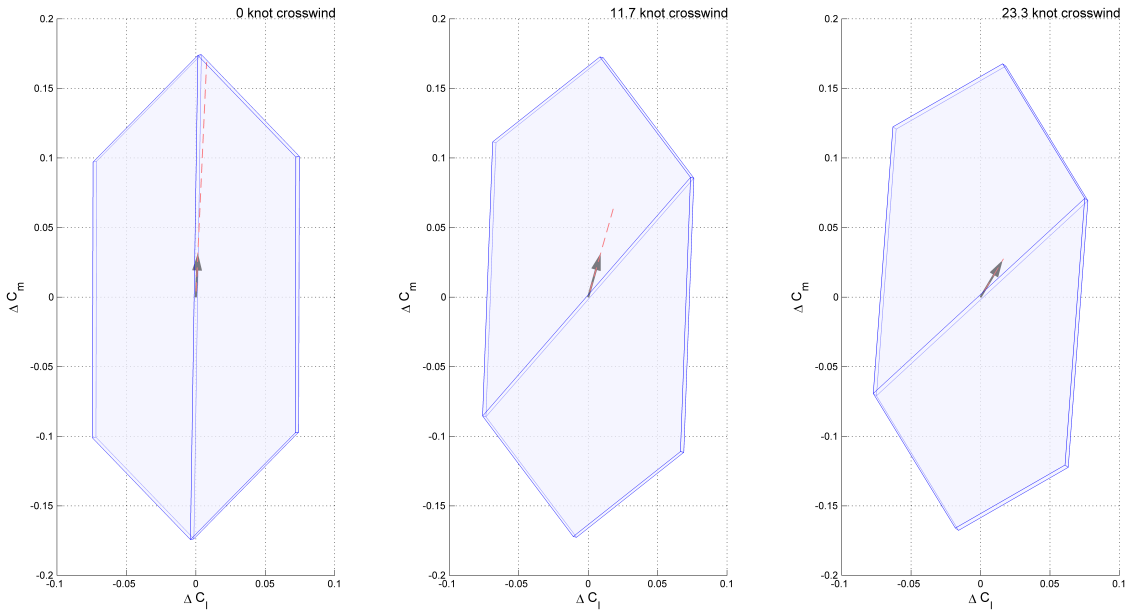

Figure 61: ΔC_m vs. ΔC_l AMS plots for increasing levels of crosswind with ganged elevons.

removed the rates in Table 21 were extremely high. In addition, the optimizer was able to find the global minimum drag trim solution (Figure 63) each time. The deflections change gradually as crosswind is increased, and at 35 knots the rudders are fully saturated. The roll angle required at full crosswind is again within the maximum five degree limit (Figure 65).

Table 21: Minimum drag results for crosswind approach without a throttle constraint.

Crosswind Mag.	Successful Conv. Rate
11.7 kts	98%
23.3 kts	97%
35 kts	78%

The elevons have much more modest deflection magnitudes compared to the throttle constrained direct allocation deflections. The cause is a combination of not having to generate extra drag and that the direct allocation deflections generated drag asymmetrically using the elevons to augment the rudder control authority. The latter effect is proven by the fact that the rudders are not saturated at 35 knot crosswind in the

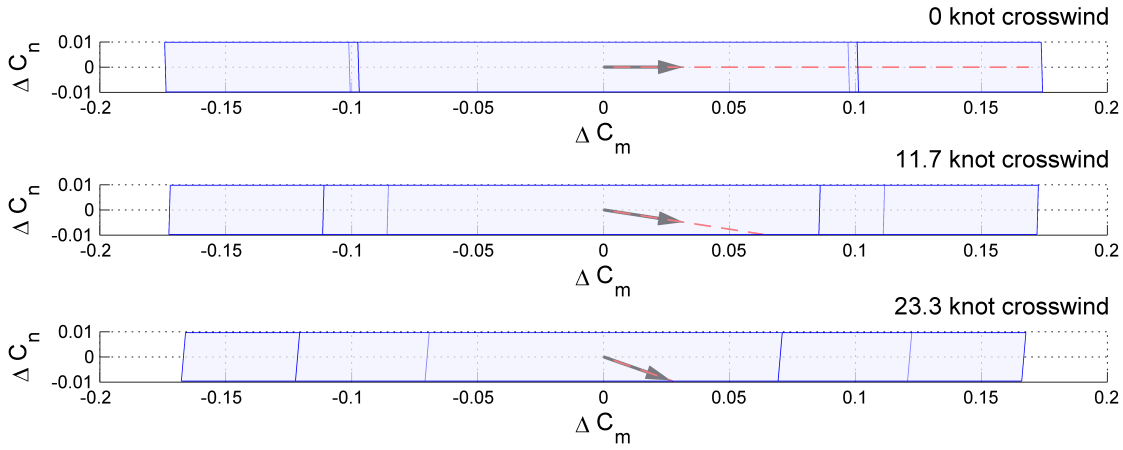

Figure 62: ΔC_n vs. ΔC_m AMS plots for increasing levels of crosswind with ganged elevons.

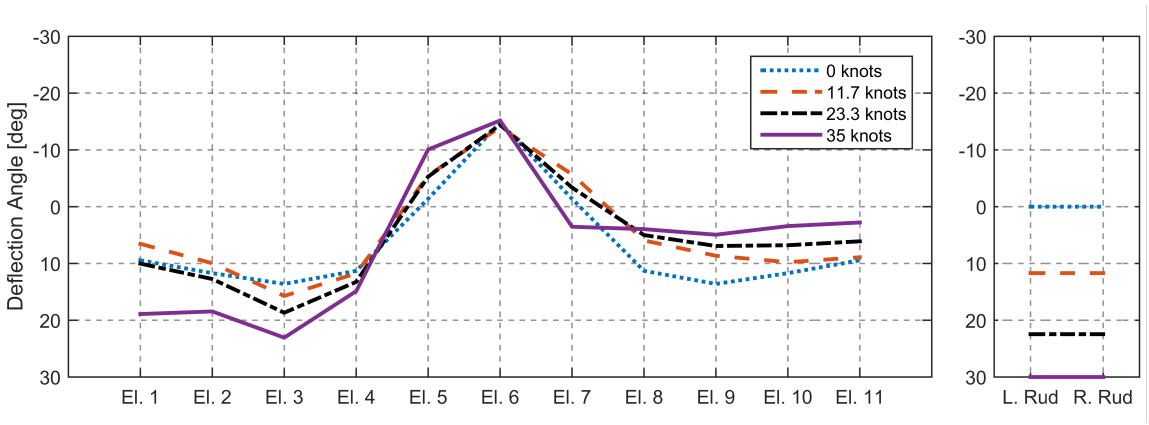

Figure 63: Minimum drag trim deflections for increasing crosswind velocity.

direct allocation solutions.

The thrust required by the minimum drag solutions to trim in the crosswind approach conditions was still very low. Figure 65 shows that thrust grows quadratically (but slowly) with crosswind magnitude. The 20% throttle line in the figure shows how far off the minimum drag solutions are from meeting that constraint. The L/D of the vehicle would need to drop by about 40% to start having more reasonable throttle settings.

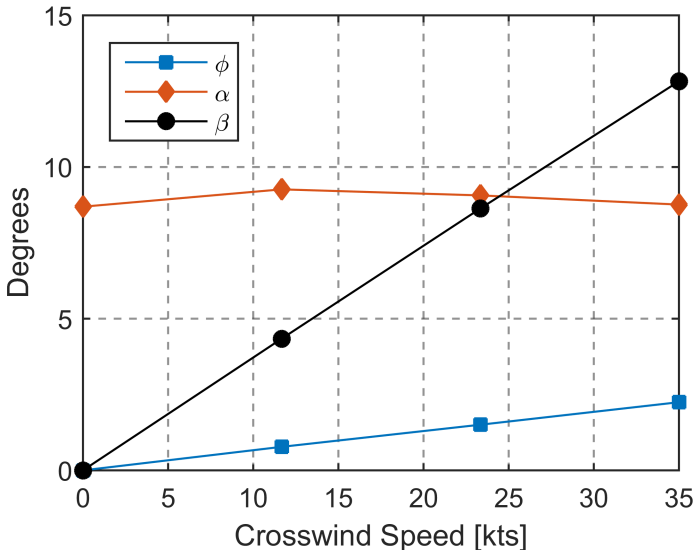

Figure 64: Angle of attack, sideslip, and roll angles for the minimum drag solutions in crosswind approach conditions.

Table 22: Minimum power method results for crosswind approach under 20% throttle constraint.

Crosswind Mag.	Successful Conv. Rate
11.7 kts	61%
23.3 kts	50%
35 kts	11%

4.6.4 Minimum Power Trim Optimization

The minimum power method in crosswind conditions was run using the same algorithm and variables (Table 20) as the minimum drag method, with the exception of an added 20% throttle constraint. This successful convergence rates are shown in Table 22. Unfortunately just as in the symmetric approach condition there is still a local optima problem (Figure 66).

All of the solutions (regardless of amount of crosswind) saturate at least one control. The objective function was supposed to penalize large deflections due to their high hinge moments. It is apparently beneficial to total power to saturate some elevons if it allows others to float near their zero hinge moment positions.

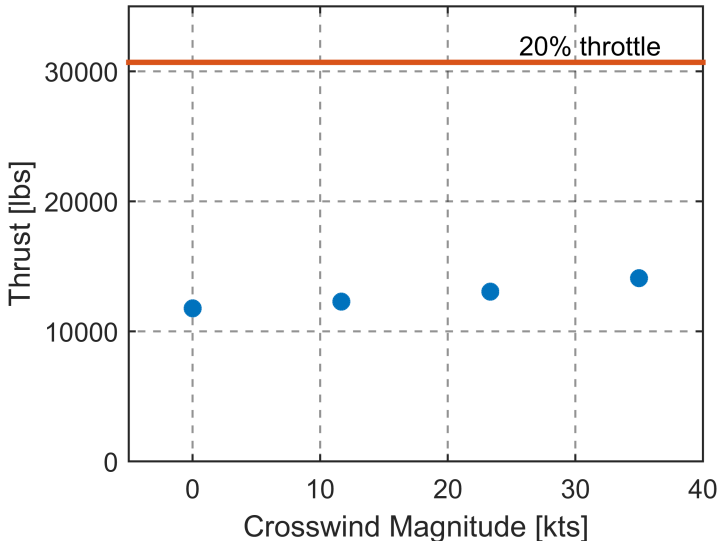

Figure 65: Total thrust with crosswind velocity for the minimum drag solutions.

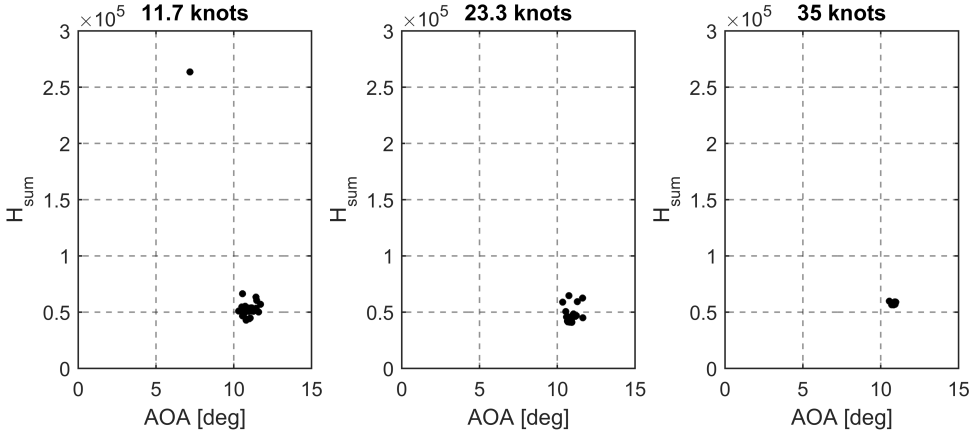

Figure 66: Minimum power crosswind approach trim solutions.

4.6.5 Summary

The direct allocation and ganging methods work best under a throttle constraint, producing consistent and unique trim deflections. At high crosswind magnitude the direct allocation deflections are rather large. The ganged elevon deflections are more reasonable but saturate the rudder sooner. A prediction was made that if ganged elevons are used during HWB MDO the tails would be over-sized. The minimum drag method does not perform well with throttle constraints. On the other hand, it

works extremely well without a throttle constraint but can only be used on vehicles with naturally higher drag. The minimum power method did not result in reasonable deflections nor reliably find the global minimum solution, and is not recommended for use in HWB MDO.

4.7 AMS Margin

RQ2.2: Are there more convenient metrics for expressing the control authority available vs. required for a set of redundant controls?

The metric being used to characterize control authority for a redundant set of controls is the AMS Margin. Trim analysis methods that do not produce unique trim solutions have the potential to make this metric noisy and to harm convergence during HWB MDO. The AMS Margin values produced by each of the trim analysis methods are shown in Figure 67. The direct allocation, ganged elevon, and minimum drag methods can produce unique solutions in symmetric and crosswind approach flight conditions. This results in unique AMS Margin values as well. The nonunique minimum power trim solutions unsurprisingly have nonunique AMS Margin values, making it unusable for HWB MDO. The AMS Margin metric behaves as expected, becoming smaller as crosswind increases. The metric is also useful for quantifying differences between trim optimization methods. These results signal that AMS Margin is able to answer research question 2.2, as a convenient measure of control authority for a set of redundant controls.

4.8 Conclusion

Conventional methods for solving the equations of motion for trim solutions formulate the problem in terms of seeking roots for the nonlinear system of equations. The main shortfall of the conventional methods is that control redundancy causes them to return nonunique solutions with wildly varying characteristics. Four alternative methods were proposed that coped with redundant controls in different ways. Two

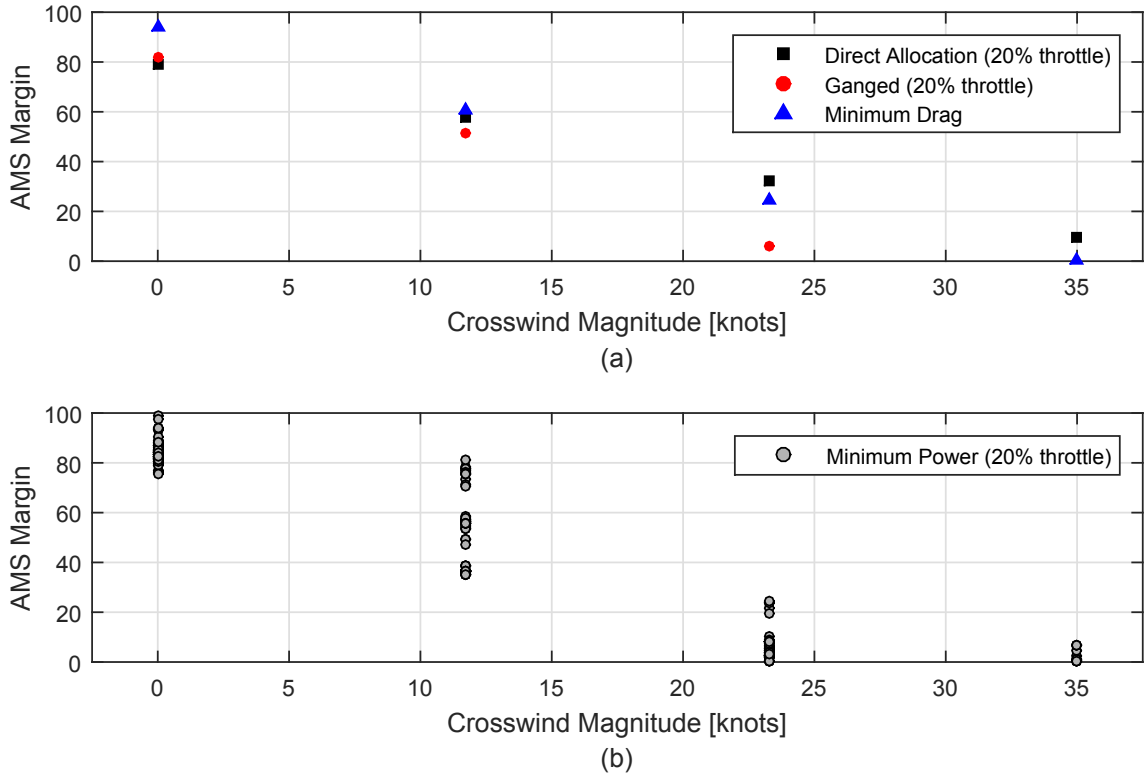

Figure 67: Crosswind approach AMS Margin values from each analysis method. The minimum drag AMS Margin values are for the unconstrained throttle scenario which had unique solutions.

methods integrated control allocation concepts into the conventional method, and the other two methods formulated the trim analysis into minimization of drag and power. All but the minimum power method were able to arrive at unique or global minimum trim solutions consistently, though the minimum drag method can only do so without minimum throttle constraints. This chapter makes a down-payment towards resolving research question 1.4, by exploring the trim analysis problem and generating options for conducting control authority assessments for the HWB configuration. The next chapter will make decisions regarding which of the trim analysis methods should be used on each off-design flight condition.

The methods of this chapter present an opportunity to develop composite cost functions for optimization. The weightings between individual objectives such as power or drag could be varied to explore whether there are combinations of these

properties that are favorable. Appendix C documents an initial exploration of this multi-dimensional Pareto frontier problem.

Another accomplishment of this chapter was to demonstrate the new AMS Margin control authority metric, giving confidence that it can satisfy research question 2.2. It was shown that how the control surfaces are utilized affects control authority, and that this can be captured by the AMS Margin. A prediction was made that vehicles sized assuming ganged elevons may result in over-sized tails and increased TOGW, and will be tested in later chapters. Methods for calculating negative AMS Margin when there is insufficient control authority are the subject of the next chapter, and must be completed in order to fully settle research question 2.2.

CHAPTER V

OFF-DESIGN TRIM ANALYSIS AND AMS MARGIN ALGORITHMS

5.1 Introduction

RQ1.4: How should the trim analysis be conducted to support HWB design optimization?

RQ2.2: Are there more convenient metrics for expressing the control authority available vs. required for a set of redundant controls?

The previous chapter explored the trim analysis problem for the HWB configuration. The problems of conventional methods were quantified and visualized, followed by the demonstration of alternative methods that could address those problems. The goal of this chapter is to establish on a case-by-case basis the most appropriate trim analysis method for each flight condition and maneuver that will be used during HWB MDO. Accomplishing this will resolve research question 1.4. Another goal is to understand how to define the AMS Margin when there is insufficient control authority, which will contribute towards resolving research question 2.2.

Insufficient control authority (i.e. the required moment is larger than that available from the controls) corresponds with a negative AMS Margin. In such situations there will be no trim solutions, leaving the AMS Margin metric undefined and an alternative method of calculating it will be necessary. It is important to estimate this negative value during HWB optimization in case the initial design starts outside of the feasible space and to indicate how much additional control authority is necessary. With this information, optimization algorithms can properly evolve the planform shape and control surface sizes. After establishing how to set up each flight

condition's trim optimization and estimate negative AMS Margin, the control authority assessment capability will be complete and ready to integrate into a larger HWB sizing and optimization environment.

5.2 Flight Conditions

Early MDO work by Boeing evaluated upwards of 20 longitudinal flight conditions in the WingMOD tool.[145] Control authority constraints (in terms of deflection angles) were checked for most of them, but the primary purpose may have been to establish operational CG limits. Wakayama has included cruise and landing phase roll maneuvers in WingMOD analyses as well, but none that would size the vertical tails (such as engine out or crosswind landing).[144] A more recent Boeing publication offers a more definitive list of flight conditions (including additional lateral-directional ones) that should be used to test the limits of HWB control authority in early design phases.[16] These longitudinal and lateral-directional flight conditions and maneuvers are summarized in Tables 23 and 24, respectively.

Table 23: Boeing flight conditions used to determine flight CG limits. Quoted text from Bonet, et al. [16]

No.	Flight Condition / Maneuver
1	"Takeoff nose wheel liftoff at 3.0 deg/s^2 pitch acceleration (nose-up longitudinal control authority)." Forward CG.
2	"Trim at Landing Reference Speed (V_{REF}) and maneuver to stall ($V_S = V_{REF}/1.23$) (nose-up longitudinal control authority)." Forward CG.
3	"Trim at Landing Reference Speed (V_{REF}) and go-around at 6.0 deg/s^2 pitch acceleration (nose-up longitudinal control authority)." Forward CG.
4	"Landing nose wheel hold-off down to stall speed (nose-up longitudinal control authority)." Forward CG.
5	"Stall recovery at -4.0 deg/s^2 pitch acceleration (nose-down longitudinal control authority)." Aft CG.

Table 24: Boeing lateral-directional flight conditions for testing control authority. Quoted text from Bonet, et al. [16]

No.	Flight Condition / Maneuver
1	Engine-Out Minimum Control Speed: "Balance engine-out on ground with no sideslip and no nose wheel steering (yaw control authority at V_{MCG})"
2	Engine-Out Minimum Control Speed: "Balance engine-out in air with no sideslip and less than 5 degrees bank angle (yaw control authority at V_{MCA})"
3	Crosswind Landing Trim: "Trim in 35 knot crosswind with no crab angle at slowest approach speed (lightest weight)"
4	Crosswind Landing Maneuver: "A 6 degree heading (sideslip) change in 2 seconds at maximum wing fuel landing weight (yaw control authority). Future work with 6 Degree-Of-Freedom (6 DOF) simulation will be required to determine requirements for yaw acceleration and steady state yaw rate."
5	Landing Roll Maneuver: "A 30 degree bank angle change in 2.5 seconds at maximum wing fuel landing weight (roll control power). This requirement equates to 20 deg/s^2 roll acceleration and 20 deg/s steady state roll rate."

Due to limitations of the tools used, it was decided not to evaluate some of the flight conditions. The second longitudinal flight condition requires maneuvering from the trimmed state to a stalled state. It is ambiguous whether this is equivalent to a conventional pull-up type maneuver or whether this requires dynamic simulation. In either case, it may require an aerodynamic model that includes separation effects not modeled in VORLAX. The other longitudinal maneuver that will not be evaluated is the fifth one requiring a nose-down pitching moment acceleration in stalled conditions. This again may not be modeled accurately by the vortex-lattice method used in this research.

The flight conditions that are implemented in this dissertation cover both longitudinal and lateral-directional scenarios, and significant effort went in to evaluating them reliably and consistently. In addition, the four tail sizing flight conditions have not been implemented in HWB MDO environments prior to this dissertation. Still, by

omitting the previously discussed flight conditions there may be some consequences that are worth mentioning. Control authority is derived in large part from the planform shape itself. If these omitted flight conditions are evaluated at a later time and happen to be active constraints, then the planform may require modification. Such a major change can add significant rework as well as cost and schedule overruns. These consequences are hypothetical, and which flight conditions are active will not be known with certainty until they are explored with HWB optimization experiments. Even then, the flight conditions that result in active control authority constraints may not be the same for all vehicles or active simultaneously.

5.3 Symmetric and Crosswind Landing Approach

The symmetric and crosswind landing approach flight conditions were explored in detail in the previous chapter for the N2A-EXTE configuration. It was discovered through additional experimentation that the lessons-learned do not necessarily apply to all HWB configurations. For designs more aerodynamically efficient than the N2A-EXTE, such as the one in Figure 68, meeting the throttle constraint requires generating an excessive amount of drag. This vehicle (referred to as Vehicle 377) originates from the design space exploration activities of Chapter 8 and was chosen to demonstrate complications that arose in the trim analyses. The elevons are responsible for generating additional drag to meet the throttle constraint, which potentially reduces the remaining control authority available for balancing moments.

Trim optimizations in the symmetric approach flight condition using the conventional method with direct allocation under a 20% throttle constraint were run for Vehicle 377, but none of the cases converged. To investigate why this might be the case the original conventional method was run as described in Chapter 4, with symmetric elevon deflections again chosen by the optimizer. One hundred randomly

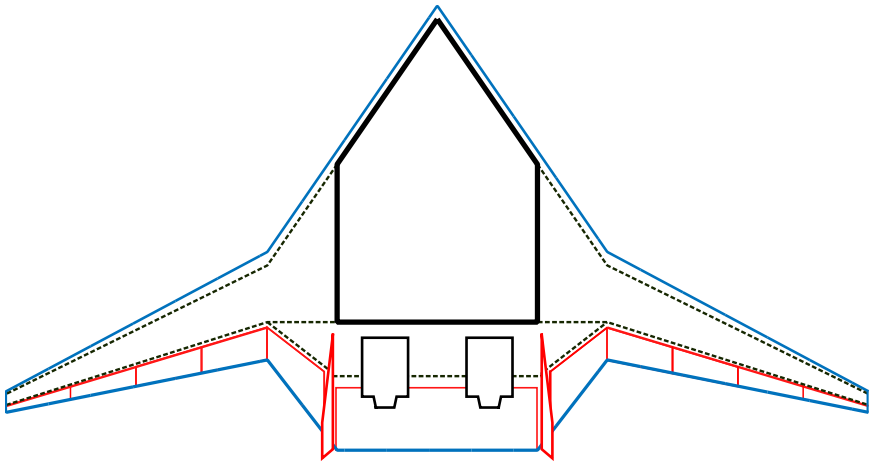

Figure 68: Vehicle 377 used for testing the trim analysis algorithms.

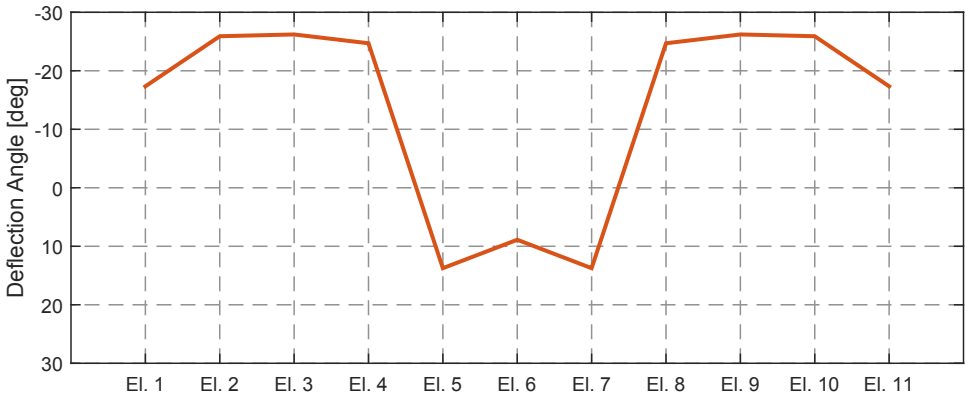

Figure 69: Large deflections were necessary to trim Vehicle 377 with a 20% throttle constraint.

generated initial conditions were run, with 59% of the cases converging to trim solutions. The trim solution with the most modest set of deflections (defined by the smallest maximum magnitude deflections) found are shown in Figure 69.

These deflections are quite large for a flight condition not known as a sizing condition. The aerodynamic model was generated with the vortex-lattice method VORLAX whose accuracy is questionable at such large deflections. Even though the elevons are nearing saturation, an AMS Margin of about 83% for this trim solution is still predicting more than adequate control authority. The metric, which measures moment required versus moment available from the control surfaces, indicates that it

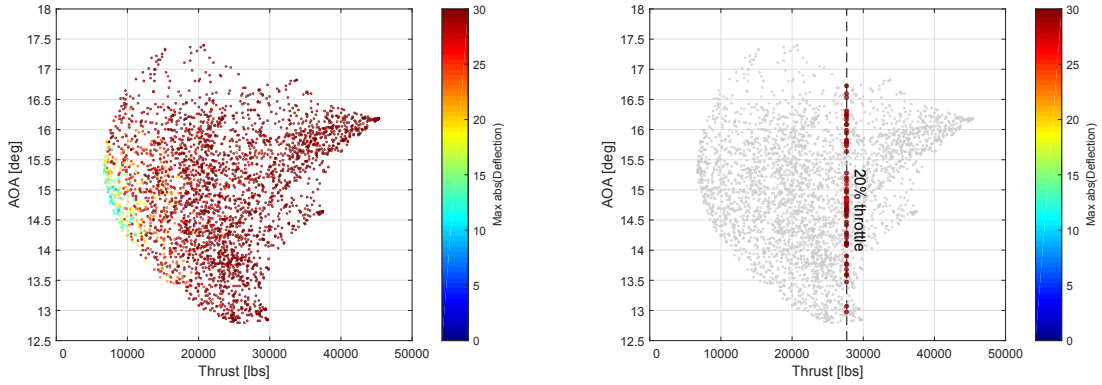

(a) (b)

Figure 70: Trim solution space for Vehicle 377 in the symmetric approach flight condition.

is not a control authority issue forcing these large deflections or causing the failure of the direct allocation trim method. In fact, the deflections on the outer wing are neutralizing lift and modifying the lift distribution in order to increase lift-induced drag.

The throttle equality constraint was suspected as being the source of the issue, and it was removed in order to see if more modest trim solutions were possible. Using the conventional method, a Monte Carlo Simulation was run with 5,000 randomly generated initial conditions. This was done in order to fill in and visualize the solution space, because a pattern had begun to emerge in early testing.

The solution space is visualized in Figure 70(a) by projecting the trim solutions onto the plane of angle of attack vs. total thrust. Each point is a distinct solution that satisfies the equations of motion, with different deflections and other state properties. The points are color-coded based on the maximum absolute value deflection in each trim solution (Equation 39), and modest deflections are defined as having low values of this metric. Trim solutions with modest deflections will have lower values of the metric. It can be observed that there is a region of modest deflections that coincides with low drag trim solutions (with corresponding low thrust) well below the assumed minimum throttle setting. As the required thrust is increased, the elevon deflections

necessary to achieve the associated drag grow quickly.

$$\delta_{max} = max\left\{|\delta_i|, \ldots, |\delta_{11}|\right\} \tag{39}$$

In the region of the 20% throttle equality constraint (Figure 70(b)), the smallest maximum absolute value deflection is on the order of 25 degrees. The deflections have to be large in order to generate enough drag to meet the throttle constraint. Sufficiently convinced that forcing the elevons to generate drag was the cause of the large deflections, a prediction was made:

Hypothesis: Freeing the controls from the responsibility of generating additional drag, through the use of speed brakes, will enable more modest trim deflections.

This hypothesis can be falsified if large deflections persist after the use of speed brakes to increase drag. If the hypothesis is supported, then a modification to the control surface layout assumed for HWB MDO is warranted. The hypothesis will be tested first by using a "virtual" speed brake, one that creates drag without influence on lift and moment. This is an idealized assumption, but is typically the design goal for speed brakes.

The 5,000 case random initial condition experiments were repeated for levels of 10 and 20k lbs of drag from a virtual speed brake that had no other incremental effects. All elevons were free to deflect symmetrically and rudders were not used. The result of adding virtual drag (with no lift or moment consequences) was to shift the trim solution space to higher angles of attack, drag, and thrust. With enough drag provided by speed brakes, the region of modest deflections could be made to intersect with the 20% throttle equality constraint as shown in Figure 71, supporting the hypothesis. The addition of 20k lbs of virtual drag enabled more moderate trim deflections, which are shown in Figure 72.

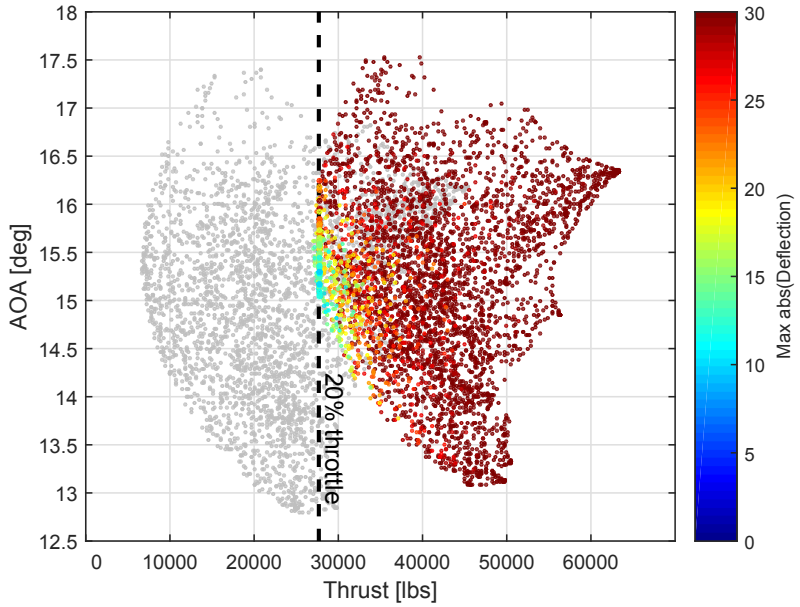

Figure 71: The effect of 20,000 lbs drag from a virtual speed brake on the trim solution space.

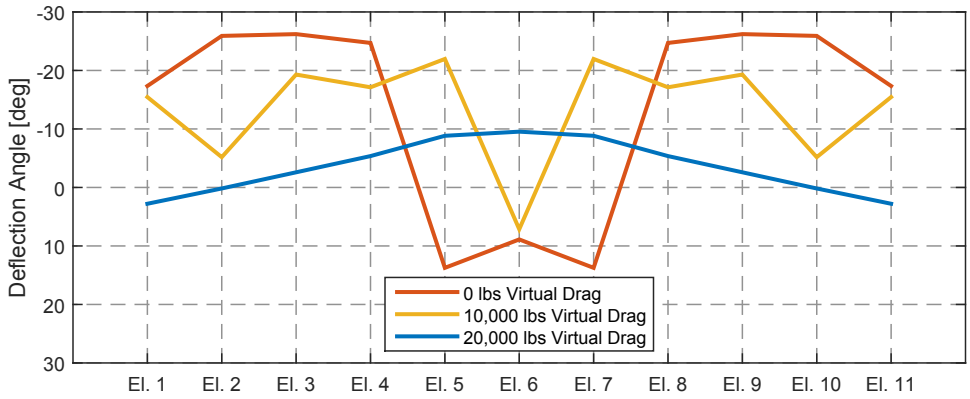

Figure 72: More modest deflections are enabled by a virtual speed brake to help meet the minimum throttle constraint.

5.3.1 Modeling Speed Brakes

A speed brake capable of generating 20,000 lbs of drag enables more practical deflections on Vehicle 377, but the question of feasibility remains. There are several types of speed brakes that can be chosen including clamshells and body/dorsal flaps.[129]

The VORLAX aerodynamic code is not able to model the form drag generated by these devices so historical methods for determining drag, lift, and moment increments will have to be used. Clamshells were chosen for further investigation due to the availability of data for sizing, as well as their potential for having negligible effects on lift and moment.

5.3.1.1 Sizing Clamshell Elevons

A first-order method for estimating the effectiveness of clamshell elevons is provided by Young which gives results similar to those from Roskam.[150, 116] Young's survey of aerodynamic data for speed brakes identifies area, geometry, chordwise position on wing, wing thickness, and lift coefficient as the primary contributors to the clamshell drag increment. For small values of C_L and when located at the trailing edge, the drag coefficient of a single flap is a function of the deflection angle β as shown in Equation 40.

$$C_D = 1.1 \sin^2 \beta \tag{40}$$

This drag coefficient is normalized by the planform area of the of the flap being deflected into the flow. When multiple flaps are used (such as upper and lower flaps forming a clamshell) the drag coefficient increments are modeled as additive. If one assumes that an elevon is split into upper and lower flaps and that the maximum allowable deflection away from neutral is 60 degrees, the panel area required to give a certain drag can be calculated from Equation 41. The resulting panel required for generating 20,000 lbs of drag at approach speeds for Vehicle 377 is compared to that available from the outboard elevons in Table 25. This analysis indicates that replacing the two outboard pairs of elevons with clamshells is sufficient for generating the required drag with less than 60 degrees of deflection. The Boeing X-48B and Preferred System Concept Subscale Test Vehicle configurations from Boeing also use

the two outboard pairs of elevons in this manner.[56, 16]

$$
\begin{aligned}
C_{D_{clamshell}} &= 2.2 \sin^2\left(\frac{60\pi}{180}\right) \\
D &= \frac{1}{2}\rho V^2 S_{panel} C_{D_{clamshell}} \\
S_{panel} &= \frac{D}{1.1\rho V^2 \sin^2\left(\frac{60\pi}{180}\right)}
\end{aligned} \tag{41}
$$

Table 25: Clamshell sizing for Vehicle 377.

Req. Drag	Req. Panel Area	Elevon 1/11 Area	Elevon 1/11 & 2/10 Area
20,000 lbs	193 ft^2	74.4 ft^2	199.5 ft^2

One final follow-up experiment was required. If the two outboard elevons are used as clamshells, they should be assumed to no longer contribute to trimming vehicle moments. The experiments were rerun with the two outboard elevon pairs fixed at zero deflection in the aerodynamic model while assuming that they are generating 20,000 lbs of drag. The purpose of the experiment was to see what happens to the solution space when those elevons are not used to trim anymore, and if the resulting trim deflections were still reasonable.

The solution space shown in Figure 73(a) has a different shape now but overall it has similar characteristics. The 20% throttle constraint again passes through the region of the solution space with modest deflection magnitudes. The variety of deflection solutions possible with the throttle constraint are shown in Figure 74, with the most modest solution highlighted. Note that the two outboard elevon pairs are constrained to zero deflection angles while the speed brakes are in use.

Smaller deflections are preferred, and by inspecting Figure 73(b), one can observe that the modest deflections are in the same region as the minimum drag deflections. Therefore, the amount of drag that should be generated is the difference between the

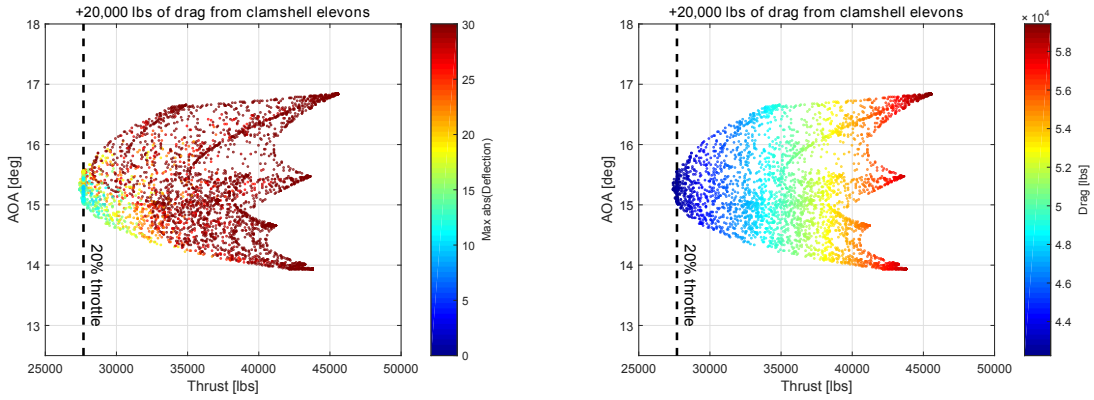

(a) Color coded by max deflection magnitude.

(b) Color coded by drag.

Figure 73: Trim solution space for Vehicle 377 in the symmetric approach flight condition with clamshells.

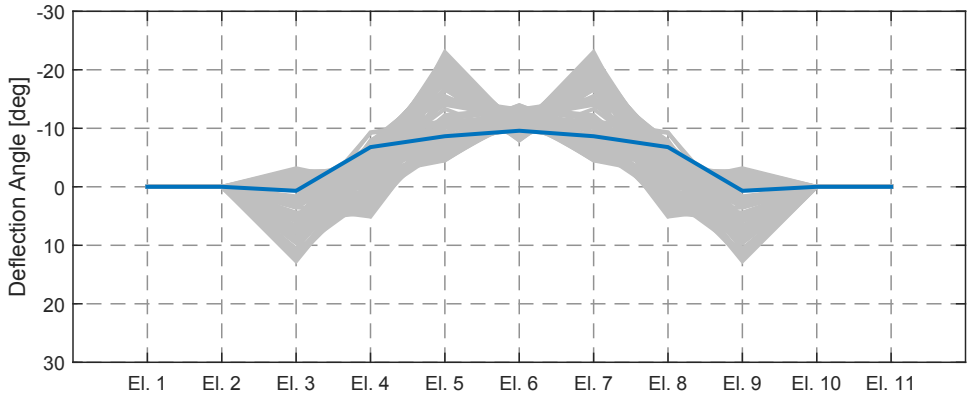

Figure 74: Trim deflections for Vehicle 377 with clamshells deployed and 20% throttle. The highlighted trim solution has the smallest maximum deflection angle.

minimum drag solution (D_{min}) and the drag required to achieve the 20% throttle constraint (Equation 42). The D_{min} term can be reliably estimated using the minimum drag trim optimization method with an unconstrained throttle. The $D_{20\%\text{ throttle}}$ term can be estimated by rearranging the rate of climb equation (Equation 43).

$$\Delta D_{\text{req}} = D_{20\%\text{ throttle}} - D_{\text{min}} \tag{42}$$

$$R/C = V \sin\gamma = V\frac{T-D}{W}$$

$$D_{20\%\text{ throttle}} = T_{20\%\text{ throttle}} - W \sin\gamma \tag{43}$$

The ΔD_{req} to be generated by the clamshells for Vehicle 377 is 21,254 lbs. Elevons 1/11 and 2/10 can produce only 20,675 lbs with 60 degree deflections at this flight condition. The ΔD imposed by the clamshells shall therefore be the minimum of ΔD_{req} and $\Delta D_{\text{avail.}}$.

The historical clamshell sizing method makes certain simplifications that should be noted. The forces are assumed aligned with the drag axis only. In reality, clamshell elevons will likely also have side force components depending on the wing trailing edge sweep angle and the angle of sideslip. The two outboard pairs of elevons may not be of sufficient size for all vehicles. A constraint should be enforced in HWB optimization that requires the available clamshell drag to be greater than or equal to the required drag. An alternative method of increasing clamshell drag would be to increase the outboard elevon span fractions, but that is not explored in this dissertation.

5.3.2 Trim Algorithm Development

After imposing this drag increment, any preferred trim optimization method can be used from here. It may be recalled from Chapter 4 that the direct allocation method also achieved low drag trim solutions. Experiments were conducted that compared the minimum drag method to the direct allocation method under different throttle constraint and clamshell usage scenarios in Appendix D. The minimum drag method was selected and this section will demonstrate the final algorithms for evaluating symmetric and crosswind landing approach trim analyses. Another decision from those experiments was that the throttle constraint was best enforced with a clamshell sizing constraint at the vehicle level, rather than at the trim optimization level.

When the minimum drag method was run with the clamshells fully deployed and no throttle equality constraint, 100% of the random initial conditions converged. There were two similar solutions but 99 of the 100 were the bold solution in Figure 162.

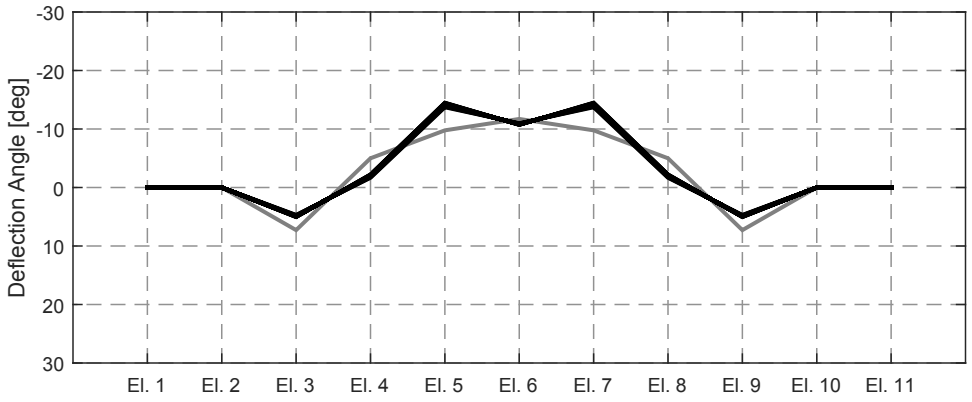

Figure 75: Minimum drag trim deflections with fully deployed clamshells.

Both had nearly identical throttle settings (20.27% vs. 20.36%) and AMS Margins (79.52% vs. 79.64%), and either would be acceptable.

The minimum drag method with fixed clamshells works well for Vehicle 377. The drag increment is merely an estimate of what is needed to shift the trim solution space to a more favorable region, and it was discovered that this can be slightly overestimated. Enforcing a 20% throttle equality constraint when the drag increment has been overestimated resulted in no feasible trim solutions. A slightly higher throttle setting is acceptable, because 20% is merely an assumed lower bound on feasible throttle settings.

The crosswind approach flight condition with clamshells was explored next. For this experiment the full 35 knot crosswind magnitude was not achievable. The method is instead tested at increasing levels of crosswind magnitude until the controls saturate and trim is no longer possible. The deflections from the minimum drag method with a fully deployed clamshell and no throttle equality constraint are shown in Figure 164. They resemble the minimum drag deflections in symmetric flight and change gradually as crosswind magnitude is increased. The rates of convergence are still very high, with 100% converged to the global minimum drag solution at a 5 knot crosswind to 92% converged to the global minimum drag solution at a 25 knot crosswind. The throttle

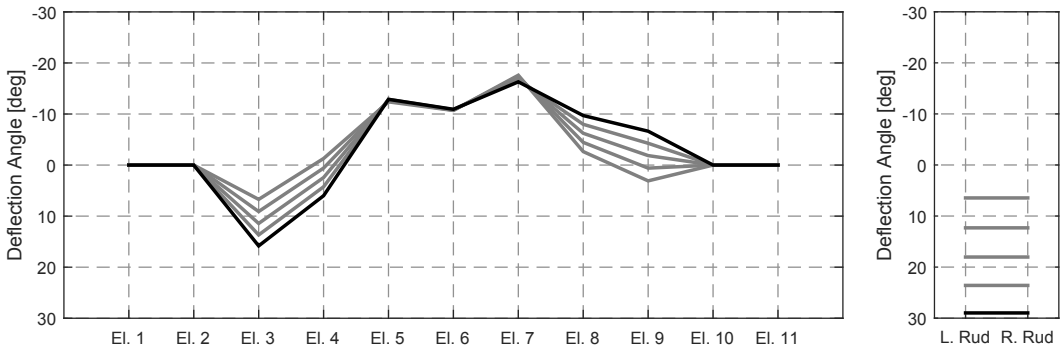

Figure 76: Minimum drag deflections with clamshells for increasing levels of crosswind.

setting variation with crosswind magnitude is quadratic but not very sensitive, and is always slightly higher than 20%.

The most important observation to make is the behavior of AMS Margin with crosswind magnitude as shown in Figure 165. It is a piecewise linear curve indicating that the control authority (from the rudder in this case) for Vehicle 377 becomes exhausted at approximately a 26.25 knot crosswind. As a reminder, the AMS Margin metric measures the remaining control authority by comparing the magnitudes of a) the moment vector required to trim, and b) a parallel vector extended to the surface of the attainable moment subset. As the crosswind magnitude is increased the moment vector required to trim shifts direction and in doing so points through different faces of the attainable moment subset. The AMS Margin is linear as the moment vector required to trim shifts across each individual face, and is readily extrapolated to the full crosswind magnitude for a value of -32.5%. Figure 164 shows that the rudder is quickly saturated and is the limiting factor. The negative AMS Margin signals that the yawing moment control authority needs to increase by nearly a third (e.g. through increased tail area).

A few visual aids will help explain what it means to have an extrapolated negative AMS Margin metric. In Figure 78, several properties of the trim solutions are plotted versus crosswind magnitude. These include the angle of attack, sideslip angle, and the

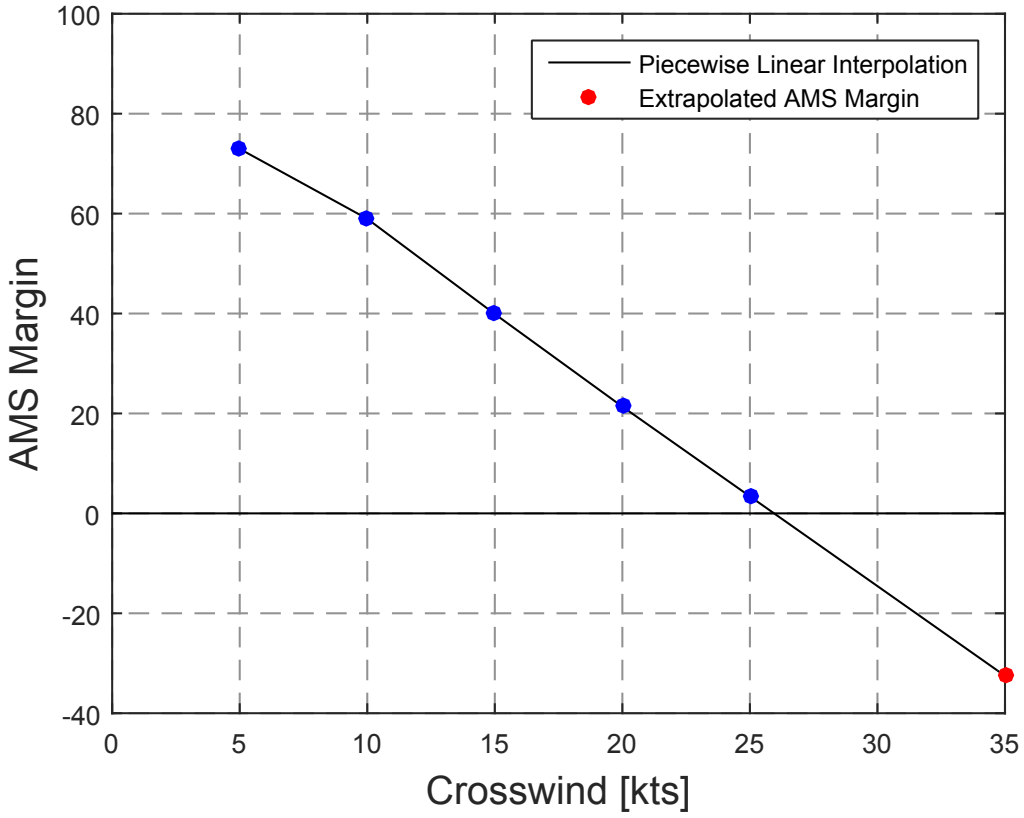

Figure 77: Crosswind approach AMS Margin trend and extrapolation for the minimum drag method with clamshells.

moment increments that the controls are required to generate. Angle of attack and the pitching moment increment follow a quadratic trend, while the others follow linear trends. The moment increments are extrapolated easily to the full 35 knot crosswind, and plotted in the attainable moment subset plots of Figure 79. This AMS axes are rescaled so that the control moment vector increments can be seen clearly. These show the AMS from various angles and how the control moment increments vary with crosswind. The converged trim solutions are the black arrows, and the extrapolated moment increment vector is in bold red. The converged trim solutions have moment vectors within the AMS boundaries and therefore have positive AMS Margin (or control authority to spare). The extrapolated moment increment vector required for a 35 knot crosswind is clearly not within the AMS and therefore has a negative AMS

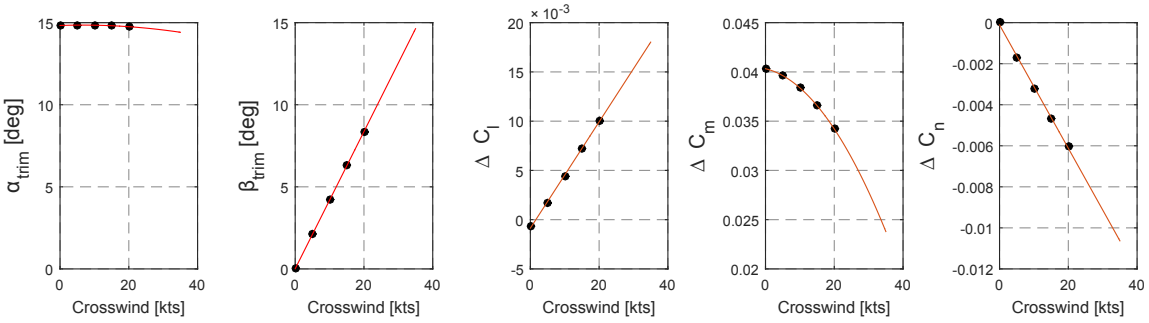

Figure 78: Trim solution properties as a function of crosswind magnitude.

Margin (insufficient control authority).

5.3.3 Final Algorithms

The final algorithm for performing trim analyses in symmetric approach:

1. Estimate D_{min} using the minimum drag trim method
    - Variable ranges defined in Tables 10 and 11 of Chapter 4. Use V_{app}, CG, weight, and the thrust upper limit from the vehicle being evaluated.
    - Elevons 1/11 and 2/10 fixed at zero deflection, no drag increment, and full throttle range allowed.
    - For high confidence that the global minimum drag solution is found, test 30 randomly generated initial conditions.
    - Some vehicles may have difficulty trimming with the two outboard elevons undeflected, or if the clamshell drag increment is inadequate. Allow approach speed increments of 10% until trim is feasible. The incremented speed replaces V_{app} in all subsequent analysis.
2. Estimate drag increment to impose with clamshell speed brakes
    - Use Equation 41 to estimate ΔD_{avail} from the clamshells.
    - Use Equation 42 to estimate ΔD_{req} needed to trim with a 20% throttle setting.

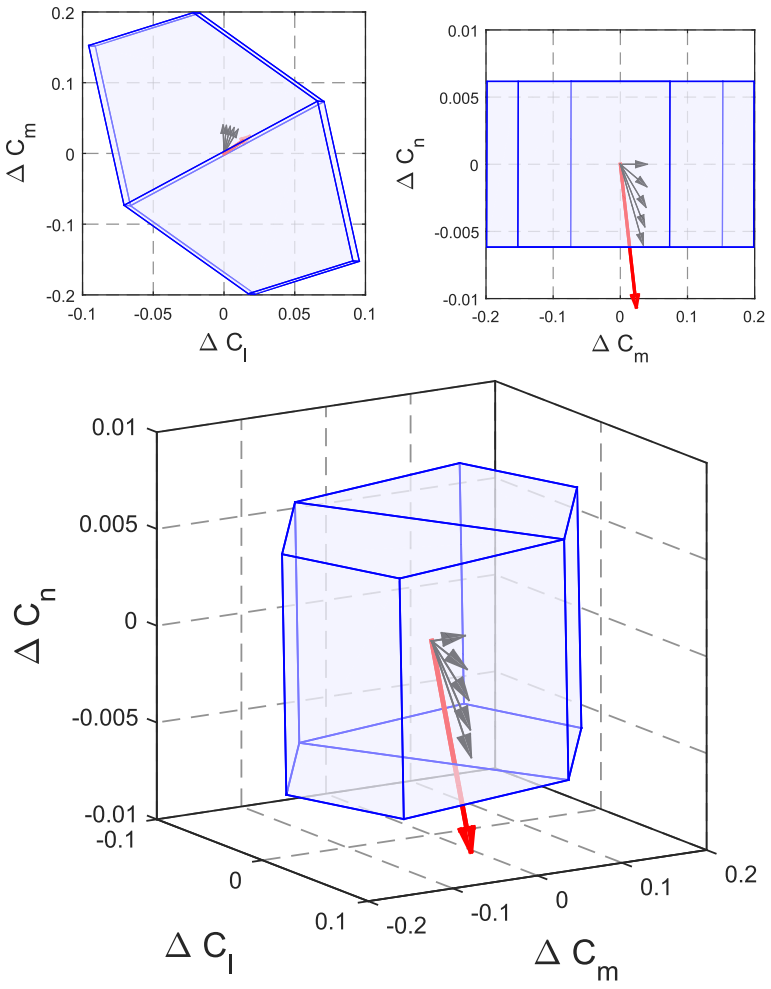

Figure 79: Control moment vector increments for increasing levels of crosswind, and the extrapolated control moment vector for a 35 knot crosswind.

- The fixed clamshell drag increment shall be: $\Delta D = min\left\{\Delta D_{req}, \Delta D_{avail}\right\}$

3. With clamshells deployed, once again find the minimum drag trim solution

   - Variable ranges defined in Tables 10 and 11 of Chapter 4. Use V_{app}, CG, and weight from the vehicle being evaluated.
   - Elevons 1/11 and 2/10 fixed at zero deflection, with ΔD imposed, and full throttle range allowed.
   - For high confidence that the global minimum drag solution is found, test 30 randomly generated initial conditions.

The final algorithm for performing trim analyses in crosswind approach:

1. Attempt to find the global minimum drag trim solution with clamshells deployed

   - Variable ranges defined in Tables 15 and 11 of Chapter 4. Impose the full 35 knot crosswind. Use V_{app}, CG, and weight from the vehicle being evaluated.
   - Elevons 1/11 and 2/10 fixed at zero deflection, with ΔD imposed, and full throttle range allowed.
   - For high confidence that the global minimum drag solution is found, test 30 randomly generated initial conditions.

2. If no trim solutions are found, run a suite of crosswind speeds and extrapolate the AMS Margin

   - Run the trim analysis with the following crosswind magnitudes: 30, 25, 20, 15, 10, 5, 2.5, and 1 knots
   - Using the minimum drag trim solutions at each successful speed, use linear piecewise extrapolation to estimate AMS Margin at the full 35 knot crosswind.

5.3.4 Other AMS Margin Assumptions

For the symmetric approach and crosswind approach flight conditions, the clamshells are always in use. Therefore, elevons 1/11 and 2/10 will not contribute to vehicle control authority or the attainable moment subset. When extrapolating AMS Margin, speeds whose AMS Margin are approximately 0 (i.e. $< 1\%$) are excluded. This occurs when rudders are fully saturated but the vehicle is still able to trim with the aid of asymmetric induced drag from the elevons. By excluding such trim solutions, the control authority limit is defined as the crosswind magnitude that saturates the rudders.

5.4 Crosswind Landing Maneuver

The crosswind landing maneuver is also known as a decrab maneuver. It requires a six degree heading change within two seconds using the maximum landing weight. The maneuver was modeled as a single axis rotation about the body z-axis (Equation 44) using the maximum takeoff weight mass properties and the leading edge drooped 30 degrees. The aerodynamic yawing moment is defined using a linear model as a function of yaw rate and sideslip angle in Equation 45. The two control derivatives N_r and N_β are calculated with VORLAX using the symmetric approach trim angle of attack and elevon deflections. The constant N_{req} term is the yawing moment required from the rudders to perform the maneuver and is to be solved for.

$$N = I_{zz}\dot{r} \tag{44}$$

$$N = N_{req} + N_r r + N_\beta \beta \tag{45}$$

The equation of motion becomes a second order ordinary differential equation when $r = \dot{\psi}$, $\dot{r} = \ddot{\psi}$, and $\beta = \psi$ are substituted (Equation 46). This equation can be integrated numerically by first converting it into two first order differential equations

(Equation 47) using the substitutions $x_1 = \psi$ and $x_2 = \dot{x_1} = \dot{\psi}$. The equations are integrated using Matlab's Runge-Kutta solver ode45 for two seconds to quantify the achievable heading angle change with a given N_{req}, assuming no initial yaw angle or rate. Several values of N_{req} are attempted, a linear curve is fit, and the yawing moment required to achieve the desired heading change is interpolated. The terms N_{req} and N_{max} are then compared using Equation 48 to calculate the AMS Margin.

$$\ddot{\psi} - \frac{N_r}{I_{zz}}\dot{\psi} - \frac{N_\beta}{I_{zz}}\psi = \frac{N_{req}}{I_{zz}} \tag{46}$$

$$\begin{bmatrix} \dot{x_1} \\ \dot{x_2} \end{bmatrix} = \begin{bmatrix} x_2 \\ \frac{N_{req}}{I_{zz}} + \frac{N_\beta}{I_{zz}}x_1 + \frac{N_r}{I_{zz}}x_2 \end{bmatrix} \tag{47}$$

$$\text{AMS Margin} = 1 - \frac{N_{req}}{N_{max}} \tag{48}$$

5.5 Landing Roll Maneuver

This maneuver requires a 30 degree bank angle change within 2.5 seconds using the maximum landing weight. The maneuver will be modeled as a single axis rotation about the body x-axis (Equation 49), using the maximum takeoff weight mass properties and the leading edge drooped 30 degrees. The term L is the external aerodynamic rolling moment which is defined using a linear model (Equation 50). A constant term, L_{req}, is the rolling moment required from the elevons to achieve the maneuver and will be some fraction of the maximum attainable rolling moment (L_{max}). The L_{max} value is achieved by deflecting all left-wing elevons 30 degrees (trailing edge down), and all right-wing elevons deflected -30 degrees. The vehicle angle of attack and centerbody elevon deflection are retained from the symmetric approach trim solution, and run through VORLAX to quantify L_{max}. The only other relevant component is a roll rate derivative, L_p, which resists rolling motion and is provided by VORLAX.

$$L = I_{xx}\dot{p} \tag{49}$$

$$L = L_{req} + L_p p \tag{50}$$

With the aerodynamic term and the substitution $p = \dot{\phi}$, the equation of motion becomes a second order ordinary differential equation (Equation 51). This equation can be integrated numerically by first converting it into two first order differential equations (Equation 52) using the substitutions $x_1 = \phi$ and $x_2 = \dot{x_1} = \dot{\phi}$. The equations are integrated using Matlab's Runge-Kutta solver ode45 for 2.5 seconds to quantify the achievable roll angle with a given L_{req}, assuming no initial roll rate and wings level. Several values of L_{req} are attempted, a linear curve is fit, and the rolling moment required to roll 30 degrees is interpolated. The terms L_{req} and L_{max} are then compared using Equation 53 to calculate the AMS Margin.

$$\ddot{\phi} - \frac{L_p}{I_{xx}}\dot{\phi} = \frac{L_{req}}{I_{xx}} \tag{51}$$

$$\begin{bmatrix} \dot{x_1} \\ \dot{x_2} \end{bmatrix} = \begin{bmatrix} x_2 \\ \frac{L_{req}}{I_{xx}} + \frac{L_p}{I_{xx}} x_2 \end{bmatrix} \tag{52}$$

$$\text{AMS Margin} = 1 - \frac{L_{req}}{L_{max}} \tag{53}$$

5.6 Go-around Maneuver

The go-around maneuver is similar to the symmetric approach flight condition, with a few key differences. It is flown at MTOW with a nose-up angular acceleration, and both engines operating at full thrust. The linear acceleration that results from this force imbalance will therefore be non-zero and a fall-out of the analysis. The range

can be bounded at zero and sea level takeoff thrust from both engines divided by the aircraft mass. A unique solution can be found by using the minimum drag trim optimization method to maximize the linear acceleration. The full set of fixed and free state variables are in Tables 26 and 27.

Table 26: Go-around maneuver fixed variables for the minimum drag method.

	Variable	Value	Units
1	V	V_{app}	
2	γ (climb angle)	0	degrees
3	ψ (heading)	90	degrees
4	θ	α	degrees
5	ϕ (roll)	0	degrees
6	$\dot{q} = \ddot{\theta}$	6	degrees/s^2
7	β	0	degrees
8	Altitude	0	ft
9	$\delta_{rudders}$	0	degrees
10	$\delta_{LEdroop}$	30	degrees
11	MTOW		lbs
12	Fwd CG		
13	Both engines $T_{max_{SL}}$		lbs
14	I_{yy}		slug-ft^2

Table 27: Go-around maneuver free variables for the minimum drag method.

	Variable	Min	Max	Units
1	α	5	20	degrees
2-7	$\delta_1 \ldots \delta_6$ (symm. elevons)	-30	30	degrees
8	$\frac{dV}{dt}$	0	$\frac{2T_{SL}}{m}$	ft/s^2

5.6.1 Sensitivity to the $C_{L_{max}}$ Assumption

Many designs in early HWB MDO experiments had difficulty performing the maneuver. One such design (Vehicle 4354), which also came from design space exploration activities of Chapter 8, is shown in Figure 80. This design will be used to demonstrate the maneuver and investigate the root causes of the trim analysis problems.

Pitching moment control authority is proportional to velocity squared, so the AMS Margin trend with velocity was expected to be useful for extrapolating to negative

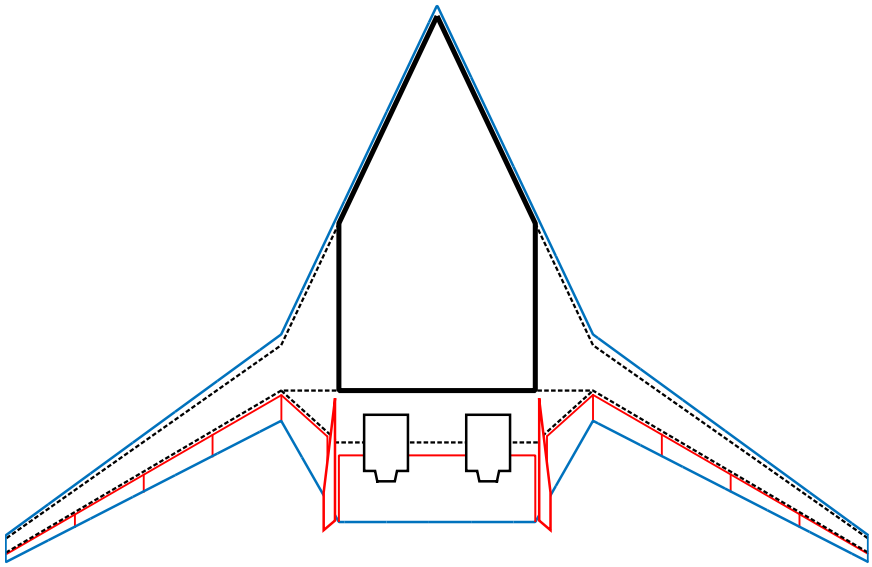

Figure 80: Vehicle 4354 used for testing the trim analysis algorithms.

values. One hundred randomly generated initial conditions were run at 5, 10, 20, and 30% greater speeds than the original V_{app} from the FLOPS performance analysis. Trim solutions from speeds approaching V_{app} had very high angles of attack near the upper bound of 20 degrees (Figure 81(a)).

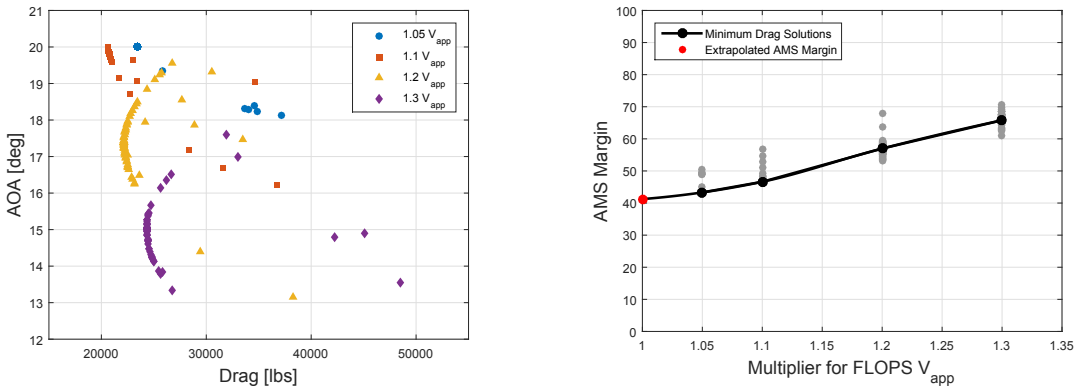

(a) (b)

Figure 81: Trim solution trends for Vehicle 4354 with speed.

The angles of attack became more moderate as speed was increased, and the AMS Margin of every solution is plotted in Figure 81(b). The minimum drag solutions were used in a piecewise cubic interpolation to generate the curve and extrapolate

AMS Margin to the desired speed. The extrapolated AMS Margin is still positive, indicating that control authority should be sufficient and was not the reason for the lack of trim solutions at V_{app}.

Since flying at greater speeds enables the trim optimizer to find valid solutions, the question became why an infeasible V_{app} was output from the FLOPS performance analysis. An investigation revealed that the $C_{L_{max}}$ assumption is the primary driver of this problem. The approach speed is generally chosen to be $1.3V_{stall}$, which can be estimated using Equation 54.

$$\begin{aligned} C_L &= \frac{L}{\frac{1}{2}\rho V^2 S} \\ L &\approx W \\ V_{stall} &= \sqrt{\frac{2W/S}{\rho C_{L_{max}}}} \end{aligned} \tag{54}$$

The $C_{L_{max}}$ had originally been treated as a technology assumption matching that of the N2A-EXTE, whose airfoil stack and drooped leading edge high lift device are shared by all designs in this dissertation. This assumption is too generous for Vehicle 4354, due to the inability to generate sufficient lift with reasonable angles of attack at the resulting approach velocity. Ideally the $C_{L_{max}}$ estimate should be a function of the airfoils, planform shape, wing twist, and high lift device performance.

Observation: The assumptions used in conceptual design of the HWB matter a great deal for the trim analyses of the vehicle. The $C_{L_{max}}$ parameter needs a good estimate that is linked to the geometry. Otherwise the vehicle may not generate enough lift within reasonable angles of attack, and the trim analysis will fail.

A computationally inexpensive method is needed to link the $C_{L_{max}}$ estimate to the geometry of each vehicle. Boeing's in-house HWB sizing environment called WingMOD solved this problem using a critical section method that: "... declares

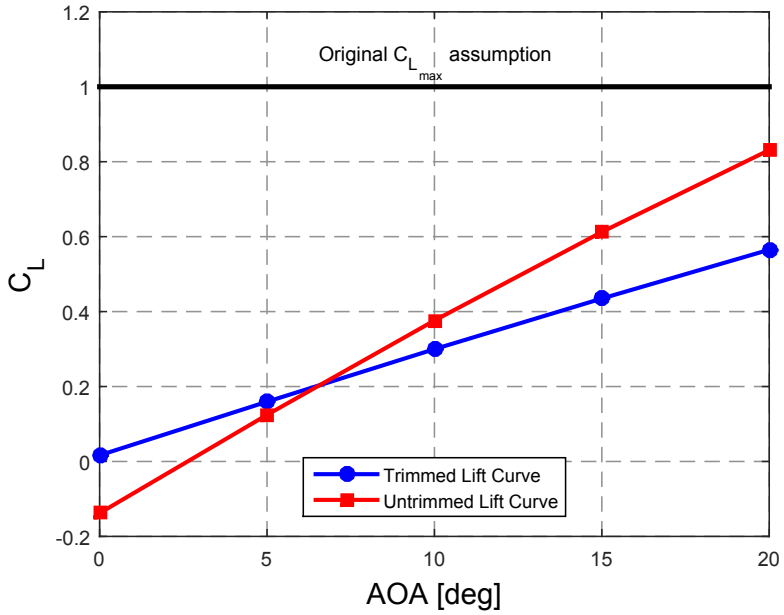

Figure 82: Lift curves for Vehicle 4354 at Mach 0.2.

the wing to be at its maximum usable lift when any section reaches its maximum lift coefficient, which is calculated from empirical data."[53] An alternative that could be implemented quickly was developed based on a heuristic. The N2A-EXTE had a maximum lift coefficient that occurred at a 20 degree angle of attack, which can be used as a guess for the maximum reasonable angle of attack for other HWBs. The VORLAX tool was used to predict the C_L at this maximum angle, however it was discovered that even this value is too generous and V_{app} was still too low. The ultimate source of the problem was the use of untrimmed lift curve data. For comparison Figure 82 shows the trimmed lift curve for Vehicle 4354 as well, which was generated by using the entire trailing edge to trim the pitching moment at each angle of attack. The effect of elevon deflection on lift and moment coefficients is linear and only two deflections at each angle of attack are necessary to estimate the trimmed C_L at each angle of attack.

The maximum realistic C_L that Vehicle 4354 can achieve in trimmed flight is 0.565, which is 43.5% lower than the initially assumed value of 1. The resulting V_{app} of 194.5

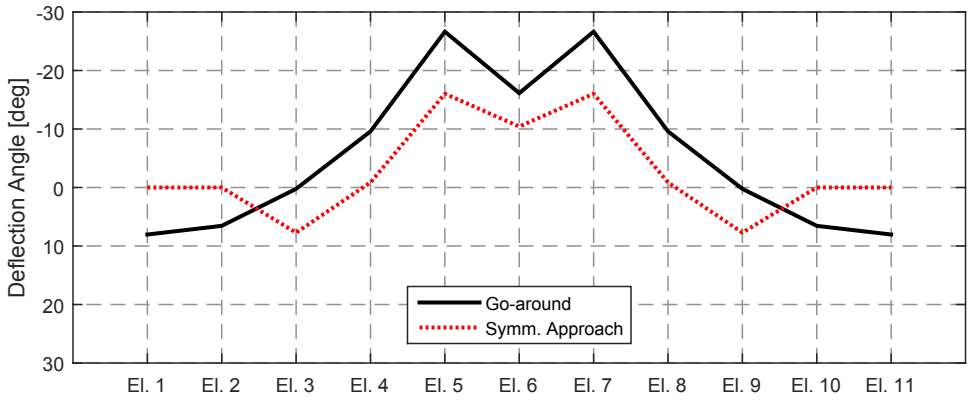

Figure 83: Minimum drag go-around deflections for Vehicle 4354.

knots is 33% faster than was originally assumed for the trim analyses, and enabled successful go-around maneuver trim solutions. The go-around minimum drag trim solution for Vehicle 4354 is shown in Figure 83, which needs more nose-up pitching moments than the approach trim solution.

5.6.2 Final Algorithm

While the new $C_{L_{max}}$ estimate drastically improves the reliability of the trim optimization, it may not always be sufficient. Similar to the symmetric approach flight condition, if the vehicle fails to trim the approach speed shall be increased in increments of 10% until a successful trim solution is found. This rarely occurred in practice, but is done to increase the robustness of the algorithm.

1. Attempt to find the global minimum drag trim solution
    - Variable ranges defined in Tables 26 and 27. V_{app} from the FLOPS performance analysis.
    - Utilize all elevons symmetrically (no clamshells).
    - For high confidence that the global minimum drag solution is found, test 30 randomly generated initial conditions.

2. Some vehicles may still have difficulty trimming with reasonable angles of attack. Allow approach speed increments of 10% until trim is feasible. The incremented speed replaces V_{app} in all subsequent analysis.

No extrapolation of the AMS Margin is necessary for this flight condition. The metric will be calculated normally with all elevons contributing normally (no clamshells) to vehicle control authority and the attainable moment subset. Elevon yawing moments are assumed to be negligible.

5.7 One Engine Inoperative in the Air

There are several ways to fly an aircraft in the event of an engine failure, as described by Anderson.[9] The method used in this dissertation requires the greatest control authority and is also recommended by Boeing.[16] This method requires banking the aircraft into the operating engine, with zero sideslip angle, a climb angle of zero, and with less than five degrees of roll angle. The flight condition will be implemented with the left engine operating, requiring a negative roll angle. As suggested by Roskam for a wind-milling high bypass ratio engine, the right engine shall have a drag of 1/4 of the maximum takeoff thrust.[115] The minimum drag trim optimization method is appropriate here and will maximize the linear acceleration. The vehicle will be trimmed at the minimum control speed, which FAR 25.149 requires to be no more than $1.13V_{stall}$. The vehicle will be trimmed at MTOW (again, FAR 25.149) and the forward-most CG allowed by fuel-shifting will be used. All elevons are used for trim optimization (no clamshells) and rudders are deflected together. The leading edge droop high lift device is deployed 30 degrees. The fixed and free state state variables for this flight condition are defined in Tables 28 and 29, respectively.

5.7.1 Calculating Negative AMS Margin

The desired speed is $1.13V_{stall}$, where V_{stall} is calculated using Equation 54 with the $C_{L_{max}}$ method developed in Section 5.6.1. Vehicle 377 with the old $C_{L_{max}}$ assumption

Table 28: One engine inoperative fixed variables for the minimum drag method.

	Variable	Value	Units
1	V	$1.13V_{stall}$	
2	γ (climb angle)	0	degrees
3	β	0	degrees
4	Altitude	0	ft
5	$\delta_{LEdroop}$	30	degrees
6	T_{left}	$T_{max_{SL}}$	lbs
7	T_{right}	$-0.25T_{max_{SL}}$	lbs
8	MTOW		lbs
9	Fwd CG		

Table 29: One engine inoperative free variables for the minimum drag method.

	Variable	Min	Max	Units
1	ψ (heading)	89	91	degrees
2	θ	5	20	degrees
3	ϕ (roll)	-5	0	degrees
4	α	5	20	degrees
5-15	$\delta_1 \ldots \delta_{11}$	-30	30	degrees
16	$\delta_{rudders}$ (linked)	-30	30	degrees
17	dV/dt	0	$\frac{0.75T_{max_{SL}}}{m}$	ft/s^2

of 1 was unable to trim at the desired speed, and will be used here to demonstrate the behavior of the AMS Margin with speed.

One hundred random initial conditions were run using the minimum drag trim method for several speeds, specified as multiples of V_{stall}. The trim optimization for this flight condition is more challenging than the others, having low convergence rates and being more susceptible to local optima. The minimum drag AMS Margin trend shown in Figure 84 is explained with the aid of Equation 55. As velocity decreases, the moment coefficients *required* grow quickly whereas the *available* moment coefficients are independent of velocity at these speeds. A second order polynomial is fit to the AMS Margin belonging to the minimum drag trim solutions at each speed and is used to extrapolate to $1.13V_{stall}$.

$$\Delta M_{req} = \frac{1}{2}\rho V^2 S\bar{c}\Delta C_{m_{req}} \rightarrow \Delta C_{m_{req}} = \frac{1}{V^2}\frac{2\Delta M_{req}}{\rho S\bar{c}} \tag{55}$$

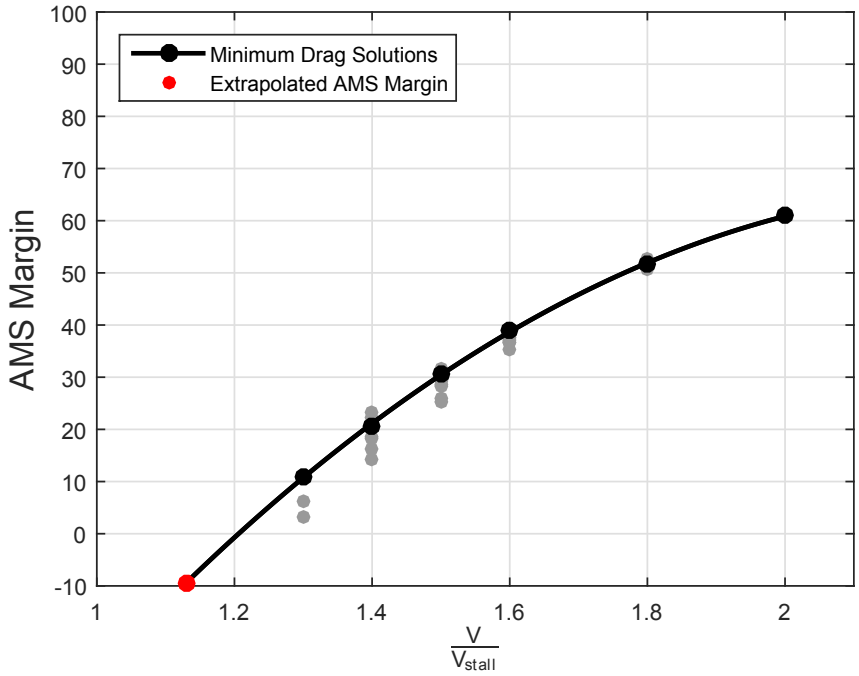

Figure 84: Behavior of AMS Margin with speed for Vehicle 377 in OEI conditions.

The extrapolated AMS Margin value is sensitive to the trim solutions selected at each speed. The presence of local optima and low rates of convergence (Table 30) were introducing variability into the metric. Experiments were conducted (Table 31) to determine the number of random initial conditions to evaluate at each speed and the number of speeds to use in the quadratic curve fit. The most consistent extrapolated AMS Margin (with least variability) occurred in experiment E, with 100 initial conditions at four different speeds. When the desired velocity is infeasible, the low V_{stall} multipliers are also likely to fail or have low convergence rates. For this reason, speeds for extrapolation are tested starting at the high end and continuing to lower speeds until the AMS Margin for four minimum drag trim solutions are available.

Table 30: One engine inoperative convergence rates.

V_{stall} multiplier	1.3	1.4	1.5	1.6	1.8	2.0
Convergence rate	3%	11%	13%	17%	37%	22%

This is a computationally expensive approach to estimating negative AMS Margin for the OEI flight condition. Improvement to convergence rates and reduction in analysis time may be possible with changes to the trim optimization input and constraint scaling. Schedule constraints prohibited further investigation into regularization techniques, but they have been identified as a possible future avenue of research.

Table 31: Various optimization and curve fit settings tested to achieve consistent results.

			Extrapolated AMS Margin	
Experiment	Cases per speed	Pts for curve fit	Mean	Range
A	50	3	-19.21	53.05
B	100	3	-7.78	7.43
C	25	4	-3.10	14.42
D	50	4	-11.34	10.96
E	100	4	-10.62	2.27

5.7.2 Sensitivity to the $C_{L_{max}}$ Assumption

The one engine inoperative flight condition had the same issues with $C_{L_{max}}$ estimates as the go-around maneuver. When it is overestimated, the speeds at which the trim analyses are conducted are too low. In such situations, as was the case for Vehicle 4354, the limiting factor becomes lift not control authority. This can be seen in Figure 85, which shows that the angle of attack necessary to support the Vehicle 4354's weight became excessive prior to reaching the desired minimum control speed. When the OEI flight condition was reevaluated using the the new $C_{L_{max}}$ method and associated V_{app}, the vehicle had sufficient lift and control authority to trim.

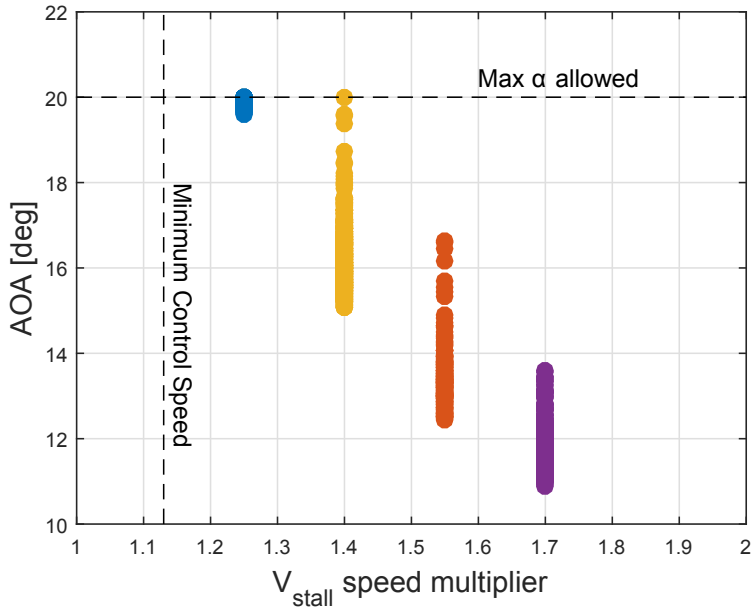

Figure 85: Feasible trim solution angles of attack for Vehicle 4354 in the OEI flight condition.

5.8 One Engine Inoperative on the Ground

This is a yawing moment control authority sizing condition that will be handled exclusively by the vertical tails and rudders. This emergency condition is used to define the minimum control speed on the ground (V_{MCG}), which is used to determine other important takeoff speeds. FAR 25.149 defines V_{MCG} as the speed at which the vehicle can recover from an engine made suddenly inoperative with a deviation from the centerline of 30 feet or less, with no sideslip or nose wheel steering. No constraint is specified for this speed, so the analysis is conducted at the takeoff rotation velocity V_R. Also, this flight condition is treated as a static single axis balance of moments in the body rather than a dynamic simulation in order to get a rough estimate of the adequacy of the yawing moment control authority. The rudders are required to balance the yawing moment generated by the left engine at full thrust, and the right engine is assumed to produce no net force. The vehicle is configured for takeoff with a 30 degree drooped leading edge, fully loaded with fuel and cargo, assuming the

forward CG.

The aerodynamic moment required (Equation 56, where Δy is the distance of the thrust line from the centerline) must oppose the engine moment and is achieved with trailing edge left rudder deflections. The maximum available moment ($M_{yaw,max}$) is estimated by running VORLAX with both rudders deflected 30 degrees in ground effect. These values are compared to quantify AMS Margin using Equation 57.

$$M_{req} = -T_{SL,max}\Delta y \tag{56}$$

$$\text{AMS Margin} = 1 - \frac{M_{req}}{M_{yaw,max}} \tag{57}$$

5.9 Takeoff Rotation Maneuver

To analyze the takeoff rotation maneuver the equations of motion had to be rederived and solved externally to the MASCOT trim analysis tool. This was necessary due to the way some of the parameters were treated by MASCOT. In particular the main gear normal force and rolling friction force were treated as unknowns when their values could have been derived. Internal MASCOT constraints bounded the normal force in a way that prevented convergence when lift was negative (consistently true for the HWB). In addition, the gear friction force (treated as a free variable) was always pushed incorrectly to zero by the trim optimizer. Both of these main gear problems led to significantly underestimated nose-down pitching moments.

This maneuver is the transition between runway acceleration and climbing flight. It occurs at the takeoff rotation speed output by the FLOPS performance analysis. This can be as low as $1.05V_{stall}$ but may be increased by FLOPS if a thrust deficiency would otherwise prevent climb constraints from being met. At that speed the vehicle must achieve a nose-up pitch acceleration of +3 deg/s^2, with a nose gear force equal to zero, and $T_{max_{SL}}$ from both engines. Linear acceleration should be positive but is

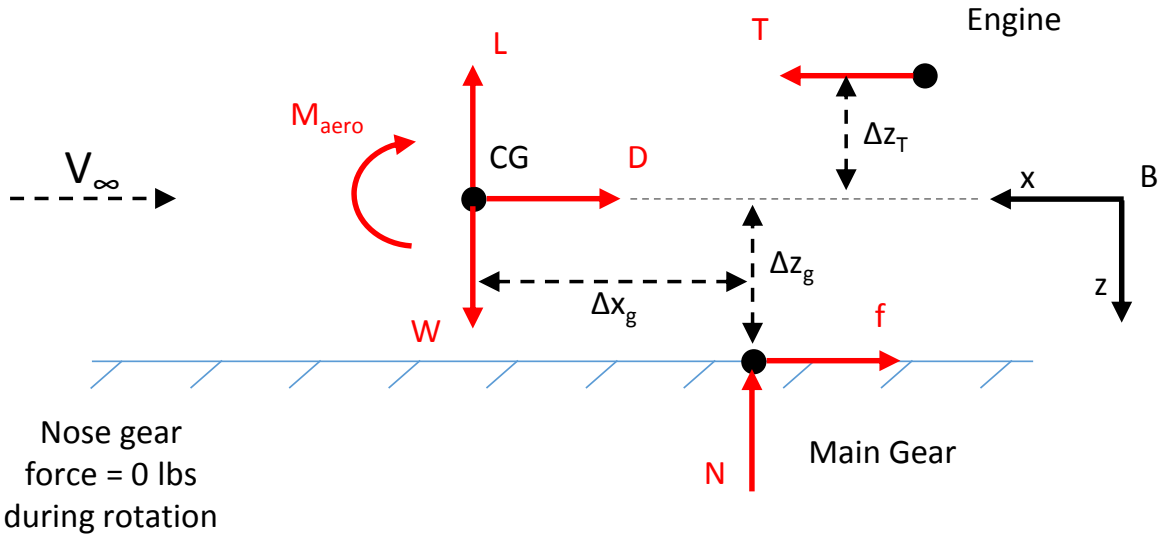

Figure 86: The free body diagram for the takeoff rotation maneuver.

otherwise unconstrained.

A free body diagram for this maneuver was constructed in Figure 86 under the assumptions listed in Table 32. Summing the forces along the body x and z axes results in Equations 58 and 59, respectively. Summing the moments about the center of gravity results in the residual equation (Equation 60) to be balanced.

Table 32: Assumptions used in the derivation of the EOMs.

Assumptions
Net force parallel to velocity unconstrained
Net force perpendicular to velocity is zero
Net moment about CG (body y-axis) is zero
Body x-axis, the thrust line, and the velocity vector are all aligned.
Angle of attack is zero.

$$\frac{dV}{dt} = \frac{T - D - f}{m} \tag{58}$$

$$N = W - L \tag{59}$$

$$\text{where} f = \mu N$$

$$residual = M_{aero} - T\Delta z_T - N\Delta x_g - f\Delta z_g - I_{yy}^{CG}\ddot{\theta} = 0 \tag{60}$$

The only parameter to be solved is the deflection angle for the elevons (Table 33). Early experiments attempted to use the centerbody elevon in isolation but that was found to provide insufficient control authority. Instead elevons 3-9 shown in Figure 87 are used, which is consistent with the way Boeing performs the maneuver.[16] The remaining state variables are fixed as specified in Table 34.

Table 33: Takeoff rotation maneuver free variables.

	Variable	Min	Max	Units
1	δ_{3-9}	-30	30	degrees

Table 34: Takeoff rotation maneuver fixed variables.

	Variable	Value	Units
1	V	$V_{R_{FLOPS}}$	
2	α	0	degrees
3	β	0	degrees
4	$\dot{q} = \ddot{\theta}$	3	degrees/sec
5	Altitude	0	ft
6	$\delta_{rudders}$	0	degrees
7	$\delta_{LEdroop}$	30	degrees
8	MTOW		lbs
9	Fwd CG		
10	Both engines $T_{max_{SL}}$		lbs

5.9.1 Challenges for HWB

With the elevon deflection the only free variable and a single residual equation, it becomes possible to visualize the residual and its contributing elements. This done in Figure 88 for Vehicle 377, which does not have enough control authority to perform the maneuver. The two primary contributors to the residual are the aerodynamic

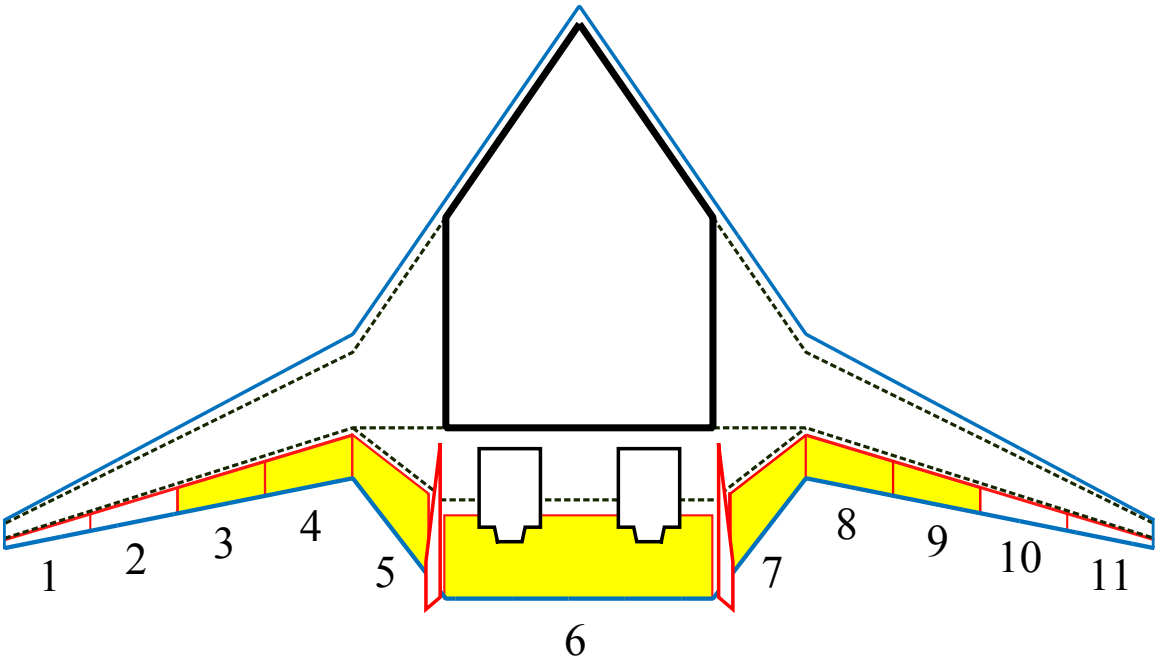

Figure 87: The highlighted elevons on Vehicle 377 are used to perform the takeoff rotation maneuver.

moment and the nose-down moment generated by the main gear normal force. The large main gear moment is caused by more than just the weight of the vehicle. The lift coefficient (Figure 89) at zero angle of attack is negative with faired controls and the negative elevon deflections necessary for nose-up aerodynamic moments create further negative lift. The weight and negative lift of the vehicle combine via Equation 59 to create a large main gear normal force applied aft of the CG which for this vehicle created an insurmountable nose-down moment.

There are several potential ways to improve maneuver performance. Angle of attack increases via longer or extendable nose gears have been proposed in the literature.[144] These would reduce main gear normal force by increasing lift at the cost of additional weight, complexity, and additional nose-down aerodynamic moment due to the increase in angle of attack. Reducing the main gear moment arm would help tremendously but this option is infeasible due to well established aft towing and tail tipping constraints.

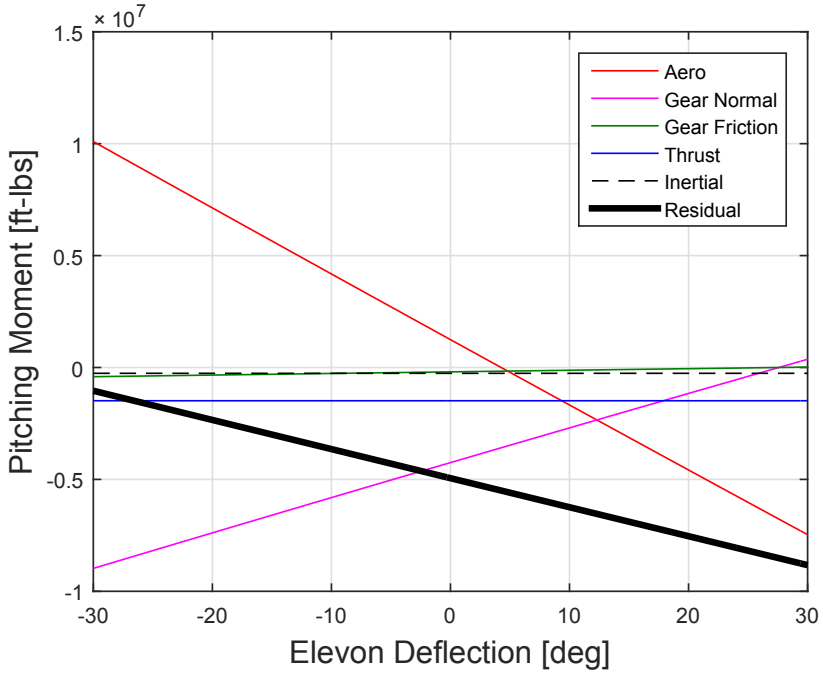

Figure 88: The pitching moment residual equation and its components as a function of elevon deflection.

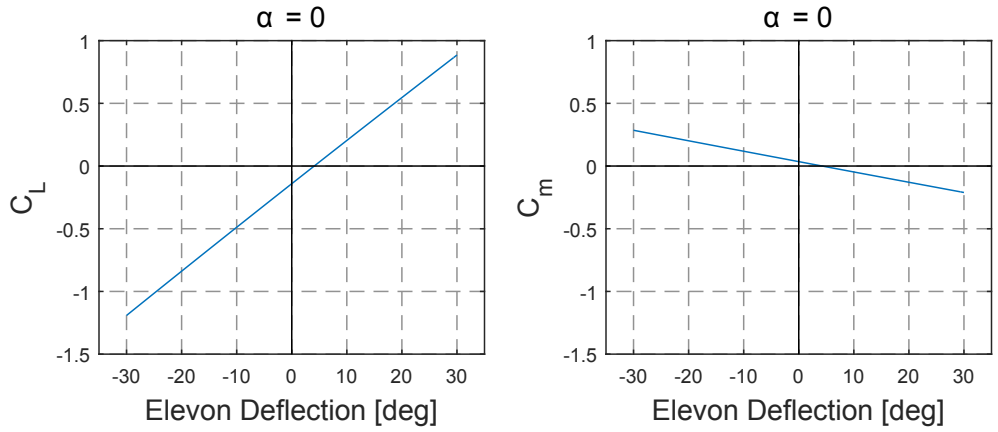

Figure 89: Takeoff lift and pitching moment coefficients for Vehicle 377 in ground effect.

Belly or ventral flaps are another technology option being explored in the literature for the HWB configuration.[129] These are aerodynamic control effectors positioned underneath the aircraft near the CG. When deflected 90 degrees into the flow they increase the static pressure in front of the CG and decrease aft, creating a nose-up pitching moment. This aerodynamic phenomenon (driven by separation effects) is not modeled in VORLAX and not enough data was available in the literature to size it with confidence. Higher fidelity modeling with CFD would be necessary to evaluate this technology.

A simple operational change such as increasing the takeoff rotation speed would give the elevons additional control authority. This option would come at the cost of increased takeoff field length. If the vehicle takeoff field length is under the maximum allowed then this trade-off could be a viable option.

Finally, the option that will be explored in this dissertation is to make changes to the vehicle geometry. Extension of the trailing edge will give the centerbody elevon a greater moment arm. The deflection of the elevon for the maneuver creates significant down force on the main gear, so a reduction in centerbody elevon chord fraction may also be beneficial.

5.9.2 Calculating Negative AMS Margin

As shown in Figure 88, the pitching moment residual equation is approximately linear with elevon deflection. Extrapolating the residual shows that a deflection of -37.9 degrees would have been capable of performing the maneuver. With this deflection the required aerodynamic moment increment can be determined and compared to the available nose-up moment from the same elevons (i.e. maximum deflection of -30 degrees). This is sufficient information to use Equation 13 from Chapter 3 to calculate negative AMS Margin, which for Vehicle 377 is -26.5%.

5.10 Landing Nose Hold-off

The landing nose hold-off trim condition ensures that upon touch-down the nose gear will not slam into the ground. The analysis is set up similarly to the takeoff rotation maneuver, using the same EOMs and elevons 3-9. This flight condition is evaluated at the weight reported at the end of descent, the stall speed (Equation 54), and with no rotational acceleration or thrust. This was again driven by the large nose-down moment from the main gear normal force. The trim condition is evaluated at angle of attack zero, which places the greatest force on the main gear.

5.11 Conclusion

In the process of setting up the control authority assessments new issues were discovered, and the root causes were found and corrected. The unexpected difficulty in meeting the minimum throttle constraint made the addition of a speed brake to the control surface layout necessary. This was an update or feedback to the initial design choices from Chapter 3, driven by the new insights generated during detailed analyses. This difficulty in generating drag for descent is probably the reason behind the X-48B's use of clamshells. This design feedback step and design rationale discovery matures the answers to research question 1.1.

Forcing the elevons to generate drag to meet the minimum throttle constraint reduces control authority remaining for trimming. The minimum drag method was robust to this issue, whereas the direct allocation method was not. The minimum drag method was also needed for sizing the clamshells, which was the determining factor for selecting it as the trim method for the HWB control authority assessments in MDO. The algorithm definitions for evaluating each flight condition are other important aspects of this chapter. The combined contributions of this chapter and the previous one are sufficient to resolve research question 1.4 regarding how the trim analysis should be conducted to support HWB MDO. Establishing the trim analysis

method is also an enabler to the control surface layout design method, which can now be implemented in the next chapter.

CHAPTER VI

MULTI-DISCIPLINARY CONTROL SURFACE LAYOUT DESIGN METHOD

6.1 Introduction

RQ1.1: What control surface type and arrangement options are available and what justifies specific choices made for HWB designs in the literature?

RQ1.2: How should the number of control surfaces be chosen?

RQ2.1: What disciplinary metrics and design considerations might influence the number of redundant control surfaces?

Hybrid Wing Body designs use a redundant number of elevons, which are multi-axis control surfaces capable of providing both pitching and rolling moments. Their division of function is not as clear-cut as it is for aileron/elevator controls on conventional tube-and-wing (T&W) aircraft. This complicates the control surface and actuator sizing process. For instance, there is some potential ambiguity with regard to Federal Aviation Regulations (FARs) that specify requirements for "the longitudinal control" or for the "aileron." Such conventional control surfaces have no clear or unique counterpart on the HWB unless a simplified linked elevon or "ganging" approach is used. Redundancy also results in the existence of non-unique deflection combinations for trimming or maneuvering the vehicle.

For the HWB designs listed in Table 35, the span-wise spacing of elevons appears to be uniform except where curvature or engine integration makes that impractical. On the outer wing the elevons typically have constant chord fractions limited by the location of the rear spar. In the transition region between the outer wing and

centerbody there is a rapid (sometimes nonlinear) change in chord, so constant chord fractions are not used. Instead the hinge lines remain parallel to the rear spar whose segments are roughly aligned with trailing edge curvature. There is unexplained variation in the number of redundant elevons in the HWB literature, and with the exception of the ACFA 2020 Final, the decision processes that led to a specific number were not found.[80]

Table 35: Variation in number of redundant elevons on HWB configurations.

Vehicle	**# Redundant Elevons**
N2A	8
B-2	9
X-48C	10
ACFA 2020	10
N2A-EXTE	11
Boeing 800 PAX	12
VELA 2	12
BWB6-250B	13
X-48B	14
VELA 1	14
OREIO	15
ACFA 2020 Final	23

As noted in Chapter 2, fixed layouts are used during planform optimization in the HWB MDO literature.[146, 86, 74, 140] The size and number of redundant elevons are determined a priori, and control authority deficiencies are resolved with planform changes alone. Justification for the decisions leading to these initial control surface layouts are absent from the literature. Bonet et al. describe Boeing's initial design stage as geometry definition where the stability and control (S&C) discipline is sometimes involved.[16] This is presumably where their CS layout decisions are made but the methods used are not revealed.

It is clear that the dimensions and number of redundant elevons on a HWB design should be determined from considerations of several disciplines. The objective of this chapter is to compare several control surface layout alternatives using a system

level metric that synthesizes key disciplinary concerns. The control surface layouts considered were variations of the layout for the N2A-EXTE HWB configuration, which was selected due to the availability of geometric and aerodynamic data in the public domain.

6.2 Potential Stakeholders in the Control Surface Layout Design Problem

6.2.1 Aerodynamics

Several studies have investigated optimizing elevon deflections to modify lift distributions and minimize drag.[5, 4, 110, 66, 30] A method from Guerreiro & Hubbard is noteworthy because the authors varied the number and spacing of trailing edge control surfaces to minimize drag, with a goal to achieve an elliptical lift distribution.[57] They observed that the error between the desired and achieved lift distribution asymptotically approached zero, and did so rapidly with diminishing returns as the number of controls was increased. In addition it was found that the optimal spacing followed an approximately cosine distribution, which implied larger surfaces inboard and smaller surfaces outboard. Using this type of approach there will be no optimal number of elevons. The designer must decide when drag minimization has reached a satisfactory level.

Minimizing drag at a design flight condition (i.e. cruise) is in the domain of the aerodynamicist. For the HWB the convention is to design the planform, twist, and camber distributions to trim without deflections at the cruise design point.[87] Therefore if convention is followed, the number and spacing of trailing edge control surfaces will not impact cruise drag via trim drag. Instead the effect will be indirect, through a change in vehicle weight (ΔW), which changes the design lift coefficient (C_L) and resulting lift-to-drag ratio (L/D).

6.2.2 Actuation Subsystem Sizing

The design of the flight control actuation system for a HWB will have to be considered relatively early in the design process, since an increase in secondary (non-propulsive) power requirements stemming from control surface actuation has already been identified as an area of concern for these concepts.[77, 113, 16] A preliminary (and overly conservative) estimate of actuation power requirements is given by the "corner power" P_{cp}, which for control surfaces may be expressed as:

$$P_{cp} = M_{h_{max}}\ \omega_{max}, \tag{61}$$

where $M_{h_{max}}$ is the maximum control surface hinge moment and ω_{max} the maximum control surface angular rate. The hinge moments would be estimated from trim analyses at various off design conditions and angular rate would be driven by stability augmentation requirements. A general expression for the hinge moment is given by

$$M_h = \bar{q} S_f c_f C_h, \tag{62}$$

where $\bar{q}, S_f, c_f, C_h$ are respectively the dynamic pressure, control surface planform area, control surface chord, and hinge moment coefficient.

The elevons on a HWB configuration have smaller moment arms as they are closer to the aircraft center of gravity (CG) than elevators on conventional aft-tail configurations.[132] In order to obtain sufficient pitch control authority, the total elevon planform area needs to be large, which leads to the apparently universal decision to make the elevons span the entire trailing edge. Roman et al. describe a "square-cube law" (also clearly seen in Eq. 62), which demonstrates that as the control surface area increases proportionally to the square of the scale ($\propto [L]^2$) and the actuating hinge moment grows proportionally to the cube of that scale ($\propto [L]^3$).[113] Therefore as the the HWB passenger class and scale increases, the magnitude of the required actuating hinge moment grows significantly.

In addition to this, stability and control requirements may result in large control surface rate demands from the flight control system. Charrier notes that for current conventional aft-tail designs, rates as high as 60°/s may be necessary to provide a satisfactory dynamic response.[23] As pointed out by Boeing, these significant actuator rate and bandwidth requirements contribute additionally to the secondary power requirement.[16]

Regarding the issue of what actuation architecture to use, centralized hydraulics have reached a point of technology saturation. Electric drive systems are experiencing a rapidly improving power-to-weight ratio, making them a viable alternative for HWBs with a target entry to service of 2025 (ERA N+2 timeline). The method developed in this chapter considers the "simplex" Electrohyrostatic Actuator (EHA) as the actuating device for all HWB control surfaces, relying heavily on the work and expertise of Chakraborty and Trawick.[19, 20] The performance of each control surface layout was considered relative to a HWB baseline for which an EHA system was also sized.

As the focus of this chapter is to investigate the optimal number and spacing of control surfaces, no detailed failure mode and effects analysis was performed. This might normally be performed in order to determine the minimum number of redundant actuators needed on each elevon in order to satisfy failure probability requirements. Instead, the following design rules (influenced by Boeing and Airbus best practices) were adopted in lieu of such a study.[149, 135]

1. A control surface, if deemed flight-critical from stability, controllability, and trim assessments, would be actuated by no fewer than three parallel electric actuators.

2. A control surface, if deemed not flight-critical, would still be actuated by no

fewer than two parallel actuators, in order to guarantee a higher level of availability.

3. The centerbody elevon, owing to its substantial actuation load and flight-criticality, would be actuated by no fewer than four parallel electric actuators. Even though three independent energy systems were assumed to exist in the airplane, no detailed investigation was performed to determine the method of supplying four parallel actuators from three independent energy sources without risking common-mode failures through the loss of a single energy system.

6.2.3 Stability and Control

The worst-case hinge moments that drove the actuator sizing requirements were estimated from trim analyses at various off-design flight conditions, maneuvers, and control failure scenarios. These analyses drew upon the experience gained in Chapters 4 and 5.

The behavior of a control surface subsequent to a failure is dependent on the type of actuation system employed. The failed control surface can be modeled as being free-floating, stuck at a neutral (faired) position, or stuck at an adverse deflection. Failure in an adverse (i.e. hard-over) deflection is a more challenging condition, and therefore a more conservative assumption. The remaining control surfaces will have to counter adverse moments due to the stuck elevon and still trim the aircraft and perform maneuvers. A flight-critical control surface is defined herein as one whose adverse failure results in a vehicle that cannot be trimmed. To enforce the set of design rules described previously, it was important to identify the flight-critical control surfaces so that the minimum number of control surface actuators could be determined.

This analysis differed from analyses by Wildschek and Maier with regard to the policy governing the inclusion/exclusion of flight-critical elevons.[147, 80] In those works, an Electromechanical Actuation (EMA) system had been considered which has

the possibility of a jamming failure scenario. In such a scenario, actuator redundancy cannot overcome the jammed actuator. As a result, a design rule was imposed to not tolerate flight-critical control surfaces. This resulted in large-span elevons being divided into two or three smaller surfaces as required to remove their flight-criticality. The design rule resulted in a CS layout featuring 23 elevons, up from the baseline design which had 10.

In this analysis, elevons are actuated by two or more EHAs. These EHAs have benign failure modes, and in the case of a failure the redundant actuators are able to continue driving the control surface. Failures that would result in a catastrophic outcome such as loss of vehicle are mandated by regulation to be extremely improbable. Further, there is potential for vehicle-level actuation system weight savings arising from the use of flight-critical elevons. If an elevon is split spanwise into two equal halves, then the hinge moment requirement for each is essentially halved but this does not lead to a corresponding halving of the weight of electric actuators. Taking into account the multiple actuators per control surface, it is likely that the sum of the weights of all actuators combined will actually increase. The combining of adjacent elevons into surfaces with larger span warranted by the above observation will be explored.

6.2.4 Selection of a Mission Level Metric for Optimization

Three primary stakeholder metrics were tracked in this study. They are 1) drag at trimmed cruise conditions, 2) actuation system weight, and 3) required actuation power during cruise. The components of the Breguet range equation are well aligned with the selected stakeholder metrics (Figure 90) and it is used in this study estimate fuel burn, a system level metric and important ERA program goal.[143] Fuel weight for a 6,000 NM design mission will be the basis for comparison between control surface layout alternatives. The equation is given below:

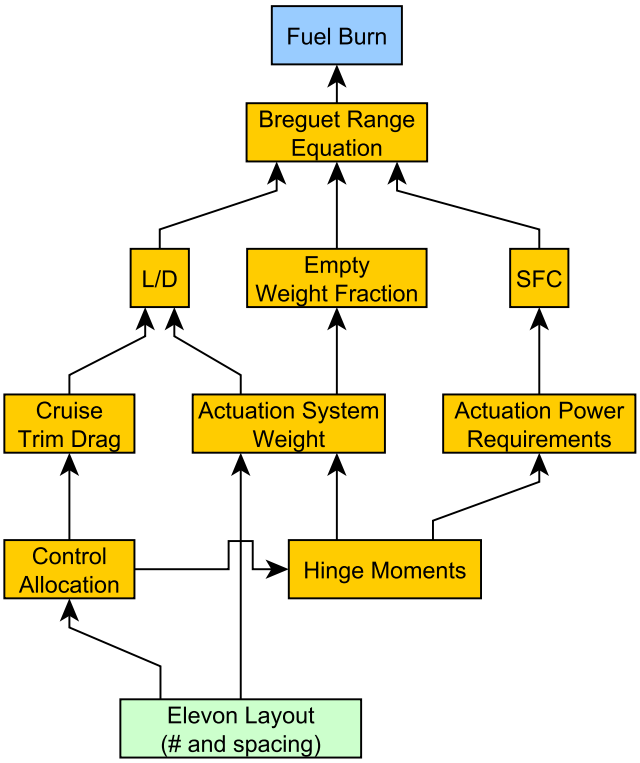

Figure 90: The elevon layout affects the system level metric through a hierarchy of disciplinary analyses and metrics.

$$R = \frac{V}{c_t}\frac{L}{D}\ln\frac{W_{initial}}{W_{final}} \tag{63}$$

where flight velocity (V), thrust specific fuel consumption (c_t), and lift-to-drag ratio (L/D) are assumed constant over the length of the cruise segment. Range (R) and V are fixed parameters defined by the mission. $W_{initial}$ must be solved for, which will then provide fuel weight: $W_{fuel} = W_{initial} - W_{final}$.

6.2.4.1 Fuel burn due to change in actuator subsystem weight

There are several effects caused by changing actuation system weights. The first is a change in the lift required for steady level flight. This requires a different angle of attack, which affects the drag, the required thrust, and therefore the required fuel flow. The change in angle of attack also changes the pitching moment, which

will require deflections to trim or retwisting of the wing. At the design cruise flight condition, the trim drag should not vary with the number of elevons because the wing is typically twisted to achieve trim without deflections.[87] In this study, vehicle geometry was fixed and the vehicle was re-trimmed at cruise using the centerbody elevon. Therefore changes in L/D were captured by re-trimming the vehicle with the new actuation system weights.

Another effect of changing actuation subsystem weight will be in the empty weight fraction of the Breguet range equation. Shifts in CG are expected to be negligible based on the actuation system mass relative to the whole vehicle. Shifting fuel between tanks could easily counter adverse changes to the CG, and therefore in this study it was fixed at its baseline position.

6.2.4.2 Fuel burn due to change in actuation power

Excessive actuation power requirements (which add to non-propulsive or secondary power requirements) have been noted frequently for the HWB configuration.[77, 113, 16] It remains a high-risk area that requires attention from a number of disciplines to solve. Both the HWB hinge moments and deflection rates are large and contribute to the problem.

Ignoring or postponing analysis of actuation power requirements may lead to a situation where the power required exceeds that available from the engines or auxiliary power units.[113] Even if the engine is adequately sized, high actuation power requirements adversely affect specific fuel consumption and reduce the HWB's ability to meet NASA's N+2 fuel burn goals. If the actuation power requirements cannot be reduced, then Boeing has suggested that it would make configuration changes despite penalties to fuel burn and noise.[16]

As will be shown in a later section, there is a large amount of uncertainty surrounding actuation power. Control law design studies under different control surface

usage scenarios are needed to reduce this uncertainty. The research described in this chapter approximates FCS activity with parametric sinusoidal deflection perturbations about the trim deflections. A physics-driven investigation into actuator power requirements under various control utilization and turbulence scenarios was explored in a follow-up study.[47]

6.3 Analysis Setup

The N2A-EXTE is a non-proprietary HWB design whose geometry, performance, and weights were available from NASA.[1] Low-speed wind tunnel data and high-speed CFD simulations serve as validation of the aerodynamic model used in this study.[49, 72] The aerodynamic model for trim analyses was generated with VORLAX, whose accuracy is limited to flight regimes with attached flow. It should be noted that the trim analyses investigated in this study sometimes require large deflections that may violate these assumptions.

The vehicle has 11 redundant elevons along the trailing edge of the wing, two centerbody mounted vertical tails with rudders, and a drooped leading edge high-lift device. An exploration of design alternatives was performed for the elevon layout. Several alternatives that were convenient to construct from the N2A-EXTE VORLAX model are shown in Figure 91. Combined control surfaces need only be ganged or operated together and their hinge moments summed. An initial analysis of the baseline elevon layout revealed that only the centerbody elevon (# 6) met the criteria for a flight-critical control surface. For this reason and the decision to use EHAs, no splitting of elevons was deemed necessary.

[1] Courtesy of Craig Nickol, aerospace engineer at the NASA Langley Research Center working on the ERA program.

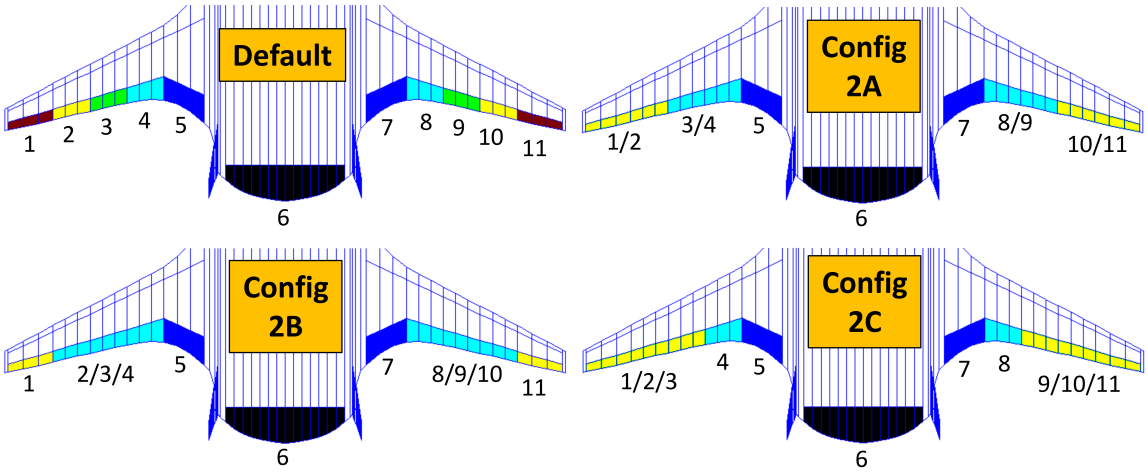

Figure 91: Proposed N2A-EXTE control surface layout alternatives.

6.3.1 Estimation of Aerodynamic Hinge Moments

For a conventional aft-tail configuration, the flight conditions yielding the maximum hinge moments are specified by the Federal Aviation Regulations (14 CFR §25) (Table 36) and should be evaluated at different points of the altitude-speed flight envelope.[1, 123, 122, 124] Unfortunately the FAR requirements do not translate well for the HWB. For instance, FAR 25.349 calls for analysis of roll rates caused by full aileron deflection to the stops. The HWB does not necessarily have any dedicated roll devices. With elevons, whose functions include generating both pitching and rolling moments, there is some ambiguity in how they should be used to comply with the FAR.

Table 36: Maximum hinge moment flight conditions for aft-tail aircraft.

Control	FAR	Description
Aileron	25.349	Rolling conditions
Elevator	25.255	Out-of-trim characteristics
Rudder	25.147	Minimum control speed
	25.351	Yaw maneuver conditions

In the ERA Subscale Test Vehicle final report, Boeing provides a list of flight

conditions used to test a HWB design for adequate control authority in early design phases.[16] These ten flight conditions should induce the largest and most saturated deflections. A subset of these flight conditions was used to demonstrate actuator sizing and control surface layout evaluation. They are 1) symmetric approach, 2) crosswind approach, 3) takeoff rotation maneuver, and 4) one engine inoperative (OEI) go-around. In addition there were $2n$ failed control surface trim analyses for the crosswind approach and OEI go-around, where n is the number of elevons. An average power draw during cruise is needed and therefore a nominal cruise flight condition was also evaluated.

Ultimately the trim and maneuver analyses provided a table of $5+4n$ trim solutions where n is the number of elevons. The actuators of each elevon were sized to its highest magnitude hinge moment experienced during any of these tests.

6.3.1.1 The Trim Analyses

The trim optimization statement used to perform the trim analyses is given below. The minimum drag method described in Chapter 4 was used to evaluate each of the flight conditions. This approach was previously found to reliably provide low drag trim solutions without unnecessarily saturated controls or otherwise undesirable deflections.[45, 48] When this study was being conducted, the minimum throttle constraint had not yet been identified as an issue and was not enforced.

$$
\begin{aligned}
\underset{S}{\text{minimize}} \quad & Drag\ (\mathbf{S}) \\
\text{subject to} \quad & S_i = a_i,\ i = 1, \ldots, l. && \textit{Flight/operating conditions} \\
& b_i \leq S_i \leq c_i,\ i = l+1, \ldots, m. && \textit{State variable side constraints} \\
& residual_j = 0,\ j = 1, \ldots, 9 && \textit{EOM residual constraints}
\end{aligned}
$$

The state vector manipulated by the trim optimization is partitioned into free and fixed variables. These partitions are flight condition specific and are specified in

Table 37. During the failure analyses, individual elevons were fixed at their minimum or maximum deflection. Elevons whose failure prevented the vehicle from achieving trimmed flight in any flight condition were designated flight-critical. The results of the failure analysis for each layout alternative are provided in Table 38. An interesting result is that, with the exception of the centerbody elevon, none of the elevons in the baseline layout are flight-critical.

Table 37: Summary of actuator sizing flight conditions.

Parameter	**Symm. App.**	**X-wind App.**	**TOR**	**OEI-GA**	**Cruise**
Elevon def. δ_i, deg	[-30, 30]	[-30, 30]	0	[-30, 30]	0
Centerbody def. δ_6, deg	[-30, 30]	[-30, 30]	[-30, 30]	[-30, 30]	[-15, 15]
Rudder def. δ_r, deg	0	[-30, 30]	0	[-30, 30]	0
L/E droop δ_{LED}, deg	30	30	30	30	0
Approach spd. V_{app}, kts	1.3 V_s	1.3 V_s	-	-	-
Rotation spd. V_R, kts	-	-	1.1 V_s	-	-
Go-around spd. V_{ga}, kts	-	-	-	1.13 V_s	-
Cruise speed M_{cr}, Mach	-	-	-	-	0.8
Fwd. accel. $\dot{V}$, ft/s^2	-	-	[0, ∞]	[0, ∞]	-
Angle of attack α, deg	[5, 20]	[5, 20]	0	[5, 20]	[0, 5]
Flt. path angle γ, deg	-3	-3	0	0	0
Heading ψ, deg	90	[89, 91]	90	[89, 91]	90
Pitch angle θ, deg	$\alpha + \gamma$	[2, 17]	0	[5, 20]	α
Roll angle ϕ, deg	0	[0, 5]	0	[-5, 0]	0
Sideslip β, deg	0	$\tan^{-1} \frac{V_{wind}}{V_{app}}$	0	0	0
Pitch accel. $\dot{q}$, deg/s^2	-	-	3	-	-
Altitude h, kft	0	0	0	0	See below
Weight W, lb	343,660	343,660	MTOW	MTOW	See below
Pitch M.o.I. I_{yy}, slug-ft^2	-	-	9.87 x 10^6	-	-
Forward CG h_{cg}, % MAC	36.1	36.1	41.7	41.7	See below
Thrust/engine T_{eng}, lbf	[0, T_{SL}]	[0, T_{SL}]	T_{SL}	T_{SL}	[0, T_{SL}]

MTOW = 471,599 lbs, T_{SL} = 76,733 lbf, V_{wind} = 35 knots
The cruise trim condition was evaluated at the most favorable CG (forward) at segment start, middle, and end (altitudes 35.3, 38.1, and 41.0 kft). Corresponding vehicle weights were 460,879 lb, 402,855 lb, and 344,830 lb. CG positions were 41.2 %, 37.8 %, and 36.2 % MAC. The average hinge moments and L/D were used to calculate inputs to the Breguet range equation

6.3.1.2 A Physics-based Approach for Estimating Hinge Moments

A physics-based approach was used to estimate the hinge moments for this study. A VORLAX geometry model for the N2A-EXTE was constructed and validated using low-speed wind tunnel test data.[49] Lift and moment curves as a function of elevon deflection were shown to have good agreement for moderate angles of attack and

Table 38: Layout flight mechanics analyses (Elevons numbered and combined as shown in Figure 91, flight-criticality denoted by (*), HM: max. hinge moment).

Baseline		**Layout 2A**		**Layout 2B**		**Layout 2C**	
Elevon #	HM (kNm)	Elevon #	HM (kNm)	Elevon #	HM (kNm)	Elevon #	HM (kNm)
1	31.0	1/2*	36.1	1	32.3		
2	16.8					1/2/3*	55.3
3	22.9	3/4	59.4	2/3/4*	75.4		
4	33.4					4	26.5
5	30.9	5	46.2	5*	25.9	5*	33.4
6*	131.7	6*	131.1	6*	144.7	6*	146.8

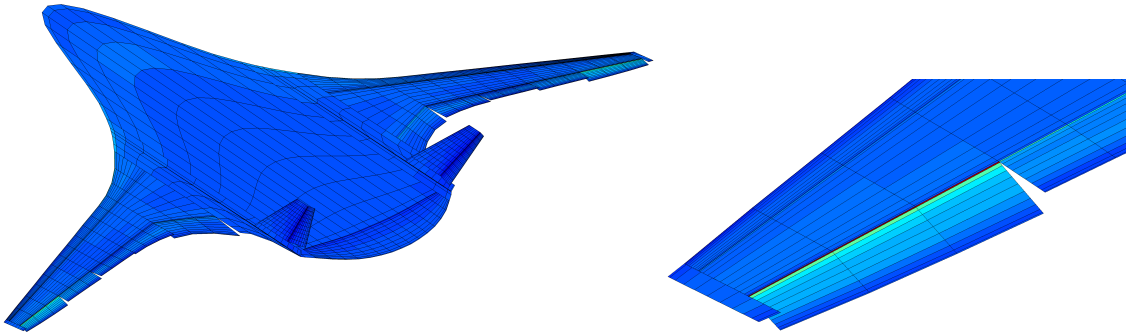

Figure 92: C_p visualization for N2A-EXTE VORLAX model.

deflections (i.e. attached flow).

The control surfaces were modeled as distinct panels from the wing as shown in Figure 92. The hinge moments were calculated by taking the moment of the control surface C_p distributions about their respective hinge lines using Equation 64. The limitations mentioned previously still apply, in that separation effects would tend to increase the hinge moment beyond what VORLAX predicts. The consequence of this is that the actuators may be undersized and the power underestimated.

$$M_{\text{hinge}}(\delta) = \sum_{\text{flap panels}} \underbrace{q_\infty S_{\text{flap panel}} C_{p_{\text{flap panel}}}(\delta)}_{\text{normal force}} \underbrace{x_{\text{flap panel}}}_{\text{moment arm}} \tag{64}$$

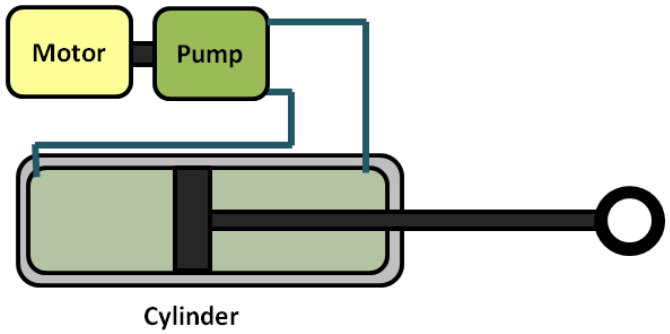

Figure 93: Simplex Electrohydrostatic Actuator (EHA).

6.3.2 Electrohydrostatic Actuator Model

A component weight build-up method is used to size electrohydrostatic actuators (Figure 93) rather than a power-to-weight ratio method. This physics-based approach sizes the actuators according to the actual loads experienced, and the models and methods to do so were developed by Chakraborty et al.[19, 20] The weight of the major components were estimated, summed, and multiplied by a 1.15 correction factor determined by comparison to data available in the literature.

The EHA models were optimized for weight (W_{EHA}) as a function of pump displacement (i.e. theoretical volume pumped per unit revolution of the pump, D_{pump}), given the following design requirements: actuator maximum output force (i.e. stall load, F_{max}), maximum ram speed (v_{max}), and stroke (Δx_{max}). An additional constraint necessary for reasonable designs was a maximum allowable motor RPM of 15,000, and maximum pump pressure was fixed at 34 MPa (5,000 psi). A surrogate model of the weight-optimized actuators as a function of the load-speed-stroke design requirements was provided by Chakraborty for use in this study.[43, 46] This optimization was performed off-line rather than in-line so that aerodynamic models and trim analyses (which supply the worst-case actuation loads) could be developed in parallel. The force-to-weight ratios of the optimized actuators were generally found

to agree with a value of 2.2 kN/kg, the reported value for electric actuators on the Airbus A380.[136]

6.3.3 Installation Geometry and Actuation Rules

6.3.3.1 Translating control surface deflection requirements to actuator requirements

This study used a minimum of two actuators per elevon. The spanwise position along the elevon (η_{rel}) and load-ratio (μ) for the actuators was dependent on the number used, and this is listed in Table 39. Flight critical elevons were given three actuators and the large centerbody elevon was given four.

Table 39: Rule-set for determining actuator relative positions and load-ratios.

# of EHAs	Rel. positions (η_{rel})	Load-ratio (μ)
1	0.50	1.00
2	0.33, 0.66	0.75
3	0.25, 0.50, 0.75	0.55
4	0.20, 0.40, 0.60, 0.80	0.40

6.3.3.2 Installation Geometry

Given elevon layout and the number of actuators, the N2A-EXTE airfoil stack was interpolated for airfoils at each actuator span location. Rear spar and elevon hinge lines estimated from three-view drawings provided the distance between airframe and control surface attachment points (Figure 94). The gearing ratio below defines the relationship between the linear motion of the actuator ram and the angular deflection of the elevon:

$$G(\delta) = \frac{\Delta\delta}{\Delta x} = \frac{\dot{\delta}}{\dot{x}} = \frac{\ddot{\delta}}{\ddot{x}} \tag{65}$$

The load requirement for the set of actuators on an elevon based on a worst-case

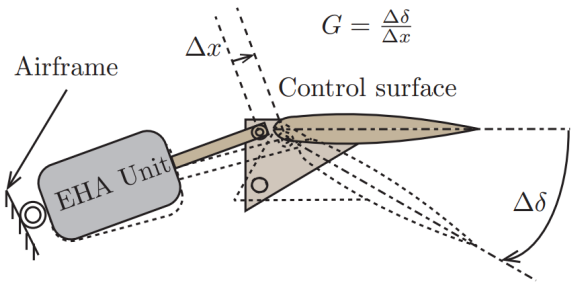

Figure 94: Kinematics of actuator and control surface linkage.

hinge moment (M_h) can be obtained from an energy balance across the linkage, where η_m is the linkage efficiency:

$$F(\delta) = \frac{M_h\ G(\delta)}{\eta_m} \implies F_{max} = \max_{\delta}\left(\frac{M_h^{max}\ G(\delta)}{\eta_m}\right), \tag{66}$$

The speed requirement for actuator sizing is determined through a similar process, where $\dot{\delta}_{max}$ is an assumed maximum deflection rate for the elevon:

$$v_{max} = \max_{\delta}\left(\frac{\dot{\delta}_{max}}{G(\delta)}\right), \tag{67}$$

The final actuator sizing requirement is the stroke of the control surface, given by:

$$\Delta x_{max} = x(\delta_{max}) - x(\delta_{min}), \tag{68}$$

where δ_{max} and δ_{min} are the maximum and minimum (hard-over) deflections of the control surface in question.

6.3.4 Optimizing Actuation System Mass

The lever arm between the elevon hinge and the actuator attachment point is limited by the airfoil geometry at each actuator's span location. This lever arm controls a trade-off between the stroke and speed design requirements for the actuator, and can be chosen to minimize actuator weight. One further optimization was conducted,

allowing the optimizer to choose the lever arm that resulted in a load-speed-stroke yielding the lowest actuator mass from the surrogate model of weight optimal actuators. This optimization was conducted for every individual elevon in a given control surface layout alternative.

The weights of the actuator sets for each control surface layout are listed in Table 40. Earlier a prediction was made that combining elevons would reduce the number of actuators required and also the weight of the actuation system relative to the baseline layout. This was generally observed but layout 2b was an outlier. This is most likely due to the magnitude of the sizing hinge moment on flight critical elevon 2/3/4, which required three actuators. Additional characteristics for the actuators sized for each control surface layout are available in the journal publication of this study by Garmendia et al.[46]

Table 40: Summary of actuation weights for control surface layouts considered.

Layout	**Actuation Weight (kg)**	**Relative to Baseline**
Baseline	1,315	
Layout 2a	1,307	-0.61%
Layout 2b	1,354	+2.97%
Layout 2c	1,257	-4.41%

6.3.5 Power Consumption

The following excerpt from Garmendia et al. is used to explain how the bus power requirements for each actuator is calculated:[46]

> The electrical power requirements for control surface actuation were estimated using the power flow diagram shown in [Figure 95]. The final mechanical output power is the product of the hinge moment and the control surface angular rate ($M_{cs}\ \dot{\delta}$). For n_{act} parallel actuators driving the surface, the hinge moment provided by each was assumed to be $M_h = M_{cs}/n_{act}$. This was used to compute the shaft power output of the motor P_m by accounting for the efficiencies of the mechanical

linkage ($\eta_{link} = 0.9$) and the hydraulic and mechanical components of the EHA ($\eta_{hm} = \eta_{pump}\ \eta_{cyl} = 0.88$):

$$P_m = \tau_m \omega_m = \frac{M_h \dot{\delta}}{\eta_{link}\ \eta_{hm}} \tag{69}$$

The input power to the electrical motor is the sum of the shaft power output P_m and the resistive losses, which are incurred whenever the motor exerts torque, even at a standstill. The resistive losses require the resistance and the current to be computed, which was done by taking a representative motor map for a brushless DC (BLDC) motor and scaling it to have the same max speed and torque as the actuator motor.[41] The motor constant K_v and resistance R were computed by solving the DC motor equations below at two points from the map, where V_{in} was assumed to be the maximum guaranteed bus voltage, one of the points being the full speed/no load point where T_m and I were zero, and another where $I = I_{max}$.

$$V_{in} = IR + K_v\ \omega_m \tag{70}$$

$$\tau_m = K_v I \tag{71}$$

The resistive power P_{res} was then computed as

$$P_{res} = I_{max}^2 R \left(\frac{\tau_m}{\tau_{max}} \right)^2 \tag{72}$$

Finally, the bus power draw P_{bus} was obtained from the motor power input by accounting for the efficiency of the power converter ($\eta_{PC} = 0.95$)

$$P_{bus} = \frac{P_m + P_{res}}{\eta_{PC}} \tag{73}$$

According to a Boeing report, significant margin had been allocated to the actuator rates and bandwidth requirements, which contributed to the excessive actuation

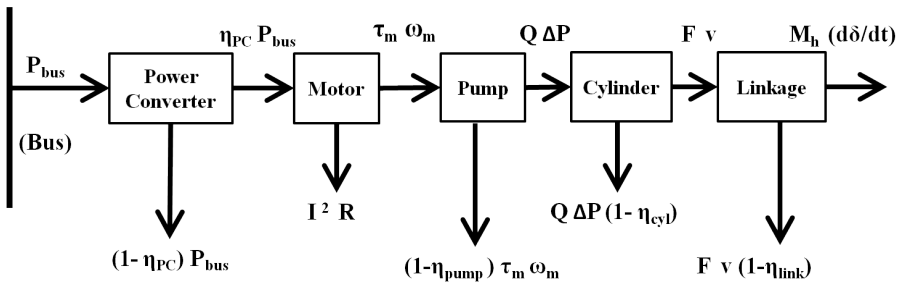

Figure 95: Power flow diagram from electrical bus to control surface.

power problem.[16] One strategy that they recommended was to perform detailed closed-loop control simulations with the aim of reducing those margins. These simulations have not been performed in this study, which led to significant uncertainty in actuation power requirements during cruise. In lieu of a detailed control law design study, the power trends for the nominal cruise condition are shown in the profiler plots of Figure 96.[2] It was assumed for this example that to satisfy stability needs the active control surfaces were deflected in equal magnitude and rate.

These plots show the sensitivity of power to its inputs, and each subplot shows the behavior of the partial derivative. The top row shows the total power required when all elevons are used in unison. The power required to hold the steady cruise trim deflections are shown at a deflection amplitude of zero degrees, and for the baseline CS layout is 80 kW. Control movements required for stabilization of the vehicle were modeled as oscillatory deflections about the cruise trim deflections. Since the centerbody elevon area was large, it was the control surface consuming the most power by far. The bottom row of the profiler plot shows an alternative scenario where the large centerbody elevon was treated as a trim-only device. The underlying assumption was that this surface would not need to be deflected rapidly, and had an irreversible actuating mechanism transmitting no steady-state loads to the driving actuators. Under this scenario the cruise power requirement for the actuation system

[2]This was investigated in greater detail in a follow-up study by Garmendia et al.[42]

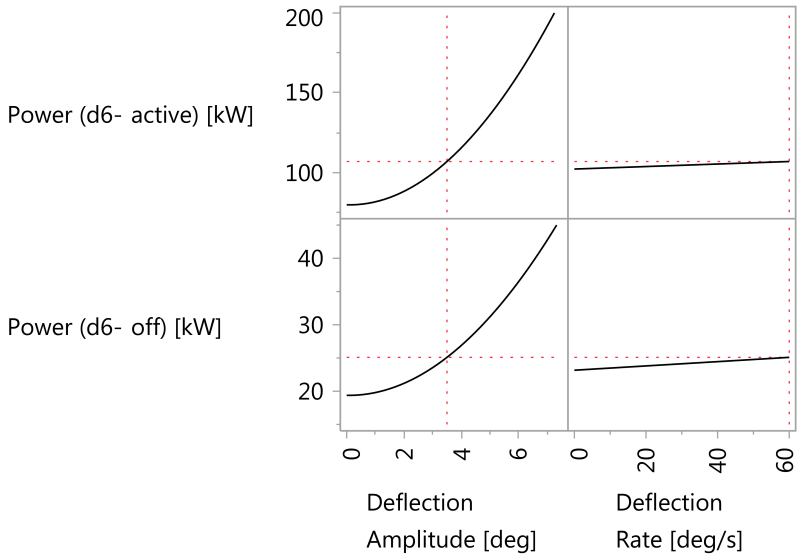

Figure 96: A profiler plot depicting the sensitivity of actuation power to its inputs. In the upper plot, the centerbody elevon is active, while in the lower plot, it is used as a trim-only device.

was seen to be reduced dramatically. That said, the feasibility of stabilizing the aircraft without use of the centerbody elevon must be determined through a control law design study.[2]

The required power for EHAs is known to be driven primarily by hinge moments. The profiler plots show that power is driven primarily by the deflection amplitude, which is correlated with hinge moments. Thus, the behavior of the profiler plot is consistent with expectations.

Fixed values of deflection amplitude and rate (3 deg and 60 deg/s, respectively) were selected for initial evaluations of the alternative control surface layouts (Table 41). The resulting power was taken to be the average power required during the cruise segment, and all of the alternative layouts required less power than the baseline layout. These results show that an actuator power requirement reduction of nearly 10 kW (or 10 %) can be achieved with a control surface layout redesign.

The effect of extracting shaft-power (secondary power) from a gas turbine engine is to increase the fuel flow rate required to continue to maintain the required level of

Table 41: Actuation power requirements at cruise with an active centerbody.

Layout	Required Power (kW)	Relative to Baseline
Baseline	99.44	
Layout 2a	96.37	-3.63%
Layout 2b	89.81	-10.19%
Layout 2c	90.65	-9.35%

thrust, i.e., an increase in the thrust specific fuel consumption (SFC). However, the magnitude of the effect varies from engine to engine, and in this study no detailed analysis of engine cycles was made. Instead, the k_p^*-factor historical method from Scholz was used.[34] Scholz showed that a large number of engines spanning a broad range of thrust showed an almost linear trend when the fuel consumption penalty was modeled as follows:

$$k_p^* = \frac{\Delta SFC/SFC}{P/T_{TO}}, \qquad \Delta SFC = SFC\ k_p^*\ \frac{P}{T_{TO}}, \tag{74}$$

where P represents the shaft-power offtake and T_{TO} the sea-level static thrust of the engine. This relationship, with $k_p^* \approx 0.0094$ N/W, was shown to have reasonable agreement with the published or known SFC penalties for a large number of engines, including those in a thrust class appropriate for the N2A-EXTE.

An example of the SFC changes can be shown for the baseline control surface layout. The average cruise SFC from the N2A final report was 0.504 lbm/(hr-lbf).[72] Uncertainty in atmospheric conditions, required control surface activity, and deflection rates propagate through the Scholz correlation to create uncertainty in the SFC penalty that would be experienced. A Monte Carlo Simulation with uniform distributions was run over the full ranges of the control surface deflection amplitudes and rates. The resulting increase in SFC is shown in Figure 97. This plot demonstrates the range of SFCs as well as a most likely value that could be experienced with the assumed input uncertainty. Reduction of this input uncertainty can be accomplished through closed-loop dynamic simulations in turbulent cruise conditions, and would

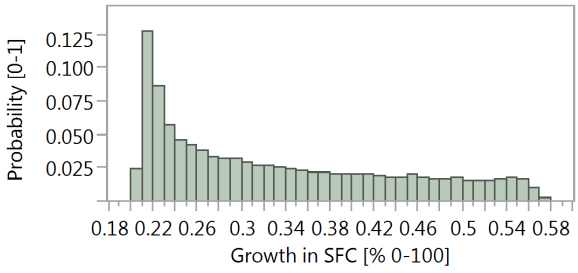

Figure 97: Growth in SFC resulting from power draw of the actuation system for the baseline layout.

result in greater confidence in the SFC increase and impact to total fuel burn.[2]

A sensitivity study was performed and it was noted that the fuel burn metric was most sensitive to SFC. Therefore, the assumed relationship between power extraction and the corresponding change in SFC is important. A higher fidelity engine modeling approach using propulsion system analysis tools such as the Numerical Propulsion System Simulation (NPSS) is recommended for future work.[79]

6.4 Comparing Control Surface Layouts at the Systems Level

The consequences of choosing each control surface layout were propagated to the system level as shown in Figure 90 to estimate required fuel weight for a design mission. Using the Breguet range equation, a constant range of 6,000 NM was imposed and the required fuel weight was post-processed. Each of the alternative layouts were compared to the baseline in the form of fuel weight differences (Eq. 75).

$$\Delta W_{fuel} = (W_{fuel})_{\text{Alt. Layout}} - (W_{fuel})_{\text{Baseline}} \tag{75}$$

In this study the aircraft was not resized, so the layouts were assessed based on their effects on a fixed vehicle. The assumption was made that there was ample volume inside the outer mold line of the vehicle to accommodate the fuel weights observed in this study. Fuel shifting was assumed to keep the center of gravity constant for

all layout alternatives. As mentioned previously, all comparisons were between EHA-driven flight control surfaces, and not between EHA and conventional centralized hydraulics.

The cruise L/D is influenced by changes to the vehicle empty weight from actuation system sizing. It is also influenced by re-trimming the aircraft using the centerbody elevon (all other surfaces faired). The deflection and associated L/D were the average of the start, middle, and end cruise segments. This set of deflections determines the steady hinge moments that drive the cruise power requirements.

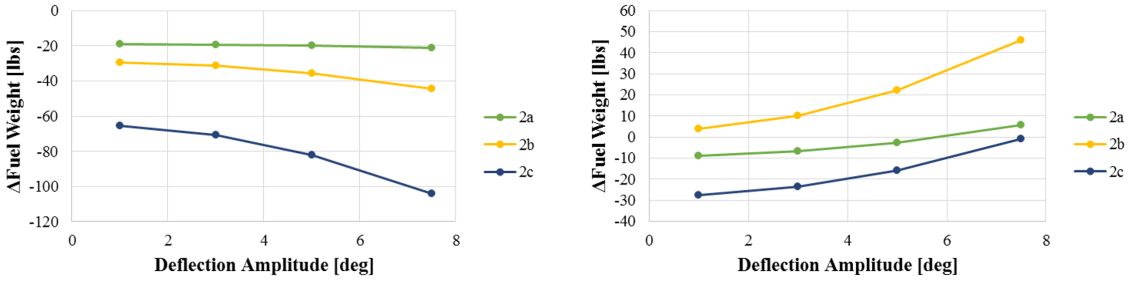

(a) Centerbody elevon active

(b) Centerbody elevon trim-only

Figure 98: W_{fuel} relative to the baseline layout.

Figure 98(a) shows the ΔW_{fuel} comparisons for a scenario in which all elevons were used to stabilize the vehicle. Each of the alternative layouts shows improvement over the baseline. The improvement of layout 2a over the baseline was not sensitive to deflection amplitude, the primary driver of uncertainty. The trends exhibit asymptotic behavior, with the fuel weight differences leveling off at the lower end of deflection amplitude. Layout 2c shows the greatest fuel burn benefit, which grows as control surface activity in cruise is increased. Referring back to Tables 40 and 41, it can be seen that layout 2c was on the low end of required power and had the lowest actuation system weight by far. The 2c layout also has two fewer control surfaces and four fewer actuators than the baseline layout. All of these considerations combined to give it an advantage in fuel burn.

An alternative scenario in which the centerbody elevon is treated as a locked

trim-only device is shown in Figure 98(b). Again similar behavior with deflection amplitude was observed and layout 2c still showed the most improvement over the baseline. The magnitude of improvement is diminished for 2a and 2c and was on-par with the baseline layout at high deflection amplitudes. Layout 2b under this scenario is always worse than the baseline, regardless of deflection amplitude.

6.5 Conclusion

A method was developed to facilitate decision making regarding the design of control surface layouts for the HWB configuration. Likely stakeholders in this design decision were explored and their interests captured in various disciplinary metrics. These were synthesized into a system level metric via the Breguet range equation to estimate fuel burn for a design mission. The method and its demonstration with the N2A-EXTE configuration settle research questions 1.1, 1.2, and 2.1. The level of effort required to perform this analysis was much greater than originally anticipated. This is recommended as a preliminary design study, rather than as an element of the aircraft sizing loop.

While the steps outlined in this method allow for a preliminary assessment of system level impacts of layout alternatives, this study will benefit from higher fidelity analyses. In particular there is great uncertainty in the flight control system requirements which drive the actuation power requirements. The layouts were evaluated on fixed vehicles, but the fuel burn benefits would grow if resizing had been performed. A sensitivity study showed that the mission fuel burn is more sensitive to SFC changes than to empty weight changes. This study would therefore benefit from a higher fidelity engine model to better predict SFC penalties due to power extraction. In addition, there were L/D penalties from trimming the vehicle at cruise with only the centerbody elevon. Re-twisting the wing would be a more appropriate course of action and would improve fuel-burn.

The decision to use EHAs enabled the consideration of control surface layouts with flight-critical elevons. While the alternative layouts were not always lighter in weight than the baseline, they did consistently use less power. In a scenario where all elevons are used by the flight control system, all alternative layouts showed reduced fuel burn. Layout 2c, which has several flight-critical elevons, was found to use the least amount of fuel in the all of the scenarios investigated. It also features a large outboard elevon (1/2/3) that resembles a conventional aileron.

CHAPTER VII

HYBRID WING BODY SIZING ENVIRONMENT

7.1 Introduction

The purpose of sizing an aircraft is to determine the appropriate geometric scale (wing area, S) and propulsive scale (max sea level static thrust, T_{SL}) for a given configuration such that performance and volumetric constraints are satisfied.[92] Determining these scales can be accomplished through iterative constraint and mission analyses which are covered thoroughly by Mattingly.[84] The constraint analysis seeks to define the feasible space for important design parameters such as thrust-to-weight (T_{SL}/W_{TO}) and wing loading (W_{TO}/S). The designer then makes a selection that minimizes engine size (low T_{SL}/W_{TO}) and planform area (high W_{TO}/S), in an effort to minimize weight. The mission analysis seeks to establish the fuel weight fractions necessary to carry out a design mission. The constraint and mission analyses depend on each other which requires initial guesses and iteration. The final step is to use parametric and empirical methods to estimate takeoff gross weight using information from the constraint and mission analyses. These three basic steps to sizing may need further repetitions if the designer wishes to seek improvements through modifications to the aircraft or propulsion configuration. For instance, the aerodynamic characteristics are only constant for 1:1 scaling ratios and if Reynold's number effects are negligible with the scale changes.

Wing loading is a useful design parameter for tube-and-wing (T&W) aircraft. Weight changes as the sizing process iterates, requiring the wing area to scale to maintain a constant wing loading. For T&W aircraft the wing area can be scaled with little impact on the longitudinal trim or dynamic stability characteristics by

shifting the wing along the fuselage to maintain the center of gravity (CG) position and by maintaining tail volume coefficients. For HWB sizing, scaling the wing is more challenging. The HWB centerbody must maintain a specific size to hold the design payload, analogous to the fuselage of a T&W. It is not appropriate to scale the centerbody cabin region up or down, as the payload does not change during sizing. Attempts have been made in the HWB literature to perform sizing with constant W_{TO}/S.[126, 97] The approach taken by Schutte et al. maintained a fixed centerbody and scaled the outer wing with a 1:1 ratio, changing the S&C characteristics in unknown ways (because they were not measured in that study). Dramatic and detrimental shifts to the vehicle CG and aerodynamic center are an example of potential problems caused by such a method. Correcting the vehicle moment balance would require configuration changes (such as changes to sweep), forcing the designer to revisit the constraint and mission analyses. In addition, Wakayama of Boeing has also identified conventional sizing approaches as problematic for the HWB configuration: "... existing tools that size thrust and wing area do not properly handle geometric changes to the BWB or account for important BWB constraints."[146]

Observation: W_{TO}/S is a difficult parameter to use independently for HWB design because wing scale cannot be decoupled from S&C metrics. Other parameters would need to change simultaneously to maintain a balanced vehicle.

An alternative approach explored in the literature and this dissertation is to allow an optimizer to simultaneously change the planform shape and scale, while seeking to satisfy performance and S&C constraints. The constraint analysis is not performed as a distinct step, and consequently the conventional design parameters T_{SL}/W_{TO} and W_{TO}/S become fall-outs of the optimization process. Wing loading in particular loses utility as a design parameter because there are potentially infinitely many geometric

variations with the same value but with wildly varying S&C properties. In addition there are many HWB degrees of freedom and constraints that may not be captured in the T_{SL}/W_{TO} vs. W_{TO}/S constraint plots, which limit their utility as design tools for the HWB.

7.1.1 Sizing through Optimization

Mody et al. have used optimization to perform HWB sizing for a design mission.[86] Their degrees of freedom were primarily engine cycle parameters and outer wing geometry (including span, chords, and leading edge sweeps). The cabin and centerbody geometry were fixed, which is similar to how T&W fuselage geometry is treated. Like Schutte et al., they are still determining geometric scale (i.e. area) with the outer wing, but with additional parameters used to meet additional constraints (Figure 99). These are S&C constraints including static margin at various mission points and pitching moment balance at a cruise design point (accomplished with wing twist). The approach flight condition is trimmed with a combination of elevon deflections (it is unclear which elevons) and thrust vectoring, whose limits are not mentioned. Lateral-directional S&C characteristics are not assessed and there does not appear to be any sizing of the elevons or vertical tails.

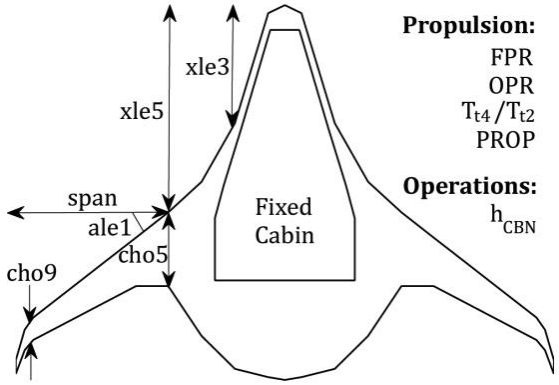

Figure 99: HWB design parameters used by Mody et al. [86]

Regarding the trim constraints, Mody et. al state: "The inability to trim the

aircraft ... at any off-design condition resulted in a non-convergent design." This disadvantage prevents the use of gradient-based optimizers unless they are initialized within the feasible design space. Their optimization strategy used a multi-objective genetic algorithm (which can accommodate failed cases) to find the feasible space and regions likely to be near the global optimum. Designs near their Pareto frontier were then run with a sequential quadratic programming algorithm.

The Boeing Wing Multidisciplinary Optimization Design (WingMOD) code uses an even greater number of degrees of freedom to size the vehicle and simultaneously meet an assortment of constraints.[145] Originally there were seven leading edge sweep and nine chord length design variables used to define the centerbody as well as the outer wing regions of the planform. In later studies the number of leading and trailing edge breaks were constrained for manufacturing reasons.[53] Unlike the work by Schutte et al. and Mody et al. the cabin dimensions are free to change as well.

There are approximately 20 longitudinal flight and loading conditions used for testing vehicle control authority in WingMOD including takeoff rotation and roll maneuvers, but no directional flight conditions to size the tails. WingMOD constraints for trim are defined in terms of elevator and aileron deflection limits, implying simplified control surface utilization (e.g., linked or "ganged" elevons). It is not clear whether the aerodynamic model allows deflections beyond these limits, or if the trim analysis fails to converge when there is insufficient control authority. There is no mention of determining appropriate throttle settings for trim, or if there were issues generating sufficient drag during approach conditions.

7.1.2 Optimization Environment Requirements

The HWB sizing environment developed in this chapter will have several basic elements in common with the other environments described earlier. The cabin shall be parametric, not fixed. The planform will be also be fully parametric, with limits

on the number of breaks in the leading and trailing edge. Performance and trim constraints will be enforced simultaneously while minimizing the conventional takeoff gross weight metric. Methods to develop the various inputs to those analyses will be developed including mass properties, landing gear placement, aerodynamic models, and others.

7.2 Geometry

7.2.1 Cabin and Planform

The cabin sizing is accomplished using algorithms described by Nickol & McCullers which has been implemented in FLOPS.[98] The 300PAX large twin aisle (LTA) class assumptions used by Nickol are used here to demonstrate the methodology.[97] The cabin will be sized to hold 24 first class, 54 business class, and 227 tourist class seats in three bays. Default values for number of passengers abreast and seat pitch in FLOPS are used. With those parameters fixed, the only remaining inputs to the cabin sizing algorithm are the centerbody leading edge sweep (Λ_{LE}) and the centerbody rear spar chord fraction (p_{ctr}) design parameters. FLOPS can be run with other vehicle parameters defaulted and the resulting cabin dimensions are extracted. Table 42 summarizes the algorithm inputs and outputs which are visualized in Figure 100.

Table 42: FLOPS cabin sizing inputs and outputs.

Inputs				
Parameter	Fixed	Min	Max	Units
Λ_{LE}	-	40	70	degrees
p_{ctr}	-	60	75	%
NPF	24	-	-	seats
NPB	54	-	-	seats
NPT	227	-	-	seats
NBAY	3	-	-	-
Outputs				
WF				ft
XL				ft
XLP				ft
XLW				ft

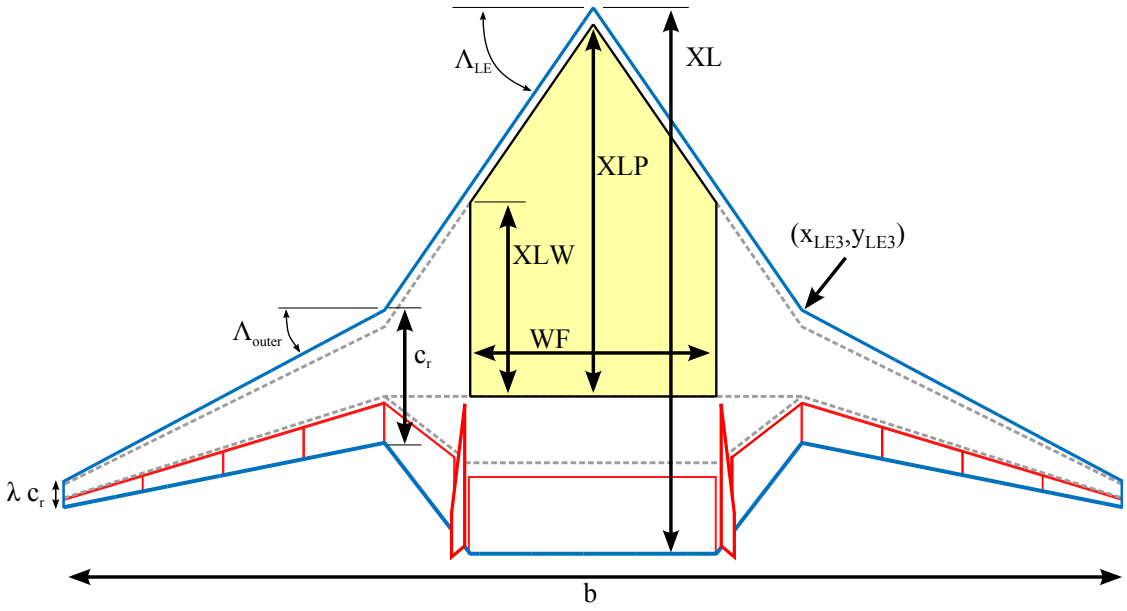

Figure 100: Cabin and planform parameterization.

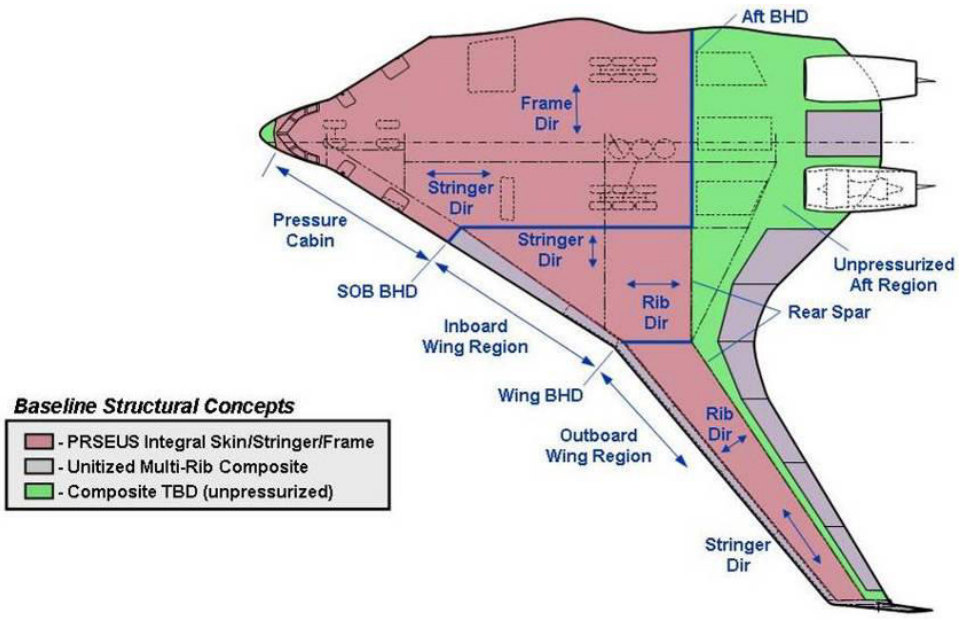

Figure 101: HWB structural layout.[139]

The cabin dimensions are necessary to define the remaining planform dimensions. The centerbody and outer wing rear spars will be aligned to match the structural arrangements observed in the literature (Figure 101). The root chord of the outer wing shall be bounded such that it does not extend farther aft than the centerbody trailing edge. This is defined by Equations 76 and 77:

$$x_{LE,2} = \frac{1}{2}\mathrm{WF}\tan\Lambda_{LE} \tag{76}$$

$$c_{r_{max}} = \frac{\mathrm{XLP} - x_{LE,2}}{p_{outer}} \tag{77}$$

where p_{outer} is the outer wing rear spar chord fraction which is fixed at 65%. The design parameter p_{rc} defines the outer wing root chord (c_r) as a fraction of $c_{r_{max}}$. Given the outer wing root chord, outer wing rear spar chord fraction, and Λ_{LE} the x and y positions of the outer wing are fully constrained:

$$x_{LE,3} = \text{XLP} + c_r \left(p_{frontspar} - p_{outer} \right) \tag{78}$$

$$y_{LE,3} = \frac{x_{LE,3}}{\tan \left(\Lambda_{LE} \right)} \tag{79}$$

where $p_{frontspar}$ is the front spar chord fraction measured from the leading edge of the outer wing and is fixed at 12.5%. The remaining outer wing geometry is defined by a taper ratio (λ), leading edge sweep (Λ_{outer}), and total wingspan (b). The afterbody consists of a straight region the width of the cabin and a straight transition region connecting the centerbody trailing edge to the outer wing trailing edge. The FLOPS algorithms place the cabin directly on the leading edge so an adjustment is needed to make space for the leading edge spar. If the rear spars are to remain aligned, the relationship in Equation 80 must hold true. The parameter XL was an output of the cabin sizing but can be adjusted to satisfy the constraint using Equation 81.

$$p_{ctr} \cdot \text{XL} = c_r \cdot p_{frontspar} + \text{XLP} \tag{80}$$

$$\text{XL}_{new} = \frac{c_r \cdot p_{frontspar} + \text{XLP}}{p_{ctr}} \tag{81}$$

The planform parameters defined so far are sufficient for defining the leading and trailing edge curves. The planform area can then be calculated by numerical integration of the curves using a trapezoidal approximation method shown in Equation 82. The mean aerodynamic chord is calculated using the same method in Equation 83.

$$\begin{aligned} S &= 2 \int_0^{b/2} \left[x_{TE} \left(y \right) - x_{LE} \left(y \right) \right] dy \\ &\approx \sum_{n=1}^{N} \left(y_{n+1} - y_n \right) \left[x_{TE} \left(y_{n+1} \right) - x_{LE} \left(y_{n+1} \right) + x_{TE} \left(y_n \right) - x_{LE} \left(y_n \right) \right] \end{aligned} \tag{82}$$

$$MAC = \frac{2}{S} \int_0^{b/2} \left[x_{TE} \left(y \right) - x_{LE} \left(y \right) \right]^2 dy \tag{83}$$

Elevons 1-4 and 8-11 are uniformly spaced on the trailing edge of the outer wing. Their hinge line sits parallel to the outer wing rear spar (fixed at 65% chord fraction) at a chord fraction of $p_{elevon,out}$, which is bounded to always be greater than (i.e. farther aft) the rear spar. Elevon 6 is the centerbody elevon and has a width equal to that of the cabin. The hinge line is parallel to the centerbody rear spar and vehicle y-axis at a chord fraction of $p_{elevon,ctr}$ relative to the centerline dimension of XL. A secondary rear spar in the centerbody is defined as 2.5% of XL forward of the elevon 6 hinge line. The secondary spar extends farther outboard to connect to the start of the outer wing rear spar. Elevons 5 and 7 occupy the trailing edge between the outer wing and centerbody regions. Their hinge lines are parallel to the secondary spar with a constant offset equal to that of the inboard edge of elevons 4 and 8. The total control surface area is an input to FLOPS, and is calculated using the trapezoidal approximation method described earlier.

The vertical tails are placed at the trailing edge with a y-position slightly outside the centerbody elevon, as defined by Equation 84. The y-position of the engine centerline is fixed at half the span fraction of the vertical tails. A trade-off between noise and installation drag penalty exists that should influence the selection of the engine x-position.[102] Quantifying this trade-off requires high fidelity simulation that is beyond the scope of this dissertation. Instead, the x-position is fixed with the core nozzle exit face placed one fan diameter forward of the trailing edge. The z-position of the engine centerline is also fixed based on measurements of the Boeing BWB-0009A configuration.[1] This position is the sum of the airfoil z-position, 17.7% of the average nacelle diameter (DNAC), and one fan radius. The dimensions of the engine are scaled relative to the baseline engine using the default FLOPS method given in Equation 85.

[1] `https://www.aiaa.org/uploadedFiles/About-AIAA/Press-Room/Key_Speeches-Reports-and-Presentations/2012/Bonet-John-Boeing-AVC-AIAA-GEPC2.pdf`

$$y_{VT} = \left(\frac{\mathrm{WF}/2}{y_{LE,3}} + 0.025 \right) y_{LE,3} \tag{84}$$

$$scale = \sqrt{\frac{T_{SL}}{T_{SL_{baseline}}}} \tag{85}$$

A study of the effect of engine location and thrust line on trim drag was conducted, and found that the cost of retrimming the aircraft at cruise with the centerbody elevon could be significant (see Appendix A). For this reason, the wing is twisted (described later) to trim the aerodynamic and thrust pitching moments at the cruise design point.

7.2.2 Airfoils and Thickness-to-Chord Distribution

A fixed airfoil stack obtained from the N2A-EXTE HWB configuration was used. Airfoil optimization is beyond the scope of this dissertation, and the use of a fixed stack appears to be the common practice for most of the HWB MDO studies reviewed in the literature survey. The airfoils will be rescaled as necessary to fit the parametric planforms. To ensure that the cabin can fit within the aircraft skin the thickness-to-chord (t/c) ratios need to be adjusted, which will have consequences for both drag and weight in FLOPS.

The t/c as a function of span fraction are plotted in Figure 102 for two non-proprietary HWB configurations. One can observe that the t/c at the centerline is not the largest. The airfoil at the side of the cabin requires greater thickness due to a smaller chord length. Other bumps or kinks in the t/c curve are to make sure that the vehicle outer mold line covers the internal components. The t/c of the outboard wing is flat, on the order of 8-8.5%.

The parametric models will be performing the same mission as the HWB301 configuration, so its t/c distribution will serve as a baseline. The height of the cabin at the centerline (h_{TCF}) and side-of-body (h_{SOB}) will be constant for all designs and

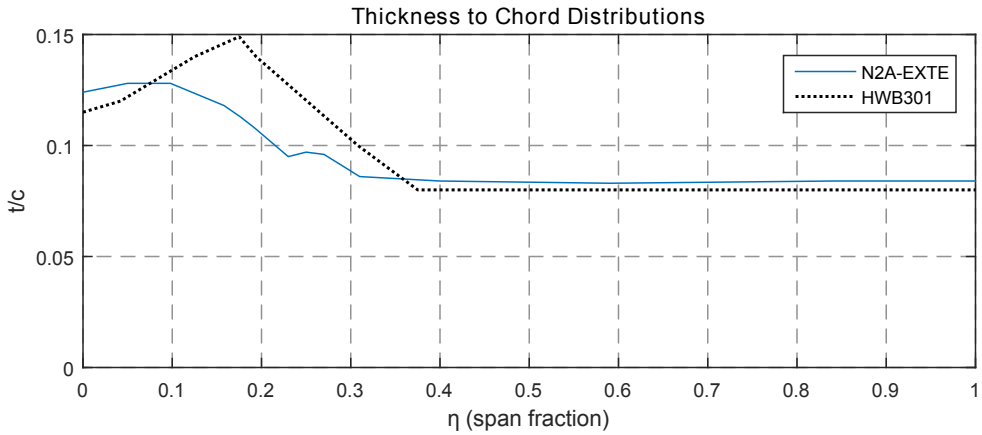

Figure 102: HWB thickness to chord distributions.

will match the HWB301 values. These properties have been estimated and placed in Table 43. New thickness-to-chord ratios are calculated by dividing these heights by their respective chord lines from the new parametric planforms (Equations 86 and 87). The outer wing sections will have a t/c equal to 8%, and all intermediate locations will be linearly interpolated from these values.

Table 43: Baseline HWB301 cabin properties

Parameter	Value	Units
XL	118.12	ft
c_{SOB} (Side-of-body chord)	77.75	ft
TCF (Center line t/c)	11.5	%
TCSOB (Side-of-body t/c)	14	%
h_{TCF}	13.58	ft
h_{SOB}	10.89	ft

$$\text{TCF}^* = \frac{h_{TCF}}{XL^*} \tag{86}$$

$$\text{TCSOB}^* = \frac{h_{SOB}}{c^*_{SOB}} \tag{87}$$

7.2.3 Available Fuel Volume

The space between the spars is used for storing fuel, and an estimate of the available volume is needed for choosing the wing scale and for estimation of mass properties. The FLOPS tool contains a parametric equation for estimating this volume based on various planform parameters (Equation 88). This equation has a tuning parameter, FWMAX, that can be defaulted (to 23) or selected by the user. The official FLOPS input files for the N2A-EXTE and HWB301 configurations use the default value, while another study used a value of 8.5.[2] This would seem to be a huge discrepancy in assumptions but it may not matter, as the HWB configuration is generally known to have an excess of available volume. Regardless, a more physics-based approach linked to the parametric geometry had to be taken for accurate estimation of the vehicle center of gravity. The fuel volume constraint was therefore enforced externally to the FLOPS tool.

$$\text{FULWMX} = \text{FWMAX}\frac{(t/c)\,S^2}{b}\left(1 - \frac{\lambda}{1+\lambda^2}\right) \tag{88}$$

The fuel tanks were defined to start at the cabin side and extend to the wing tip. Three tanks were assumed including one in the transition region and two splitting the outer wing (Figure 103). The volume of each tank was approximated by summing the volumes of several extruded airfoil sections. These airfoils were truncated where the leading and trailing edge spars intersected them. The areas of these sections are then multiplied by a length determined from the number of discretized sections used in the approximation. The summation of these volumes are then multiplied by a volume efficiency of 90%, matching the assumption used for the N2A-EXTE.[72] A convergence study was performed and found that 10 slices per fuel tank accurately approximated the available fuel volume. Pumping fuel inboard or outboard enables

[2]Personal communication with Craig Nickol of NASA Langley Research Center and Jeff Schutte of Georgia Tech's Aerospace Systems Design Laboratory

CG shifting, and will be used to determine forward and aft CG positions.

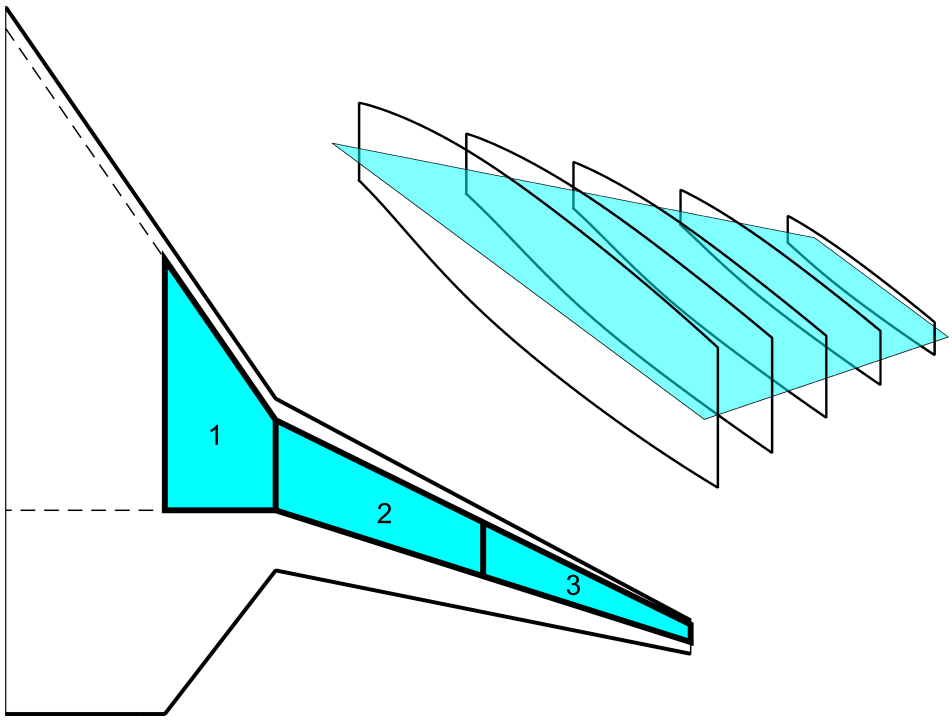

Figure 103: Fuel tanks and cross sections used to estimate volume.

7.2.4 Initial Vertical Tail Sizing

Over the course of vehicle optimization, the vertical tails will be sized to satisfy various trim constraints. Vertical tail sweep should be enough so that the tail's critical Mach number is greater than the wing's. In addition, high tail sweep moves the tail aerodynamic center farther aft providing a larger moment arm. The vehicles in this dissertation used a fixed vertical tail planform shape that is approximately equivalent to the Boeing 0009A design (Table 44), and only the scale (e.g., area or span) will need to be established.[3] As a first guess for sizing, a vertical tail volume coefficient from the Boeing OREIO (a design with centerbody mounted tails) can be used.[4] The tail area can be estimated using Equation 89 based on properties of the

[3] https://www.aiaa.org/uploadedFiles/About-AIAA/Press-Room/Key_Speeches-Reports-and-Presentations/2012/Bonet-John-Boeing-AVC-AIAA-GEPC2.pdf

[4] http://ntrs.nasa.gov/archive/nasa/casi.ntrs.nasa.gov/20110023250.pdf

wing and tail position:

Table 44: Vertical tail parameters

Parameter	Value	Units
$\Lambda_{VT,LE}$	55	degrees
$\Lambda_{VT,c/4}$	45.4	degrees
λ_{VT}	0.3115	-
AR_{VT}	1.2197	-
C_{VT}	0.01265	-

$$C_{VT} = \frac{L_{VT} S_{VT}}{b_W S_W}$$
$$S_{VT} = \frac{C_{VT} b_W S_W}{L_{VT}} \tag{89}$$

where L_{VT} is defined as the distance between the wing MAC quarter chord and the vertical tail MAC quarter chord. Because the tail is positioned flush with the trailing edge, this distance is dependent on tail size requiring a few iterations for these parameters to converge. The rudder hinge line is fixed at 25% of the chord line measured from the trailing edge.

7.3 Performance Analysis

It was mentioned in Section 7.2.1 that the LTA class mission defined by Nickol would be used in this research.[97] This 301 passenger mission is defined in part by the performance constraints listed in Table 45. The mission profile is a simple takeoff, climb, cruise, descent, and landing with all FLOPS settings defaulted unless otherwise noted. FLOPS is set up to analyze the input configuration by computing weights, drag polars, and evaluating mission performance. The ramp weight is estimated with

a fixed range and planform. An engine deck is provided to FLOPS which it scales as necessary.

The takeoff segment is run with ground effects active using a wing height above ground of 20 ft, a 0.009 landing gear drag coefficient, a 0.005 delta drag coefficient for an engine out condition, and a maximum angle of attack equal to the tail clearance angle. The climb segment is a minimum fuel to climb profile. Cruise takes place at a fixed 0.84 Mach number, optimum altitude for specific range, and a maximum altitude of 45,000 ft. The descent segment occurs with an optimum lift-to-drag ratio. The landing segment starts with an approach segment 500 ft above the ground and flight path angle of -3 degrees. Spoilers and thrust reversers are not used during landing or aborted takeoff segments.

Table 45: Large Twin Aisle 300PAX mission performance constraints from Nickol 2012.[97]

Name	**Value**	Units
Range	7,500	nm
Approach speed	< 150	knots
TO field length	$< 10{,}100$	ft
Missed approach thrust	> 0	lbf
2nd segment climb thrust	> 0	lbf
Excess fuel capacity	> 0	lbf
ROC at altitude	> 300	ft/min

For each vehicle a takeoff and landing drag polar is generated as an input to FLOPS. An angle of attack sweep from 1 to 16 degrees is run through VORLAX with the leading edge drooped 30 degrees. A viscous drag correction for the VORLAX drag polar was made using the FLOPS internal aerodynamic model at Mach 0.2 sea level conditions. For conceptual design work it is not uncommon to assume a

fixed value of $C_{L_{max}}$ as a type of technology level assumption. However, the HWB configuration lift is sensitive to deflections required to trim. This penalty is vehicle specific and has strong influence over the resulting stall speed, takeoff rotation speed, takeoff field length, approach speeds, and control authority. It is therefore important to estimate *trimmed* $C_{L_{max}}$ for each vehicle rather than assuming a fixed value. The $C_{L_{max}}$ assumed for each vehicle is the trimmed C_L achieved at a 20 degree angle of attack (the upper bound assumed for all low speed trim analyses) or one (the N2A-EXTE's value), which ever is smaller. This upper limit is imposed as a technology level assumption.

VORLAX was used to estimate trimmed $C_{L_{max}}$ and the details of the algorithm are in Section refsec:CLmaxMethod. Limitations of this method include the inability model separation effects which would determine the angle of attack corresponding to the maximum lift coefficient. Boeing's method of critical sections uses higher fidelity empirical airfoil data, but it is not clear if it produces a trimmed lift coefficient. A higher fidelity approach that would capture the relevant physics is beyond the means of a conceptual design study, but would involve RANS CFD-based evaluation and optimization of the high lift devices.

7.3.1 Miscellaneous FLOPS Issues

The performance analysis had to be made robust to a climb failure error in FLOPS. Certain vehicles would cause FLOPS to fail due to a negative rate of climb at the beginning of the climb segment. The FLOPS manual identifies this as an aerodynamic problem that can be overcome by increasing the start-of-climb Mach number (CLMMIN). The initial Mach number used in these analyses is 0.3 and if this error is encountered it is incremented by 0.01 up to 10 times.

The FLOPS analysis requires an initial guess for the takeoff gross weight. Based on experiences with the trim analyses, there was a concern that the output TOGW

would depend on the initial guess. A uniform distribution of 0 to 1,000,000 lbs was sampled in a Monte Carlo Simulation on the TOGW weight guess for Vehicle 377. The range of converged TOGW values was trivially small so FLOPS does not appear to have problems with local minima. Any TOGW guesses that were more than 30-40k lbs below the converged TOGW values resulted in failed FLOPS cases due to lack of weight available for fuel. FLOPS was made robust to this error by using an initial guess of 1,000,000 lbs.

7.4 Engine Model

A geared turbofan engine deck generated by the Aerospace Systems Design Laboratory is used and scaled for these experiments (Figure 104).[5] The fixed engine cycle is described in Table 46 and the ERA Task 2.1 Year 2 Deliverables documentation, which assumes a combination of Reference Technology Collector (RTC) and Integrated Technology Demonstrator (ITD) technology packages. Using a rubberized engine is important for these experiments, as many of the designs to be explored are likely to have poor performance. Including an engine cycle analysis in-the-loop for such designs would not be a judicious use of time. This is left as an avenue of future research once the feasible design space has been discovered.

7.5 Mass-Properties

The vehicle center of gravity is needed for positioning the landing gear, for defining the moment reference point in VORLAX, and for the trim analyses. Moment of inertia estimates are also needed for any flight condition that experiences angular acceleration. The FLOPS analysis provides an itemized weight table whose items can be grouped and positioned on the aircraft planform (Figure 105). The weights for certain items such as the outer wing, fuel tanks, and cabin were placed at their

[5]Courtesy Dr. Jimmy Tai, Senior Research Engineer, Aerospace Systems Design Laboratory

Table 46: A geared turbofan engine deck with RTC and ITD technology packages.

Description	Value	Units
SLS Thrust	57,046	lbs
SLS Airflow	2,735	pps
Takeoff Thrust (M0.25/0K, Hot)	45,965	lbs
Cruise TSFC	0.491	lb/(lbf-hr)
Total Engine Weight	9,963	lbs
Engine Nacelle Length	12.96	ft
Fan / Nacelle Diameter	113.5/131.0	in
FPRD / HPCPRD / OPRD (M0.80/35K)	1.35/20.52/60	-
BPRD (M0.80/35K)	19.05	-
OPR SLS Uninstalled	49.86	-
T4max (M0.25/0K)	3,550	deg R
Fan Tip Mach No.	1.06	-
LPC / HPC / HPT / LPT Stages	4/8/2/4	-

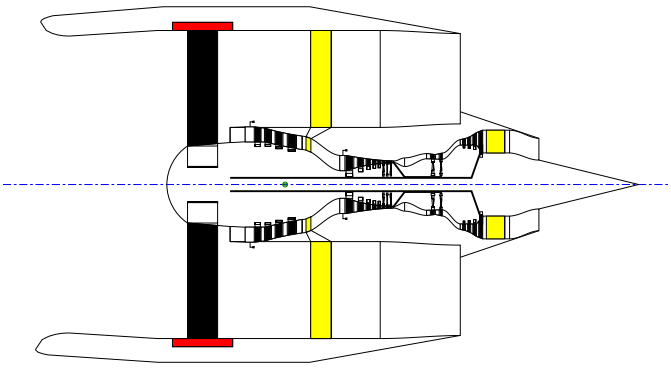

Figure 104: Baseline engine flow path.

2-dimensional geometric centroid defined by Equations 90 and 91:

$$x_c = \frac{1}{6A} \sum_{i=0}^{n-1} (x_i + x_{i+1}) (x_i y_{i+1} - x_{i+1} y_i) \tag{90}$$

$$y_c = \frac{1}{6A} \sum_{i=0}^{n-1} (y_i + y_{i+1}) (x_i y_{i+1} - x_{i+1} y_i) \tag{91}$$

where A is the component planform area. Equation 92 was then used to estimate the center of gravity location for the vehicle. The CG is assumed to sit on the aircraft centerline in the x-y plane (i.e. $z_{CG} = 0$). For the body moments of inertia, aircraft components were similarly modeled as point masses (larger components such as the wing and cabin were approximated as a series of flat plates) and integrated using Equations 93-95. Figure 106 shows the CG and I_{yy} generated for the N2A-EXTE under various loading conditions. A similar analysis was performed on the N2A geometry and weight table and was shown to have good agreement with published CG locations (Table 47).[72]

$$x_{CG} = \frac{1}{m} \sum_{i=1}^{n} m_i x_i \tag{92}$$

$$I_{yy} = \sum_{i=1}^{n} I_{yy_i} + \sum_{j=1}^{m} m_i \left[(z_i - z_{cg})^2 + (x_i - x_{cg})^2 \right] \tag{93}$$

$$I_{xx} = \sum_{i=1}^{n} I_{xx_i} + \sum_{j=1}^{m} m_i \left[(z_i - z_{cg})^2 + (y_i - y_{cg})^2 \right] \tag{94}$$

$$I_{zz} = \sum_{i=1}^{n} I_{zz_i} + \sum_{j=1}^{m} m_i \left[(x_i - x_{cg})^2 + (y_i - y_{cg})^2 \right] \tag{95}$$

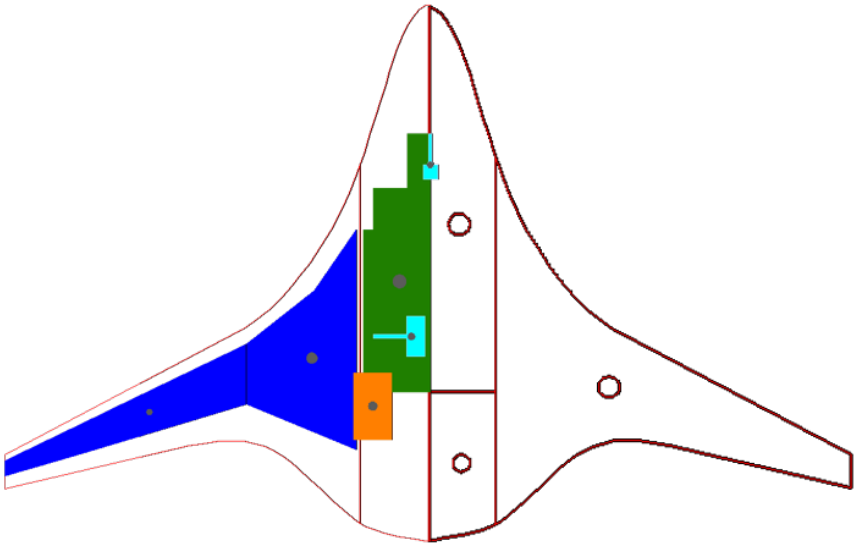

Figure 105: The layout of components and their respective geometric centroids / assumed CG for the N2A.

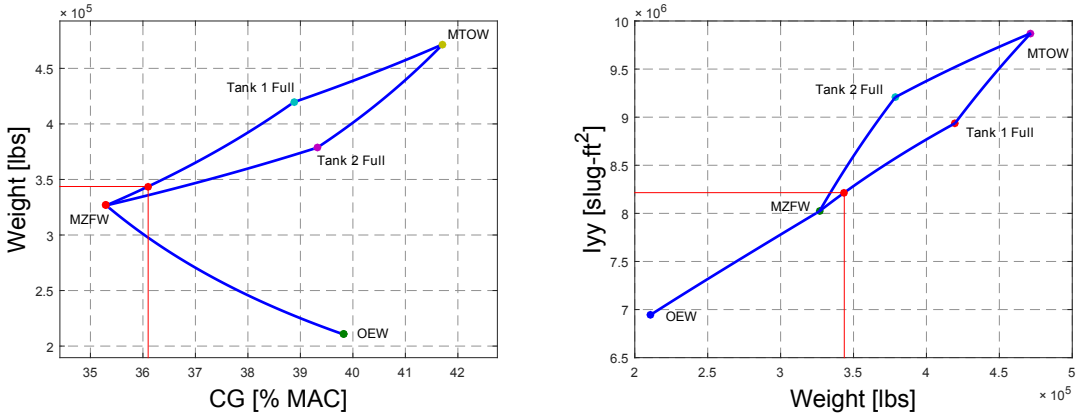

Figure 106: N2A-EXTE mass model with the forward approach loading condition highlighted.

Table 47: Mass model validation by comparison with reported N2A values.

Loading Condition	Estimated CG [% MAC]	Reported CG [% MAC]	% Error
OEW	43.02	44.31	2.91
MZFW	37.55	39.21	4.24

The landing gear will need to be positioned relative to the aft-most CG position. It is expected that this will occur with an empty cabin and mission fuel filling the outboard tanks first. To be certain, six loading conditions are evaluated and the aft-most CG is used. The loading conditions are combinations of 1) a full vs. empty cabin, and 2) no fuel vs. mission fuel filling inboard tanks first vs. mission fuel filling outboard tanks first. An initial guess of the landing gear positions are required to estimate the center of gravity. The nose gear is initially positioned at the centerline leading edge and the main gear are placed at the aft cabin corners.

7.6 Landing Gear Placement

The landing gear is placed relative to the CG, which in turn modifies the CG making this an iterative process. The placement of the CG also determines the gear length, requiring recalculation of their weights and iteration with FLOPS. The CG location is very important for vehicle trim at cruise with twist, so the iteration continues until the CG (in units of % MAC) convergences within a tolerance of 1e-4 feet. The z and x-position of the main gear is determined from the intersection of two lines: 1) a line drawn 15 degrees aft of the aft-most CG, and 2) a line defining a tail clearance angle of 15 degrees. This is visualized in Figure 107, and the main gear coordinates are derived below:

$$\Delta x_m = \Delta z_m \tan \theta_{CG}$$

$$\Delta z_m = \Delta x_t \tan \theta_{tail}$$

$$\Delta x_t = XL - CG_x - \Delta x_m$$

$$\Delta z_m = (XL - CG_x - \Delta x_m) \tan \theta_{tail} \tag{96}$$

$$\Delta x_m = \frac{(XL - CG_x) \tan \theta_{tail} \tan \theta_{CG}}{1 + \tan \theta_{tail} \tan \theta_{CG}} \tag{97}$$

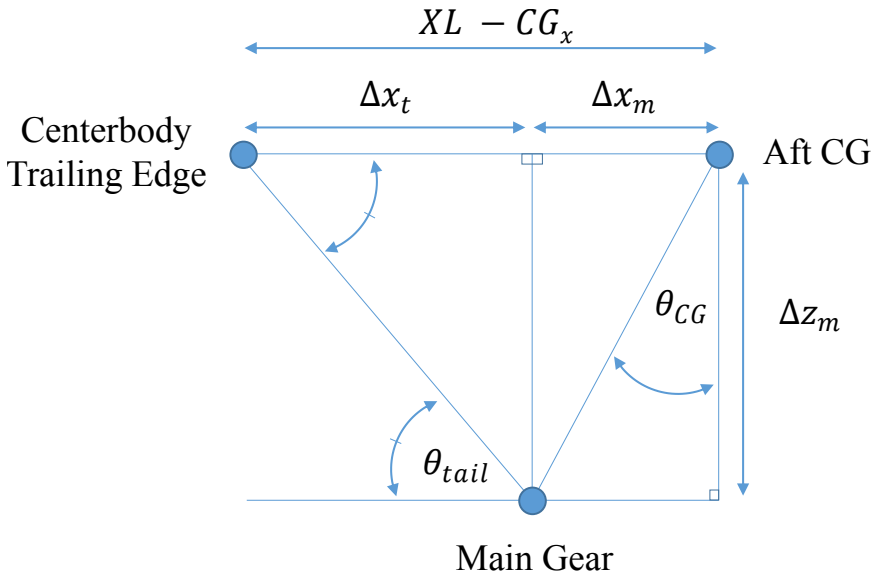

Figure 107: Main landing gear position geometry.

These rules are used to prevent issues with aft towing and tail tipping. Currey explains: "The 15 deg figure has been used for many years and is based on two parameters: aft towing and tail tipping. For aft towing, it ensures that the aircraft will not tip if the brakes are applied to cause a deceleration of 8 ft/s/s. Tail tipping is prevented because the aft fuselage and/or tail bumper design will not permit the tail to be lowered by as much as 15 deg in most aircraft and the c.g. will not, therefore, rotate over and aft of the main gear."[6]

The nose gear x-position is chosen such that it carries 8% of the vehicle weight in the aft-most loading condition and the nose gear z-position matches that of the main gear. This rule ensures that the nose gear is useful for steering.[119] There is plenty of space to position the main gear practically anywhere in the centerbody,

[6]Currey, Norman S. (1988). Aircraft Landing Gear Design - Principles and Practices. Ch3, pg 25-42.

including underneath the cabin. Technically there is a turnover angle requirement, but given the analyses that will be conducted there is no consequence for simply picking the y-location to match the cabin sides (+/- WF/2), which is also consistent with Nickol's assumptions.[97] The length of the main and nose gear are calculated from their z-locations to the airfoil surface at their respective y-locations.

7.6.1 Wing Dihedral Angle

Typical values of dihedral for low wing aircraft is 2-3 degrees, rarely exceeding 5 degrees.[7] The dihedral for the parametric HWB configurations investigated here will be zero, or if necessary large enough to avoid a wingtip strike during takeoff. The dihedral will start outside of the centerbody region at $y_{LE,3}$ as shown in Figure 100. The algorithm for choosing the dihedral angle is shown below:

1. After the landing gear is sized, calculate the x, y, and z locations of the wingtip trailing edge.

2. Rotate a vector pointing from the main gear to the wingtip about the y-axis passing through the main gear by 15 degrees.

3. If the rotated wingtip vector points below the horizontal (i.e. wingtip strikes the ground), increase the dihedral by one degree.

4. Repeat steps 1-3 until the wingtip is clear of the ground.

7.7 Twisting the Wing to Trim at Cruise

With the landing gear position, vehicle weight, and center of gravity converged the wing can be twisted to trim at a start-of-cruise design point without deflections. Trimming without deflections is done in an effort to minimize drag, which is the

[7]Kundu, Ajoy Kumar (2010). Aircraft Design. Cambridge University Press. Online version available at: http://app.knovel.com/hotlink/toc/id:kpAD000013/aircraft-design/aircraft-design

convention in the HWB literature. Linear wing twist starting at a span fraction just past the cabin and vertical tail will be used to trim the vehicle. This is done to avoid possible packaging issues with the cabin. If the vehicle is tail heavy, positive tip twist is needed (right hand rule using a y-axis pointing out the right wing). If the vehicle is nose heavy, negative tip twist is needed. Given the weight and altitude table from the FLOPS mission analysis the design lift coefficient at the start of cruise can be calculated:

$$C_{L_{design}} = \frac{W}{\frac{1}{2}\rho V^2 S} \tag{98}$$

The net pitching moment must equal zero, so the wing must counteract the nose-down moment from the engines. The thrust required at the start of cruise can again be obtained from the FLOPS mission analysis and is used to determine the design pitching moment coefficient for the planform:

$$C_{m_{design}} = \frac{T\Delta z}{\frac{1}{2}\rho V^2 S\bar{c}} \tag{99}$$

where T is the thrust at start of cruise and Δz is the distance between the thrust line and CG along the body z-axis. In order to determine the amount of tip twist that is required to achieve the design C_L and C_m simultaneously a set of VORLAX experiments must be conducted. Initially, the tip twists of magnitude -5, -2.5, 0, and 2 are investigated. For each tip twist setting, the geometry is run through VORLAX at angles of attack of 0 and 3 degrees. The angle of attack necessary to achieve the design C_L is determined using linear extrapolation. VORLAX is then rerun at that angle of attack to determine the C_m at the design C_L. This is done for each candidate tip twist and is shown in Figure 108. The trend appears linear, which can be interpolated for the tip twist that achieves the design C_m simultaneously with the design C_L. Subsequent iterations between the performance and tip twist analyses will

use the previous iteration's tip twist +/- 3 degrees. The twist and lift distributions for Vehicle 377 are shown in Figure 109.

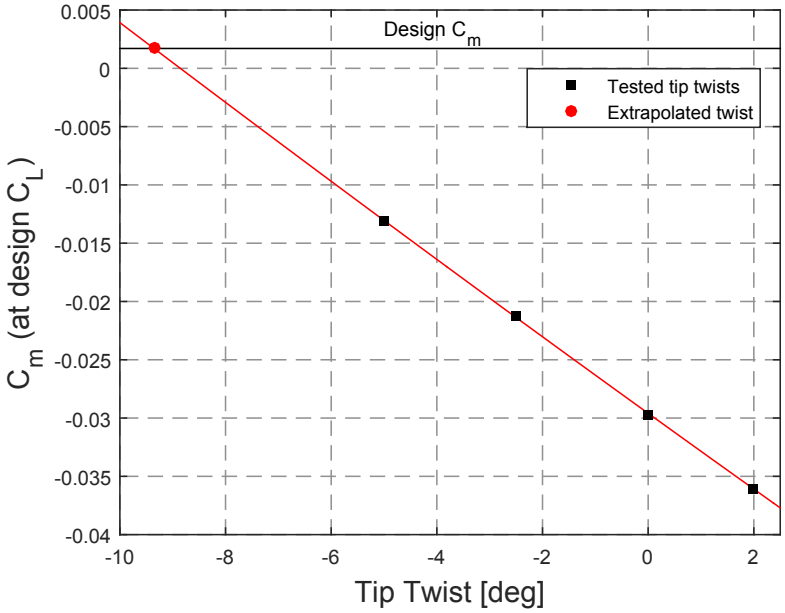

Figure 108: Finding the tip twist that achieves design C_L and C_m simultaneously for Vehicle 377.

The aerodynamic model used by FLOPS needs to be updated to reflect the changes caused by twisting the wing. The internal aerodynamic model is being used (much faster than generating tables with VORLAX) and there are several methods for tuning it. The FCDI tuning parameter (or k-factor), which is a multiplier on lift-induced drag, was determined to be most appropriate because wing twist is affecting primarily the lift distribution. In order to tune FCDI, the FLOPS analysis must output the drag polar at start-of-cruise conditions for comparison to the VORLAX drag polar. The two drag polars are interpolated at the design lift coefficient and divided to obtain FCDI using Equation 100. As seen in Figure 110, the VORLAX and tuned FLOPS drag polars have excellent agreement in the design C_L region.

$$FCDI = \frac{C_{D_{i,VORLAX}}}{C_{D_{i,FLOPS}}} \tag{100}$$

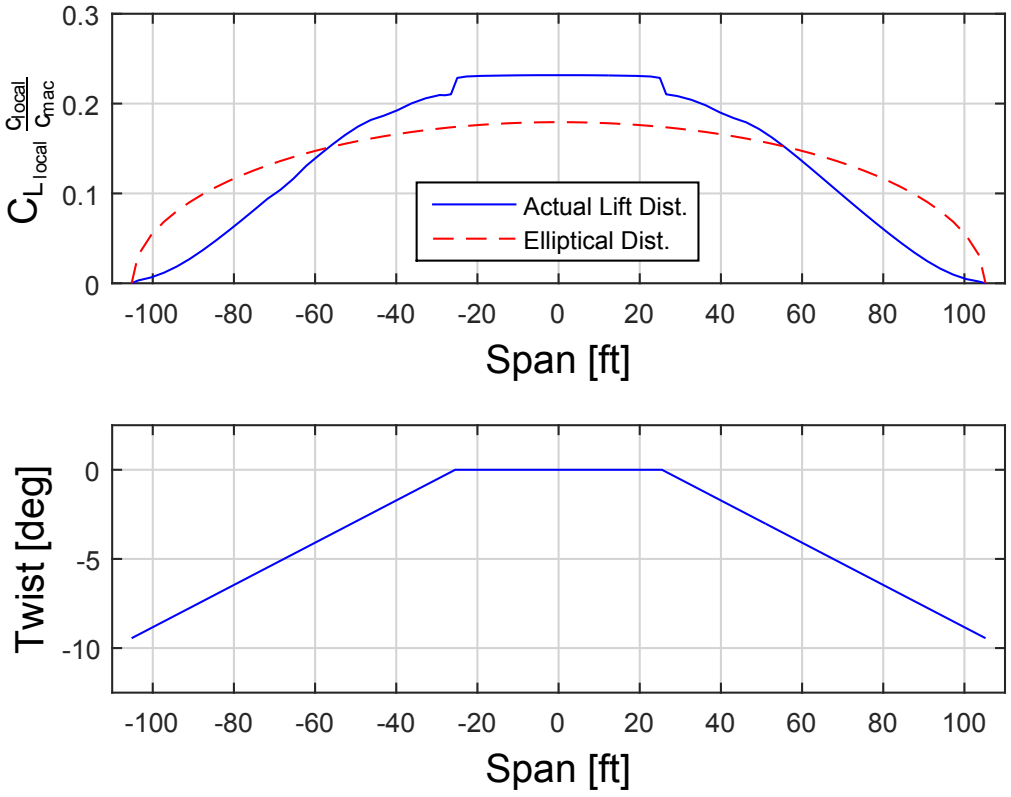

Figure 109: Twist and lift distributions for Vehicle 377.

Updating the FCDI input to FLOPS requires FLOPS and the landing gear placement loop to be rerun. Initial experiments testing this feedback revealed that the loop was unstable, causing oscillation of TOGW with ever growing amplitude. A damping mechanism (via Equation 101) was able to solve this problem. The wing twist feedback outer loop continues until the TOGW converges within 0.1% of the previous iteration, which is on the order of 4000 lbs.

$$FCDI_{i+1} = \frac{FCDI_i + FCDI_{i-1}}{2} \tag{101}$$

The wing twist feedback loop serves to penalize planforms that are poorly balanced or require excessive twist. An external constraint enforced during HWB MDO requires a negative tip twist angle. Positive twist will cause the wingtips to stall first, which

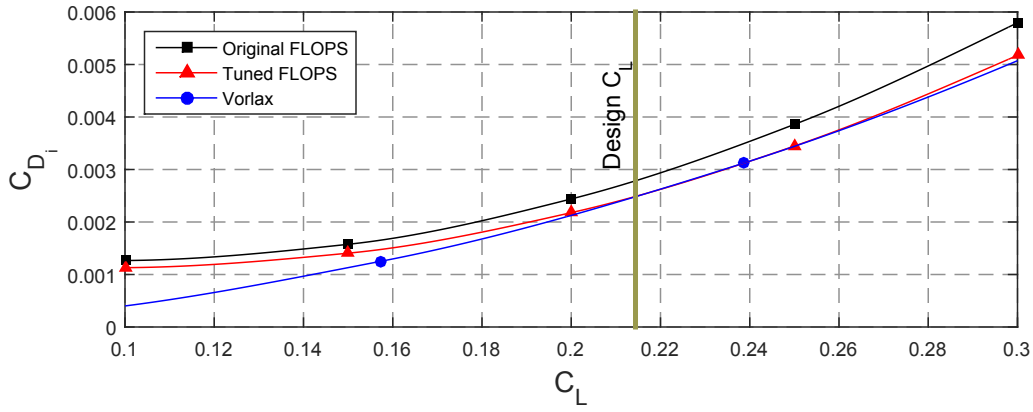

Figure 110: FLOPS aerodynamic model tuned with FCDI at the cruise design point.

should be avoided so that the outboard elevons remain effective at high angles of attack. The Nickel and Wohlfarht design text for tailless aircraft notes that tip twist greater than 15 degrees would be excessive.[94] The lower bound for twist is not constrained explicitly, but is penalized through greater induced drag via FCDI feedback. Finally, the takeoff and landing drag polars for FLOPS are also regenerated with the new geometry in VORLAX.

Limitations: There is some uncertainty regarding whether a vortex-lattice method such as VORLAX can accurately predict the pressure distribution at transonic cruise conditions. This is a limitation of inviscid linearized potential flow theory.[85] No pitching moment coefficient wind tunnel or CFD-based data was available for comparison. To capture the all of the relevant effects would require CFD, such as capturing the effects of engine integration on the flow field, but this is not practical for conceptual design studies. The vortex-lattice method is adequate for demonstrating the methodology, with the understanding that the wing twist required for trim may need to be revisited in a later design phase with higher order tools.

7.8 Off-design Trim Analyses

The importance of including control authority constraints during optimization of a control configured vehicle such as the HWB cannot be understated. Wakayama and

Kroo note the following: "For the BWB, this could be disastrous: the wing shape that maximizes L/D is unlikely to lead to a balanced airplane with the control authority to rotate for takeoff."[146] In addition, they noted the following based on their experiences with HWB MDO: "Wing area, which is a primary design variable for conventional sizing methods, is virtually unchanged, meaning that improvements were made through much finer manipulation of the geometry. This shows a fundamental advantage of multidisciplinary optimization over conventional sizing processes." These findings justify the extra effort involved in evaluating control authority for the HWB in an MDO setting.

A list of Boeing recommended flight conditions that may provide active control authority constraints was discussed in Chapter 3. The nine flight conditions that will be evaluated in this dissertation are listed in Table 48. The AMS Margin control authority metric for redundant control surface layouts will be generated for each flight condition, and be constrained during HWB optimization experiments. The only flight condition omitted from the full list recommended by Boeing was the stall recovery maneuver. VORLAX does not model separation effects, which are expected to be important in that maneuver. This flight condition could be included if reliable empirical data were available to correct the vortex-lattice method results, or if higher fidelity aerodynamic modeling is utilized.

Table 48: Flight conditions providing control authority constraints during optimization.

No.	Flight Condition / Maneuver
1	Takeoff rotation maneuver with forward CG and 3.0 deg/s^2 pitch acceleration at V_R reported by FLOPS
2	Symmetric approach at V_{app} reported by FLOPS with forward CG
3	Symmetric go-around with forward CG, 6.0 deg/s^2 pitch acceleration, at V_{app} reported by FLOPS
4	Landing nose wheel hold-off with forward CG, $\alpha = 0$, at V_{stall}
5	One engine inoperative in the air with forward CG, no sideslip, less than 5 degrees bank angle, at the maximum allowable minimum control speed $V_{MCA} = 1.13V_{stall}$
6	Crosswind approach with forward CG, 35 knot crosswind, no crab angle, at V_{app} reported by FLOPS
7	One engine inoperative on the ground with the fully loaded configuration (MTOW) at V_R reported by FLOPS
8	Crosswind landing maneuver for six degree heading change in two seconds with the fully loaded configuration (MTOW) at V_{app} reported by FLOPS
9	Landing roll maneuver for 30 degree bank angle change in 2.5 seconds with fully loaded configuration (MTOW) at V_{app} reported by FLOPS

The additional control authority needed by the flight control system to stabilize the vehicle will not be estimated. In lieu of closed loop stability analyses an additional control authority margin should be imposed for all flight conditions. A successful test case for the N2A-EXTE configuration was documented and published.[42] In that publication, control laws were designed and actuation power requirements under various continuous turbulence and control utilization scenarios were investigated.

7.8.1 S&C Aerodynamic Models

The FLOPS internal aerodynamic model was sufficient for the mission analysis but it is not a full S&C model. VORLAX is used again to generate aerodynamic models as functions of α, β, and deflections needed for the trim analyses. The force and moment coefficients are not sensitive to Mach number at low speeds (on the order of Mach 0.2), so several flight conditions can use the same aerodynamic model. The following flight conditions use a model developed at the Mach number corresponding to V_{app} from FLOPS at sea level conditions: Symmetric approach, symmetric go-around, OEI, and crosswind approach. All flight conditions assume that the leading edge droop is deployed 30 degrees.

The behavior of the force and moment coefficients in this flight regime were expected to be linear and quadratic functions of angle of attack, sideslip angle, and deflections. Therefore the models were constructed with 2nd order response surface equations (whose general form is given in Equation 102) constructed from a Box-Behnken Design of Experiments (DOE). The 15 design parameters and their ranges are listed in Table 49, requiring 421 VORLAX experiments. Each DOE case is an individual run of VORLAX, multiple instances of which can be run in parallel on separate CPU cores. On a 3.4 GHz 4 core (8 thread) processor the entire DOE run serially takes 17 minutes and in parallel takes 5 minutes.

$$\hat{y} = \hat{\beta}_0 + \sum_{i=1}^{k} \hat{\beta}_i x_i + \sum_{i=1}^{k} \hat{\beta}_{ii} x_i^2 + \sum_{i=1}^{k} \sum_{j=1}^{i-1} \hat{\beta}_{ij} x_{ij} \tag{102}$$

The aerodynamic surrogate models are generated automatically in Matlab and are not checked for each vehicle. The accuracy of the Box-Behnken DOE and 2nd order RSE combination was tested for Vehicle 377. The surrogates are compared to VORLAX generated data in Figures 111 and 112. Figure 111 sweeps through the angle

Table 49: Design variables and ranges for the Box-Behnken DOE.

	Variable	Min	Max
1	α	5	20
2	β	0	17
3	δ_1	-30	30
...	...	...	...
13	δ_{11}	-30	30
14	$\delta_{L.rud}$	-30	30
15	$\delta_{R.rud}$	-30	30

of attack at a constant 5 degree sideslip angle for various levels of right wing elevon (7-11) deflection. The RSEs are able to capture the trends very accurately. Figure 112 shows a different scenario in which sideslip is zero and the elevons are deflected symmetrically. The lift, induced drag, and pitching moment coefficient RSEs show excellent agreement with VORLAX data. VORLAX predicts the sideforce, rolling moment, and yawing moment coefficients as zero (or trivially small), but the RSEs have trouble recreating that precisely. In this example, the values that the RSEs predict for the rolling and yawing moment coefficients are for all intents and purposes zero. The sideforce coefficient predictions are greater in magnitude and therefore more troublesome. This poor prediction only occurs in symmetric conditions where it is safe to simply hard code the lateral-directional coefficients to zero.

If a different center of gravity than the one used to generate the aerodynamic model is desired, one can use Equation 103 to calculate the moments at a new reference point:

$$\mathbf{T}_B = \mathbf{T}_A + \mathbf{r} \times \mathbf{F}_A \tag{103}$$

where vector $\mathbf{r}$ points from reference point A to reference point B. In this case the original reference point (A) used to run the VORLAX DOE was the forward approach CG, and the flight condition requiring a different CG (ref. point B) is the one engine inoperative condition.

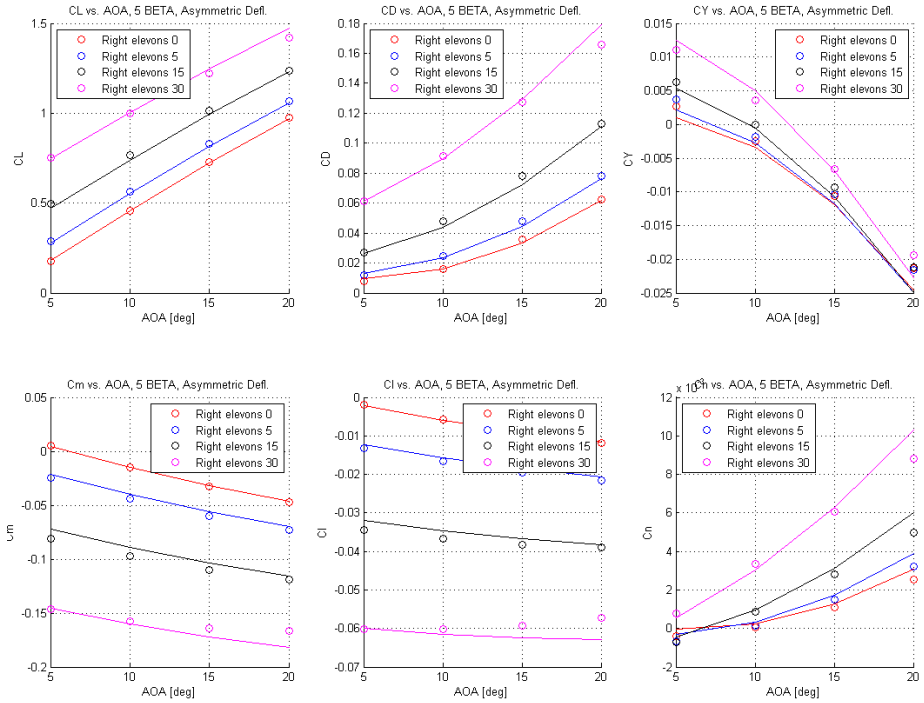

Figure 111: 2nd order RSEs (solid lines) accurately model the VORLAX force and moment coefficients from the DOE (circles).

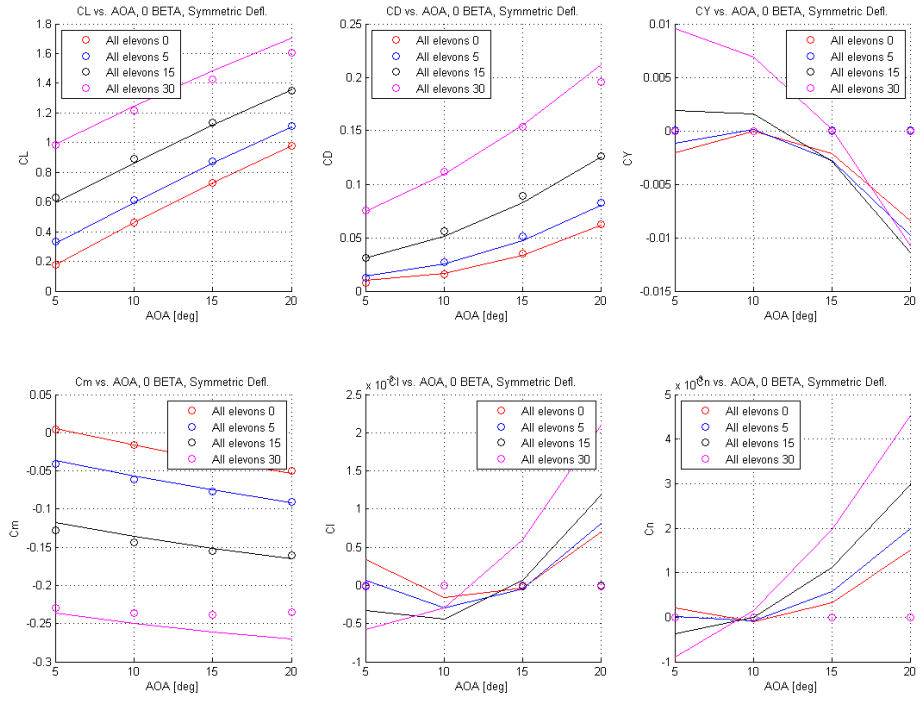

Figure 112: The RSEs (solid lines) can have some trouble predicting zero coefficients in symmetric conditions.

VORLAX only provides a lift-induced drag estimate, so a semi-empirical viscous drag correction developed by Gern was used and is added to the VORLAX drag estimate in Equation 104.[51] The viscous drag offset is derived from a skin friction relationship in Equation 105. The wetted area ratio is assumed relatively constant for the HWB configuration, and the N2A's value of 2.14 is used. The $C_{f,comp}$ term is a compressibility corrected Hoerner relationship (Equation 106) between skin friction drag and Reynold's number, using $m = 7$ and $K = 0.03$ for Reynold's numbers at the vehicle scales investigated here. The ff_{HWB} term is a form factor derived by comparing Equation 105 to N2A low speed wind tunnel data, resulting in a value of approximately 4.5.[50]

$$C_D = C_{D_i} + C_{D_v} \tag{104}$$

$$C_{D_v} = C_{f,comp} \frac{S_{wet}}{S_{ref}} ff_{HWB} \tag{105}$$

$$C_{f,comp} = \frac{C_f}{T} = \frac{K/RE^{1/m}}{1 + 0.155M^2} \tag{106}$$

The aerodynamic model for the takeoff rotation maneuver is much simpler, having only two parameters (Table 50). The effect of angle of attack is included in case the effects of extendable nose gear are investigated for aiding the maneuver. The other parameter deflects elevons 3-9, which are used together as a large pseudo-elevator. Other assumptions include a leading edge high lift device drooped 30 degrees and ground effects on. A 9-case face centered central composite design is used to generate data for creating a 2nd order RSE. This combination creates a surrogate model with excellent agreement with VORLAX data. VORLAX is run at a Mach number corresponding to the FLOPS takeoff rotation speed at sea level and with the forward takeoff CG. The landing nose hold-off aerodynamic model is a 2nd order RSE

Table 50: Design variables and ranges for takeoff rotation maneuver aerodynamic model.

	Variable	Min	Max
1	α	0	5
2	δ_{3-9}	-30	30

constructed from a five point deflection sweep of elevons 3-9, with angle of attack fixed at zero. VORLAX is run at a Mach number corresponding to V_{stall} (Equation 107) at sea level conditions. The viscous drag correction described earlier is again used for takeoff and landing aerodynamic models.

$$V_{stall} = \sqrt{\frac{2W/S}{\rho C_{L_{max}}}} \tag{107}$$

Limitations: Separation effects would introduce other nonlinear and higher order effects, but those are not modeled in VORLAX. VORLAX will therefore overpredict control effectiveness at large deflection angles and maximum attainable moments. Consequences for the short-comings of the vortex-lattice method might include undersized controls. As mentioned in previous chapters, control authority is linked in part to the planform shape which may need modification in later design stages. These inaccuracies and their consequences are avoided if modest angles of attack and deflections are used during the trim analyses. The off-design flight conditions of greatest concern are the takeoff rotation maneuver (large elevon deflections) and the directional flight conditions that saturate the rudder. The AMS Margin metrics for these flight conditions should be well above 0% unless higher fidelity tools or reliable empirical corrections are used.

7.9 Design Variables and Constraints

All of the elements necessary to complete the HWB sizing environment have been described. Once stitched together they form the environment shown in Figure 113 which evaluates TOGW, performance constraints, geometric constraints, and control

authority. As mentioned previously there are several feedback loops: 1) the center of gravity and landing gear placement convergence loop, 2) the TOGW and cruise trim with wing twist convergence loop, and 3) the feedback of TOGW and the constraints to the optimizer.

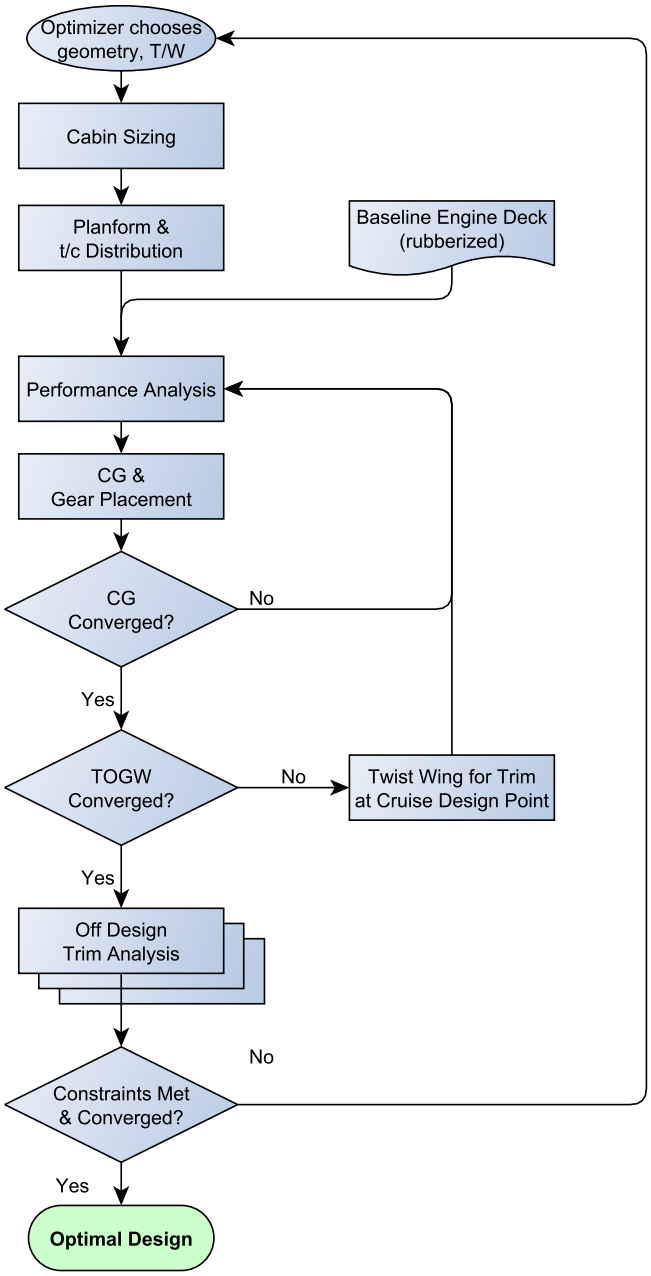

Figure 113: The primary elements and feedback loops in the HWB sizing environment.

Table 51: HWB Design Variables.

	Design Variable	Min	Max	Units
1	T_{SL}/W_{TO}	0.1	0.5	-
2	Λ_{ctr}	40	70	degrees
3	p_{ctr}	60	75	%
4	b_W	100	213	ft
5	Λ_{outer}	10	70	degrees
6	λ	0.1	0.5	-
7	p_{rc}	0.05	0.95	-
8	b_{VT}	5	20	ft
9	$p_{elevon,ctr}$	0.8	0.95	-
10	$p_{elevon,out}$	0.7	0.9	-

The assorted design variables from the previous sections have been collected in Table 51. The ranges selected for these variables are initial guesses that will be refined in the coming chapters. The upper bound for the wingspan, b_W, is set by ICAO Annex 14 code E airport regulations.

Various HWB optimization constraints discussed previously and some additional constraints are collected together in Table 52. The mission performance constraints (1-4) match those from Nickol's LTA mission (300PAX), plus an additional minimum climb ceiling constraint present in ASDL EDS missions. The range requirement is handled internally to FLOPS and does not need to be enforced at the optimizer level. Nickol's "missed approach thrust" and "2nd segment climb thrust" are not explicitly enforced in FLOPS or the HWB optimizer. To enforce them within FLOPS would require running it in optimization mode. The engine cycle parameters are fixed and the deck is scaled by max sea level takeoff thrust. Not meeting the thrust constraints results in a FLOPS failure which can be resolved by increasing the T_{SL}/W_{TO} design parameter.

The geometry constraints (5-7) serve several purposes. The excess fuel volume constraint ensures that the fuel tanks are large enough to fly the design mission. A negative twist angle prevents stall from initiating at the wingtips. Requiring the outer wing sweep to be less than that of the centerbody ensures reasonable looking

Table 52: Optimization constraints.

	Constraint	Target	Units
Performance			
1	Approach speed	< 150	knots
2	TO field length	$< 10{,}100$	ft
3	ROC @ Mach 0.84, 35k ft	> 300	ft/min
4	Climb ceiling	$> 35{,}000$	ft
Geometry			
5	Excess fuel capacity	> 0	lbs
6	Wingtip twist	< 0	degrees
7	Λ_{outer}	$< \Lambda_{ctr}$	degrees
Control Authority			
8	AMS Margin$_{Sym.\ Appr.}$	> 10	%
9	AMS Margin$_{Go-around}$	> 10	%
10	AMS Margin$_{Cross.\ Appr.}$	> 10	%
11	AMS Margin$_{OEI,air}$	> 10	%
12	AMS Margin$_{TO\ Rot.}$	> 10	%
13	AMS Margin$_{Lnd.\ nose\ hold}$	> 10	%
14	AMS Margin$_{OEI,ground}$	> 10	%
15	AMS Margin$_{Decrab}$	> 10	%
16	AMS Margin$_{Roll\ maneuv.}$	> 10	%
Other			
17	Start-of-cruise α	< 5	degrees
18	Excess clamshell drag	> 0	lbf

planforms.

The AMS Margin metric proposed in Chapter 3 must be positive in all nine off-design flight conditions. If the metric is at least zero, then there is sufficient control authority to trim. The exact amount of margin desired for each flight condition is a designer preference and they do not all need to be the same. Some additional margin beyond zero should be required as reserve for emergency maneuvers or for stability augmentation. A cruise AMS Margin is not included because it is 100% by design, since twist alone is used to trim the vehicle.

Finally, two additional constraints (17-18) have been added based on recommendations from the literature and findings from previous chapters. The start-of-cruise angle of attack is constrained for passenger comfort and is a commonly used HWB

constraint. A positive excess clamshell drag constraint ensures that elevons 1/11 and 2/10 can produce enough drag to reach a 20% throttle setting in approach conditions. This simultaneously sizes the clamshells and prevents the optimizer from relying too heavily on the centerbody elevon for pitch trim. Static margin is tracked at cruise and approach conditionsto see where optimization pushes it, but they are not constrained in this study.

7.10 Summary

The purpose of this chapter was to set up the HWB sizing and optimization environment. Conventional sizing techniques involving scaling of the wing were rejected in favor of a more integrated optimization approach. Instead, the entire planform (centerbody and outer wing) will be free to change in order to satisfy performance, geometric, and control authority constraints. The fixed engine cycle will be scaled for each planform. A modest set of design variables have been defined and initial ranges established, and design constraints have also been selected. In the chapters to follow, the HWB sizing and optimization environment will be used to explore the design space and conduct optimizations under a variety of scenarios. Together the models and their intended use for sizing contribute towards resolving RQ3.1, regarding how sizing should be performed for the HWB configuration.

CHAPTER VIII

HYBRID WING BODY DESIGN SPACE EXPLORATION

8.1 Introduction

The ranges established for each of the design variables are educated guesses and not all values will produce feasible designs. A Monte Carlo Simulation (MCS) will be useful for identifying promising regions of the design space, and to revise the design variable ranges for use in optimization. One of the research objectives was to use the assembled MDO environment to test or discover trends, correlations, and design heuristics to aid in HWB conceptual design. The MCS will also support this objective and aid in the characterization of the design space.

A complete evaluation of an HWB configuration takes on the order of 10 to 20 minutes, with the control authority assessments taking up 50% to 75% of that time. The variation in execution time is caused by follow-up trim analyses for vehicles with insufficient control authority so that negative AMS Margin can be estimated. It is suspected that many of the designs in the MCS will not meet performance constraints, and therefore assessing their control authority would be wasted effort. In an effort to discover the feasible design space more rapidly the performance constraints will be assessed first, and the control authority constraints will be assessed only for the performance-feasible designs. This modified work-flow is depicted in Figure 114. The HWB designs that remain after application of all the constraints will be good starting points for the optimization experiments, which are discussed in the next chapter.

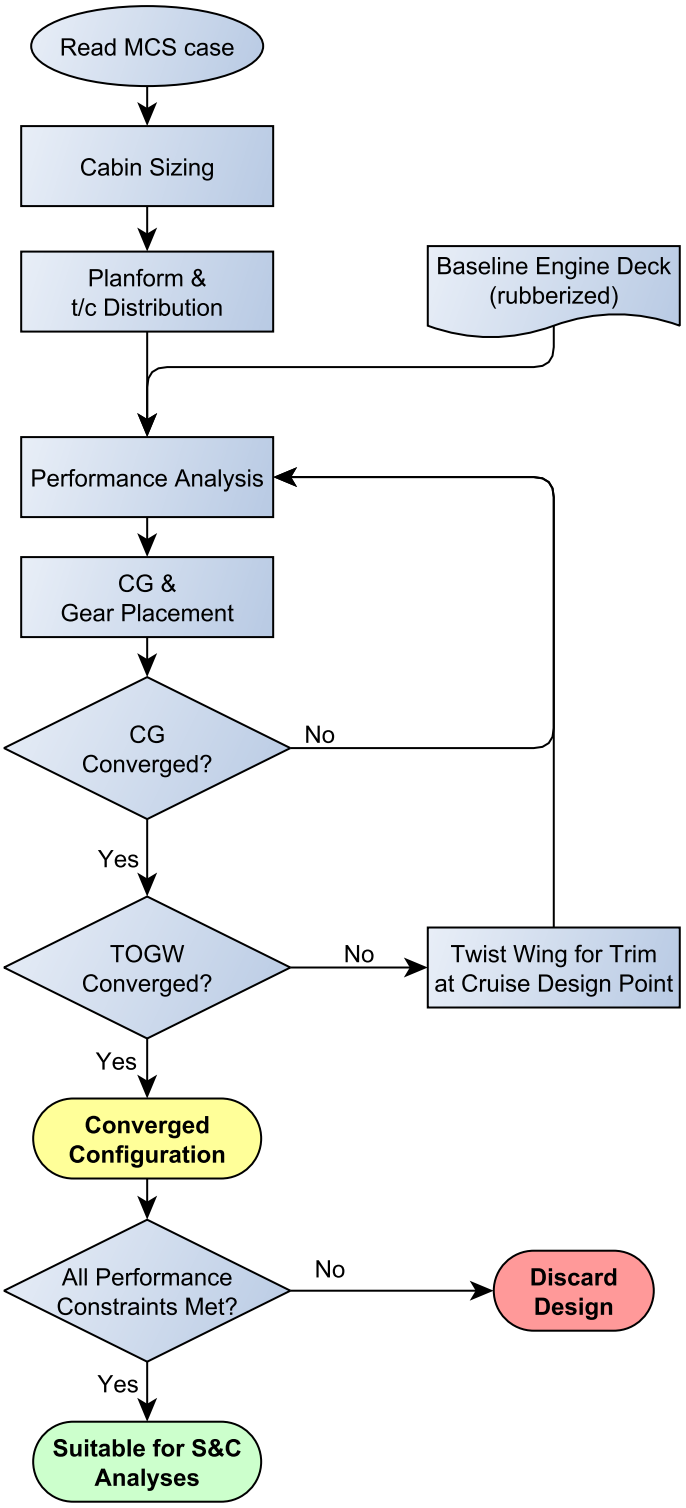

Figure 114: A reduced modeling environment for rapid identification of the feasible design space.

Table 53: HWB design variables for the initial Monte Carlo Simulation.

	Design Variable	Min	Max	Units
1	T/W	0.1	0.5	-
2	Λ_{ctr}	40	70	degrees
3	p_{ctr}	60	75	%
4	b_W	100	213	ft
5	Λ_{outer}	10	70	degrees
6	λ_W	0.1	0.5	-
7	p_{rc}	0.05	0.95	-
8	$\Lambda_{VT,c/4}$	20	60	degrees
9	λ_{VT}	0.2	0.6	-
10	AR_{VT}	1	5	-
11	$p_{elevon,ctr}$	0.8	0.95	-
12	$p_{elevon,out}$	0.7	0.9	-

8.2 Initial Monte Carlo Simulation

The parameters in Table 53 were sampled with uniform distributions bound by the minimum and maximum values. These ranges match those proposed in Section 7.9, but have additional vertical tail parameters which were included primarily to test the environment. A tail volume of 0.01265 was used to set the scale of the tail.[107]

Of the 2,000 randomly generated HWB configurations, only 341 (or 17%) of them converged while the rest were failed cases for an assortment of reasons. The most common error resulting in a failed case was due to a FLOPS climb error, which occurred for roughly 50% of all cases run. This error indicates that the rate of climb was less than or equal to zero at the beginning of the climb segment. This issue can be sometimes overcome by increasing the start-of-climb Mach number, and this fix was implemented in Section 7.3.1. Other errors were related to degenerate geometry, which were also corrected when possible. Under certain circumstances a very small centerbody elevon (large $p_{elevon,ctr}$) caused VORLAX to crash, and this issue could not be resolved.

The ranges of some of the design variables consistently resulted in failed solutions,

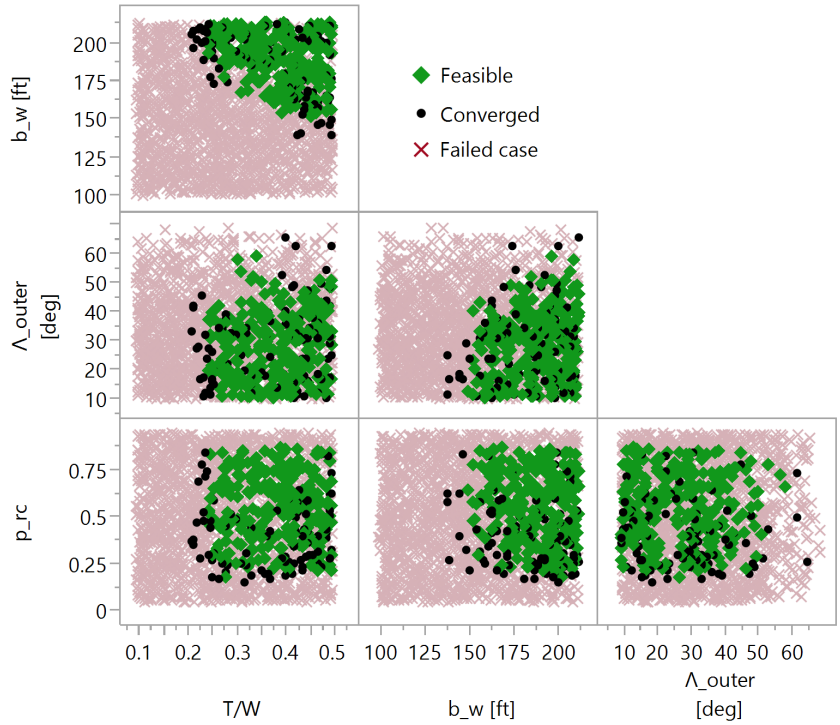

Figure 115: A multivariate scatterplot of design variables that need to be rebounded.

and are shown in Figure 115 with red X symbols. The designs whose TOGW successfully converged are black dots and those that satisfied the mission performance constraints are green diamonds. These four design variables were rebounded (see next section) to avoid wasted effort in future experiments. This initial design space exploration was also helpful for verifying that there is a performance-feasible design space given the all the assumptions made up to this point.

FLOPS is set up to analyze the input configuration by computing weights, drag polars, and evaluating mission performance. The ramp weight is estimated with a fixed range and planform. An alternative to restricting design variable ranges would be to run FLOPS in a mode with fixed ramp weight and derived range, with a range constraint imposed at the vehicle optimizer level. This was not explored in this dissertation but has the potential to reduce the number of failed cases and improve optimizer performance.

Table 54: Updated design variable bounds shown in bold font.

	Design Variable	Min	Max	Units
1	T/W	***0.25***	0.5	-
2	Λ_{ctr}	40	70	degrees
3	p_{ctr}	60	75	%
4	b_W	***160***	213	ft
5	Λ_{outer}	***20***	***55***	degrees
6	λ	0.1	0.5	-
7	p_{rc}	***0.2***	0.95	-
8	b_{VT}	5	20	ft
9	$p_{elevon,ctr}$	0.8	0.95	-
10	$p_{elevon,out}$	0.7	0.9	-
	$\Lambda_{VT,LE}$	55		degrees
	λ_{VT}	0.31		-
	AR_{VT}	1.22		-

8.3 Follow-up Monte Carlo Simulation

A follow-up MCS was performed after many iterations of bug fixes and with new design parameter ranges in Table 54. The vertical tail planform shape parameters were not strong drivers of vehicle performance in the initial MCS, and are fixed in all subsequent experiments. Values for these parameters now match those of the BWB-0009A, a recent Boeing design with centerbody mounted vertical tails and similar cruise Mach number.[15] Vertical tail span is used as the sizing parameter. The $C_{L_{max}}$ issues discovered in Section 5.6.1 have been corrected, resulting in a more realistic V_{app}. The trimmed C_L value at the maximum allowed α of 20° is used as $C_{L_{max}}$, capped at a maximum of 1 to avoid unrealistic values from VORLAX.

A total of 2,500 cases were run, again sampling from uniform distributions for each of the design variables. Of those 1,637 (or 65.5%) converged, which is a significant improvement over the initial MCS experiments. A sequence of constraints were applied to filter the design space and find the feasible regions, and the statistics are shown in Table 55. First the mission constraints from Table 45 of Chapter 7 are imposed. Next a negative twist angle and an angle of attack less than 5° are necessary

Table 55: Sequentially imposed constraints to identify the feasible design space.

	Constraint type	% of cases passing
1	Converged (no failures)	1,637/2,500 (65.5%)
2	Mission constraints from Table 45 of Chapter 7	828/2,500 (33.1%)
3	Negative tip twist to trim and $\alpha \leq 5^\circ$ at start-of-cruise design point	653/2,500 (26.1%)
4	Takeoff Rotation AMS Margin $\geq 0\%$	13/2,500 (0.5%)
5	All[1] AMS Margin constraints $\geq 0\%$	4/2,500 (0.16%)

for a well balanced and feasible design at the start-of-cruise design point. At this point only the control authority constraints remain, but they are quite expensive to generate. The takeoff rotation maneuver is known to be an active pitching moment control authority constraint, and requires the least computational effort to evaluate. Therefore this flight condition was evaluated, which reduced the feasible designs to 13 vehicles making the full suite of control authority constraints affordable to evaluate. These final constraints reduced the number of feasible designs down to four vehicles, or approximately 0.16% of all the cases evaluated.

Imposing the sequential constraints hones in on the feasible design space without wasting effort. This is visualized in Figure 116, which is a multivariate scatterplot of the mission performance and cruise trim metrics. The black dots are designs that converged, the green dots satisfied the performance constraints, the blue dots satisfy cruise trim constraints, and the red dots can perform the takeoff rotation maneuver. The region of the design space that remains feasible under all of these constraints is

[1]The following flight conditions are not included in constraint set 5: OEI on the ground, decrab maneuver, and roll maneuver. These flight conditions were implemented after the design space exploration studies had been completed, and are therefore not quantified in this chapter.

very narrow.

Some of the responses are correlated with each other, such as the top-of-climb rate-of-climb with the maximum ceiling. Takeoff field length is positively correlated with V_{app}, both driven by V_{stall} through the trimmed $C_{L_{max}}$ metric. Tip twist shows negative correlation with the start-of-cruise angle of attack. Negative twist reduces the amount of lift generated by the wing at a given angle, and requires a greater angle of attack to make up for it.

A multivariate scatterplot of the design variables was not useful for generating insights. Instead a parallel plot is shown in Figure 117, which shows each design variable with a normalized scale. Each design traces a line through this plot and is color-coded by the constraints satisfied. The designs that can perform the takeoff rotation maneuver tend to have lower thrust-to-weight ratios and outer wing root chord parameters. The maneuver is performed at full thrust, so a higher thrust-to-weight ratio increases $T_{SL_{max}}$ and the adverse nose-down pitching moment associated with it. Increasing the outer wing root chord parameter adversely affects the aerodynamic pitching moment curve (i.e., C_{m_0}) so that the wing produces stronger nose down pitching moments at zero angle of attack. Greater elevon deflections would be needed to overcome these adverse nose-down pitching moments.

The final four designs that satisfied all sets of constraints are shown in Figure 118, and their characteristics listed in Table 56. Requiring positive AMS Margin for the lateral-directional flight conditions favors designs with larger vertical tail spans. Since the VT spans were chosen randomly in the follow-up MCS, a more fair comparison between the final 13 designs would have been to give each the maximum allowed span or to have continued using the vertical tail volume coefficient. Ultimately it does not matter, because these designs are sufficient for demonstrating the utility of the AMS Margin metric in HWB optimization.

The TOGW of the designs in Table 56 are within 5% of each other. For most

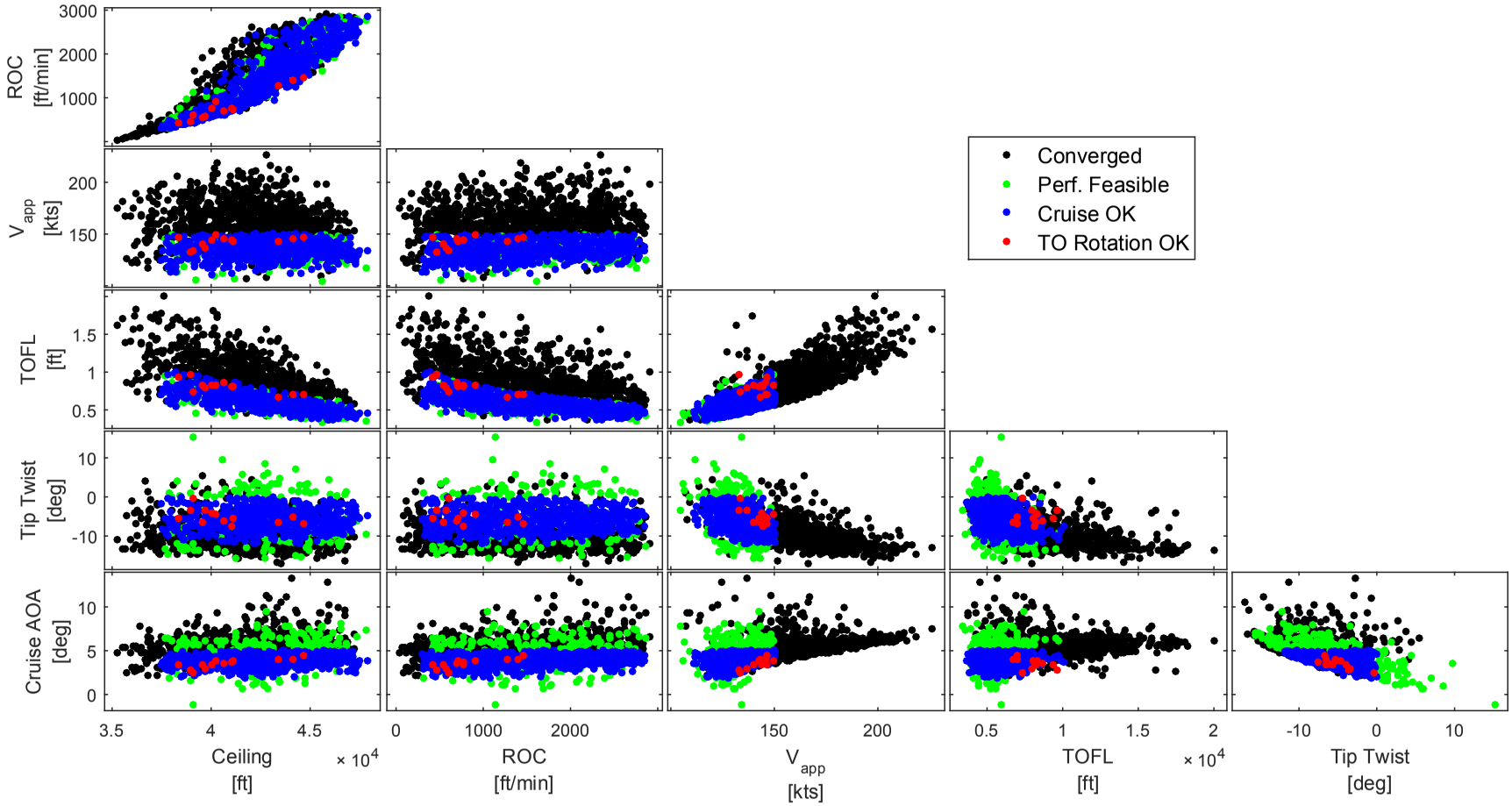

Figure 116: Performance and cruise trim responses in a multivariate scatterplot.

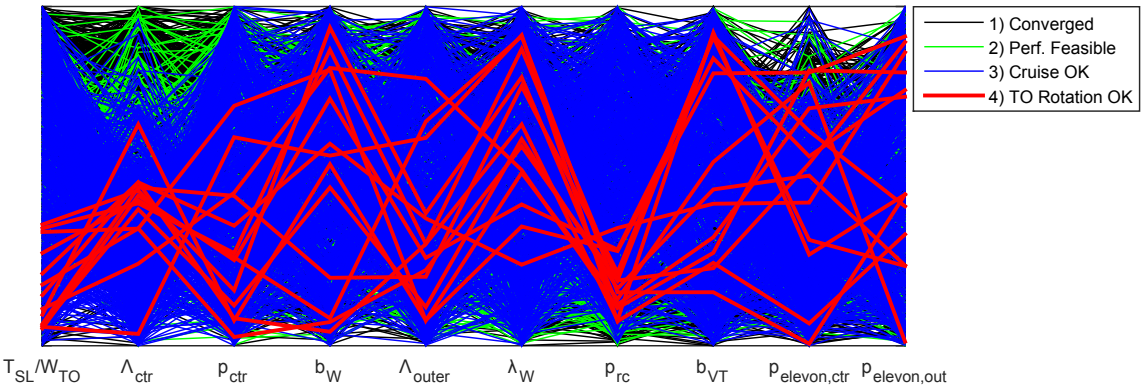

Figure 117: A parallel plot of the design variables.

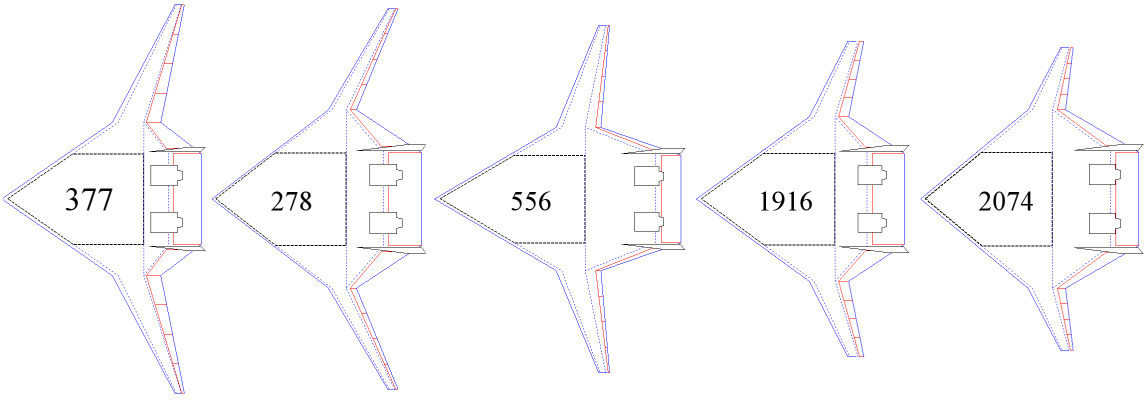

Figure 118: Four designs that satisfy all constraints (and Vehicle 377).

of these designs, the takeoff rotation maneuver and crosswind approach trim flight conditions have the lowest AMS Margin values[1] (i.e., the least remaining control authority). Vehicle 377, used for testing the trim analyses, has negative crosswind approach AMS Margin (i.e., cannot trim with a 35 knot crosswind) and also a low AMS Margin for the one engine inoperative trim flight condition. Static margin constraints have not been imposed but most of the designs are statically stable for both cruise and approach conditions. The static margin in low speed conditions is always less than that at cruise and may be the more challenging regime to stabilize. Automated flight control system design is beyond the scope of this dissertation, but was investigated for several static margins, control utilization scenarios, and turbulence scenarios in a separate publication.[47] Vehicle 2074 is statically unstable at both speeds and simultaneously being the heaviest configuration, so it was not optimized in the next chapter.

8.4 Additional Analyses

There is an opportunity for deeper investigation into the characteristics of the design space using the follow-up MCS data set. Discovering new trends, understanding the physical phenomena driving them, and creating or verifying design heuristics would all support the research objectives of this dissertation. In the following sections the accuracy of the FLOPS available fuel weight model is assessed, trends regarding wing twist and feasible CG ranges are discussed, and a few comments are made on the appropriateness of the engine deck used in these analyses. Finally, there is a discussion on conventional constraint analysis plots and their relevance to HWB design.

8.4.1 Tuning the FLOPS Available Fuel Weight Model

As mentioned in Chapter 7, FLOPS uses a tuned function of wing geometry parameters to predict the available fuel weight (Equation 108). FULWMX is the total fuel

Table 56: Four designs that satisfy all constraints (and Vehicle 377).

		Vehicle				
		377	278	556	1916	2074
Sizing	TOGW [lbs]	433,011	441,145	427,921	434,588	448,410
	T_{SL}/W_{TO}	0.32	0.34	0.27	0.27	0.30
	W_{TO}/S [lbs/ft^2]	53.22	53.44	48.46	54.67	51.92
Perf. Constraints	Max Ceiling [ft]	42,850	44,145	40,653	38,327	39,084
	ROC [ft/min]	1,160	1,393	703	422	601
	V_{app} [knots]	153	145.7	145.7	146.2	133.4
	TOFL [ft]	8,094	6,980	8,694	9,364	7,335
AMS Margin Constraints	Takeoff Rotation [%]	8.9	3.1	11.6	14.9	0.8
	Landing Nose Hold-off [%]	48.9	53.3	44.0	43.2	43.8
	Symmetric Approach [%]	83.4	95.6	89.9	92.5	97.3
	Go-around [%]	67.5	71.5	70.3	76.1	79.0
	Crosswind Approach [%]	-2.8	4.2	3.5	9.4	2.3
	One Engine Inop. [%]	3.3	29.2	43.6	44.5	41.9
Cruise	AOA [deg]	4.56	4.03	3.49	3.37	2.42
	Tip Twist [deg]	-9.45	-5.28	-6.19	-5.59	-0.42
	Static Margin [%]	9.99	5.69	5.17	3.46	-0.64
Low Speed	Trimmed $C_{L_{max}}$ (at $\alpha = 20°$)	0.79	0.89	0.80	0.87	0.97
	Static Margin [%]	8.58	3.03	4.21	2.78	-1.82

capacity of the wing in lbs, FWMAX is the configuration dependent tuning parameter, TCA is the average thickness to chord ratio, SW is the wing area in ft^2, SPAN is wingspan in ft, and TR is the outer wing taper ratio.

$$\text{FULWMX} = \text{FWMAX}\frac{\text{TCA} \cdot \text{SW}^2}{\text{SPAN}}\left(1 - \frac{\text{TR}}{1 + \text{TR}^2}\right) \tag{108}$$

The FLOPS fuel weight equation is only for the wing of a conventional aircraft, and the user-specified parameter FULFMX is supposed to account for fuel stored in the wing carry-through. Regarding the parametric geometry used in this dissertation, this might correspond to the inboard fuel tank. FLOPS has no equation for FULFMX, so the FULWMX equation will be tuned to best match data from the geometry environment. A statistical analysis software named JMP was used to fit this model, including an intercept term, to the data from the Monte Carlo simulation. This regression is shown in Equation 109.

$$\text{FULWMX} = -16752 + 9.83\frac{\text{TCA} \cdot \text{SW}^2}{\text{SPAN}}\left(1 - \frac{\text{TR}}{1 + \text{TR}^2}\right) \tag{109}$$

The FWMAX parameter takes a value of 9.83 assuming an intercept term correction factor, similar to the value of 8.5 used by the Aerospace Systems Design Laboratory[1]. The model fit is not very accurate as demonstrated by the actual-by-predicted and residual-by-predicted plots shown in Figure 119, and an R^2 of just 0.64.

The FLOPS model was intended for use with T&W configurations and with other assumptions that may not have been explicitly stated in the manual. An alternative model based on the HWB geometry parameters used here can be generated using a third order response surface equation (RSE) with stepwise regression. The goodness of fit indicators shown in Figure 120, an R^2 of 0.99, and the model fit error comparison

[1]Based on inspection of HWB FLOPS files for NASA ERA work, courtesy Dr. Jeffrey Schutte.

of Figure 121 indicate that this model is a better predictor of available fuel weight. Future versions of FLOPS would therefore benefit from a modified model or regression for available fuel weight. The negative consequences of using the existing FLOPS model are negligible, however, if used strictly in the context of sizing and not S&C analyses. Volume available for fuel in these models is always greater than that required for the design mission, so for sizing it is not a critical issue.

8.4.2 Observations on Tip Twist

Figure 122 shows the tip twist angle required to trim without deflections at the start-of-cruise design point for all converged designs. One of the requirements for the tip twist angle is that it be less than or equal to zero, to avoid tip stall at high angles of attack. Such vehicles are poorly balanced or "tail-heavy" as indicated in Figure 122(a) by the higher % MAC (farther aft).

Those designs with positive tip twist also suffer significant aerodynamic penalties resulting in higher takeoff gross weights, indicated by the color map. The maximum takeoff gross weights are on the order of 720,000 lbs but are clipped to a maximum of 550,000 lbs in the color map to better distinguish the low weight designs in blue. This shows a cluster of designs with start-of-cruise CGs between 30 and 37% MAC that have low weight and modest negative tip twist. The designs chosen for optimization in Section 8.3 are also in this region.

This "sweet spot" of low weight designs is also observed in Figure 122(b), with start-of-cruise static margins ranging from 10% to just under 0%. As a reminder, static margin describes the position of the CG relative to the vehicle aerodynamic center. If the CG is forward of the aerodynamic center, then the static margin is positive and the vehicle experiences restoring moments when perturbed from trim and positive static stability. As the CG moves aft closer to the aerodynamic center, the static margin is reduced and can become negative. Vehicles with low and negative

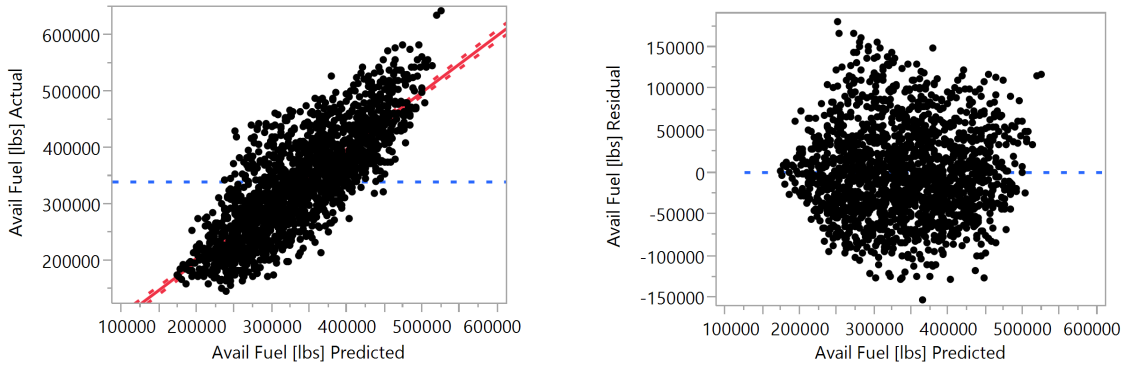

(a) Actual by predicted

(b) Residual by predicted

Figure 119: Goodness-of-fit indicators for the tuned FLOPS equation of available fuel in lbs.

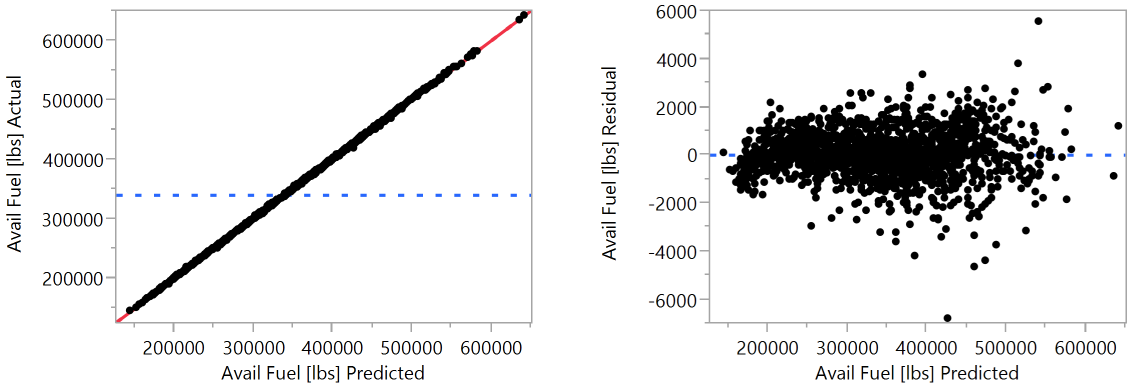

(a) Actual by predicted

(b) Residual by predicted

Figure 120: Goodness-of-fit indicators for the 3rd order RSE of available fuel in lbs.

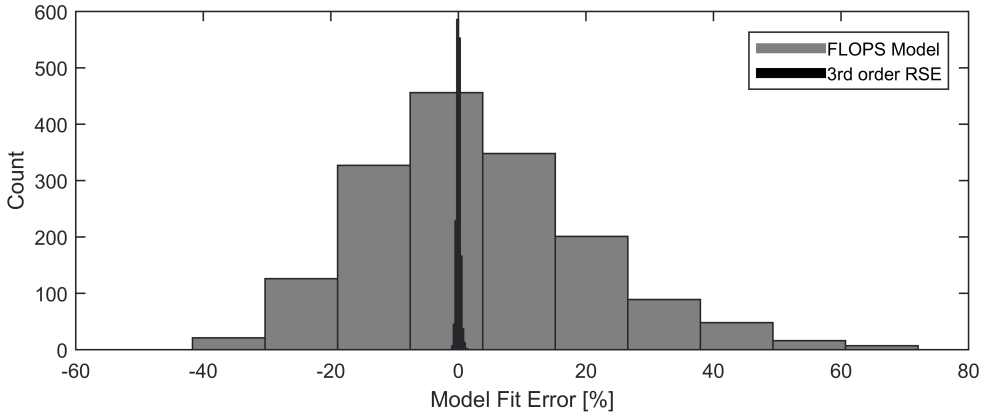

Figure 121: A comparison of model fit error of the two available fuel volume models.

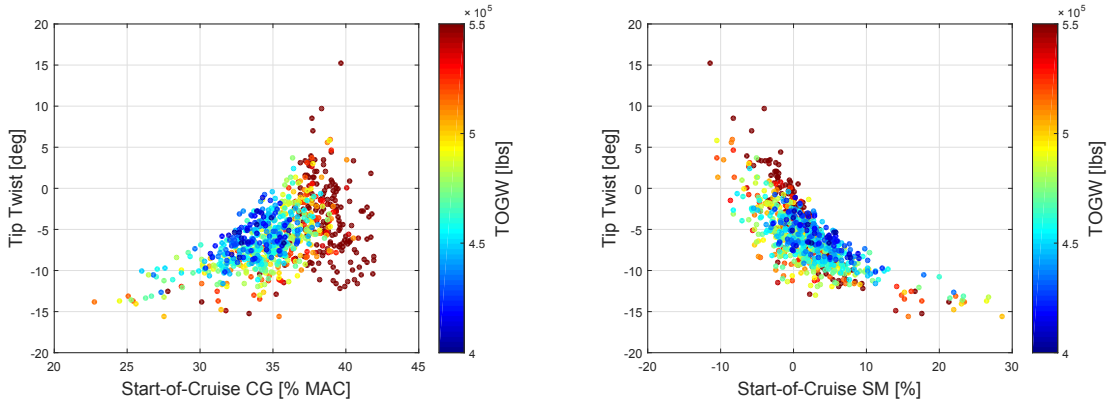

(a) (b)

Figure 122: Tip twist trends color coded by TOGW.

static margins require stability augmentation systems to ensure acceptable dynamic stability performance.

A design heuristic from Boeing that Nickol also employed was that vehicle designs with neutral static margins (i.e., 0%) at cruise conditions can be balanced (and would require stability augmentation).[97, 107] The trends shown in Figure 122(b) are consistent with this heuristic, but show that it may be overly constraining. Another component of the Boeing heuristic stated that neutral static margin should occur with CGs and aerodynamic centers near the 40% MAC position. The results of Figure 122(a) show that well balanced and low weight designs occur with CGs that are forward of this mark by 3 to 10 points.

It is not known whether the planform layout rules and assumptions used in this dissertation are fully compatible with those of the Boeing heuristic. Such differences might explain the discrepancy here. In addition, the CGs and static margins plotted here are the forward-most possible at the start-of-cruise using fuel shifting. The CGs are still able to be shifted aft by several points if fuel is pumped to the outboard tanks. This demonstrated in Figure 123, which plots tip twist (still designed for the forward CG) against the aft-most CG available from fuel shifting. The low takeoff gross weight designs are able to achieve aft CG positions of 40% MAC. Unless the

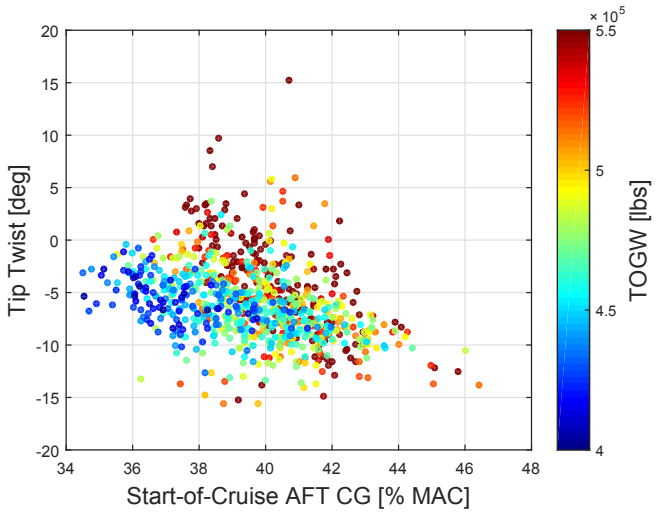

Figure 123: Tip twist (designed for forward CG) plotted against alternative aft CGs generated by shifting fuel to outboard tanks.

wing is twisted for the aft CG, deflections will be needed to retrim the vehicle. The consequences of these deflections for a CG aft of design condition are outlined by Garmendia & Chakraborty, namely that steady state actuation power requirements can increase dramatically.[47]

8.4.3 Feasible CG Ranges

The CG ranges discussed in the previous section were for designs that met the mission performance constraints. In this section the cruise trim constraints and takeoff rotation maneuver feasibility constraints are imposed to observe what happens to the feasible CG range. In Figure 124 the CGs for three loading scenarios are plotted for the follow-up MCS designs: forward takeoff, forward cruise, and aft cruise. It was mentioned previously that it is possible for the CG of performance-feasible designs to cross the 40% MAC mark with outboard fuel shifting. However, performance-feasible designs that can also perform the takeoff rotation maneuver have a much narrower range. An alternative heuristic based on these findings is offered:

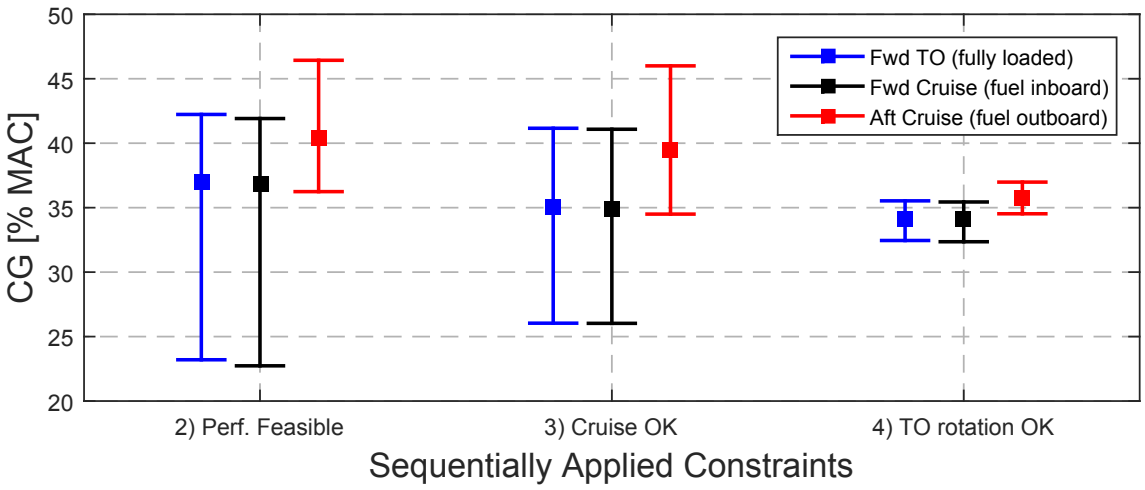

Figure 124: CG ranges for the follow-up MCS designs under the sequential constraints.

Heuristic: HWB configurations that meet mission performance constraints, can be balanced in cruise, *and* perform the takeoff rotation maneuver tend to have CGs around 35% MAC.

8.4.4 Engine Deck Scaling

It is preferable to keep the scale of the rubberized engine within ±10% of the baseline thrust it was designed for. Otherwise some iteration with a new engine deck may be necessary, or simultaneous optimization of the engine cycle with the aircraft. Figure 125 shows the range of engine scales required for the follow-up MCS data set under each of the sequential constraints. Fortunately the vehicles that meet performance constraints, cruise trim constraints, and can perform the takeoff rotation maneuver have engine scales near unity. This indicates that the baseline engine was properly selected for this class of HWB and mission.

8.4.5 Constraint Analysis Plots

Mission performance constraints can frequently be translated into relationships between the thrust-to-weight ratio and wing loading sizing parameters. Certain assumptions have to be made regarding the vehicle's drag polar and thrust lapse as a function of

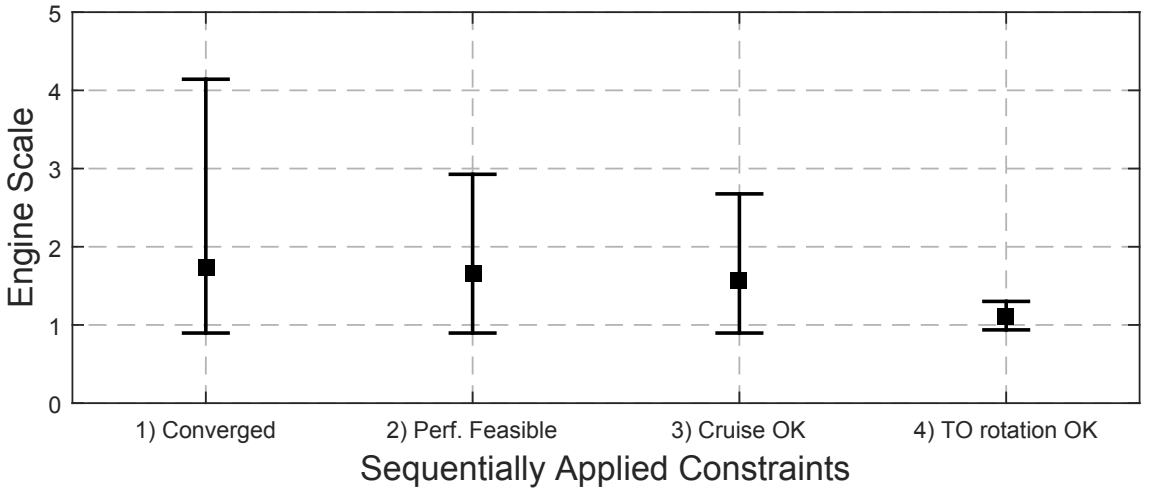

Figure 125: Upper/lower bounds and mean engine scale multiplier for designs that pass each constraint gate.

altitude and Mach number. Mattingly notes that: "It is not necessary that these assumptions be exact, but greater accuracy reduces the need for iteration."[84] For the drag polar to be accurate across vehicle scales, geometric similarity must be maintained. This assumption is unrealistic for the HWB configuration. If the centerbody region is held constant due to the fact that the payload has a fixed size, then that leaves the outer wings to scale in isolation which violates the geometric similarity assumption. As established in previous sections, achieving a CG within a relatively narrow band is extremely important for this configuration. Multiple outer wing parameters would likely have to change simultaneously in order to achieve this, further violating the geometric similarity assumption.

The violation of assumptions in typical constraint analyses makes their definition of the feasible design space questionable. The constraint lines might only be accurate in the immediate vicinity of the baseline design's wing loading, which itself may not satisfy all of the performance constraints. This is the challenge of trying to use wing loading as a design parameter and the conventional sizing process to size the planform of the HWB. The sized wing area that is an output of conventional sizing methods is insufficient information for determining trimmed $C_{L_{max}}$ (for V_{app} or V_{stall}),

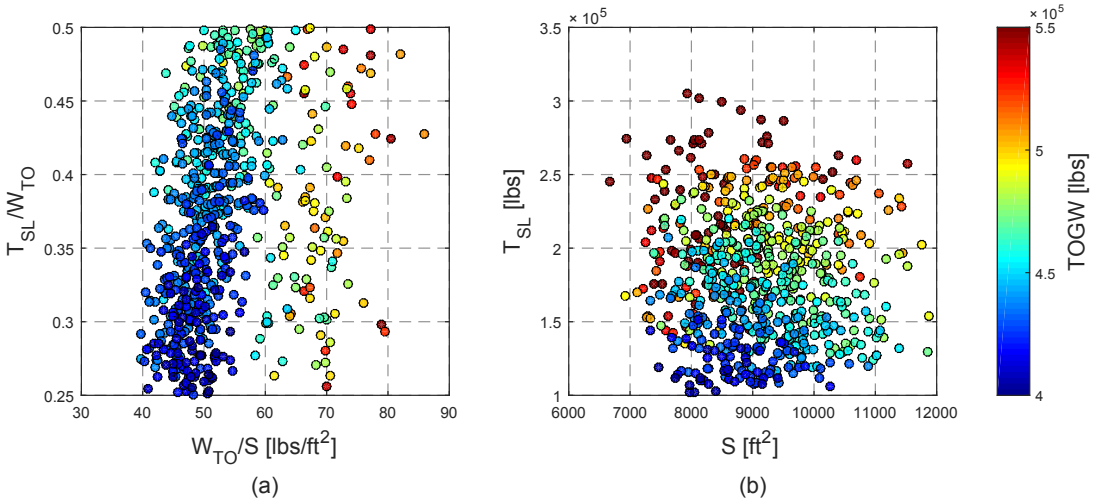

Figure 126: The follow-up MCS data that meet performance constraints visualized using conventional sizing charts, and color-coded by takeoff gross weight.

whether the vehicle can trim at cruise with reasonable twist and angle of attack, or whether it can perform the takeoff rotation maneuver. Resolving issues with any of those constraints requires a planform change and repetition of the constraint analysis, mission analysis, and weight estimation.

For the reasons described above, a conventional constraint analysis was not performed. Instead, the results of the follow-up MCS are shown in a thrust-to-weight ratio vs. wing loading plot and a thrust vs. planform area plot shown side by side in Figure 126. There are several very heavy designs with wing loading in the 60 to 85 lbs/ft^2 range, and they were ignored. The low weight designs occupy a region of the thrust-to-weight / wing loading plot where one would expect them to be: low thrust-to-weight and high wing loading. In the thrust vs. planform area plot low TOGW occurs in the bottom left, though is more strongly correlated with thrust.

If the constraint plots are recolored by which sequential set of constraints they satisfy an interesting trend emerges. Figure 127 shows designs that satisfy performance constraints and cruise trim requirements in gray, and designs that can perform the takeoff rotation maneuver are red. The vehicles that can perform the maneuver occupy the same space that the low weight designs occupy. An upper bound for feasible

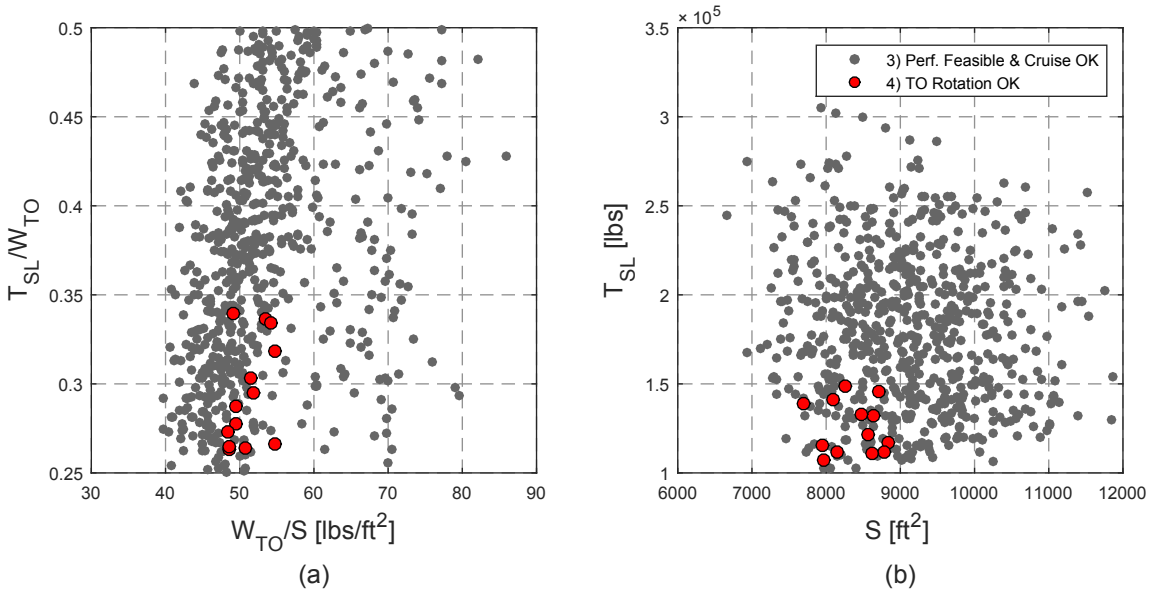

Figure 127: The follow-up MCS data that meet performance constraints visualized using conventional sizing charts, with red dots indicting that the vehicle can perform the takeoff rotation maneuver.

thrust-to-weight is about 0.35, but an analytical relationship could not be established. The takeoff rotation maneuver occurs at full thrust, so higher thrust-to-weight values produce higher adverse nose-down pitching moments.

As shown in Figure 128, the vehicles that can perform the takeoff rotation maneuver are also in regions of high approach speed (e.g., stall and rotation speed) and high TOFL. In Section 5.9 a trade-off between control authority, speed, and TOFL was identified and its critical importance can now be recognized. The vehicles that cannot perform the takeoff rotation maneuver have low approach speeds and therefore lower stall and rotation speeds. The rotation speed is by default $V_R = 1.05V_{stall}$ in FLOPS. Pitching moment control authority is proportional to velocity squared ($M = \frac{1}{2}\rho V^2 S\bar{c}C_m$), so low stall speeds are actually detrimental to the rotation maneuver. Vehicles with low approach and stall speeds also happen to have takeoff field lengths well below the maximum allowed. It may be reasonable to extend their takeoff distance in order to achieve a higher rotation speed, granting greater pitching moment control authority. This operational change would be a much simpler method of

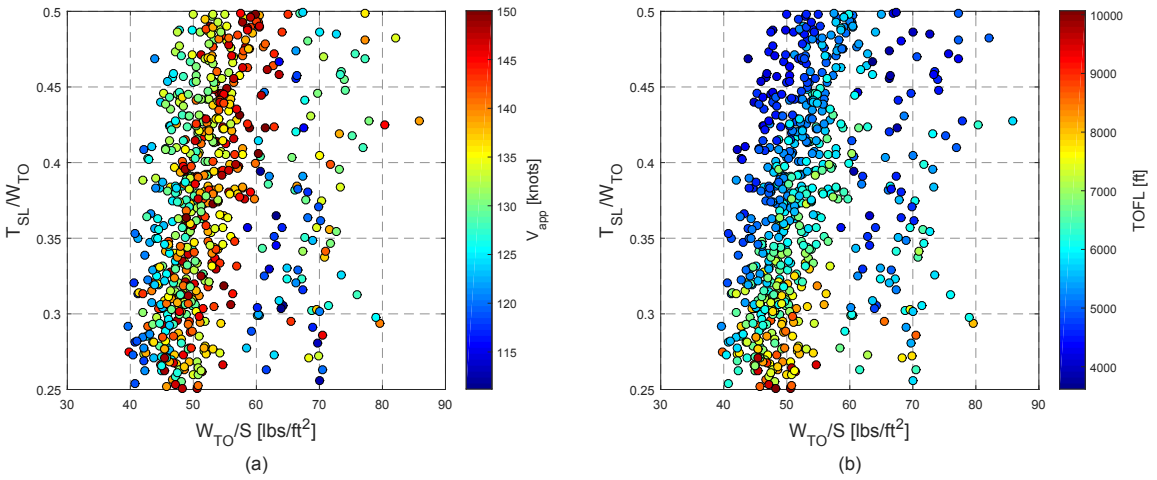

Figure 128: The follow-up MCS data that meet performance constraints visualized using conventional sizing charts, and color-coded by various constraint metrics.

opening up the feasible design space than the infusion of technologies such as thrust vectoring or body flaps. This is an important finding and is summarized below. Designers should be aware that the increase in speed may have a negative impact on noise, but this trade-off cannot be quantified with the assembled tools of this method.

Observation: The feasible design space can be expanded by increasing V_R, trading increased TOFL (up to the max allowed) for greater pitching moment control authority during the takeoff rotation maneuver.

8.5 Conclusion

This chapter has successfully demonstrated the integrated modeling environment for HWB sizing and design space exploration. The many investigations and discoveries within this chapter contribute to the secondary research objective. A Monte Carlo simulation was used to rigorously test the environment, identify better design variable ranges, and draw other useful insights from the data in support of the research objectives. The feasible design space was discovered rapidly by evaluating the expensive control authority constraints only for those designs that satisfied the performance

and cruise trim constraints. Less than 1% of all evaluated designs were able to satisfy the performance, cruise trim, and off-design control authority constraints. These designs served as good starting points in the optimization experiments described in Chapter 9.

Other important contributions from this chapter come from the analysis of the Monte Carlo simulation data set. Tuning parameters for the FLOPS available fuel weight relationship were generated by least squares regression on the geometry driven outputs of the HWB modeling environment. Trends regarding placement of the center of gravity were discovered and were compared to design heuristics from the literature. A new extended design heuristic regarding desirable CG locations was offered based on the results and assumptions from this chapter. Finally, a deeper investigation into the feasible design space used conventional constraint analysis plots to generate insights. One of the discoveries was an untapped trade-off between takeoff rotation maneuver control authority and takeoff field length that could expand the feasible design space.

There are opportunities for future or follow-up research, including the generation of surrogate models for rapid design space exploration. Surrogates will be very computationally expensive to make given the environment's long run time, which up to this point was frequently being modified. The environment has since stabilized, making the effort for surrogates worthwhile. Finally, the CG design heuristic discovered in Section 8.4.3 should be verified for or generalized to other passenger classes and mission profiles.

CHAPTER IX

HYBRID WING BODY OPTIMIZATION

9.1 Introduction

The primary goal of this chapter is to make recommendations regarding how to conduct HWB optimization for conceptual design studies. This will be supported by the selection of an optimization algorithm and discovery of good optimizer settings. In addition, various control utilization scenarios will be investigated to observe their effect on final optimized designs. The tail volume coefficient method for tail sizing will be revisited to see if it performs well compared to actual lateral-directional constraints. These efforts will be the final step in achieving the sub-research objective and demonstrating the capabilities of the integrated suite of models to perform HWB sizing (RQ3.1). In addition, demonstrating the AMS Margin control authority metric in an optimization problem will be the final step necessary to resolve RQ2.2. The optimization experiments were conducted using Vehicles 377 and 278, which were discovered during the design space exploration studies.

9.2 Optimization Setup

The optimization statement for the experiments conducted in this chapter is given below. Takeoff gross weight will be minimized by manipulating thrust-to-weight ratio and the geometry variables, subject to mission performance and control authority constraints. Initial experiments in Section 9.3 were conducted while utilizing all elevons independently in the control authority assessments. These initial tests omitted the OEI on the ground, decrab maneuver, and roll maneuver flight conditions. The resulting tails were suspected to be under-sized so two follow-up optimization

Table 57: Updated design variable bounds shown in bold font.

	Design Variable	Min	Max	Units
1	T/W	0.25	0.5	-
2	Λ_{ctr}	40	70	degrees
3	p_{ctr}	60	75	%
4	b_W	160	213	ft
5	Λ_{outer}	20	55	degrees
6	λ	0.1	0.5	-
7	p_{rc}	0.2	0.95	-
8	b_{VT}	5	**25**	ft
9	$p_{elevon,ctr}$	0.8	**0.93**	-
10	$p_{elevon,out}$	0.7	0.9	-
	$\Lambda_{VT,LE}$	55		degrees
	λ_{VT}	0.31		-
	AR_{VT}	1.22		-

experiments were conducted. The experiments of Section 9.4 attempt to prevent unintended elevon behavior and force increased reliance on the vertical tails. Section 9.6 introduces the omitted flight conditions to observe how the optimized vehicles change. Finally, Section 9.5 tests whether the tail volume coefficient method is competitive with the physics-based control authority assessment method.

$$\begin{aligned} \underset{x}{\text{minimize}} \quad & TOGW(x) \\ \text{subject to} \quad & \text{1) x side constraints in Table 57} \\ & \text{2) Performance, geometry, control authority constraints in Table 58} \\ & \text{3) Control utilization scenario} \end{aligned}$$

The design space exploration chapter used Monte Carlo Simulation to discover the feasible space and select candidate designs for optimization. Gradient-based algorithms are preferred over global search or stochastic methods because the objective function and constraints are continuous, and the feasible designs space was already discovered. In addition, the long function call evaluation time might make a global optimizer take an excessive amount of time. The MCS experiments revealed that cases

Table 58: Revised optimization constraints.

	Constraint	Target	Units
Performance			
1	Approach speed	< 150	knots
2	TO field length	$< 10{,}100$	ft
3	ROC @ Mach 0.84, 35k ft	> 300	ft/min
4	Climb ceiling	$> 35{,}000$	ft
Geometry			
5	Excess fuel capacity	> 0	lbs
6	Wingtip twist	< 0	degrees
7	Λ_{outer}	$< \Lambda_{ctr}$	degrees
Control Authority			
8	AMS Margin$_{Sym.\ Appr.}$	> 10	%
9	AMS Margin$_{Go-around}$	> 10	%
10	AMS Margin$_{Cross.\ Appr.}$	> 10	%
11	AMS Margin$_{OEI,air}$	> 10	%
12	AMS Margin$_{TO\ Rot.}$	> 10	%
13	AMS Margin$_{Lnd.\ nose\ hold}$	> 10	%
14	AMS Margin$_{OEI,ground}$	> 10	%
15	AMS Margin$_{Decrab}$	> 10	%
16	AMS Margin$_{Roll\ maneuv.}$	> 10	%
17	Crosswind roll angle, ϕ	< 5	degrees
Other			
18	Start-of-cruise α	< 5	degrees
19	Excess clamshell drag	> 0	lbf

can still fail due to FLOPS or VORLAX errors that were not resolvable. Matlab's sequential quadratic programming (SQP) implementation in fmincon is therefore a good choice because it is able to accommodate these failures so long as they do not happen during the gradient calculation phase of the algorithm. If a case failure occurs during the line search segment of the algorithm, fmincon will reduce the step size and try again. The SQP algorithm also works well for optimization problems like this one in which there are more constraints than design variables. Comparison of alternative algorithms was prohibitively expensive, but would be enabled by surrogate models of the environment and would be a useful avenue of future research.

A series of optimization experiments were conducted to establish best practices and select optimizer settings. Initially experiments were unable to reduce TOGW or

find designs that satisfied all constraints simultaneously. Rescaling techniques were used to improve optimizer performance. The design variables, which had different units and magnitudes, were rescaled to a have a range of 0-1. A flag within fmincon was enabled, which divides the objective function and constraints by their initial values to scale them. These steps prevent any single design variable or constraint from dominating the others during the selection of a search direction, by rescaling them to have similar orders of magnitude.

The TOGW objective function is reported by FLOPS in integers. The finite difference step size for calculating the gradient therefore had to be large enough to make noticeable difference in TOGW. With the design variables scaled between 0 and 1, a finite difference step of 1e-2 was found to work well and enable approximation of the gradient. The constraint tolerance was left at the default value of 1e-6. The tolerance for the scaled objective function was set to 1e-3, which for a 400,000 lb initial design would correspond to 400 lbs. A maximum of 400 iterations was imposed, but the default step size constraint of 1e-6 was usually the termination condition met first. Due to the 10-20 minute function call evaluation each optimization experiment can take several days to complete. Multiple desktop computers were utilized to conduct optimization experiments simultaneously.

Starting the optimizations at designs that satisfied all or most of the constraints was critical for good optimizer performance. AMS Margin constraints were also initially required to be 25% or greater simultaneously, but it became apparent that this was not a realistic goal. It caused the optimizer to perform poorly, unable to find the feasible space or reduce TOGW. The AMS Margin constraints were reduced to 10%, which could be achieved simultaneously.

The final designs from the MCS were only required to trim successfully, not necessarily with AMS Margin greater than 10%. Vertical tail span was increased in order to start the optimization experiments with OEI in the air and crosswind approach

AMS Margins in the feasible region. In retrospect, more designs from the MCS of the previous chapter may have satisfied all constraints if their tail spans had been increased. However, the purpose of this chapter is not to discover a global optimum solution, but instead to establish optimization best practices.

A consequence of using over-sized tails was that some vehicles would require large roll angles to trim side force in crosswind conditions. Air worthiness regulations require this angle to be less than 5 degrees, but when enforced by the trim analyses it would prevent vehicles with otherwise adequate control authority from returning a trim solution. The constraint was therefore moved to the HWB vehicle optimization level, and is listed in Table 58. This avoided unnecessary trim analysis failures or computationally expensive AMS Margin extrapolations.

Early optimization and MCS experiments indicated that centerbody elevon chord fractions ($p_{elevon,ctr}$) at the maximum value of 0.95 (i.e. the smallest allowed elevon) were causing the VORLAX aerodynamic tool to return nonsense answers, crash, or freeze. Optimization experiments were frequently attempting to evaluate designs with such small centerbody elevons, so the upper bound on this design variable was changed to 0.93 to avoid this problem.

9.3 HWB Optimization Utilizing Independent Elevons

In this section optimization results for Vehicles 377 and 278 are presented. As a reminder the control authority metrics were generated based on the minimum drag trim solutions, which were shown in Chapters 4 and 5 to have modest deflections and no unnecessary saturation of the controls when paired with clamshells to meet throttle constraints. The trim optimizer was free to use all elevons independently to balance the forces and moments as well as minimize drag. The rudders were linked and deflected together. The results of the optimization will be shown in terms of before and after geometry, iteration history, as well as the before and after constraints, design

variables, and other important metrics. These optimization experiments were conducted prior to the implementation of 1) OEI on the ground, 2) the decrab maneuver, and 3) the landing roll maneuver in the MDO environment.

9.3.1 Vehicle 377 Optimization Results

Prior to optimization, the vertical tail span was increased from 15 to 19.5 ft in order to satisfy the 10% or greater AMS Margin for the crosswind approach flight condition. This condition appeared to be the most constraining lateral-directional flight condition. The optimizer was discovered to be sensitive to this particular constraint, and would struggle to find the feasible design space if it was initially violated. The optimizer was able to cope with the initially infeasible V_{app} (a few knots too high) and takeoff rotation maneuver AMS Margin (a few points too low).

First the TOGW history over the course of the optimization shown in Figure 129 will be inspected, where the start of each iteration is denoted with a black dot. There were no failed cases during this optimization run, which would have shown as breaks in the line. In the first 100 function calls the algorithm is cycling between calculating the gradient (flat regions) and performing a line search seeking the feasible space (the peaks). At function call 126 the optimizer discovers a way to gain a significant improvement to TOGW, but after this point achieves no further improvement. Optimization was terminated at function call 398 when the step size became smaller than the tolerance setting, after running for nearly 67 hours. All constraints were satisfied and a local optimum was obtained.

The AMS Margin constraint histories are plotted in Figure 130. The gray transparent regions of the plots indicate the infeasible space, where AMS Margin is below 10%. Figure 130(a) shows that of the longitudinal flight conditions only the takeoff rotation maneuver and landing nose hold-off ever dip below the required AMS Margin. During the early gradient calculation iterations those two AMS Margin constraints

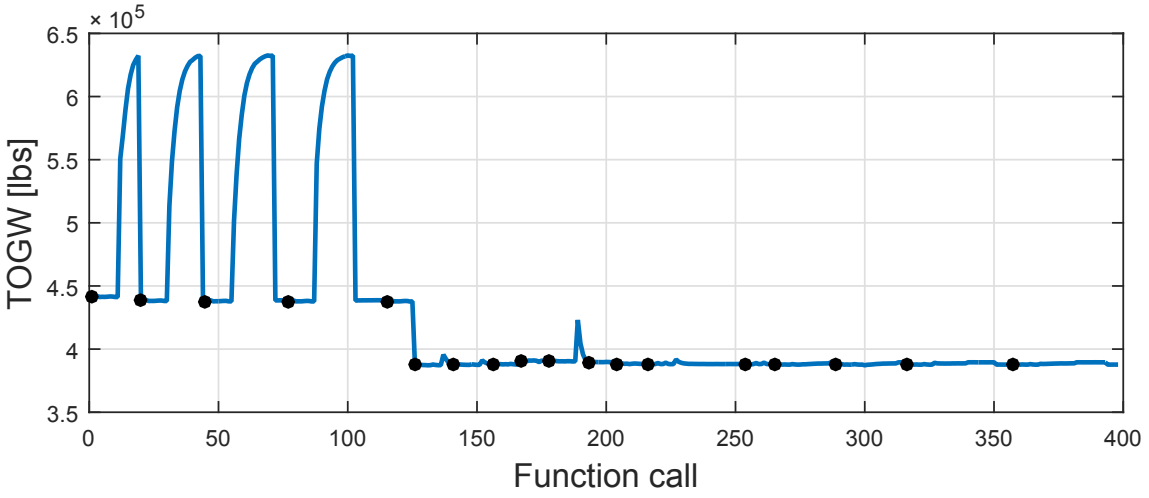

Figure 129: Vehicle 377 iteration history for the TOGW objective function.

dip into the negative hundreds range. As a reminder, the AMS Margin is a measure of *remaining* control authority and negative values indicate inadequate control authority to perform the maneuver. The takeoff rotation maneuver AMS Margin dips down to -374% at one point, indicating that to perform the maneuver that vehicle would require a nose-up pitching moment 3.74 times greater than what was available. Throughout the optimization run the takeoff rotation maneuver is consistently the most constraining longitudinal flight condition.

Figure 130(b) shows the function call history of the two lateral-directional flight conditions evaluated during this optimization experiment. Only once during the optimization does the OEI in the air AMS Margin dip below 10%, but the vehicles can always successfully trim using the available control authority. The crosswind approach AMS Margin constraint on the other hand is frequently violated, frequently negative, and by the end of the optimization is an active constraint. The 126th function call that brought a large improvement to TOGW also degraded the takeoff rotation maneuver, landing nose hold-off, and crosswind approach AMS Margin constraints. It took approximately 100 additional function calls and several iterations for these control authority constraints to become feasible again. After about function call 225

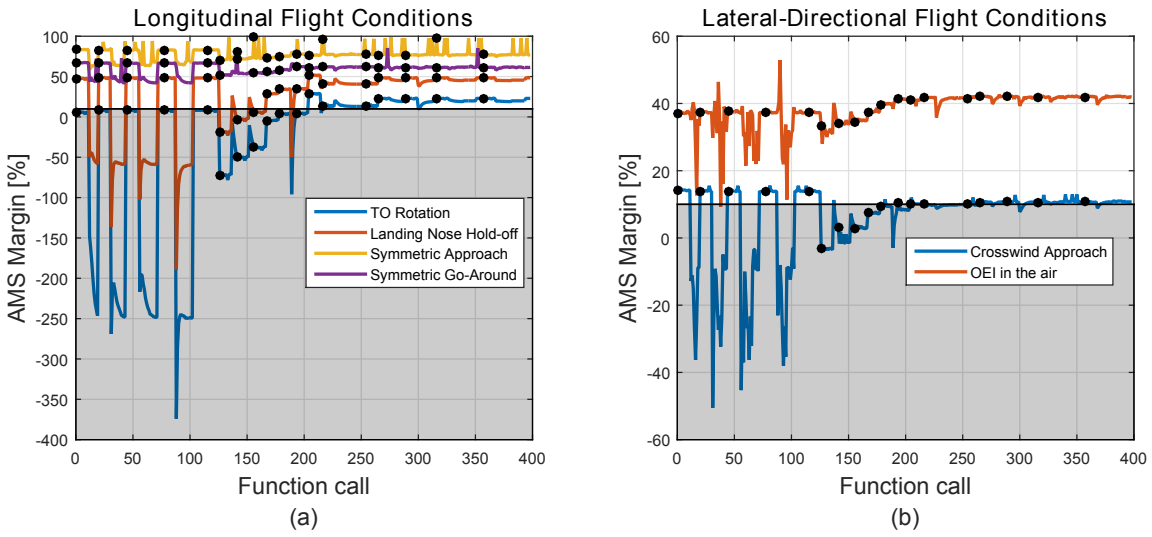

Figure 130: Vehicle 377 iteration history for the control authority constraints.

there is no significant change in the AMS Margin constraint values.

The function call history for a selection of performance constraints and design variables are shown in Figure 131. The excess clamshell drag (a) was expected to be driven by the outer wing elevon chord fraction (d), but the latter essentially constant over the course of optimization. The initial wide variation in clamshell effectiveness is likely driven by the approach speed, and the later variation by more subtle changes to the outer wing planform shape. By the end of the optimization run, TOFL (b) is near the maximum allowed and approach speed (c) is an active performance constraint.

The AMS Margin constraints are correlated with approach velocity which makes sense because control moments are proportional to V^2. Increasing the vehicle's speed appears to be the optimizer's strategy for achieving adequate control authority. It is important to note that the only mechanism in these experiments available to the optimizer for increasing the velocity is through reduction of the trimmed $C_{L_{max}}$ estimate. Planform geometry is therefore being evolved in a way that increases static margin starting around function call 126.

Two other design variables besides the outer wing elevon chord fraction were limited by their lower side bounds. By function call 126 the thrust-to-weight ratio

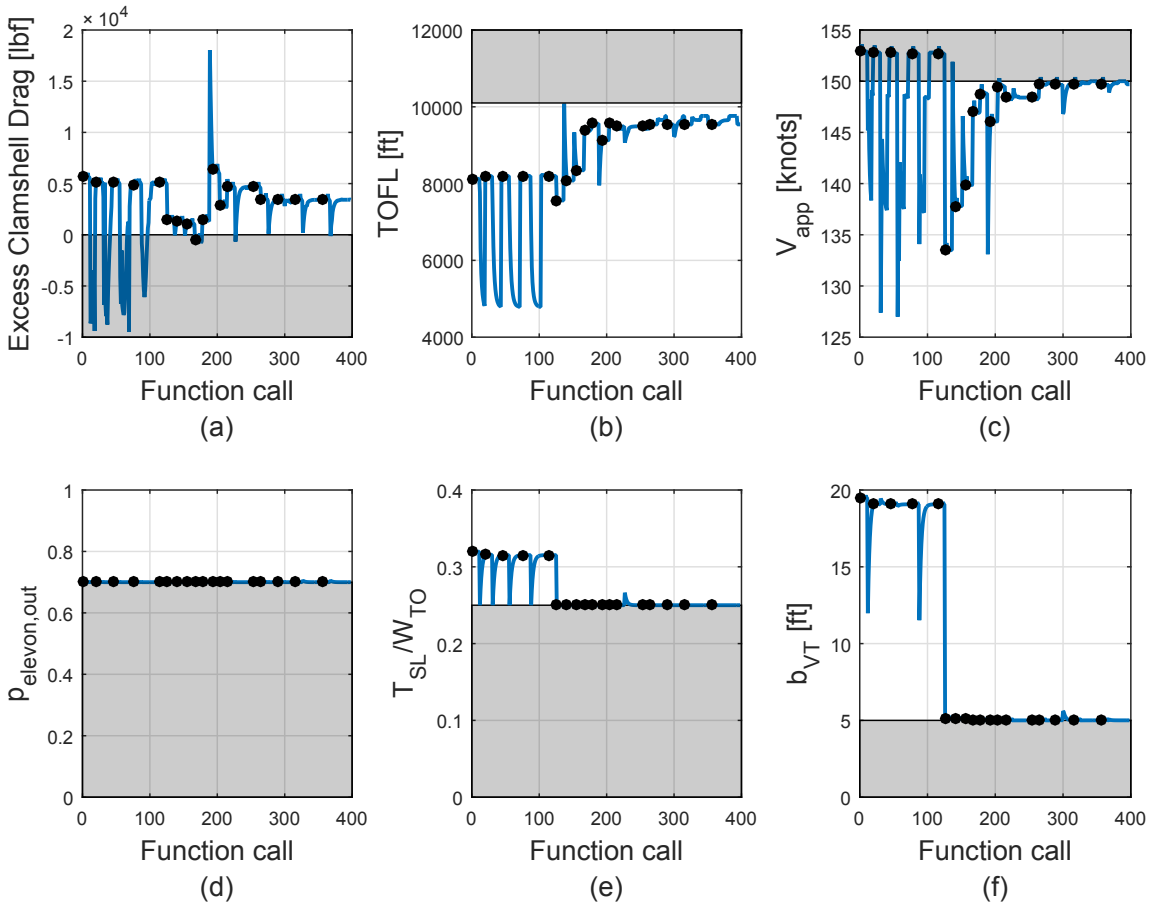

Figure 131: Vehicle 377 iteration history for the active performance constraints (a-c) and design variable side constraints (d-f).

(e) remains essentially fixed at a value of 0.25, and greater weight reduction would probably have been achieved if the bound was relaxed. The vertical tail span (f) was also forced to its smallest allowed value of 5 ft, and is probably the cause of the large decrease in TOGW. The lateral-directional AMS Margin constraints indicate that the vehicle can still trim with such small tails, and an explanation for how this was possible was sought.

It was originally suspected that the vehicle could not trim, triggering the AMS Margin extrapolation algorithm which was assumed to be malfunctioning. However, it was discovered that the minimum drag trim optimizer was able to converge to an actual trim solution that did not saturate the rudders. The trim deflections for the

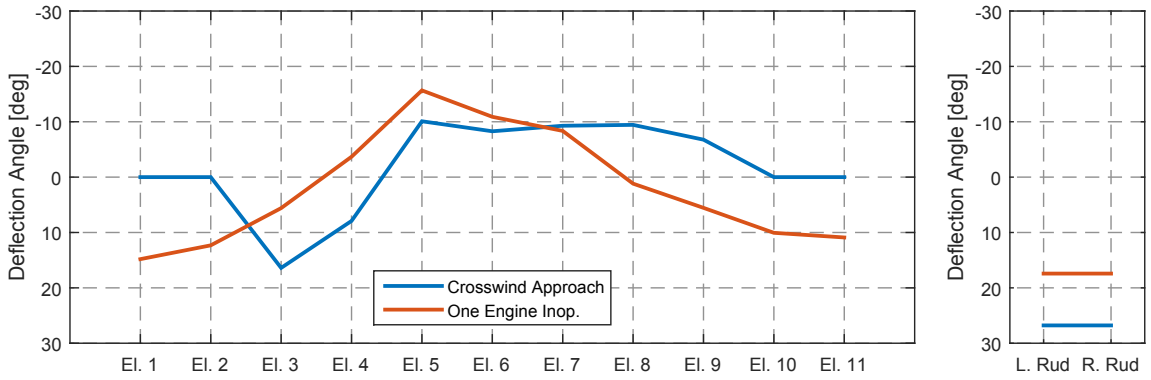

Figure 132: Lateral-directional flight condition deflections for optimized Vehicle 377.

lateral-directional flight conditions are shown in Figure 132. To trim in crosswind the vehicle needs to have a positive roll angle (right wing down) and positive rudder (negative yaw to keep the nose pointed down the runway). The rudders *should* have been saturated (and then some), but the trim optimizer was able to exploit asymmetric lift-induced drag from the elevons for additional yawing moment. The large positive deflection of elevon 3, and to a lesser extent elevon 4, are able to maintain the required roll angle and generate excessive lift-induced drag. Likewise, the elevon deflections on the right wing serve to decrease lift and lift-induced drag, creating a favorable nose-left yawing moment. This was an unintended use of the elevons that the optimizer was able to exploit.

Despite being able to trim with such a small tail, it appeared that a vertical tail sizing constraint had been omitted. Two of the Boeing recommended flight conditions that were omitted from this initial experiment rely exclusively on the rudder and actually be active constraints. These are the landing heading change (or decrab) maneuver and the one engine inoperative on the ground flight conditions. This issue was anticipated in Chapter 1, which warned of the risk of missing active constraints when evaluating unconventional configurations. Clearly, iteration will be part of the design process as new problems arise and lessons are learned. Section 9.6 looks into what happens when these constraints are added back in. If the tail is still minimized

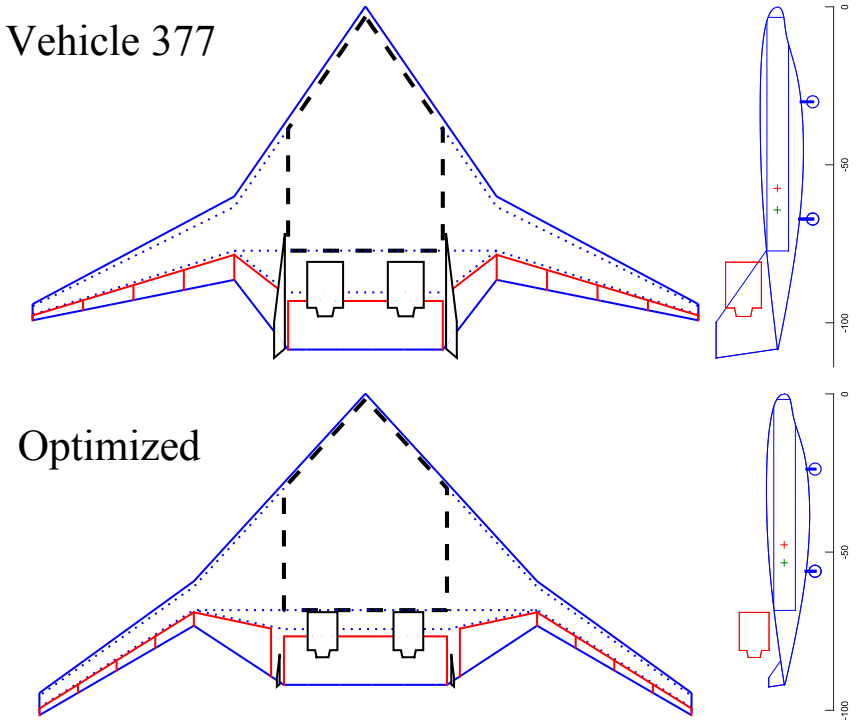

Figure 133: Vehicle 377 original and optimized HWB geometry. The small vertical tails indicate a constraint is likely missing.

despite the new constraints, then a totally tailless aircraft may be possible.

The planform and side views of Vehicle 377 and the final optimized design are shown in Figure 133. The asymmetric drag for the outer wing elevons was made more effective by decreasing the outer wing root chord (Table 59), which due to the rear spar alignment rule had the effect of starting the outer wing at a greater span fraction and giving the outer wing elevons a longer moment arm for yaw. The large sweep of the outer wing has caused the wing tips to extend aft of the centerbody trailing edge, and this required the addition of three degrees of dihedral to avoid tip strike issues during takeoff and landing. An alternative control utilization scenario that can prevent the unintended use of the elevons was investigated in Section 9.4, as a quick follow-up before implementing the missing flight conditions.

Table 60 contains conventional sizing outputs and an assortment of other metrics. The weight is reduced by about 12.1% over the course of optimization., and wing

Table 59: Vehicle 377 initial and final design variables. Active and near-active side constraints for the optimized design are bold.

	Parameter	Vehicle 377	Optimized	Units
1	T_{SL}/W_{TO}	0.32	**0.25**	-
2	Λ_{ctr}	55.39	47.54	degrees
3	p_{ctr}	71.18	**74.35**	%
4	b_W	210.42	206.10	ft
5	Λ_{outer}	28.09	35.89	degrees
6	λ	0.19	0.50	-
7	p_{rc}	0.44	0.24	-
8	b_{VT}	19.5	**5.0**	ft
9	$p_{elevon,ctr}$	0.86	0.83	-
10	$p_{elevon,out}$	0.70	**0.70**	-

Table 60: Responses of interest for the optimization of Vehicle 377.

	Vehicle 377	Optimized	Units
TOGW	441,285	387,741 (-12.1%)	lbs
T_{SL}/W_{TO}	0.32	0.25	-
W_{TO}/S	54.24	53.38	lbs/ft^2
T_{SL} (& scale)	70,536 (1.24)	48,468 (0.85)	lbs/engine
S	8,136	7,264	ft^2
Wing tip twist	-9.36	-6.02	degrees
Cruise FWD CG	34.37	33.60	% MAC
Cruise Static Margin	9.71	7.87	%
Approach Static Margin	8.24	6.93	%
Trimmed $C_{L_{max}}$ (at $\alpha = 20°$)	0.81	0.86	-

area reduces proportionally to weight keeping the wing loading relatively constant. The CG and tip twist to trim at the start-of-cruise design condition is consistent with the lowest weight designs found among the MCS results visualized in Figure 122 of Chapter 8. Static margin at cruise and landing approach conditions is positive. Had the optimization results chosen neutral or negative static margin a constraint might have been imposed in follow-up experiments. In a side study based on the N2A-EXTE configuration, static margin values of this magnitude were found to not require stability augmentation during cruise segments.[47]

Overall this optimization experiment was marginally successful. It helped demonstrate that the novel AMS Margin control authority constraint can guide an optimizer

towards reduced weight vehicle that can trim in all off-design flight conditions. It also helped demonstrate that the modeling environment as a whole is functional, though not always as intended. Results indicate that how the control surfaces are utilized may make a difference in the final optimized geometry, in tail size and planform shape. The comparison of trim methods and their AMS Margins as a function of crosswind in Chapter 4 provided early indications that this might be true, but at the time it only caused suspicion that the tail size would vary. This will now be formalized into a hypothesis:

Hypothesis: Control utilization assumptions will have significant influence over the planform shape and vertical tail size of optimized HWBs.

This hypothesis will be tested in Section 9.4, where experiments are conducted under a different control utilization assumption. If the optimized geometry is identical or similar to the results in this section, then the control utilization assumption is not important and the hypothesis would be falsified. Prior to investigating this hypothesis, Vehicle 278 will be optimized with independent elevons first to see if similar issues are experienced from a different starting point in the design space.

9.3.2 Vehicle 278 Optimization Results

Another optimization experiment was conducted using Vehicle 278, selected from the feasible designs found during the design space exploration studies of Chapter 8. It experienced the same issue as Vehicle 377, where the optimizer chose to minimize vertical tail span at function call 65 and rely on asymmetric elevon drag and increased V_{app} to make up for it. The TOGW objective function and constraint values were stable for another 85 function calls, at which point the optimization was aborted.

The final design shown in Figure 134 met all constraints and had characteristics remarkably similar to Vehicle 377's optimized design. The only noticeable geometry

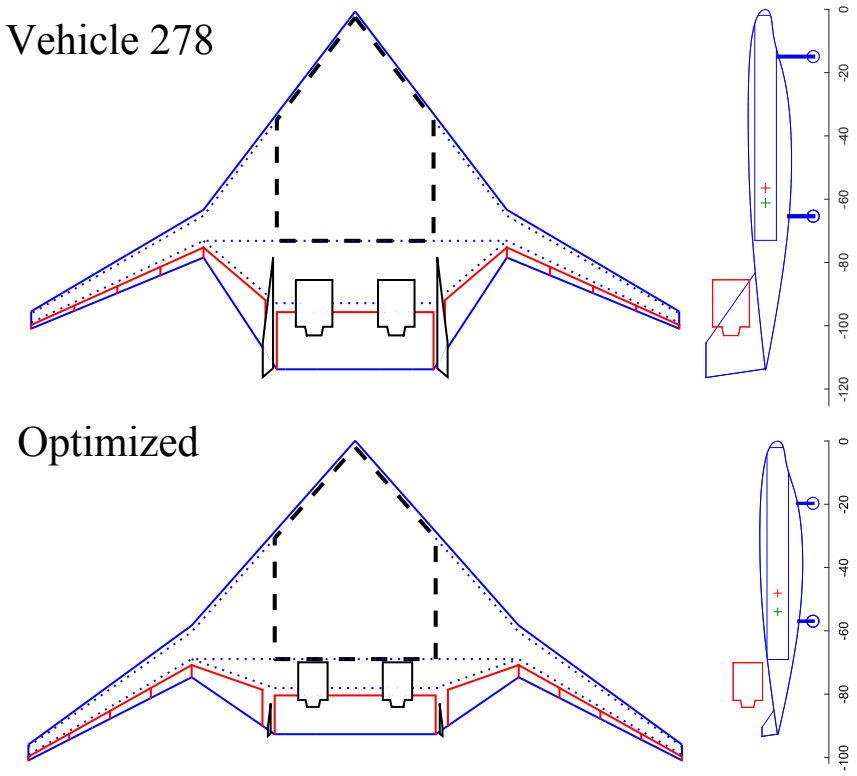

Figure 134: Vehicle 278 original and optimized HWB geometry. The small vertical tails indicate a constraint is likely missing.

differences are a slightly more tapered outer wing and smaller elevons (see Table 61). The clamshell sizing constraint was active for Vehicle 278 due to the smaller two outboard elevon pairs, which produced only 12 lbs in excess of what was required to achieve the 20% throttle setting. A comparison of Table 62 for Vehicle 278 with Table 60 for Vehicle 377 shows that the sizing metrics (thrust-to-weight ratio, wing loading, planform area, maximum sea level thrust, and TOGW) for the optimized designs are also very similar. These two different initial conditions converged to essentially the same local optimum.

The crosswind approach trim deflections for Vehicle 278 are shown in Figure 135. The vehicle planform and elevon positions are very similar to Vehicle 377, but the outer wing elevon chord fractions are smaller. As a result elevons 3 and 4 were fully saturated by the trim optimizer to achieve the needed asymmetric lift-induced drag.

Table 61: Vehicle 278 initial and final design variables. Active and near-active side constraints for the optimized design are bold.

	Parameter	Vehicle 278	Optimized	Units
1	T_{SL}/W_{TO}	0.34	**0.25**	-
2	Λ_{ctr}	52.59	48.48	degrees
3	p_{ctr}	64.10	**74.41**	%
4	b_W	206.25	208.01	ft
5	Λ_{outer}	30.53	36.12	degrees
6	λ	0.36	0.31	-
7	p_{rc}	0.26	0.28	-
8	b_{VT}	18.8	**5.0**	ft
9	$p_{elevon,ctr}$	0.84	0.87	-
10	$p_{elevon,out}$	0.79	0.77	-

Table 62: Responses of interest for the Vehicle 278 optimization.

	Vehicle 278	Optimized	Units
TOGW	441,145	384,664 (-12.8%)	lbs
T_{SL}/W_{TO}	0.34	0.25	-
W_{TO}/S	53.44	52.69	lbs/ft^2
T_{SL} (& scale)	74,236 (1.3)	48,083 (0.84)	lbs/engine
S	8,254	7,300	ft^2
Wing tip twist	-5.28	-6.84	degrees
Cruise FWD CG	34.54	33.42	% MAC
Cruise Static Margin	5.69	8.90	%
Approach Static Margin	3.03	7.87	%
Trimmed $C_{L_{max}}$ (at $\alpha = 20°$)	0.89	0.84	-

The deflections for the symmetric flight conditions are shown in Figure 136, and no control surfaces are saturated. Overall the trim solutions of Vehicles 377 and 278 have very similar characteristics, but are not identical due to the subtle differences in geometry.

It should be noted that the takeoff rotation deflections are rather large for both vehicles, and VORLAX may be over-predicting their effectiveness. This AMS Margin constraint in part drives the size of the elevons and shape of the planform, so uncertainty in control effectiveness propagates to uncertainty in vehicle geometry. Future work should look into reducing this uncertainty by testing the design sensitivity to the takeoff rotation maneuver AMS Margin constraint, as well as incorporating higher

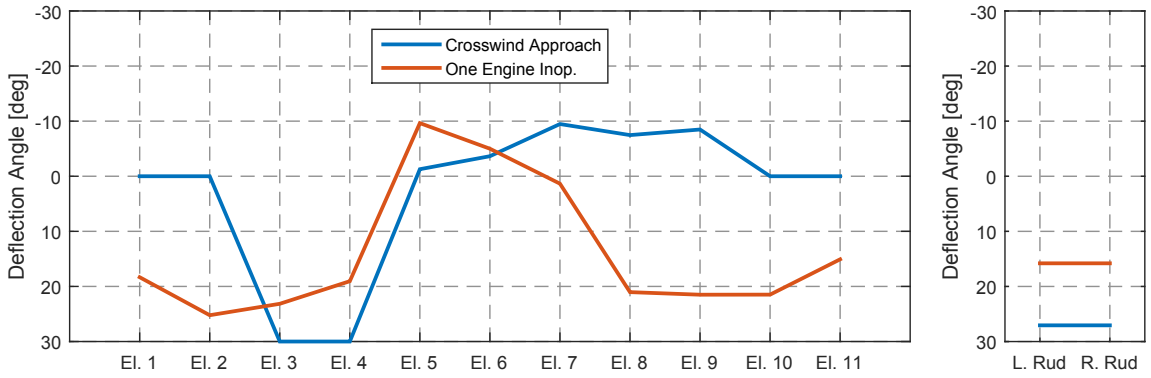

Figure 135: Lateral-directional flight condition deflections for optimized Vehicle 278.

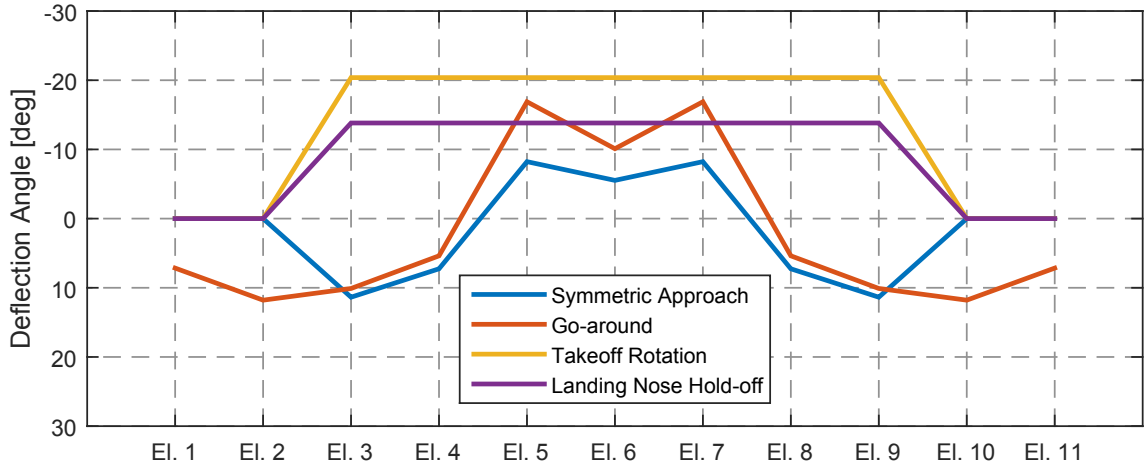

Figure 136: Longitudinal flight condition deflections for optimized Vehicle 278.

fidelity aerodynamic modeling or empirical corrections to the VORLAX data. Similar issues arise with the rudder and tail sizing constraints, which would also benefit from uncertainty reduction efforts.

9.4 Follow-up HWB Optimization Utilizing Ganged Elevons

The optimization experiments in the previous section likely omitted an active tail sizing constraint, but also experienced unintended usage of the elevons with the consequence of under-sizing the vertical tails. A prediction was made that imposing more rational utilization of the elevons would have a beneficial effect on the vertical tail, but also potentially the shape of the planform. This hypothesis will be tested by

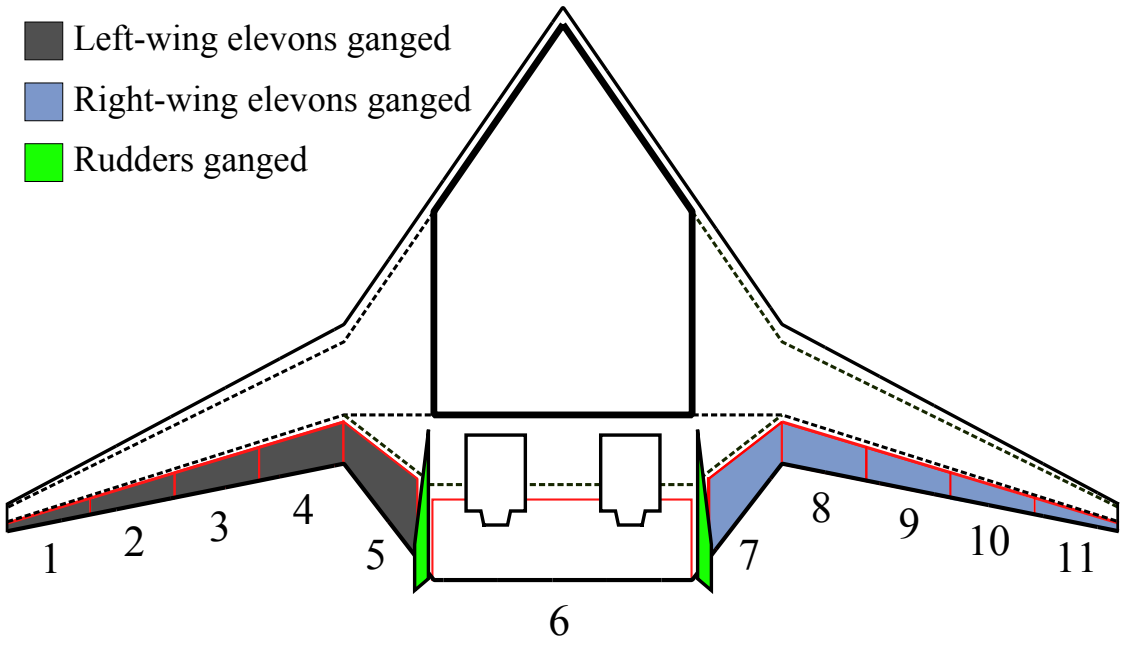

Figure 137: Ganged elevon arrangement to force greater reliance on the rudders for yawing moment needs. Note that elevons 1/2 and 10/11 are not used when clamshells are active.

implementing the ganging concept from control allocation, and the experiment will also test the strategy as a way to hedge against negative effects of accidental omission of active tail sizing constraints.

The ganging arrangement shown in Figure 137 is based on the allocation of function given to the controls on the Boeing STV configuration during their control authority analyses.[16] All of the left wing elevons (1-5) are ganged together to operate as a single large pseudo-aileron. The same is true for elevons on the right wing (7-11). These pseudo-ailerons are not constrained to provide rolling moments exclusively, instead the trim optimization algorithm may also use them to generate pitching moments. The rudders in this dissertation have always been ganged together and remain so for these experiments.

The ganged elevon experiments of the trim methodology chapter had been conducted with the conventional optimization method. The ganged elevon trim experiments under a 20% throttle constraint were unique, and the same deflection would

have been found regardless of trim optimization method or algorithm. The HWB optimization experiments have been conducted using the minimum drag trim analysis method, and will continue to do so. It is expected that this ganging layout will prevent the trim optimizer from using the elevons to generate excessive asymmetric induced drag, which will force greater reliance on the rudder resulting in a larger tail. The prediction in Chapter 4 was that this would over-size the tails, but given that they are currently being under-sized this would be a favorable consequence of ganged elevons.

9.4.1 Vehicle 278 Optimization Results

The TOGW history of Vehicle 278 with ganged elevons is shown in Figure 138. It does not feature large swings in TOGW in early iterations, and this is probably because more of the constraints for the initial design are feasible. There is a steady decrease of TOGW up until approximately function call 150 when it levels off. Occasionally the optimizer would choose a geometry that would crash FLOPS or VORLAX, and these are shown as discontinuities in the lines. Fortunately these failures occurred during the line step segment of the algorithm, when the SQP algorithm can accommodate them. The step size tolerance criteria terminated the optimization.

Figure 139 shows the control authority metric iteration history for Vehicle 278 with ganged elevons. All of the longitudinal flight conditions start and end in the feasible space. The crosswind approach AMS Margin did not start in the feasible design space, but was able to reach the 10% level quickly. This was the only active control authority constraint from the flight conditions tested.

The iteration history for constraint metrics of interest are collected in Figure 140. The excess clamshell drag (a) takeoff field length (b), and approach speed (c) constraints are still active or nearly so by the end of the optimization experiment. The thrust-to-weight ratio (e) is again very quickly reaching its lower bound. Greater

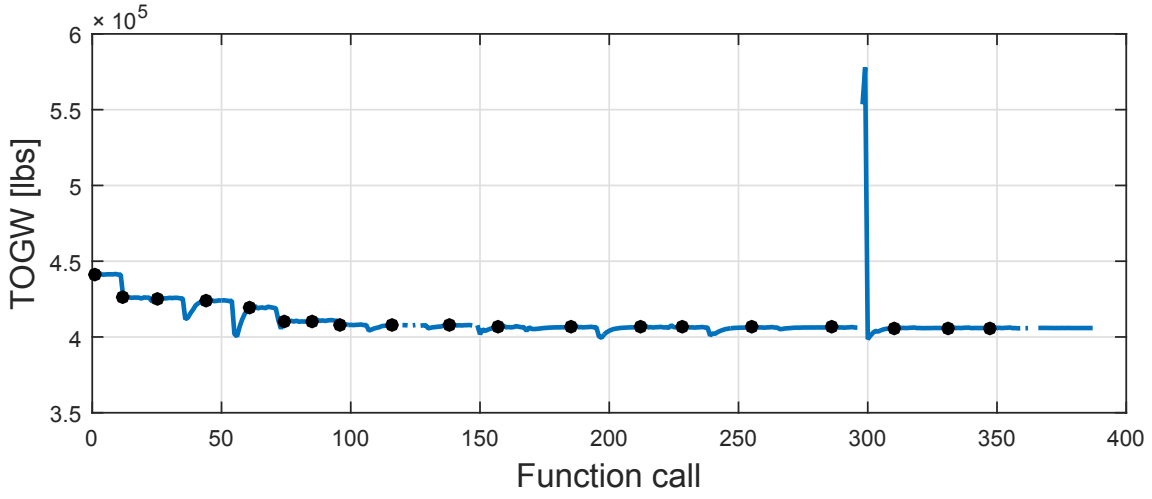

Figure 138: Vehicle 278 iteration history for the TOGW objective function, using ganged elevons.

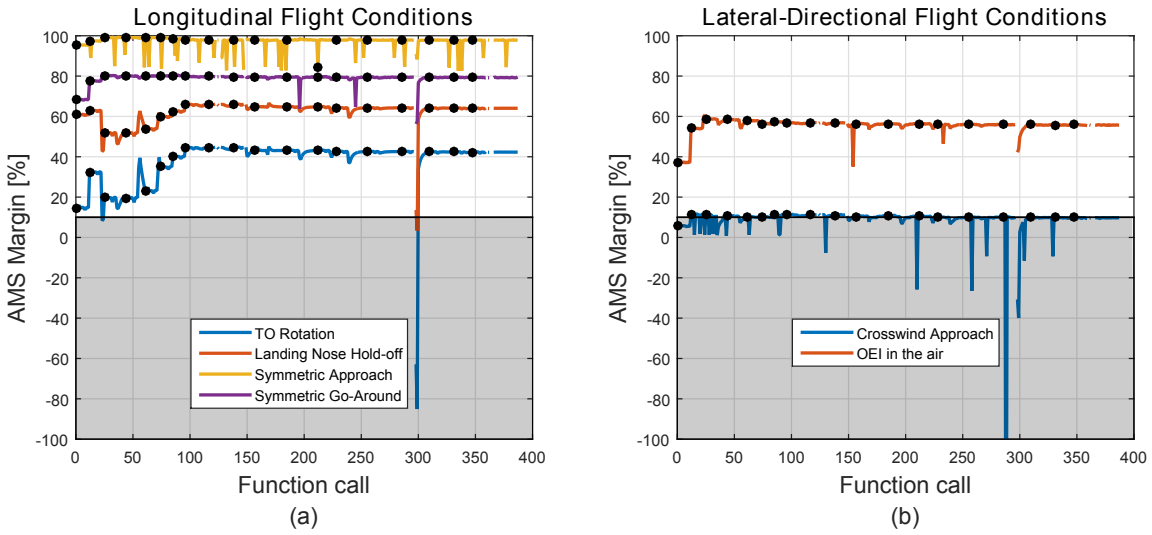

Figure 139: Vehicle 278 iteration history for the control authority constraints, using ganged elevons.

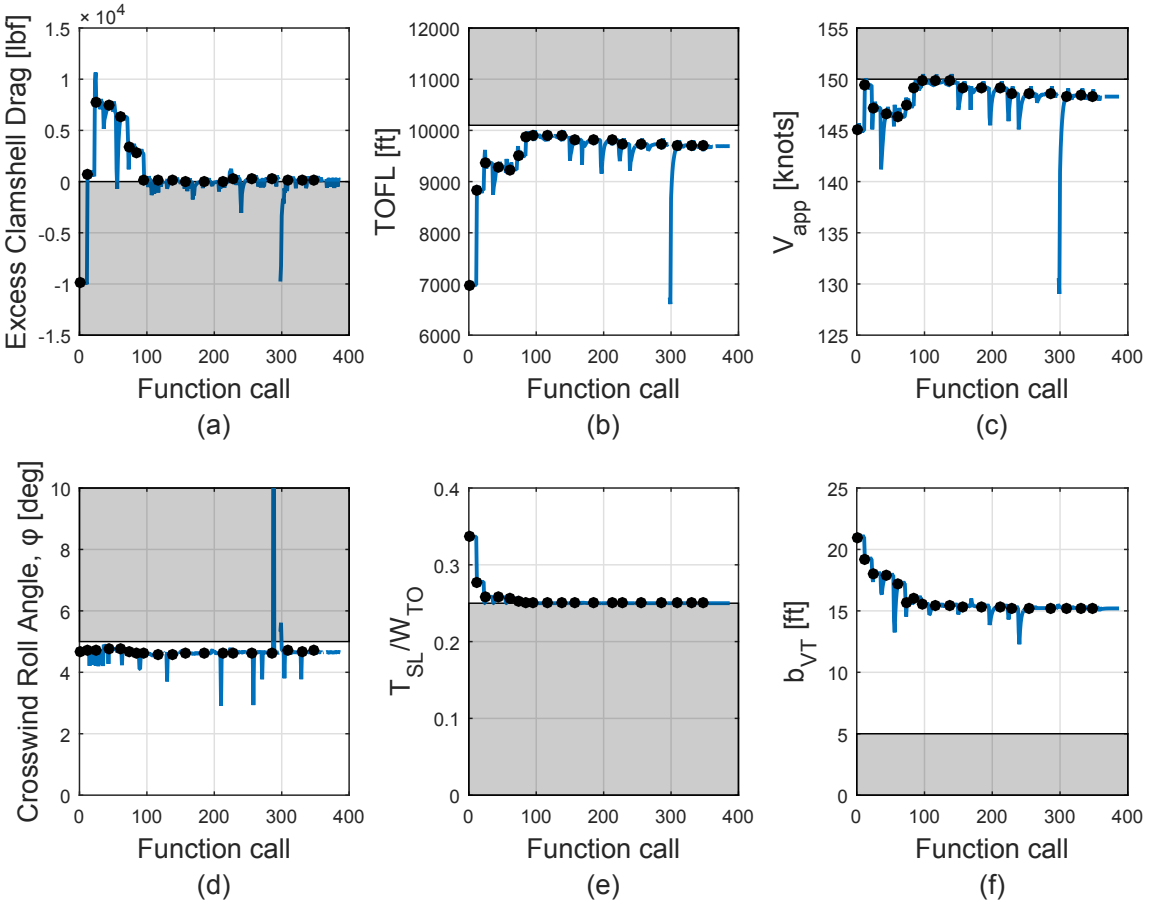

Figure 140: Vehicle 278 (with ganged elevons) iteration history for the active performance constraints (a-d) and design variable side constraints (e-f).

reduction in TOGW is possible if the lower bound is decreased further, but it was left unmodified so that fair comparisons could be made across vehicles and control utilization scenarios. The vertical tail span (f) iteration history appears to show that the ganged control utilization scenario was successful in forcing increased reliance on the rudder for yawing moment control authority. The crosswind approach flight condition is driving the size of the vertical tail, which stabilizes at about 15 ft in span.

The trim deflections for the lateral-directional flight conditions of Vehicle 278 optimized with ganged elevons is shown in Figure 141. The rudder is primary provider of yawing moment, and in these flight conditions the AMS Margin correlates with rudder deflection angle. The crosswind approach AMS Margin is an active constraint

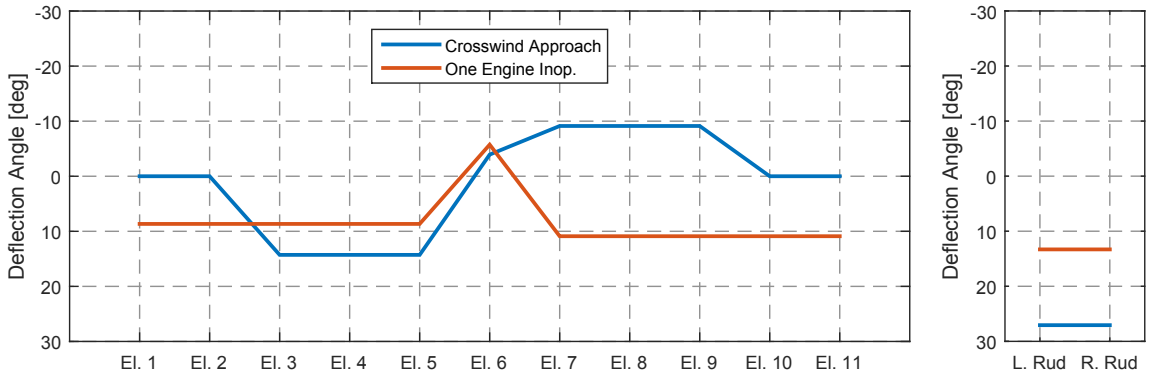

Figure 141: Lateral-directional flight condition deflections for optimized Vehicle 278 using ganged elevons.

set at 10%, which corresponds with the roughly 27 degree deflection seen here (i.e., 90% of the maximum 30 degree deflection). This is essentially the same rudder deflection angle seen for the vehicles optimized with independent elevons. However now that the elevons are ganged they cannot be deflected to extremes to generate asymmetric induced drag, and the tail must be larger to achieve trimmed flight with 10% AMS Margin. Figure 142 shows the symmetric flight condition trim deflections for the same vehicle. As a reminder, all symmetric flight conditions except go-around have the clamshells deployed (shown as undeflected elevons). For the go-around maneuver, elevons 1-5 and 7-11 are ganged together (no clamshells used) and the minimum drag method trimmed with only a centerbody elevon deflection.

The final design from the ganged elevon optimization for Vehicle 278 is shown on the lower right of Figure 143, and shown to scale with the initial geometry and geometry optimized with independent elevons. A reduction of TOGW was still achieved, but to a lesser extent. The ganged elevon design now has vertical tails that look proportional to the vehicle, and the outer wing elevons are no longer pushed outboard in an effort to increase their moment arm for yawing moment. In fact, the optimized geometry looks very similar to the initial geometry. The primary differences are decreased outer wing sweep, smaller engines, a decreased trailing edge extension (smaller p_{ctr}), and larger vertical tails. The design variables for the initial Vehicle 278

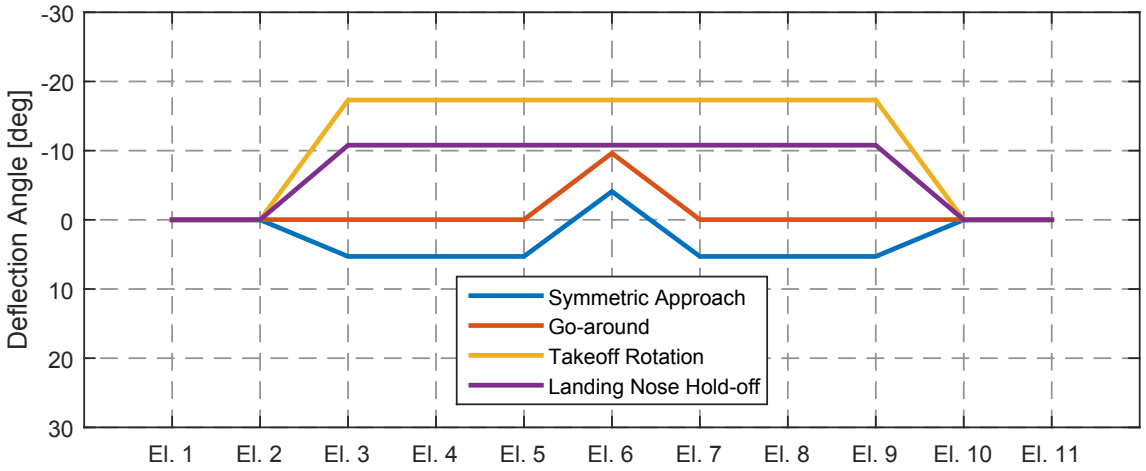

Figure 142: Longitudinal flight condition deflections for optimized Vehicle 278 using ganged elevons.

Table 63: Design variables for Vehicle 278 optimized under independent and ganged elevon control utilization scenarios. Values near side constraints are in bold.

		Vehicle 278			
	Parameter	Initial	Independent	Ganged	Units
1	T_{SL}/W_{TO}	0.34	**0.25**	**0.25**	-
2	Λ_{ctr}	52.59	48.48	53.04	degrees
3	p_{ctr}	64.10	**74.41**	67.98	%
4	b_W	206.25	208.01	207.95	ft
5	Λ_{outer}	30.53	36.12	25.79	degrees
6	λ	0.36	0.31	0.39	-
7	p_{rc}	0.26	0.28	0.26	-
8	b_{VT}	18.8	**5.0**	15.2	ft
9	$p_{elevon,ctr}$	0.84	0.87	0.86	-
10	$p_{elevon,out}$	0.79	0.77	0.79	-

and the two optimized derivatives are shown in Table 63.

The prediction that the control utilization scenario would change the final design is supported by these results. The more reasonable optimization result that came from using ganged elevons is an important finding in part because ganged elevons might be usable for minimizing the effect of accidental omission of critical flight conditions. This method has fewer independent controls and therefore a smaller DOE can be used to build the aerodynamic surrogate model. The original model was a function of α, β, 11 elevons, and two independent rudders which required 421 VORLAX cases using

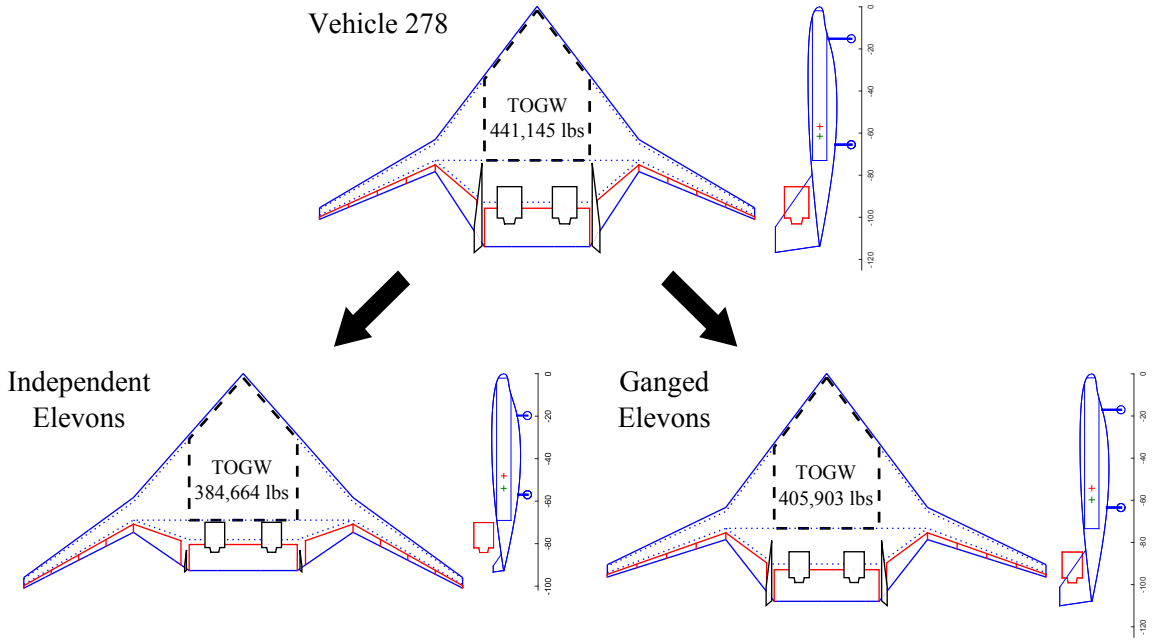

Figure 143: A comparison of optimized planforms for Vehicle 278 under different control utilization scenarios.

a Box-Behnken design. For a ganged control arrangement the new model would be a function of α, β, five elevons, and one rudder which would require only 113 VORLAX cases. In addition, the trim analyses themselves are completed more rapidly when the trim optimizer manipulates fewer parameters. Both factors reduce the computational burden for HWB conceptual design.

The constraints for the initial design and two optimized designs are collected in Table 64. The approach speed, crosswind approach AMS Margin, and excess clamshell drag are still active constraints. The AMS Margin for both optimized vehicles is just shy of the required 10%, and is close enough. Achieving 10% exactly would require restarting the optimization at those designs for better constraint scaling. Imposing a multiplier on the AMS Margin constraint might also help in follow-up optimizations of these designs. The larger tail on the ganged elevon vehicle produces more side force during the crosswind approach flight condition that must be balanced by vehicle roll angle, and this angle is nearly at the upper limit of five degrees. The remaining

Table 64: Constraint metrics for Vehicle 278 optimized under independent and ganged elevon control utilization scenarios.

			Vehicle 278			
		Target	Initial	Independent	Ganged	Units
Performance Constraints						
1	Approach speed, V_{app}	< 150	145.7	**149.9**	**148.3**	knots
2	TO field length	$< 10{,}100$	6,980	9,597	9,692	ft
3	ROC @ Mach 0.84, 35k ft	> 300	1,393	545	518	ft/min
4	Climb ceiling	$> 35{,}000$	44,145	39,962	39,896	ft
Geometry Constraints						
5	Excess fuel capacity	> 0	160,120	230,820	173,722	lbs
6	Wing tip twist	< 0	-5.28	-6.84	-6.81	degrees
7	$\Lambda_{outer} - \Lambda_{ctr}$	< 0	-22.1	-12.4	-27.3	degrees
Control Authority Constraints						
8	AMS Margin$_{TO\ Rot.}$	> 10	3.1	32.1	42.3	%
9	AMS Margin$_{Lnd.\ nose\ hold}$	> 10	53.3	53.9	64.0	%
10	AMS Margin$_{Sym.\ Appr.}$	> 10	95.6	88.7	97.8	%
11	AMS Margin$_{Go-around}$	> 10	71.4	79.2	79.5	%
12	AMS Margin$_{OEI,air}$	> 10	29.2	47.3	55.7	%
13	AMS Margin$_{Cross.\ Appr.}$	> 10	4.1	**9.8**	**9.8**	%
14	Crosswind roll angle, ϕ	< 5	4.0	4.0	**4.7**	degrees
Other Constraints						
15	Start-of-cruise α	< 5	4.03	3.62	3.98	degrees
16	Excess clamshell drag	> 0	-10,803	**12**	**192**	lbf

metrics of interest are collected in Table 65. The ganged elevon design's wing loading is still near the initial value. The weight and wing area are lower than the initial design but higher than that of the independent elevon design. The engine scale is 11% smaller than the baseline design, making it still reasonable to use this engine deck.

9.4.1.1 Vertical Tail Volume Coefficient

The vertical tail volume coefficient for Vehicle 278 optimized with ganged elevons was calculated using Equation 110 below, for comparison with recent Boeing BWB designs. The moment arm L_{VT} is assumed to be measured between the forward MTOW CG (takeoff) and the vertical tail quarter mean aerodynamic chord, and the S_{VT} term is taken to be the combined area of the two tails. Vehicle 278 optimized

Table 65: Other results for Vehicle 278 optimized under independent and ganged elevon control utilization scenarios.

	Vehicle 278			
Metric	Initial	Independent	Ganged	Units
TOGW	441,145	384,664	405,903	lbs
T_{SL}/W_{TO}	0.34	0.25	0.25	-
W_{TO}/S	53.44	52.69	51.99	lbs/ft^2
T_{SL} (& scale)	74,236 (1.3)	48,083 (0.84)	50,739 (0.89)	lbs/engine
S	8,254	7,300	7,807	ft^2
Wing tip twist	-5.28	-6.84	-6.81	degrees
Cruise FWD CG	34.54	33.42	34.03	% MAC
Cruise Static Margin	5.69	8.90	7.92	%
Approach Static Margin	3.03	7.87	5.86	%
Trimmed $C_{L_{max}}$ (at $\alpha = 20°$)	0.89	0.84	0.84	-

with ganged elevons had a vertical tail volume coefficient of 0.01222. For comparison the tail volume coefficient of the Boeing OREIO design is 0.01265, indicating that the ganged elevon control utilization scenario was successful in producing a more reasonably sized tail.[107]

$$C_{VT} = \frac{L_{VT} S_{VT}}{b_W S_W} \tag{110}$$

Initial expectations (see Chapter 2) were that the short-cut tail sizing methods such as the tail volume coefficient were not mature enough to justify skipping lateral-directional S&C analyses during HWB conceptual design. Given how closely C_{VT} for Vehicle 278 optimized with ganged elevons matches the more mature Boeing design, utilizing a tail volume coefficient to size the tail may be a viable option for rapid design space exploration and optimization in conceptual design. A prediction is made below:

Hypothesis: Utilizing the Boeing tail volume coefficient to size the vertical tails (while omitting the lateral-directional control authority constraints during optimization) will result in a vehicle with similar geometry, performance, and S&C characteristics.

An experiment will be designed in Section 9.5 to test this hypothesis. If it is

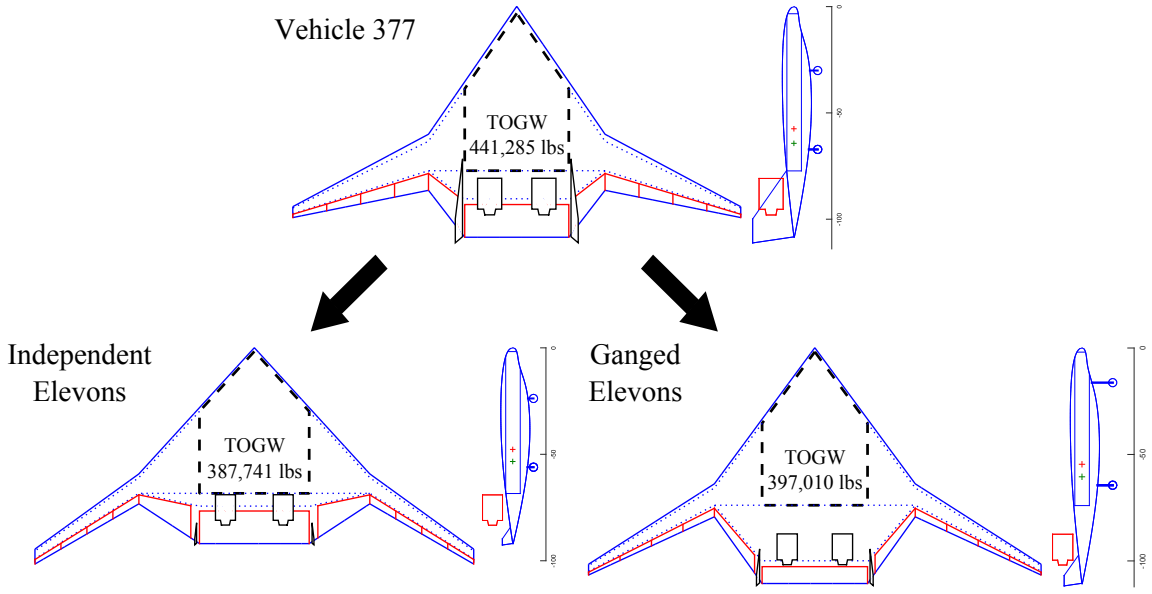

Figure 144: A comparison of optimized planforms for Vehicle 377 under different control utilization scenarios.

supported, the conceptual designer stands to benefit from an extremely reduced work load. Otherwise, the harder path with more lateral-directional S&C constraints must be taken to arrive at reasonable HWB designs.

9.4.2 Vehicle 377 Optimization Results

Vehicle 377 was also optimized utilizing ganged elevons to see if the results would be consistent from a different starting point. The final geometry is in the lower right hand corner of Figure 144, and the vertical tail is still quite small. The tail volume coefficient for Vehicle 377 optimized with ganged elevons is only 0.00458, just over a third of Boeing value and is likely under-sized for the omitted flight conditions. The results of this experiment indicate that the ganged elevon control utilization scenario is not always sufficient to produce reasonably sized vertical tails. When performing physics-based control sizing there is no subsitute for using the full suite of flight conditions likely to be active constraints.

9.5 Simplified HWB Optimization with Tail Volume Coefficients

The experiments in this section will be used to test the hypothesis regarding the use of tail volume coefficients and attempt to establish best practices for doing so. The Boeing OREIO tail volume coefficient of 0.01265 (and implicit assumptions that come with it) will be used to size the tails at every function call including the initial design for Vehicle 278.[16] None of the lateral-directional flight conditions will be evaluated, nor will most of the longitudinal ones. Of the latter, only the takeoff rotation maneuver AMS Margin will be included since it is the most constraining. Again, the purpose of this section is to test whether the tail volume coefficient method is a suitable substitution for a physics-based method.

The clamshell sizing constraint as implemented can only be calculated from the S&C aerodynamic database and the results from the symmetric approach flight condition. This makes it a relatively expensive constraint to calculate and it would be convenient to omit it. The optimization experiment will be conducted under three alternative scenarios to determine if it is possible to drop the clamshell constraint.

In scenario (a), the takeoff rotation maneuver AMS Margin constraint and the clamshell sizing constraint are enforced as usual. The lateral-directional flight conditions are implicitly met (supposedly) by using the tail volume coefficient, and the other longitudinal flight conditions are not active control authority constraints. All design variables are available to the optimizer to minimize TOGW except for vertical tail span which is a fall-out of using the tail volume coefficient.

Scenario (b) enforces the takeoff rotation maneuver constraint but not the clamshell sizing constraint. All design variables are available to the optimizer to minimize TOGW except for vertical tail span. This scenario has the potential to minimize the outer wing elevons as a weight reduction measure, and might make the rolling maneuver (not evaluated) infeasible and the clamshells ineffective.

Finally in scenario (c) the takeoff rotation maneuver control authority constraint is enforced, the clamshell sizing constraint is not enforced, and the outer wing elevon parameter $p_{elevon,out}$ is fixed at its lowest value (i.e., biggest elevon). The outer wing elevon was fixed because it was suspected that scenario (b) might under-size them otherwise. HWB optimization environments in the literature (see Chapter 2) have similarly fixed elevon chord fractions in their studies. An important distinction here is that the centerbody elevon is still free to change because of its large and complex effect on the takeoff rotation maneuver.[1] Vertical tail span is again a fall-out of using the tail volume coefficient.

9.5.1 Vehicle 278 Optimization Results

The optimized vehicles for each scenario are shown together in Figure 145. As expected for scenario (b), removing the clamshell sizing constraint but still allowing the optimizer to control $p_{elevon,out}$ made the outer wing elevons very small. A follow-up analysis evaluated the excess clamshell drag constraint (Table 66) which revealed that the outer wing elevons are in fact under-sized. It is not simply the outer wing elevon size that determines whether this constraint is satisfied or not, because the other two optimization scenarios also cannot produce enough drag with their clamshells either. Scenario (c) had maximized outer wing elevons and scenario (a) included the constraint in the optimization problem. For scenario (a) this may be an issue with constraint scaling, and if the optimization was performed again a multiplier on the excess clamshell constraint might help. Manual follow-up design iterations could potentially make the following changes to resolve this issue: 1) deflect the clamshells more than 60 degrees, 2) increase span fraction of two outboard elevon pairs, or 3) decrease outer wing tapering.

[1] Bigger is not always better in this case, because the centerbody elevon dumps lift when deflected for nose-up pitching moment. This increases the nose-down moment from the main gear normal force. A smaller centerbody elevon would dump less lift, and despite a reduced pitching moment control derivative might still be adequate for the maneuver.

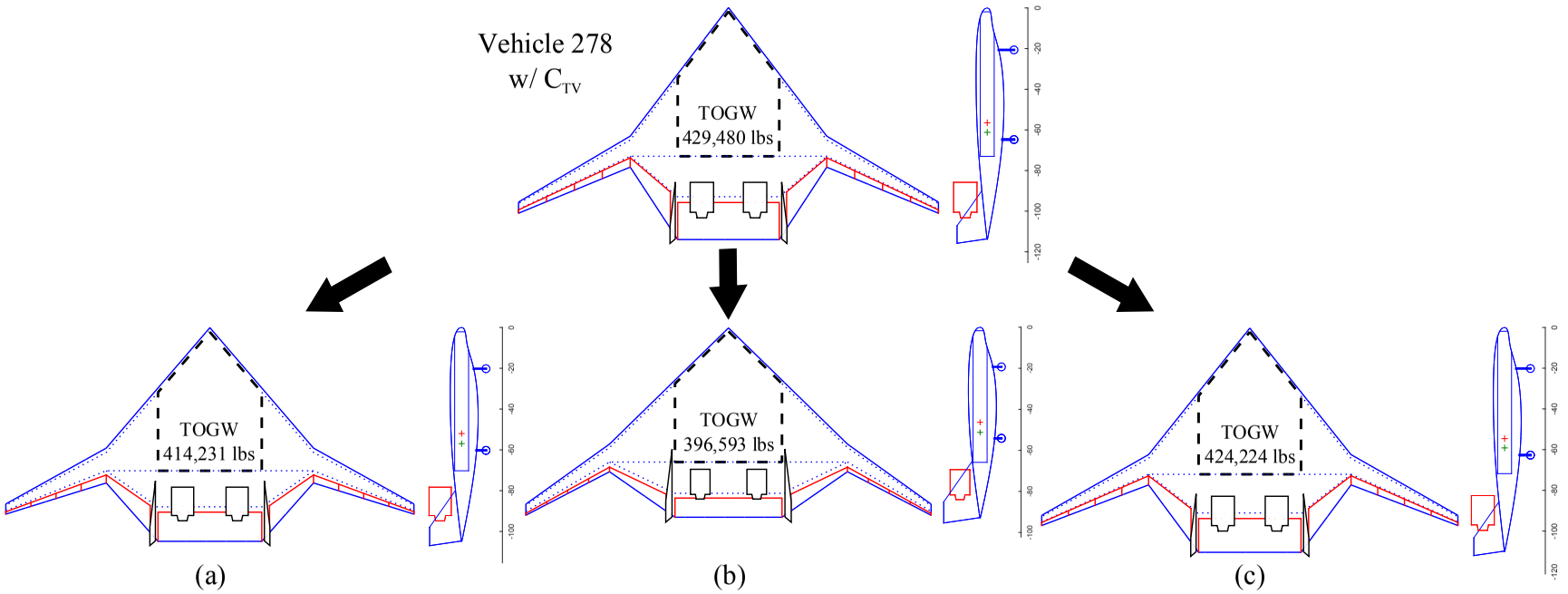

Figure 145: Vehicle 278 optimized using a tail volume coefficient under a takeoff rotation maneuver constraint and (a) clamshell sizing constraint + all DOF, (b) no clamshell constraint + all DOF, (c) no clamshell constraint + maximum $p_{elevon,out}$.

Table 66: Constraint metrics for Vehicle 278 optimized with a tail volume coefficient, under various scenarios. Violated constraints are bold.

			Vehicle 278 - Tail Vol.			
		Target	(a)	(b)	(c)	Units
Performance Constraints						
1	Approach speed, V_{app}	< 150	138.9	135.1	143.3	knots
2	TO field length	$< 10{,}100$	6,788	7,889	6,926	ft
3	ROC @ Mach 0.84, 35k ft	> 300	1,116	450	1,308	ft/min
4	Climb ceiling	$> 35{,}000$	43,038	38,955	43,871	ft
Geometry Constraints						
5	Excess fuel capacity	> 0	206,292	260,934	177,571	lbs
6	Wing tip twist	< 0	-5.21	-4.10	-4.65	degrees
7	$\Lambda_{outer} - \Lambda_{ctr}$	< 0	-20.2	-8.6	-21.7	degrees
Control Authority Constraints						
8	AMS Margin$_{TO\ Rot.}$	> 10	14.2	16.9	19.5	%
9	*AMS Margin$_{Lnd.\ nose\ hold}$	> 10	54.3	45.9	60.7	%
10	*AMS Margin$_{Sym.\ Appr.}$	> 10	94.3	94.1	94.9	%
11	*AMS Margin$_{Go-around}$	> 10	68.9	70.3	70.1	%
12	*AMS Margin$_{OEI,air}$	> 10	11.2	13.5	10.9	%
13	*AMS Margin$_{Cross.\ Appr.}$	> 10	**-7.5**	**-7.4**	**-6.9**	%
14	*Crosswind roll angle, ϕ	< 5	3.78	3.97	3.69	degrees
Other Constraints						
15	Start-of-cruise α	< 5	3.62	2.95	3.85	degrees
16	Excess clamshell drag	> 0	**-8,559**	**-8,112***	**-6,780***	lbf

* = Not a constraint during MDO, evaluated after the fact.

In the optimization experiments of Section 9.3.1, the excess clamshell drag constraint was correlated with approach speed which the vehicle optimizer was increasing as a way to meet control authority constraints. The designs from the tail volume method did not have any active control authority constraints, so the vehicle optimizer could relax static margin, increase $C_{L_{max}}$, and decrease the flight speeds. This reduction in speed is beneficial from a noise point of view but comes at the cost of lateral-directional control authority. This can be seen in Table 66 which shows the vehicle cannot trim in crosswind, which was evaluated in a follow-up analysis and not as part of the optimization. This critical interaction between control authority and speed is missed by relying on a tail volume coefficient. Either the speed must increase or the tail size (and tail volume coefficient) must increase to have feasible designs. Without evaluating the lateral-directional flight conditions, it will not be known if the right balance has been struck. Also, the vehicle can be permitted to fly at higher speeds that prescribed by $C_{L_{max}}$ and FLOPS if the V_{app} constraint is still satisfied. Higher speeds come with the benefit of greater control authority but to the detriment of noise, and this trade-off is not quantifiable with the proposed method. Enabling this trade-off should be the subject of future work.

None of the tail volume coefficient optimization scenarios tested are adequate replacements for a physics-based control authority assessment method that includes all active constraints. The hypothesis that predicted similar results between the methods was falsified. The final planforms of the physics-based vs. tail volume coefficient based optimizations are visually different. Also, the performance discrepancy caused by the coupled AMS Margin, static margin, $C_{L_{max}}$, and V_{app} issue goes against the predictions of the hypothesis.

9.6 Best Practice: HWB Optimization Utilizing Independent Elevons and the Complete Set of Flight Conditions

The following constraints had been omitted from the earlier optimization experiments and were later implemented for a follow-up experiment: 1) OEI on the ground, 2) decrab maneuver, and 3) landing roll maneuver. The elevons are once again operated independently, because the ganged elevon scenario did not always adequately compensate for missing constraints. The purpose of this optimization experiment was to test whether the two new directional flight conditions were more constraining than crosswind approach, and to determine whether the landing roll maneuver was an active constraint.

It is important for good optimizer performance that the initial design start in the feasible design space if possible. Vehicle 278 and Vehicle 377 both required larger vertical tails than in previous experiments to satisfy all directional flight conditions. In addition, Vehicle 278 required larger outer wing elevons than before in order to satisfy the landing roll maneuver constraint. The initial and optimized vehicle geometries are shown in Figure 146, and the tails are clearly larger and the new directional control authority constraints were active. The design parameters for these designs are listed in Table 67, where the tail spans are significantly larger than in previous experiments.

Table 67: Design variables for Vehicle 278 optimized under independent and ganged elevon control utilization scenarios. Values near side constraints are in bold.

	Parameter	Vehicle 278	Vehicle 377	Units
1	T_{SL}/W_{TO}	**0.25**	**0.25**	-
2	Λ_{ctr}	53.41	48.62	degrees
3	p_{ctr}	68.17	**74.66**	%
4	b_W	**212.38**	**212.10**	ft
5	Λ_{outer}	30.51	34.78	degrees
6	λ	**0.5**	0.42	-
7	p_{rc}	0.28	0.26	-
8	b_{VT}	18.1	21.0	ft
9	$p_{elevon,ctr}$	**0.93**	**0.92**	-
10	$p_{elevon,out}$	0.83	**0.70**	-

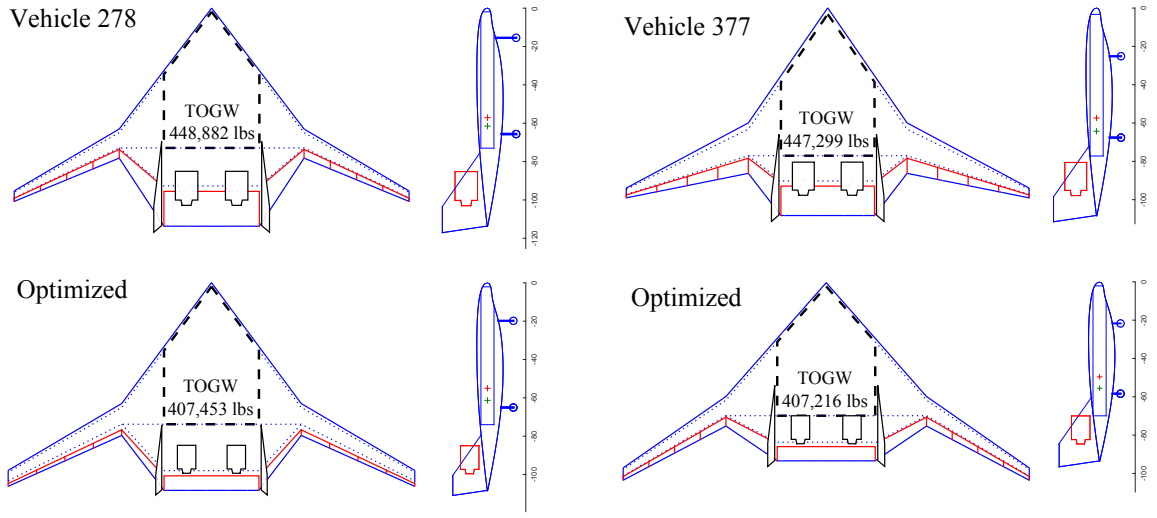

Figure 146: Optimized planforms under the full set of nine control authority constraints.

The AMS Margin constraints for Vehicle 278 over time are plotted in Figure 147. For both vehicles OEI on the ground became the constraining directional control authority constraint that sized the tail. The elevons were not utilized at all in that flight condition, and were unable to augment yaw capability with asymmetric drag. The landing roll maneuver AMS Margin is also an active constraint. The decrab maneuver was on par with OEI in the air and was not an active constraint, despite being performed with only the rudders.

Tables 68 and 69 contain the constraints and other important parameters for the new optimized designs. The weights of the two optimized vehicles are extremely close to each other, but the optimized version of Vehicle 278 has better qualities than Vehicle 377. First, the outer wing elevons on Vehicle 278 are smaller which provides more space between the hinge line and the outer wing rear spar. This smaller surface area would result in smaller hinge moment loads, and the additional space provides the actuation subsystem designer greater flexibility to minimize actuation power. The tail volume coefficient for Vehicle 377 is actually smaller than on Vehicle 278 but due to the small moment arm the tail is extremely large.

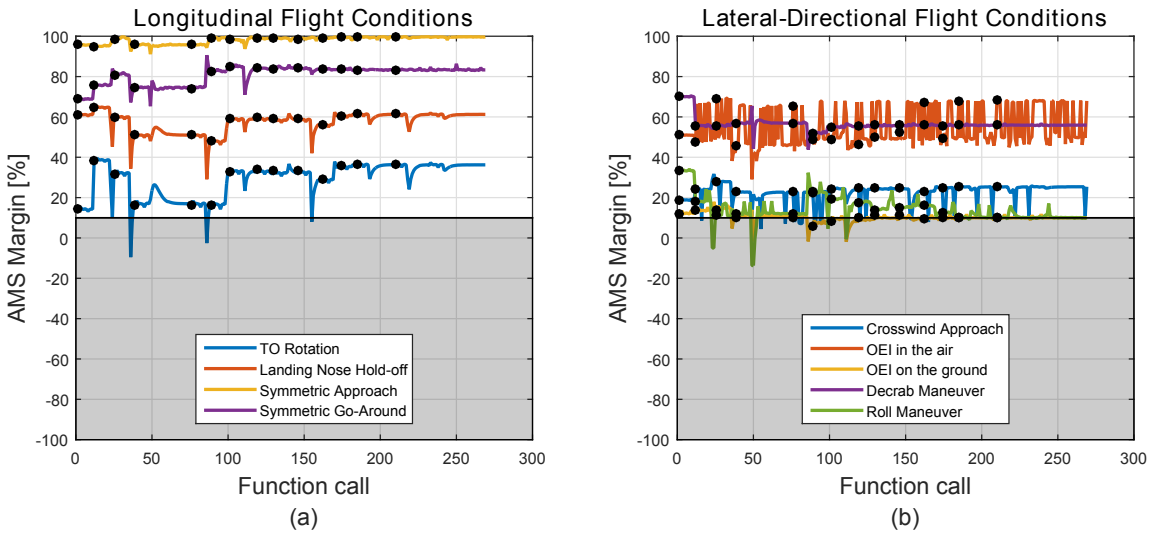

Figure 147: Full suite of AMS Margin constraints for Vehicle 278.

This method of optimizing the vehicle, independently deflected elevons with the full suite of off-design flight conditions, is considered to be HWB sizing best practice. The ganged elevon control utilization scenario can helped force greater reliance on the vertical tail in crosswind but is no substitute for evaluating control authority at all flight conditions. This requires additional model development and analysis but is important to do for unconventional configurations with no historical sizing methods. The best practice vehicle optimization method now enables exploring other vehicle classes and hopefully the generation of reliable trends.

Once a sufficient amount of data has been generated using this physics-based method, there may be the potential to employ historical methods such as the tail volume coefficient method. The tail volume coefficient for the optimized Vehicle 278 in this case is 0.0172. This is larger than the Boeing value, and the discrepancy may be due to different assumptions. For instance, some Boeing designs feature double hinged rudders and all-moving vertical tails. These control surface layout choices increase yawing moment control authority and enable smaller tails. The OEI on the ground was the tail sizing condition, which does not actually have a formal definition in the FARs or in Boeing documentation. The simplification of the analysis (static

Table 68: Constraint metrics for Vehicle 278 and 377 optimized with all control authority constraints and independent elevons.

		Target	Vehicle 278	Vehicle 377	Units
Performance Constraints					
1	Approach speed, V_{app}	< 150	**149.6**	**150**	knots
2	TO field length	$< 10{,}100$	9,874	9,880	ft
3	ROC @ Mach 0.84, 35k ft	> 300	508	453	ft/min
4	Climb ceiling	$> 35{,}000$	39,814	39,117	ft
Geometry Constraints					
5	Excess fuel capacity	> 0	179,035	217,345	lbs
6	Wing tip twist	< 0	-7.94	-6.64	degrees
7	$\Lambda_{outer} - \Lambda_{ctr}$	< 0	-22.9	-13.8	degrees
Control Authority Constraints					
8	AMS Margin$_{TO\ Rot.}$	> 10	36.2	29.0	%
9	AMS Margin$_{Lnd.\ nose\ hold}$	> 10	61.2	53.1	%
10	AMS Margin$_{Sym.\ Appr.}$	> 10	99.7	79.0	%
11	AMS Margin$_{Go-around}$	> 10	83.3	57.1	%
12	AMS Margin$_{OEI,air}$	> 10	67.9	63.8	%
13	AMS Margin$_{Cross.\ Appr.}$	> 10	25.4	20.4	%
14	AMS Margin$_{OEI,ground}$	> 10	**10.0**	**10.0**	%
15	AMS Margin$_{Decrab}$	> 10	55.9	37.3	%
16	AMS Margin$_{Roll\ maneuv.}$	> 10	**10.1**	**10.0**	%
17	Crosswind roll angle, ϕ	< 5	**5.1**	**5.1**	degrees
Other Constraints					
18	Start-of-cruise α	< 5	4.19	3.75	degrees
19	Excess clamshell drag	> 0	585	4,064	lbf

moment balance vs. dynamic ground roll simulation) and the unknown speed at which it should be performed create some uncertainty as well.

9.7 Conclusion

The optimization experiments of this chapter have resulted in significant contributions to the primary and secondary research objectives. The active performance and control authority constraints have been identified. Conceptual design of unconventional configurations such as the HWB is made difficult by the lack of knowledge regarding active control sizing flight conditions. Early optimization experiments omitted the most constraining vertical tail sizing flight condition. As a consequence, the vehicle

Table 69: Other results for Vehicle 278 and 377 optimized with all control authority constraints and independent elevons.

Metric	Vehicle 278	Vehicle 377	Units
TOGW	407,453	407,216	lbs
T_{SL}/W_{TO}	0.25	0.25	-
W_{TO}/S	50.53	55.62	lbs/ft^2
T_{SL} (& scale)	50,931 (0.89)	50,902 (0.89)	lbs/engine
S	8,063	7,321	ft^2
Wing tip twist	-7.94	-6.64	degrees
Cruise FWD CG	32.47	33.92	% MAC
Cruise Static Margin	10.55	9.23	%
Approach Static Margin	8.66	7.95	%
Trimmed $C_{L_{max}}$ (at $\alpha = 20°$)	0.80	0.87	-

and trim optimizers were able to exploit asymmetric drag from the elevons (an unintended usage) to drive the tail span to its lower bound. A ganged elevon utilization scenario was able to reduce this effect, but it was not a good substitute for evaluating the full set of flight conditions. The physics-based control authority assessment with AMS Margin constraints for the full suite of off-design flight conditions was established as the best practice for HWB optimization in conceptual designs.

This chapter also successfully demonstrated the utility of the AMS Margin control authority metric in an MDO setting. This was the final step necessary to resolve research question 2.2. It was discovered that the most constraining flight conditions for this design mission were the takeoff rotation maneuver, OEI on the ground, and the landing roll maneuver. The AMS Margin metrics for the first two flight conditions were correlated with the pseudo-elevator and rudder deflections, respectively. If desired the AMS Margin constraints could be replaced by those deflection angles. The AMS Margin concept may be the more intuitive option if the control effectors have nonlinear effects, or if the flight conditions with active control authority constraints require more significant overlap of control function.

Future avenues of research have been enabled by the work in this chapter. The modeling environment has been demonstrated to function as intended, resulting in

feasible HWB designs whose weights were successfully minimized. If historical tail sizing methods can be generalized to the HWB configuration, designers stand to benefit from a reduced analysis burden. However, initial experiments with the tail volume coefficient method identified issues that require resolution in future work. In particular the air speed, static margin, control authority, and noise trade-off requires must be explored in greater detail before historical methods can be recommended. The creation of surrogate models for the environment would enable more rapid optimization and design space exploration experiments, as well as enable algorithm performance comparisons. Other opportunities for future work enabled by the methods and models of this dissertation include quantifying the effects of new technologies on control authority constraints and the optimized vehicle. Examples include the use of body or ventral flaps during the takeoff rotation maneuver or active flow control for increased vertical tail effectiveness.

CHAPTER X

CONCLUSION

The elements of the Hybrid Wing Body - Control Authority Testbed (HWB-CAT) methodology have been developed and demonstrated throughout this dissertation and are now complete. Figure 148 captures the primary elements of the methodology. This final chapter will summarize the contributions of the dissertation in the context of the research questions posed through-out. Important new models, methods, and discoveries that contribute to the research objectives will also be discussed. Opportunities for future work including additional design studies enabled by this dissertation, improvements to the trim analyses, and extension of AMS Margin metric to other configurations.

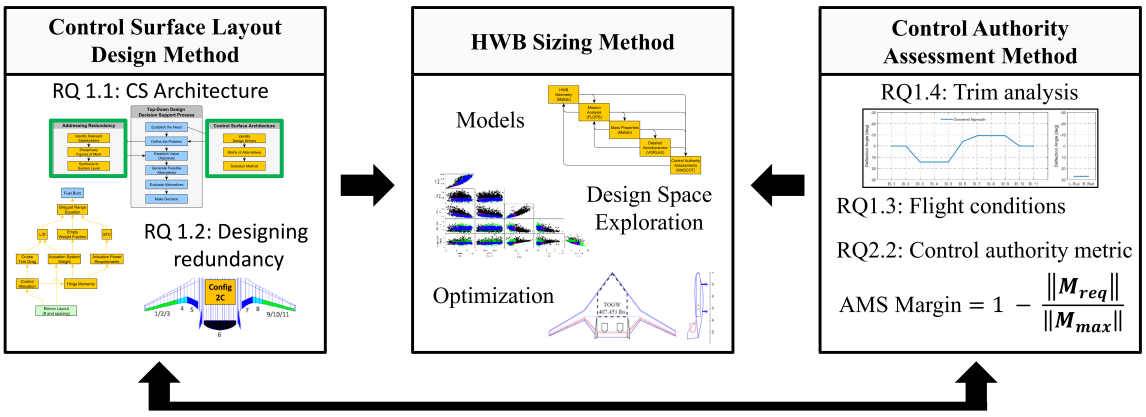

Figure 148: Hybrid Wing Body - Control Authority Testbed (HWB-CAT) Methodology.

10.1 Progress in and Resolution of the Research Questions

10.1.1 Design of Control Surface Layouts

RQ1.1: What control surface type and arrangement options are available and what justifies specific choices made for HWB designs in the literature?

→**RQ1.2**: How should the number of control surfaces be chosen?

→**RQ2.1**: What disciplinary metrics and design considerations might influence the number of redundant control surfaces?

The large amount of variability in the number of control surfaces among HWB designs in the literature and insufficient explanation of design rationale was the main motivation behind this series of research questions. Design drivers for control surface layout options were collected including the need to influence each moment axis, the need to fit controls on the available aerodynamic surfaces, and other considerations such as noise and mission requirements. Alternatives for the types of control surfaces were identified and stored in a matrix of alternatives. Decision making methods were suggested when the choices are not obvious. The control surface layout chosen for this dissertation was based on the N2A-EXTE configuration, and later modified to include speed brakes. This work was covered in Chapter 3 and resolves research question 1.1.

Chapter 5 discovered that the 20% minimum throttle constraint was challenging for a lot of HWB configurations to achieve. The elevons could be used to generate additional drag, but it was decided that dedicated speed brakes were a more appropriate option. This shows how design can be iterative, and some decisions need to be revisited as new information is learned. The MDO studies of Chapter 9 found that the two outboard elevons pairs from the default control surface layout were typically sufficient for achieving the 20% throttle constraint.

The literature survey did not find adequate answers regarding the appropriate amount of control redundancy on the HWB or other configurations. This required a new method to be developed and motivated the creation of research questions 1.2 and 2.1. In Chapter 3 the basic steps to answer these questions were identified but were fully explored and resolved in Chapter 6. Various disciplinary stakeholders were speculated upon and important metrics were identified. These included aerodynamics

(drag), actuation subsystem sizing (power, weights), and flight mechanics (trim deflections, loads generation). Alternative control surface layouts defined by the number and spacing of elevons needed to be compared based on their effects at the system level. The Breguet range equation was used to synthesize the disciplinary concerns and generate a fuel burn metric for comparing the layouts. This method was demonstrated successfully using the N2A-EXTE configuration and found that combining adjacent outer wing elevons into a larger pseudo-aileron had both weight, power, and fuel burn reduction benefits. Speed brakes were not required in this study, but the method could accommodate them without modification if desired. This design trade-off study was very computationally intensive and was not integrated into the larger HWB design environment. Due to the level of detail and analysis required to investigate the control surface layout alternatives, this is certainly a preliminary or detailed design issue.

10.1.2 Sizing HWB Control Surfaces

RQ1.3: What flight conditions are most likely to result in active control authority constraints for the Hybrid Wing Body?

The time and resources available to designers during the conceptual design phase are limited, and the evaluation of off-design flight conditions must be prioritized. As Chapter 1 noted, evaluating a limited number of flight conditions creates a risk of missing an active control authority constraint. Consequences to this may include degraded vehicle performance, accidents, or late phase redesign which can be costly. A survey of the literature regarding the sizing of unconventional control surfaces and unconventional configurations was conducted in Chapter 2, which uncovered the AeroMech methodology. This methodology was intended for use on unconventional vehicles and control surface layouts, and recommended evaluating on the order of 30 flight conditions to avoid missing a design critical one. Fortunately Boeing offered

a reduced set of more likely flight conditions based on approximately 25 years of experience with the HWB configuration.

Boeing's list of flight conditions for control authority assessments was sufficient to answer research question 1.3, but additional insights were generated during the HWB optimization experiments of Chapter 9. One recommended flight condition was not evaluated due to limitations of the VORLAX aerodynamic model used in this dissertation. Of the remaining nine conditions the takeoff rotation maneuver, OEI on the ground, and landing roll maneuver were discovered to be active constraints. Early optimization constraints omitted three lateral-directional flight conditions, and the consequences for missing an active constraint were observed.

RQ1.4: How should the trim analysis be conducted to support HWB design optimization?

Chapter 4 presented the conventional method for performing trim analyses from the literature. This method was predicted to perform poorly due to the control redundancy on HWB configurations, and experiments confirmed this using a model of the N2A-EXTE. Four alternative trim optimization formulations were proposed to deal with this issue. Two methods borrowed concepts from the control allocation literature, with the aim of creating unique trim solutions. Integrating the direct allocation method required swapping deflection angle parameters in the state vector with "commanded moments" for which the method could provide unique deflections. The ganging approach to control allocation also reduced the number of free parameters by linking elevons together to act as one larger control surface. Both methods were successful in achieving unique trim solutions.

Another pair of trim analysis methods were proposed that modified the trim optimization problem from root seeking to minimization of a secondary metric. These methods utilized the redundancy to choose from the nonunique solutions ones that

minimized drag and actuation power requirements. The minimum drag method could reliably achieve the global minimum trim solution. A global minimum power trim solution existed, but required an excessive number of randomly generated initial conditions to achieve due to the non-differentiability of the objective function and the presence of nonlinear constraints. In addition, the method was predicted and shown to under-utilize large control surfaces at the expense of saturating smaller ones.

Minimum throttle constraints were discovered to be necessary during the landing approach condition for the HWB. The two control allocation based methods were able to accommodate this constraint on the N2A-EXTE test configuration, whereas the minimum drag method would no longer return unique solutions. Chapter 5 experiments revealed that generating additional drag to meet the minimum throttle constraints required extreme elevon deflections for some designs, and caused the direct allocation method to fail. This issue was resolved by modifying the control surface layout, swapping the two outboard elevon pairs for clamshells. The minimum drag method was discovered to work well with clamshells and enabled small magnitude deflections. This settled for research question 1.4 which trim optimization problem formulation should be used to support HWB MDO. The rest of Chapter 5 would continue to formally define the algorithms for assessing each flight condition using the minimum drag method.

RQ2.2: Are there more convenient metrics for expressing the control authority available vs. required for a set of redundant controls?

One of the novel contributions of this dissertation was the introduction of a metric for assessing the control authority of a set of redundant multi-axis control surfaces. The AMS Margin metric is based on the attainable moment subset concept from the control allocation literature, and converts an N-dimensional trim deflection vector into a scalar measure of remaining control authority. A trim solution that requires

no deflections has an AMS Margin of 100%. A vehicle at the absolute limits of control authority has an AMS Margin of 0%. Finally, a vehicle with insufficient control authority to trim would have a negative AMS Margin, meaning the moment increments required were greater than what the controls could provide. Chapter 4 was able to demonstrate the metric on the trim solutions from all four alternative trim methods, and revealed that how the controls are utilized influences the control authority of the vehicle.

The AMS Margin metric was intended to be a continuous measure of remaining control authority, and a method needed to be established for estimating it when there was no valid trim solution. A negative AMS Margin would provide an indication of how much additional control authority was needed, and would be useful during gradient-based optimization of the vehicle. Chapter 5 performed experiments to demonstrate the behavior of the AMS Margin with key parameters defining each flight condition, which could be used to extrapolate the metric. For the crosswind approach flight condition, the behavior of the metric was shown to be piecewise linear with crosswind magnitude. For OEI in the air the metric was proportional to the V^{-2}. Of the longitudinal flight conditions, only the takeoff rotation maneuver ever experience control deficiencies. The AMS Margin metric was shown to be a linear function of the pseudo-elevator deflection angle, which was the only degree of freedom in that trim analysis.

The AMS Margin metric was successfully employed as the control authority constraint during the HWB MDO experiments of Chapter 9. It is useful because only one metric or constraint is required per flight condition regardless of the number of control surfaces, and makes for a cleaner optimization problem statement. The AMS Margin metric is also therefore a conceptually simpler control authority constraint than the alternative. It was able to provide the gradient-based optimizer a continuous constraint, even when the vehicle could not trim. Had control surface deflection

limits been used in place of the AMS Margin, the independent elevon optimization experiments would have had 55 additional constraints (or 12 deflections per flight condition). This alternative using independent deflection constraints would have resulted in failed function calls in cases with inadequate control authority, because the trim analysis was not permitted to extrapolate the aerodynamic surrogate model.

10.1.3 Sizing the HWB Configuration

RQ3.1: How should HWB sizing be conducted?

Chapter 3 established requirements and identified the basic elements required to model the HWB configuration. Chapter 7 went into greater detail for each of the steps in Chapter 3. It was decided that wing loading, a conventional sizing design parameter for T&W aircraft, was inappropriate to define independently for the HWB configuration. Reasons included the fact that the centerbody region of the planform should not be scaled, and that scaling the outer wing in isolation could lead to poorly balanced designs. Other parameters would need to change simultaneously to maintain a balanced vehicle. For this reason an optimizer driven approach to sizing was chosen. Vehicle planform geometry and the thrust-to-weight parameter were chosen as the independent design variables, and wing loading became an output of the sizing process.

Chapter 5 identified the sensitivity of HWB control authority to the $C_{L_{max}}$ parameter, which is an input to the FLOPS performance analysis. It was initially assumed to be a fixed parameter and technology level indicator but this value was not realistic for many designs. The resulting approach speed would be too low requiring extremely large angles of attack to trim. This constant was replaced with the maximum trimmed $C_{L_{max}}$, which was estimated to occur at a 20 degree angle of attack. This linked the parameter to each vehicle's geometry and resulted in more realistic approach velocities.

The trim analysis methodology study of Chapter 4 gave the first indications that how the controls are used will influence the optimized vehicle. A hypothesis was presented that predicted elevon ganging would cause over-sized tails. HWB optimization experiments in Chapter 9 with independent elevons showed that the tails were initially grossly under-sized due to missing lateral-directional control authority constraints, and the ganged elevon scenario could help compensate for this. However it was decided to implement the missing constraints, and best practice was determined to be optimization under the full suite of AMS Margin constraints with independent elevon control utilization assumptions.

Chapter 9 also investigated the feasibility of HWB optimization utilizing a vertical tail volume coefficient in lieu of the more expensive physics-based control authority assessment. However, initial experiments with the tail volume coefficient method identified issues that require resolution in future work. In particular the air speed, static margin, control authority, and noise trade-off requires further attention before historical methods can be recommended.

10.1.4 Research Objectives

Primary Research Objective: Develop an HWB sizing and control surface layout design methodology

Chapters 3, 4, 5, and 7 established methods and models to enable HWB conceptual design and control authority assessments. The resolution of research questions 1.3, 1.4, and 2.2 by these chapters contributed to resolving research question 3.1 as well. Chapters 8 and 9 demonstrated how these models and methods should be used to perform design space exploration and optimization in support of HWB conceptual design. Chapter 3 and 6 together resolve the series of research questions (1.1, 1.2,

2.1) regarding design of control surface layouts. Chapter 6 was successful in defining and demonstrating the control surface layout design method on the N2A-EXTE configuration. The creation and demonstration of the two methods, for HWB vehicle/control sizing and control surface layouts, satisfies the primary research objective of this dissertation.

Secondary Research Objective: Use the assembled MDO environment to test or discover trends, correlations, and design heuristics to aid in HWB conceptual design.

Chapter 8 made significant contributions towards meeting the secondary research objective by identifying and characterizing the feasible design space through filtered Monte Carlo Simulation experiments. This resulted in the selection of four candidate designs that were suitable optimization and more detailed analysis. The large Monte Carlo Simulation data set also supported several other analyses and discoveries. The geometry driven fuel volume data were utilized to tune the FLOPS fuel weight model for HWB configurations, and found good agreement with current practice within ASDL. An important trade-off between takeoff rotation control authority, takeoff field length, and rotation speed was discovered that can be used to expand the feasible design space or extract greater weight reductions. If this trade-off is not exploited, an optimizer may choose geometric changes that are detrimental to trimmed $C_{L_{max}}$ in an effort to increase V_{stall} (and related speeds) to increase control authority. A Boeing design heuristic regarding CG placement was scrutinized and determined to be plausible, though overly constraining. An alternative heuristic backed by evidence from the Monte Carlo Simulation and optimization experiments was proposed. HWB designs that had good cruise trim characteristics, and satisfied all performance and off-design control authority constraints fell within a narrow band of CGs centered at about 35% MAC. The HWB optimization experiments of Chapter 9 also made important contributions to this research objective by identifying active performance

and control authority constraints.

10.2 Opportunities for Future Work

Design Studies: There were several unturned stones that can be explored due to the availability of the models developed in this dissertation. The Monte Carlo Simulation of Chapter 8 resulted in an observation that vehicles which could perform the takeoff rotation maneuver tended to have high approach speed and TOFL. It was predicted but never demonstrated that trading TOFL (when feasible) for increased rotation velocity would expand the feasible design space. This is a low hanging fruit worth exploring in future work.

Chapter 8 also established that designs which could satisfy performance, cruise trim, and the takeoff rotation maneuver control authority constraint had forward takeoff CGs within a narrow range centered about 35% MAC. This information might be utilized to generate scaling rules for the outer wing on HWB configurations. With a constant outer wing sweep angle, increasing the scale or span of the outer wing push the CG aft. Therefore, there is potentially a gearing ratio between outer wing scale and outer wing sweep that maintains a relatively constant CG. This might enable conventional constraint analysis to be performed, because this gearing ratio would act as a stand-in for the expensive S&C constraints that have no analytical relationship to wing loading or thrust-to-weight ratio.

There is an opportunity to use this physics-based design environment to evaluate the impact of certain technologies on the HWB configuration. Body flaps are a possible control surface layout addition that augment pitching moment control authority during the takeoff rotation maneuver. Installing this type of control surface might reduce the extension of the centerbody required to perform the maneuver for reduced weight.

Now that the modeling environment development has stabilized, it may be worth

the effort to invest in generating a surrogate model of the environment. Currently, the environment may experience the occasional case failure during gradient calculation phases of the SQP algorithm from which it cannot recover. Considering the fact that the optimization runs presented in Chapter 9 took several days to complete, such a failure can be extremely frustrating. A surrogate model of the TOGW objective function and all of the constraints would help protect against breaking the optimization algorithm, or at least make it inconsequential due to the rapid design evaluation.

And finally the optimization environment should be used to further investigate the tail volume coefficient method. For instance it is not known whether the tail volume coefficient is sensitive to HWB passenger class, but the HWB sizing and optimization environment developed in this dissertation would be able to observe this. If the vertical stabilizers are mounted on the wing tips, it is suspected that the traditional tail volume coefficient would not be appropriate. In such a situation the effectiveness of the tails/rudders would be coupled with the planform, whereas centerbody mounted tails are not. This would also make an interesting follow-up study.

Trim Analyses Scaling of the objective function and constraints was discovered to greatly improve performance of the vehicle optimization experiments. The one engine inoperative flight condition in particular was a difficult flight condition for the minimum drag method, and it required a large number of random trials to be confident that the global optimum trim solution had been found. The force, moment, and navigation equations have different units and scales, which likely resulted in a poorly scaled problem. This and the other flight conditions may achieve the global minimum drag trim solutions more rapidly and reliably if these regularization methods are applied to the trim optimizer as well.

The minimum power trim method also suffered from many local optima, and rescaling may improve optimizer performance. The hinge moment model developed

from the VORLAX code does not model separation effects from large deflection angles. Such separation causes the pressure distribution over the control surfaces to increase dramatically. An accurate hinge moment model would not likely result in saturated elevon deflections as seen in Chapter 4. More realistic minimum power deflections could be achieved if empirical data were available to correct the vortex-lattice method results.

Extension of the AMS Margin Metric The aerodynamic models used in this dissertation predicted linear moments with control surface deflection. If an aerodynamic model with nonlinear control effectors were used, the AMS Margin metric would require a slight modification to remain accurate. The linear programming method used to estimate the maximum attainable moment vector in the required direction would need to be replaced by a piece-wise linear programming method. This extension of direct allocation methods to nonlinear controls has already been explored in the literature, and is expected to be a low hanging fruit.[14]

A loss of control authority caused by the need to generate excessive drag to meet minimum throttle constraints was discovered in Chapter 5. The AMS Margin metric was unable to capture this because drag is a nonlinear function of elevon deflection and was not included in the control effectiveness matrix (B). The piece-wise linear programming technique would resolve this issue, assuming a target drag force is included among the target moments. This would result in a more accurate AMS Margin when throttle constraints are met by elevons alone (no clamshells). The expected behavior for increasing minimum throttle constraints would be monotonically decreasing AMS Margin.

APPENDIX A

THE COST OF ENGINE LOCATION PERTURBATION ON CRUISE DRAG

A.1 Introduction

The metric decomposition for ITD-51A is shown in Figure 149. The top level includes the ERA program goals most directly impacted by HWB propulsion airframe integration. The bottom level includes the degrees of freedom available to designers for engine integration. These include engine location (x-y-z), engine orientation (Euler angles), vehicle outer mold line (OML), and nacelle shape. The intermediate levels map, through various disciplines, the degrees of freedom to the ERA program goals.

Boeing has spent significant effort optimizing these degrees of freedom using CFD. In fact, the configuration could be considered frozen. However, low speed wind tunnel tests on the N2A-EXTE revealed the possibility of low speed engine operability issues that were not predicted by CFD. The ability of CFD to accurately predict leading edge vortices has created uncertainty regarding the feasibility of the current engine location. If the vortices caused by the leading edge are ingested into the inlet or degrade engine operability beyond acceptable thresholds, the nacelles will have to be moved from their optimized location. Therefore, there is uncertainty in the final engine location with potentially nontrivial consequences to the ERA program goals.

The effect of the engine on vehicle trim and overall drag is highlighted in Figure 149. Moving the engine or changing its orientation will change the moments caused by thrust (Figure 150). Convention in HWB design is to trim the vehicle at a cruise design point by wing twist alone. At other points along the cruise segment, control surfaces would have to be used to balance the moments.

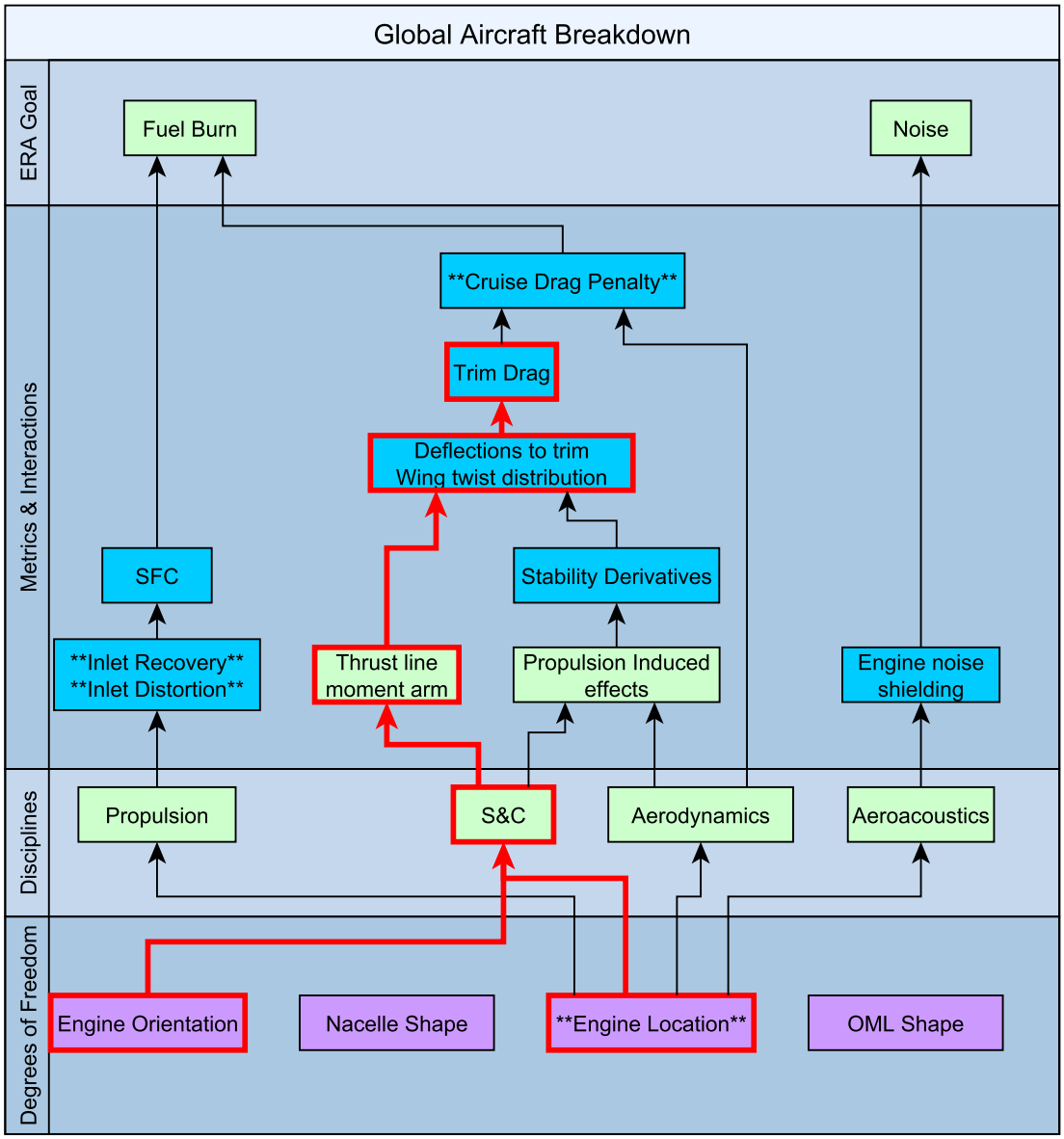

Figure 149: ITD-51A metric decomposition.

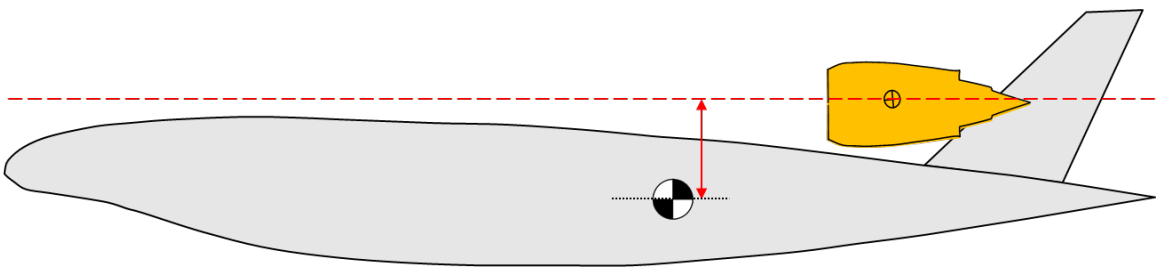

Figure 150: Engine location affects the thrust line.

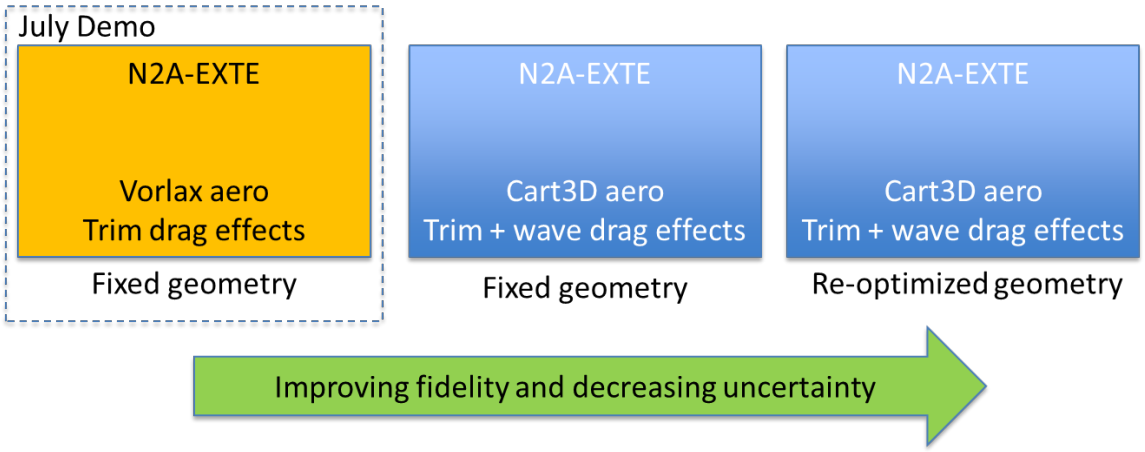

Figure 151: Modeling approaches of varying fidelity, accuracy, and effort.

In order to demonstrate uncertainty propagation for ITD-51A, an experiment was conducted to measure drag at a mid-cruise design point. Engine location and orientation parameters were varied and the vehicle was re-trimmed using the centerbody elevon. This was presented at the July MRB.

A.2 Discussion of Fidelity

Ideally the uncertainty propagation study would use Boeing proprietary geometry, a viscous CFD code, and optimization of vehicle OML and nacelle geometry with every new engine location. The unavailability of proprietary geometry and the computation expense of running many CFD cases led to the generation alternative approaches for studying this problem (Figure 151). The N2A-EXTE is a nonproprietary geometry available to ASDL for use in this study. Previous in-house studies have analyzed this geometry using vortex-lattice method (VORLAX) and inviscid CFD (Cart3D), and their models were available.

For the study presented at the MRB, a low fidelity approach was used as a first step. The N2A-EXTE geometry was represented in Vorlax to generate aerodynamic models for use in a trim analysis. A viscous drag correction from viscous CFD was applied to the inviscid Vorlax results. Shock effects were not captured in this study. In

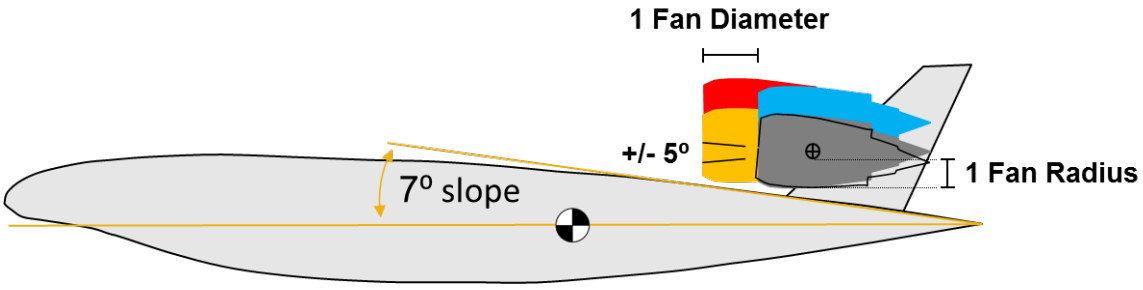

Figure 152: Engine degrees of freedom for the uncertainty propagation study.

addition, vehicle geometry is fixed and the vehicle is retrimmed using control surfaces alone. These issues will be addressed in future work described in a later section.

A.3 Method

A screening test was first performed on the engine location and orientation degrees of freedom. The results of this test indicated that spanwise engine location (y-location) and engine orientation in the horizontal plane were not significant contributors to trim drag. The degrees of freedom selected for the full study are shown in Figure 152. These are engine x-location in terms of fan diameters aft of the baseline, fan radii above the vehicle surface, and the engine orientation in the vertical plane. When the engine x-location is changed, it is moved relative to a 7 degree ramp. This is to avoid infeasible engine locations that would cause the nacelle to intersect with the OML. The CG x-location was updated with engine was movements.

An aerodynamic model of the N2A-EXTE at the cruise design point was generated using VORLAX. The VORLAX geometry and representative C_p distribution are shown in Figure 153. The control surfaces were modeled as distinct panels, which was found predict control surface effects better than conventional camber line modification. Low speed wind tunnel data with elevon deflections was used to validate the model (Figure 154), as well as cruise CFD for calibrating the viscous drag correction (Figure 7). Surrogate models of the force and moment coefficients were generated as a function of angle of attack, elevon deflections, and CG location.

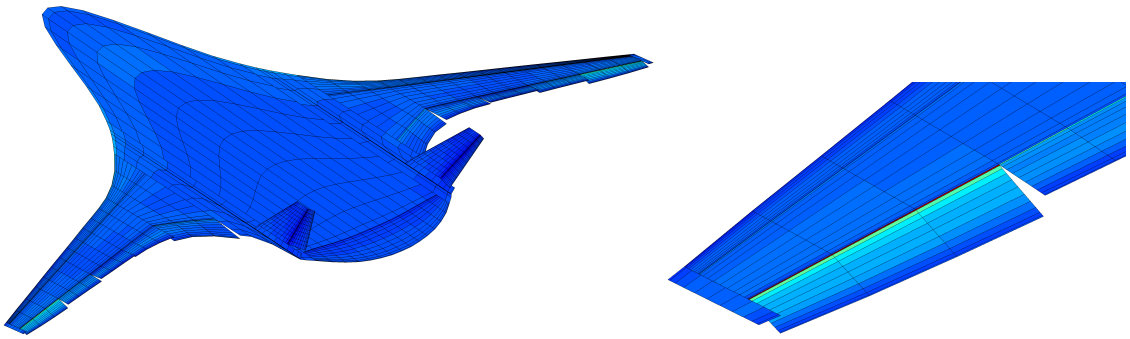

Figure 153: C_p visualization for the N2A-EXTE VORLAX model.

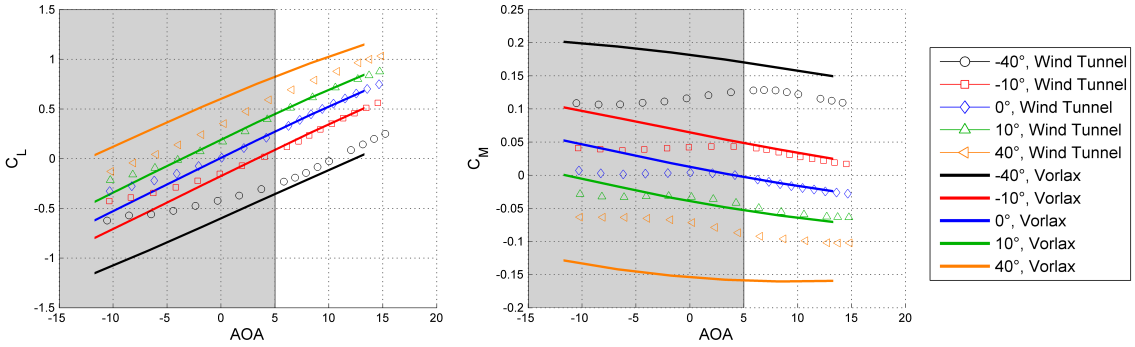

Figure 154: VORLAX and wind tunnel data for the N2A-EXTE in high lift configuration at Mach 0.2.

Table 70: Mid-cruise design point.

Parameter	Value	Units
Weight	402,855	lbs
Altitude	38,145	ft
Mach	0.8	
Center of gravity	Aft	-

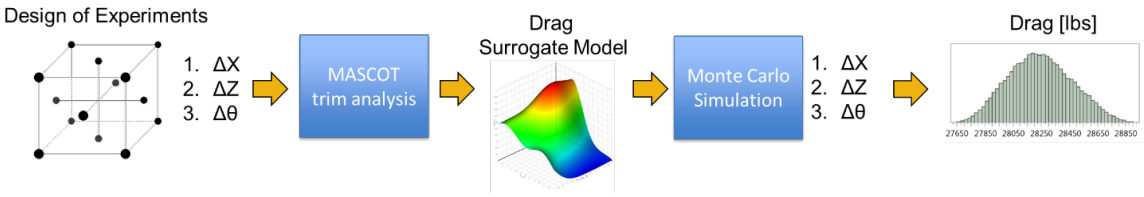

Figure 155: VORLAX and wind tunnel data for the N2A-EXTE in high lift configuration at Mach 0.2.

The trim analysis was performed using the NASA Matlab Stability and Control Toolbox (MASCOT). It has been modified by ASDL to accommodate vehicles like the HWB with redundant multi-axis control surfaces. The centerbody elevon alone was used to balance the pitching moments as necessary. Table 70 describes the cruise design point flight condition evaluated in MASCOT. The drag of the trimmed vehicle is collected for every engine location.

A surrogate model of the trimmed vehicle drag was regressed as a function of engine location and orientation. This step was necessary to generate a drag distribution based on engine location uncertainty via Monte Carlo Simulation. A central composite design was used to choose the engine parameters, and a 2nd order response surface equation was able to accurately model the trimmed vehicle drag. The full sequence of steps for the method is shown in Figure 155.

Using the trimmed vehicle drag surrogate model a prediction profiler can be generated (Figure 10). It shows the sensitivity of the response (drag) to each of the input parameters. The effects of engine location shown here are linear in drag, and this is strictly due to the cost of retrimming the aircraft. The Vorlax model did not include nacelles, nor would it have made a large difference. CFD is necessary to capture the

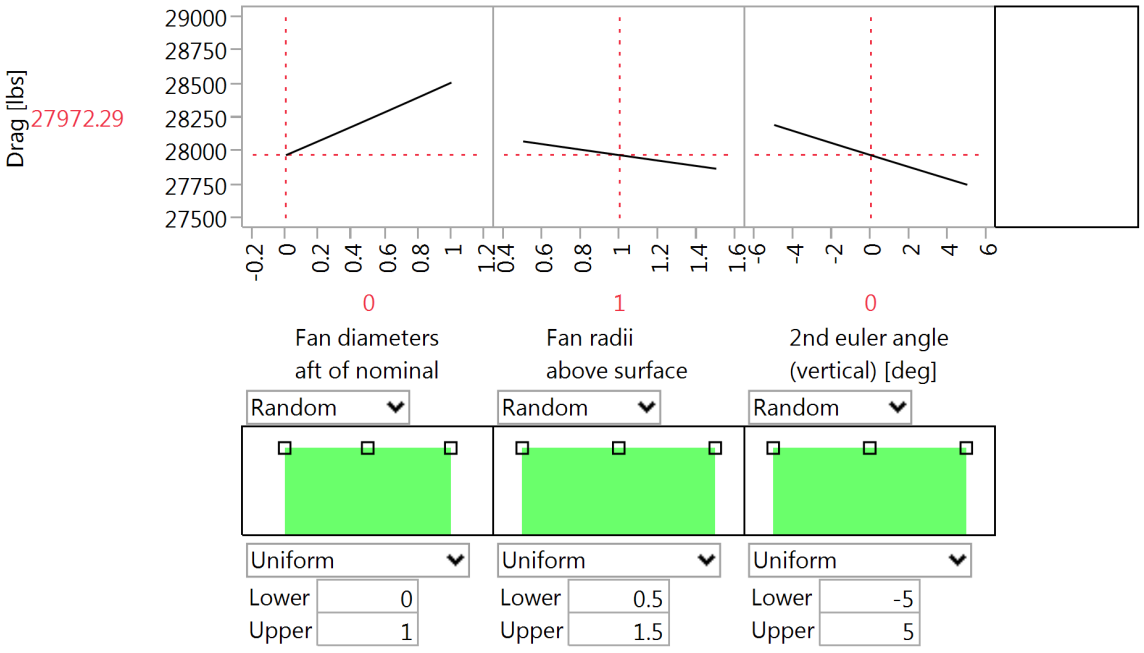

Figure 156: Trimmed vehicle drag prediction profiler.

true total cost of moving the engines around.

The Monte Carlo Simulation is performed using this dialog in the JMP software. Below each input parameter are options for choosing distributions. A 100,000 case Monte Carlo Simulation was performed by sampling each input parameter from uniform distributions.

The resulting drag distribution from the simulation is shown in Figure 157. There is nontrivial variation in mid-cruise drag caused by engine movement. It ranges from -1% to +3% of the baseline drag value. This result should make it clear that a certain level of vehicle redesign is necessary whenever the engine is moved. In this case, the wing can be retwisted to reduce or eliminate trim drag penalties. The final step to complete the uncertainty propagation study was not performed for the July MRB. The EDS environment, which uses FLOPS for the performance analysis, would require some additional manipulation of the drag distribution. The FLOPS input is a percentage installation drag penalty, which is also a distribution on account of the engine location uncertainty. FLOPS would be run many times while sampling from

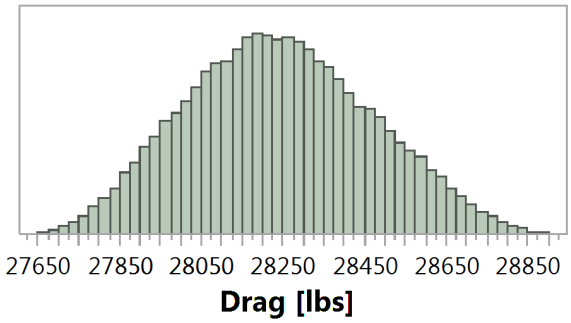

Figure 157: Trimmed vehicle drag distribution due to engine location uncertainty.

the installation drag penalty distribution. This final step will be performed with higher fidelity Cart3D aerodynamic results at a later time.

APPENDIX B

ADDITIONAL MINIMUM POWER TRIM OPTIMIZATION EXPERIMENTS

B.1 Further Analysis of the Minimum Power Trim Optimization Symmetric Approach Results

B.1.1 Different H_{sum} definition

The local optima problem motivated an additional test, where the elements of H_{sum} were squared instead of absolute value. Success would be defined as greater convergence rates or being more likely to hit the optimal solution. The rate of convergence was about the same. The deflection trade space, optimal solution, etc were different. There was no compelling reason to switch to this version of the H_{sum} metric.

B.1.2 Centerbody Elevon as a Trim-only Device

The centerbody elevon is the largest in terms of surface area and has the largest hinge moment derivative, but is also the most effective for controlling pitching moment. Minimizing H_{sum} avoids using this elevon for steady state trim. If the functions of the stability augmentation system could be performed without the use of this elevon, then it could be possible to make it a trim-only device. This entails fitting the centerbody elevon with an irreversible mechanism and operating it like rotatable horizontal tails on current passenger transports. The movements would be slow, but there would be no steady state power requirements for that elevon.

This scenario was investigated to see how it influences H_{sum} magnitudes and trim deflections. Another 500 randomly generated initial conditions were run, with a modified objective function that neglected the centerbody elevon hinge moment. As seen in Figure 158, there are still local optima causing premature gradient-based

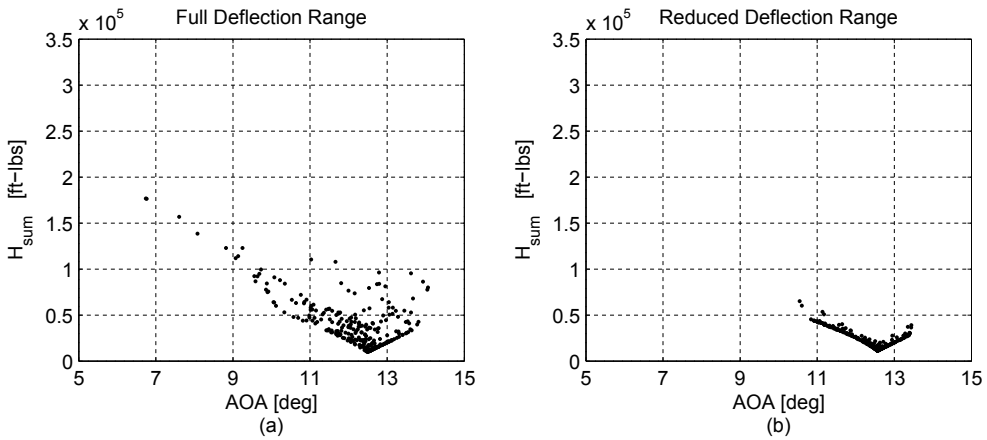

Figure 158: H_{sum} vs. AOA with the centerbody elevon (no. 6) as trim-only device for (a) full deflections allowed and (b) reduced deflections.

optimizer termination for most of the solutions. Power is minimized at a specific angle of attack that is higher than before, and there is no longer an H_{sum} "bucket." What is striking is that the minimum power trim solution has an H_{sum} that is 80% lower than the minimum in the previous scenario. If conversion of the centerbody elevon to a trim-only device is feasible, then there is a lot to be gained by doing so.

Plots of the trim solutions for the full and reduced deflection ranges are shown in Figure 159. In the full deflection range solution the centerbody elevon is able to trim the vehicle with most of the remaining elevons free floating. The elevon 1/11 pair are powered and saturated, however. The reduced deflection angle range trim solution is an excellent compromise that reduces the risk of flow separation with trivial difference in H_{sum}.

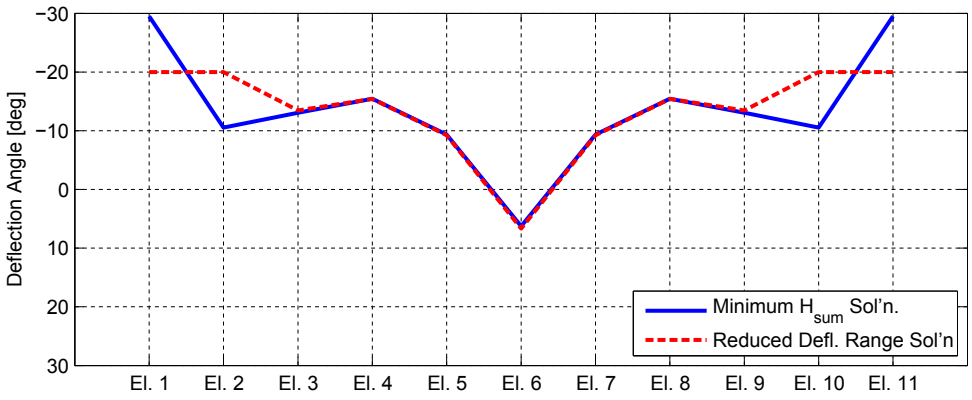

Figure 159: Minimum H_{sum} deflections with the centerbody elevon (no. 6) as trim-only device.

APPENDIX C

MULTI-DIMENSIONAL TRIM SOLUTION PARETO FRONTIERS

The experiment in this appendix investigates the trade-off between a minimum power and a minimum drag cost function for trim analyses, which had been previously investigated in isolation. The N2A-EXTE model used extensively in Chapter 4 is again used here in a symmetric landing approach flight condition. The fixed vs. free elements of the state vector are the same as those used in the minimum drag trim optimization experiments of Section 4.5.5 (Tables 10 and 11, respectively). In these experiments the 20% throttle constraint will not be enforced.

The new cost function given in the optimization statement below is a parametric weighting between the H_{sum} and drag cost functions. The cost functions are divided by their lowest observed values from previous experiments in an attempt to rescale them to the same order of magnitude. The range of the tuning parameter is from 0 to 1. The extremes of α minimize H_{sum} or drag in isolation, and values in between are used to define the Pareto frontier between between the two cost functions.

$$
\begin{aligned}
\underset{S}{\text{minimize}} \quad & \alpha \frac{H_{sum}(S)}{H_{min}} + (1-\alpha)\frac{Drag(S)}{Drag_{min}} & \\
\text{subject to} \quad & S_i = a_i,\ i = 1, \ldots, l. & \text{Flight/Operating conditions} \\
& b_i \leq S_i \leq c_i,\ i = l+1, \ldots, m. & \text{State variable side constraints} \\
& residual_j = 0,\ j = 1, \ldots, 9 & \text{EOM residual constraints}
\end{aligned}
$$

For this experiment, α was varied from 0 to 1 in increments of 0.25. Two hundred random initial conditions were run with the fmincon / active-set algorithm at each

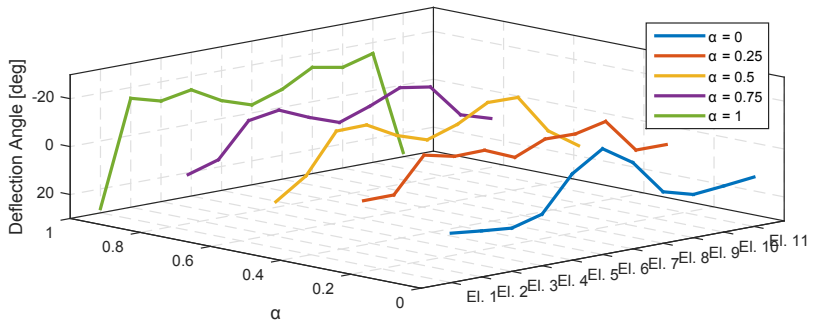

Figure 160: Optimal trim solutions in symmetric approach for various weightings between H_{sum} and Drag.

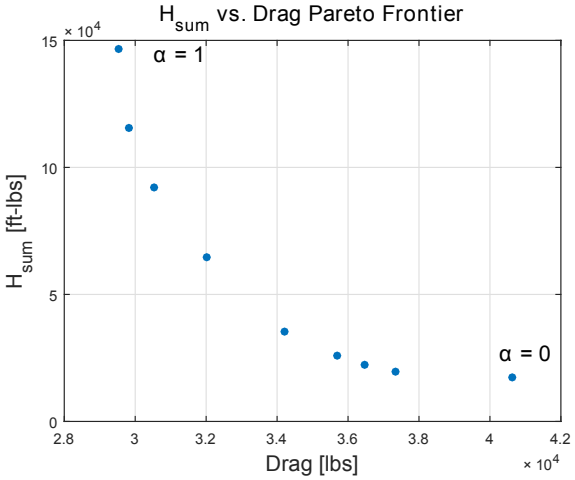

Figure 161: The Pareto frontier for H_{sum} and Drag.

value of α and the trim solution that minimized the composite cost function was retained. The optimal trim deflections are plotted in Figure 160 as a function of α. In the foreground are the minimum drag trim deflection plotted in blue, and in the background are the minimum H_{sum} trim deflections in green. These are different from the ones presented in Section 4.5.6, which imposed a throttle constraint. The Pareto frontier for these and some additional values of α are shown in Figure 161. An interesting avenue of future work would be to investigate additional cost functions and their trade-offs in multiple dimensions. Other example cost functions of interest include the sum squared deflection and noise.

APPENDIX D

SELECTION OF A TRIM ANALYSIS METHOD FOR SYMMETRIC AND CROSSWIND APPROACH WITH CLAMSHELLS

The use of clamshells for achieving modest trim deflections under throttle constraints was explored with the conventional trim method, which required a large number of random initial conditions. Next it had to be determined which of the alternative trim methods from Chapter 4 would still perform well with the use of clamshells. In this section a set of experiments is conducted in order to evaluate and compare several options. The option determined from the matrix of alternatives in Table 71 that works well in both symmetric and crosswind conditions will be selected. The preferred results are high rates of convergence, unique solutions, and the ability to meet the 20% throttle constraint with modest deflections. The full set of experiments is enumerated in Table 72.

Table 71: Clamshell test matrix of alternatives.

Option	1	2
Flight Condition	Symmetric Approach	Crosswind Approach
Trim method	Min Drag	Direct Allocation
Clamshell utilization	Fixed ΔD	Variable ΔD

Table 72: Tests to determine the best method to use with clamshells.

Exp. #	Flight Condition	Trim Method	Clamshell Utilization	Throttle
1	Symmetric Approach	Min Drag	Fixed ΔD	(a) Unconstrained (b) Constrained
2	Symmetric Approach	Direct Allocation	Fixed ΔD	(a) Unconstrained (b) Constrained
3	Symmetric Approach	Min Drag	Variable ΔD	Constrained
4	Symmetric Approach	Direct Allocation	Variable ΔD	Constrained
5	Crosswind Approach	Min Drag	Fixed ΔD	Unconstrained
6	Crosswind Approach	Direct Allocation	Fixed ΔD	Unconstrained
7	Crosswind Approach	Min Drag	Variable ΔD	Constrained
8	Crosswind Approach	Direct Allocation	Variable ΔD	Constrained

Notably absent from Table 72 is the minimum power trim optimization method, which will not be explored further in this dissertation. The VORLAX code from which the hinge moment models are generated does not take into account separation effects at high deflections. This would change the pressure distribution downstream of the hinge, resulting in higher hinge moments than are currently predicted. As a result, the minimum power method produces deflections with some extreme angles. Another issue is the difficulty in finding the global minimum power solutions, which required a large number of random initial conditions.

For the first method of using clamshell elevons in the trim analysis, a fixed drag increment of either $\Delta D = D_{20\% \text{ throttle}} - D_{min}$ or $D_{clamshell_{max}}$ (the smaller of the two) will be assumed. The two outboard elevon pairs will be assumed to be dedicated drag generating clamshells for the approach flight condition in which they are needed. As a consequence they will not be available for generating moments for trim nor will they

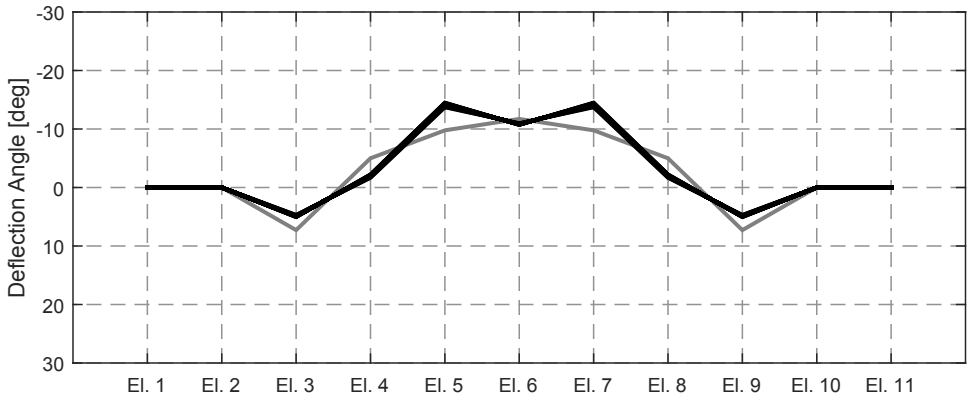

Figure 162: Minimum drag trim deflections with fully deployed clamshells.

contribute to the attainable moment subset. They will remain "undeflected" as far as the VORLAX aerodynamic model is concerned. They will also operate symmetrically and will not be able to augment the rudder yaw control authority.

Each of the experiments will optimize 100 randomly generated initial conditions. The experiments with fixed clamshell drag increments have some properties in common that are described here. Again, the fixed drag increment is the minimum of either 1) the drag available from the clamshells, or 2) the drag difference between the global minimum drag solution and Equation 43. The drag increment needed to bring the global minimum drag (22,730 lbs) up to a drag achieving 20% throttle is 20,779 lbs. The drag available from the clamshells on Vehicle 377 is 20,675 lbs at full 60 degree deflection, which is the smaller of the two values and will serve as the fixed drag increment.

Experiment 1 When the minimum drag method was run with the clamshells fully deployed and no throttle equality constraint, 100% of the random initial conditions converged. There were two similar solutions but 99 of the 100 were the bold solution in Figure 162. Both had nearly identical throttle settings (20.27% vs. 20.36%) and AMS Margins (79.52% vs. 79.64%), and either would be acceptable.

The minimum drag method with fixed clamshells works well for Vehicle 377. The

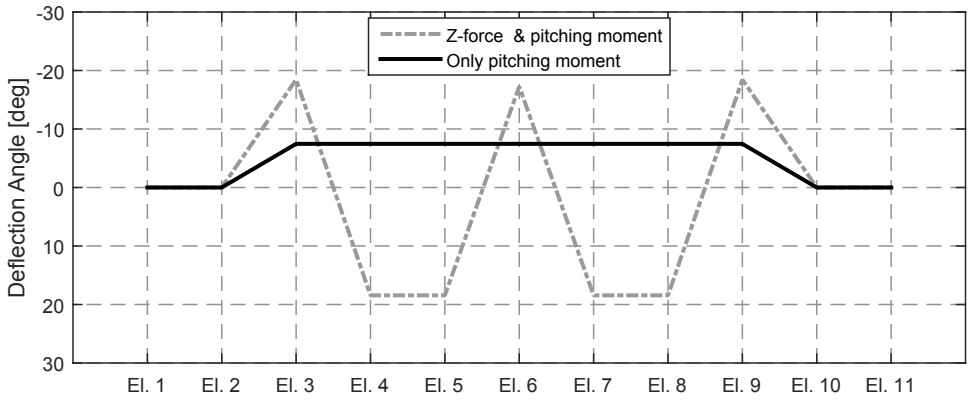

Figure 163: Direct allocation trim deflections with fully deployed clamshells.

drag increment is merely an estimate of what is needed to shift the trim solution space to a more favorable region, and it was discovered that this can be slightly overestimated. Enforcing a 20% throttle equality constraint when the drag increment has been overestimated resulted in no feasible trim solutions. A slightly higher throttle setting is acceptable, because 20% is merely an assumed lower bound on feasible throttle settings.

Experiment 2 The conventional method with direct allocation was also successful in achieving trim solutions with a fixed clamshell drag increment. Direct allocation was conducted with 1) a sole pitching moment command, and 2) both body axis Z-force and pitching moment commands. The former resulted in smaller deflections, though both resulted in 100% convergence and unique solutions (Figure 163). In the latter case, the Z-force was constrained by its lower bound of zero pounds. Follow-up tests allowing negative Z-force (e.g. positive lift) resulted in non-unique solutions. The trim solution throttle settings were approximately 21%, again a reasonable result. The direct allocation solution found with pitching moment commands only had an AMS Margin of 75.13%, which is comparable to the minimum drag method.

Experiment 3 The minimum drag trim method with a throttle equality constraint and clamshell drag as a degree of freedom did not perform well. Despite a 100% rate of convergence and exactly 20% throttle, the solutions were not unique.

Experiment 4 When commanded Z-force was a degree of freedom the results were not unique, regardless of the bounds allowed on it. When only pitching moment was commanded, 100% of the trials converged to a unique trim deflection that was similar to those in Experiment 2 and Figure 163.

Experiment 5 This is the first of the experiments to test the crosswind approach flight condition with clamshells. For this and the following experiments, the full 35 knot crosswind magnitude was not achievable. The methods are instead tested at increasing levels of crosswind magnitude until the controls saturate and trim is no longer possible.

The deflections from the minimum drag method with a fully deployed clamshell and no throttle equality constraint are shown in Figure 164. They resemble the minimum drag deflections in symmetric flight and change gradually as crosswind magnitude is increased. The rates of convergence are still very high, with 100% converged to a unique solution at a 5 knot crosswind to 92% converged to a unique solution at a 25 knot crosswind. The throttle setting variation with crosswind magnitude is quadratic but not very sensitive, and is always slightly higher than 20%.

The most important observation to make is the behavior of AMS Margin with crosswind magnitude as shown in Figure 165. It is a piecewise linear curve indicating that the control authority (from the rudder in this case) for Vehicle 377 becomes exhausted at approximately a 26.25 knot crosswind. As a reminder, the AMS Margin metric measures the remaining control authority by comparing the magnitudes of a) the moment vector required to trim, and b) a parallel vector extended to the surface of the attainable moment subset. As the crosswind magnitude is increased the moment

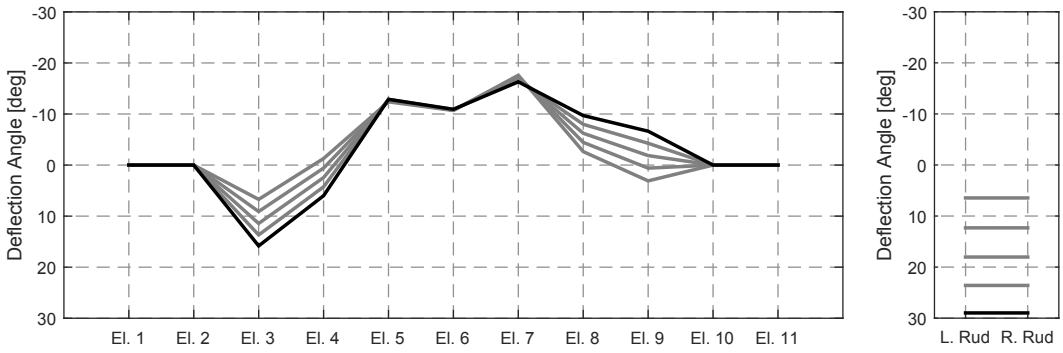

Figure 164: Minimum drag deflections with clamshells for increasing levels of crosswind.

vector required to trim shifts direction and in doing so points through different faces of the attainable moment subset. The AMS Margin is linear as the moment vector required to trim shifts across each individual face, and is readily extrapolated to the full crosswind magnitude for a value of -32.5%. Figure 164 shows that the rudder is quickly saturated and is the limiting factor. The negative AMS Margin signals that the yawing moment control authority needs to increase by nearly a third (e.g. through increased tail area).

Experiment 6 The heading angle (ψ) range from the previous chapter was too restrictive for Vehicle 377 using direct allocation in crosswind conditions and had to be expanded to $\pm 1^{\circ}$ about 90 degrees. Once that was changed, the trim method was tested using only the moment commands (no Z-force), full symmetric clamshell deployment, and no throttle equality constraint. The convergence rates shown in Table 73 were not as good as the minimum drag trim method, but the solutions at each crosswind magnitude were unique (Figure 166). If the worst observed rate of successful convergences (43%) is assumed, then to have a 99% likelihood of finding a trim solution the trim analysis should be run at least 9 times per crosswind magnitude. However, since they are all unique only the first successful solution is needed. The throttle settings were all slightly above the 20% minimum.

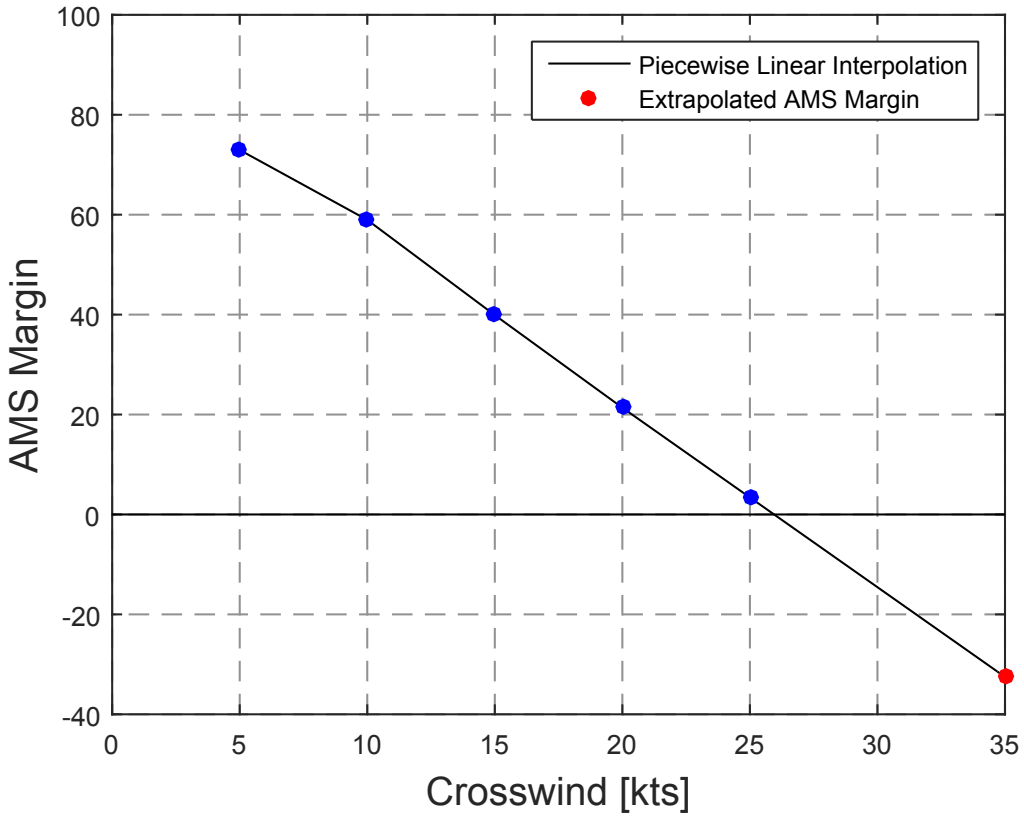

Figure 165: Crosswind approach AMS Margin trend and extrapolation for the minimum drag method with clamshells.

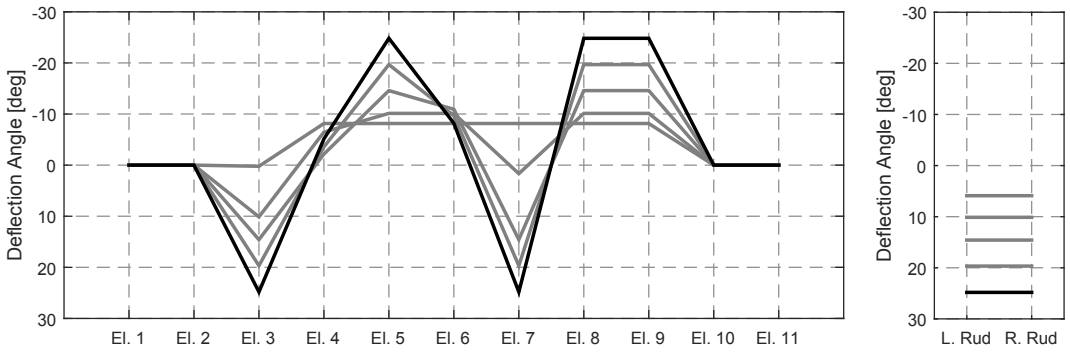

Figure 166: Direct allocation deflections with clamshells for increasing levels of crosswind.

Table 73: Convergence rates as function of crosswind magnitude for Experiment 6.

Crosswind Mag. [kts]	5	10	15	20	25
Convergence Rate	80%	63%	43%	84%	63%

The unique trim solutions also have piecewise linear AMS Margin trends shown in Figure 167. The control authority for Vehicle 377 using direct allocation deflections becomes exhausted at approximately 30 knots, which is an improvement over the minimum drag method. This method appears to have achieve greater yawing moment control authority indirectly through favorable asymmetric elevon drag. This comes at the cost of increased elevon deflection magnitudes, and several are nearly saturated at 25 knots. The extrapolated AMS Margin at full crosswind is approximately -17%.

Experiment 7 The minimum drag method in crosswind conditions under a throttle equality constraint with clamshell drag as a degree of freedom did not perform well. There was nontrivial variation in their trim solutions and their respective AMS Margins. This combination of settings is not recommended.

Experiment 8 The direct allocation trim solutions under a throttle equality constraint and variable clamshell drag were successful. The results are able to achieve

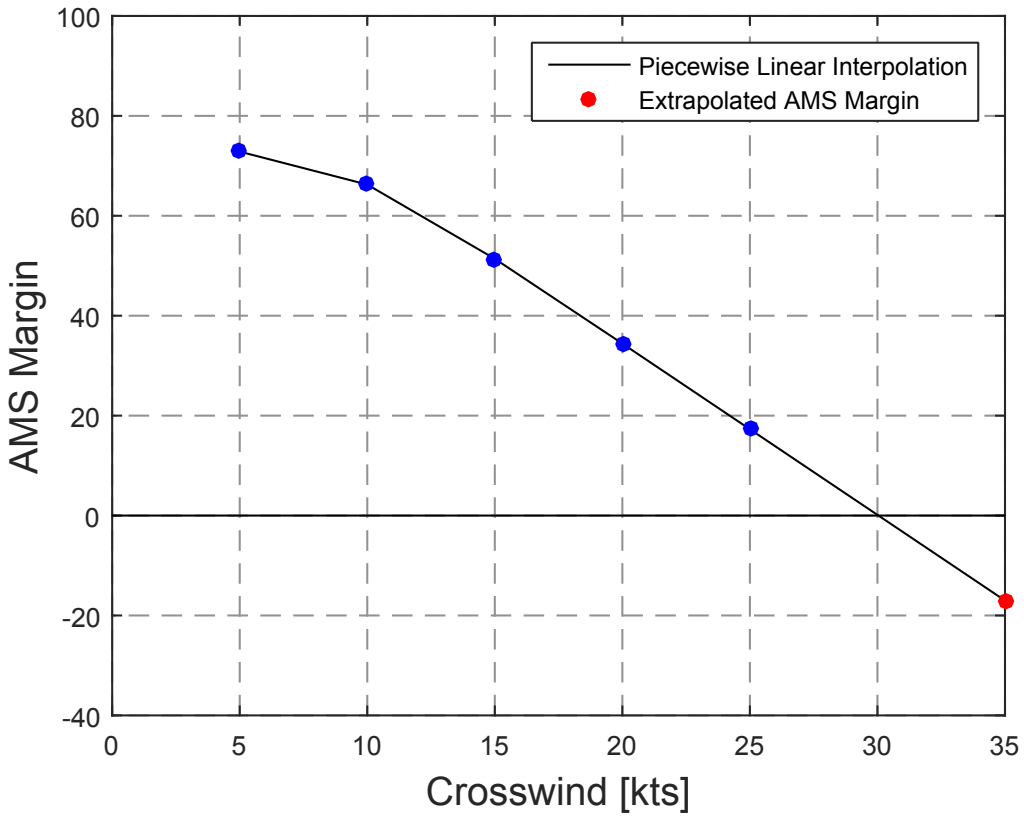

Figure 167: Crosswind approach AMS Margin trend and extrapolation for the direct allocation method with clamshells.

an exact 20% throttle setting, but are otherwise very similar to those in Experiment 6 (fixed clamshell, no throttle constraint).

Summary of Results A summary of the experimental results for the minimum drag method and conventional method with direct allocation are in Tables 74 and 75, respectively.

Table 74: Summary of results for the minimum drag method.

Minimum Drag Method	Symmetric Approach	Crosswind Approach
1) Fixed Clamshell	Global minimum drag solution is unique. Infrequent outliers (local optima). Throttle > 20%	Global minimum drag solution is unique. Throttle > 20% Max Crosswind 25 kts
2) Variable Clamshell	Non-unique solutions Throttle = 20%	Non-unique solutions Throttle = 20% Max Crosswind 25 kts

Table 75: Summary of results for the conventional method with direct allocation.

Direct Allocation Method	Symmetric Approach	Crosswind Approach
1) Fixed Clamshell	Unique solution (pitching moment command only). Throttle > 20%	Unique solutions (moment commands only). Throttle > 20% Max Crosswind 30 kts
2) Variable Clamshell	Unique solution (pitching moment command only). Throttle = 20%	Unique solutions (moment commands only). Throttle = 20% Max Crosswind 30 kts

Earlier results in Chapter 4 showed that the minimum drag method could not achieve unique solutions under a throttle constraint with the original control surface layout. When properly sized clamshells are used to generate the drag needed to achieve at least a 20% throttle, the minimum drag method performs well. With a throttle inequality constraint and fixed clamshell drag increment, the method can reliably achieve the global minimum drag solution with modest deflection magnitudes in both symmetric and crosswind approach flight conditions. The conventional method with direct allocation consistently produced unique solutions using both methods of generating drag with the clamshells (e.g., fixed increment vs. degree of freedom).

During HWB optimization it is possible that designs with inadequately sized clamshells will be evaluated. In that situation there may not be a feasible trim solution space if a throttle equality constraint is imposed. This reduces the choice of trim method to either the minimum drag method or the conventional method with direct allocation using a fixed clamshell drag increment. Vehicle 377 is able to trim at slightly greater crosswind magnitudes using the conventional method with direct allocation, but at the cost of near saturation of several elevons. The minimum drag method achieves similar crosswind magnitudes with more modest deflections and therefore is the method chosen for symmetric and crosswind approach flight conditions. This method is also able to deal with issues caused by low $C_{L_{max}}$ (described in Section 5.6.1), making it the best choice.

REFERENCES

[1] "Federal aviation regulations (far) part 25 - airworthiness standards: Transport category airplanes, federal aviation administration (faa), code of federal regulations title 14." `http://www.ecfr.gov/`.

[2] "Global market forecast 2012-2031," tech. rep., Airbus, Blagnac Cedex, France, September 2012.

[3] "Current market outlook 2013-2032," tech. rep., Boeing, Seattle, WA, 2013.

[4] Abdulrahim, M., "Flight dynamics and control of an aircraft with segmented control surfaces," in Aerospace Sciences Meeting, no. AIAA-2004-128, American Institute of Aeronautics and Astronautics, Jan. 2004.

[5] Abdulrahim, M. and Lind, R., "Investigating segmented trailing-edge surfaces for full authority control of a uav," in Guidance, Navigation, and Control and Co-located Conferences, no. AIAA-2003-5312, American Institute of Aeronautics and Astronautics, Aug. 2003.

[6] Alston, K., Doyle, S., Kim, H., Ragon, S., and Winter, T., "High fidelity multidisciplinary optimization (hfmdo)," in Aerospace Sciences Meetings, pp. –, American Institute of Aeronautics and Astronautics, Jan. 2010.

[7] Alston, K. and Winter, T., "Balancing high fidelity mdao with robust system design," in Aerospace Sciences Meetings, pp. –, American Institute of Aeronautics and Astronautics, Jan. 2011.

[8] Anderson, J. D., Aircraft performance and design. Boston : WCB/McGraw-Hill, 1999.

[9] Anderson, J. D., Aircraft performance and design. Boston : WCB/McGraw-Hill, 1999.

[10] Anderson, M. R. and Mason, W., "An MDO approach to control-configured-vehicle design," in AIAA, NASA, and ISSMO, Symposium on Multidisciplinary Analysis and Optimization, (Bellevue, WA), Sept. 1996.

[11] Bjorck, A., Numerical Methods for Least Squares Problems. Handbook of Numerical Analysis, Society for Industrial and Applied Mathematics, 1996.

[12] Bodson, M., "Evaluation of optimization methods for control allocation," Journal of Guidance, Control, and Dynamics, vol. 25, no. 4, pp. 703–711, 2002.

[13] Bolender, M. A. and Doman, D. B., "Nonlinear control allocation using piecewise linear functions," Journal of Guidance, Control, and Dynamics, vol. 27, no. 6, pp. 1017–1027, 2004.

[14] Bolender, M. and Doman, D., "Nonlinear control allocation using piecewise linear functions: A linear programming approach," JOURNAL OF GUIDANCE CONTROL AND DYNAMICS, vol. 28, pp. 558–562, MAY-JUN 2005. AIAA Guidance Navigation and Control Conference, Providence, RI, AUG 16-19, 2004.

[15] Bonet, J. T., "Boeing era n+2 advanced vehicle concept results," in 50th AIAA Aerospace Sciences Meeting, American Institute of Aeronautics and Astronautics, Jan. 2012.

[16] Bonet, J. T., Schellenger, H. G., Rawdon, B. K., Elmer, K. R., Wakayama, S. R., Brown, D. L., and Guo, Y., "Environmentally responsible aviation (era) project - n+2 advanced vehicle concepts study and conceptual design of subscale test vehicle (stv) - final report," tech. rep., Boeing Research and Technology, Huntington Beach, CA, 2011. To Appear.

[17] Bordignon, K. A. and Durham, W. C., "Closed-form solutions to the constrained control allocation problem," Journal of Guidance Control and Dynamics, vol. 18, no. 5, pp. 1000–1007, 1995.

[18] Cameron, D. and Princen, N., "Control allocation challenges and requirements for the blended wing body," (Denver, CO), Aug. 2000.

[19] Chakraborty, I., Jackson, D., Trawick, D., and Mavris, D., "Development of a sizing and analysis tool for electrohydrostatic and electromechanical actuators for the more electric aircraft," in AIAA Aviation 2013 Conference, no. AIAA 2013-4282, (Los Angeles, California), August 12-14, 2013.

[20] Chakraborty, I., Trawick, D., Jackson, D., and Mavris, D., "Electric control surface actuator design optimization and allocation for the more electric aircraft," in AIAA Aviation 2013 Conference, (Los Angeles, California), AIAA, August 12-14, 2013.

[21] Chakraborty, I., Mavris, D. N., Emeneth, M., and Schneegans, A., "A methodology for vehicle and mission level comparison of more electric aircraft subsystem solutions: Application to the flight control actuation system," Proceedings of the Institution of Mechanical Engineers, Part G: Journal of Aerospace Engineering, vol. 229, no. 6, pp. 1088–1102, 2015.

[22] Chambers, J. R., "Innovation in flight: Research of the nasa langley research center on revolutionary advanced concepts for aeronautics," tech. rep., NASA, Hampton, VA, 2005.

[23] Charrier, J. and Kulshreshtha, "Electric actuation for flight and engine control system: Evolution, current trends and future challenges," in 45th AIAA Aerospace Sciences Meeting and Exhibit, no. AIAA 2007-1391, (Reno, Nevada), January 2007.

[24] Chudoba, B., Coleman, G., Smith, H., and Cook, M., "Generic stability and control for aerospace flight vehicle conceptual design," Aeronautical Journal, vol. 112, no. 1132, p. 293306, 2008.

[25] Chudoba, B., Development of a Generic Stability and Control Methodology for the Conceptual Design of Conventional and Unconventional Aircraft Configurations. PhD thesis, Cranfield University, 2001.

[26] Chudoba, B. and Cook, M., "Identification of design-constraining flight conditions for conceptual sizing of aircraft control effectors," in AIAA Atmospheric Flight Mechanics Conference and Exhibit, Guidance, Navigation, and Control and Co-located Conferences, American Institute of Aeronautics and Astronautics, Aug. 2003.

[27] Chudoba, B. and Smith, H., "A generic stability and control methodology for novel aircraft conceptual design," in AIAA Atmospheric Flight Mechanics Conference and Exhibit, Guidance, Navigation, and Control and Co-located Conferences, American Institute of Aeronautics and Astronautics, Aug. 2003.

[28] Coleman, G., "A generic stability and control tool for flight vehicle conceptual design: Aeromech software development," Master's thesis, The University of Texas at Arlington, 2006.

[29] Crespo, L. G. and Kenny, S. P., "Matlab stability and control toolbox: Trim and static stability module," Tech. Rep. NASA/TM-2006-214536, NASA Langley Research Center; Hampton, VA, United States, Langley Research Center Hampton, Virginia 23681-2199, 2006.

[30] Cusher, A. and Gopalarathnam, A., "Drag reduction methodology for adaptive tailless aircraft," in Fluid Dynamics and Co-located Conferences, pp. – , American Institute of Aeronautics and Astronautics, June 2006.

[31] De Marco, A., Duke, E., and Berndt, J., "A general solution to the aircraft trim problem," in AIAA Modeling and Simulation Technologies Conference and Exhibit, no. AIAA 2007-6703, American Institute of Aeronautics and Astronautics, Aug. 2007.

[32] Diedrich, A., Hileman, J., Tan, D., Willcox, K., and Spakovszky, Z., "Multidisciplinary design and optimization of the silent aircraft," in Aerospace Sciences Meetings, pp. –, American Institute of Aeronautics and Astronautics, Jan. 2006.

[33] Dieter, G., Engineering Design: A Materials and Processing Approach. McGraw-Hill series in materials science and engineering, McGraw-Hill, 2000.

[34] Dieter Scholz, Ravinka Seresinhe, I. S. C. L., "Fuel consumption due to shaft power off-takes from the engine," in Workshop on Aircraft System Technologies 2013, (Hamburg, Germany), American Institute of Aeronautics and Astronautics, 2013.

[35] Donaldson, A., Gibbs, J., and Mody, P., "Design of a hybrid wing-body aircraft to maximize market disruption," in 49th AIAA Aerospace Sciences Meeting, (Orlando, Florida), Jan. 2011.

[36] Durham, W., "Constrained control allocation," Journal of Guidance, Control, and Dynamics, vol. 16, pp. 717–725, Aug. 1993.

[37] Durham, W., "Attainable moments for the constrained control allocation problem," Journal of Guidance, Control, and Dynamics, vol. 17, no. AIAA 21360-514, pp. 1371–1373, 1994.

[38] Durham, W., "Constrained control allocation - 3-moment problem," Journal of Guidance Control and Dynamics, vol. 17, pp. 330–336, Apr. 1994. WOS:A1994NC78900015.

[39] Etkin, Bernard., R. L. D., Dynamics of flight : stability and control. New York: Wiley, 1996.

[40] Faleiro, L., "Beyond the more electric aircraft," in AIAA Aerospace America, 2005.

[41] Frischemeier, S., "Electrohydrostatic actuators for aircraft primary flight control - types, modelling and evaluation," in 5th Scandinavian International Conference on Fluid Power, SICFP 1997, Linkoping, Sweden, May 1997.

[42] Garmendia, D., Chakraborty, I., and Mavris, D. N., "Uncertainty quantification for the actuation power requirements of a hybrid wing body configuration with electrically actuated flight control surfaces," in AIAA SciTech 2015 Conference, no. AIAA-2014-2428, (Kissimmee, FL), 2015.

[43] Garmendia, D., Chakraborty, I., Trawick, D., and Mavris, D. N., "Assessment of electrically actuated redundant control surface layouts for a hybrid wing body concept," in AIAA Aviation 2014 Conference, no. AIAA-2014-2428, (Atlanta, GA), 2014.

[44] Garmendia, D. and Mavris, D., "Power efficient trim solutions for the hybrid wing body in approach conditions," in AIAA Atmospheric Flight Mechanics Conference, no. AIAA 2015-0754, (Orlando, FL), Jan. 2015.

[45] Garmendia, D. and Mavris, D., "Alternative trim analysis formulations for vehicles with redundant multi-axis control surfaces," in AIAA Aviation 2014 Conference, no. AIAA-2014-2058, American Institute of Aeronautics and Astronautics, 2014.

[46] Garmendia, D. C., Chakraborty, I., and Mavris, D. N., "Method for evaluating electrically actuated hybrid wing–body control surface layouts," Journal of Aircraft, 2015.

[47] Garmendia, D. C., Chakraborty, I., and Mavris, D. N., "Uncertainty quantification for the actuation power requirements of a hybrid wing body configuration with electrically actuated flight control surfaces," in 53rd AIAA Aerospace Sciences Meeting, no. AIAA 2015-1683, American Institute of Aeronautics and Astronautics, Jan. 2015.

[48] Garmendia, D. C. and Mavris, D. N., "Alternative trim analysis formulations for vehicles with redundant multi-axis control surfaces," Journal of Aircraft, 2015.

[49] Gatlin, G., Vicroy, D., and Carter, M., "Experimental investigation of the low-speed aerodynamic characteristics of a 5.8-percent scale hybrid wing body configuration," in Fluid Dynamics and Co-located Conferences, pp. –, American Institute of Aeronautics and Astronautics, June 2012.

[50] Gatlin, G., Vicroy, D., and Carter, M., "Experimental investigation of the low-speed aerodynamic characteristics of a 5.8-percent scale hybrid wing body configuration," in 30th AIAA Applied Aerodynamics Conference, Fluid Dynamics and Co-located Conferences, American Institute of Aeronautics and Astronautics, June 2012.

[51] Gern, F., "Improved aerodynamic analysis for hybrid wing body conceptual design optimization," in 50th AIAA Aerospace Sciences Meeting including the New Horizons Forum and Aerospace Exposition, (Nashville, Tennessee), Jan. 2012.

[52] Gern, F., "Artificial intelligence based control power optimization on tailless aircraft," in NASA Aeronautics Research Mission Directorate (ARMD) 2014 Seedling Technical Seminar, Feb. 2014.

[53] Gilmore, R., Wakayama, S., and Roman, D., "Optimization of high-subsonic blended-wing-body configurations," in 9th AIAA/ISSMO Symposium on Multidisciplinary Analysis and Optimization, Multidisciplinary Analysis Optimization Conferences, American Institute of Aeronautics and Astronautics, Sept. 2002.

[54] Goldthorpe, S., Rossitto, K., Hyde, D., and Krothapalli, K., "X-48b blended wing body flight test performance of maximum sideslip and high to post stall angle-of-attack command tracking," in Guidance, Navigation, and

Control and Co-located Conferences, pp. –, American Institute of Aeronautics and Astronautics, Aug. 2010.

[55] Grellmann, H., "B-2 aerodynamic design," in AIAA Aerospace Engineering Conference and Exhibit, (Los Angeles, CA), Feb. 1990.

[56] Griffin, B., Brown, N., and Yoo, S., "Intelligent control for drag reduction on the x-48b vehicle," in AIAA Guidance, Navigation, and Control Conference, no. AIAA 2011-6470, 2011.

[57] Guerreiro, N. and Hubbard, J., "Trailing-edge flap optimization for lift distribution control," in 46th AIAA Aerospace Sciences Meeting and Exhibit, Aerospace Sciences Meetings, American Institute of Aeronautics and Astronautics, Jan. 2008.

[58] Hahn, A., "Staging airliner service," in 7th AIAA ATIO Conf, 2nd CEIAT Int'l Conf on Innov & Integr in Aero Sciences,17th LTA Systems Tech Conf; followed by 2nd TEOS Forum, Aviation Technology, Integration, and Operations (ATIO) Conferences, American Institute of Aeronautics and Astronautics, Sept. 2007.

[59] Hileman, J. I., Spakovszky, Z. S., Drela, M., Sargeant, M. A., and Jones, A., "Airframe design for silent fuel-efficient aircraft," Journal of Aircraft, vol. 47, pp. 956–969, May 2010.

[60] Hileman, J., Spakovszky, Z., Drela, M., and Sargeant, M., "Aerodynamic and aeroacoustic three-dimensional design for a "silent" aircraft," in Aerospace Sciences Meetings, pp. –, American Institute of Aeronautics and Astronautics, Jan. 2006.

[61] Hileman, J., Reynolds, T., de la Rosa Blanco, E., Law, T., and Thomas, S., "Development of approach procedures for silent aircraft," Jan. 2007.

[62] Holloway, R. B., "Introduction of ccv technology intro airplane design," Tech. Rep. AGARD CP-147, October 1973.

[63] Holzapfel, F., Lenz, J., Leitner, R., and Sachs, G., "Aircraft performance assessment based on nonlinear constraints imposed on complex flight simulation models," in AIAA Atmospheric Flight Mechanics Conference and Exhibit, Guidance, Navigation, and Control and Co-located Conferences, American Institute of Aeronautics and Astronautics, Aug. 2006.

[64] Hrkegrd, O., "Dynamic control allocation using constrained quadratic programming," Journal of Guidance, Control, and Dynamics, vol. 27, no. 6, pp. 1028–1034.

[65] Jensen, S., Jenney, G., and Dawson, D., "Flight test experience with an electromechanical actuator on the f-18 systems research aircraft," in 19th Digital Avionics Systems Conference, 2000, vol. 1, pp. 2E3/1 – 2E310, 2000.

[66] Jepson, J. and Gopalarathnam, A., "Computational study of automated adaptation of a wing with multiple trailing-edge flaps," in Aerospace Sciences Meetings, pp. –, American Institute of Aeronautics and Astronautics, Jan. 2005.

[67] Jimenez, H., Pfaender, H., and Mavris, D., "Fuel burn and co2 system-wide assessment of environmentally responsible aviation technologies," Journal of Aircraft, vol. 49, pp. 1913–1930, Nov. 2012.

[68] Jones, A., Willcox, K., and Hileman, J., "Distributed multidisciplinary optimization of aircraft design and takeoff operations for low noise," in Structures, Structural Dynamics, and Materials and Co-located Conferences, pp. –, American Institute of Aeronautics and Astronautics, Apr. 2007.

[69] Jong, Y., "An augmented smoothing method of l1-norm minimization and its implementation by neural network model," arXiv preprint arXiv:1207.1931, 2012.

[70] Jung, D. and Lowenberg, M., "Stability and control assessment of a blended-wing-body airliner configuration," (San Francisco, California), Aug. 2005.

[71] Juran, J. M., "The non-pareto principle; mea culpa," Quality Progress, vol. 8, no. 5, pp. 8–9, 1975.

[72] Kawai, R., "Nasa armd subsonic fixed wing project acoustic prediction methodology and test validation for an efficient low-noise hybrid wing body subsonic transport - final report," Tech. Rep. NASA Contract Number NNL07AA54C, The Boeing Company, Huntington Beach, CA, February 2011.

[73] Kawai, R., "Quiet cruise efcient short take-off and landing subsonic transport system," Tech. Rep. NASA/CR–2008-215141, Boeing Technology / Phantom Works, Huntington Beach, California, 2008.

[74] Laban, M., Arendsen, P., Rouwhorst, W., and Vankan, W. J., "A computational design engine for multi-disciplinary optimisation with application to a blended wing body configuration," in Multidisciplinary Analysis Optimization Conferences, pp. –, American Institute of Aeronautics and Astronautics, Sept. 2002.

[75] Liebeck, R., "Design of the blended-wing-body subsonic transport," in Aerospace Sciences Meetings, pp. –, American Institute of Aeronautics and Astronautics, Jan. 2002.

[76] Liebeck, R. H., Page, M., Rawden, B. K., Scott, P., and Wright, R., "Concepts for advanced subsonic transports," Tech. Rep. NASA CR-4624, September 1994.

[77] Liebeck, R., "Design of the blended wing body subsonic transport," Journal of Aircraft, vol. 41, pp. 10–25, Feb. 2004.

[78] Liebeck, R., Page, M., and Rawdon, B., "Blended-wing-body subsonic commercial transport," in 36th AIAA Aerospace Sciences Meeting and Exhibit, Jan. 1998.

[79] Lytle, J. K., "The numerical propulsion system simulation: An overview." NASA/TM-2000-209915, http://ntrs.nasa.gov/archive/nasa/casi.ntrs.nasa.gov/20000063377.pdf, June 2000.

[80] Maier, R., "ACFA 2020 summary of achievements," Tech. Rep. Deliverable D0.9, EADS Innovation Works, Munich, Germany, Oct. 2012.

[81] Markish, J. and Willcox, K., "Multidisciplinary techniques for commercial aircraft system design," in Multidisciplinary Analysis Optimization Conferences, pp. –, American Institute of Aeronautics and Astronautics, Sept. 2002.

[82] Markish, J. and Willcox, K., "Value-based multidisciplinary techniques for commercial aircraft system design," AIAA Journal, vol. 41, pp. 2004–2012, Oct. 2003.

[83] MARQUARDT, D., "AN ALGORITHM FOR LEAST-SQUARES ESTIMATION OF NONLINEAR PARAMETERS," JOURNAL OF THE SOCIETY FOR INDUSTRIAL AND APPLIED MATHEMATICS, vol. 11, no. 2, pp. 431–441, 1963.

[84] Mattingly, Jack D., H. W. H. P. D. T. American Institute of Aeronautics and Astronautics, 2002.

[85] Miranda, L. R., Elliot, R. D., and Baker, W. M., "A generalized vortex lattice method for subsonic and supersonic flow applications," tech. rep., Dec. 1977. If the discrete vortex lattice is considered as an approximation to the surface-distributed vorticity, then the concept of the generalized principal part of an integral yields a residual term to the vorticity-induced velocity field.

[86] Mody, P., Sato, S., Hall, D., De la Rosa, E., Hileman, J., and Wen, E., "Conceptual design of an n+3 hybrid wing body subsonic transport," in 28th AIAA Applied Aerodynamics Conference, (Chicago, Illinois), June 2010.

[87] Mohr, B., Paulus, D., Baier, H., and Hornung, M., "Design of a 450-passenger blended wing body aircraft for active control investigations," Proceedings of the Institution of Mechanical Engineers, Part G: Journal of Aerospace Engineering, vol. 226, no. 12, pp. 1513–1522, 2012.

[88] Morris, J. and Ashford, D. M., "Fuselage configuration studies," in Society of Automotive Engineers, (New York, New York), SAE 670370, Apr. 1967.

[89] MORRIS, S. J., "Integrated aerodynamics and control system design for tailless aircraft," in AIAA Guidance, Navigation and Control Conference, (Hilton

Head, South Carolina), American Institute of Aeronautics and Astronautics, Aug. 1992.

[90] Mukhopadhyay, V., "A conceptual aerospace vehicle structural system modeling, analysis and design process," in Structures, Structural Dynamics, and Materials and Co-located Conferences, pp. –, American Institute of Aeronautics and Astronautics, Apr. 2007.

[91] Mukhopadhyay, V., Hsu, S.-Y., Mason, B., Sleight, D., Jones, W., Chu, J., Hicks, M., Spangler, J., Kamhawi, H., and Dahl, J., "Adaptive modeling, engineering analysis and design of advanced aerospace vehicles," in Structures, Structural Dynamics, and Materials and Co-located Conferences, pp. –, American Institute of Aeronautics and Astronautics, May 2006.

[92] Nam, T., A Generalized Sizing Method for Revolutionary Concepts under Probabilistic Design Constraints. PhD dissertation, Georgia Institute of Technology, Atlanta, GA, Apr. 2007.

[93] Navarro, R., "Performance of an electro-hydrostatic actuator on the f-18 systems research aircraft," in 16th Digital Avionics Systems Conference, Irvine, California, October 1997.

[94] Nickel, K. and Wohlfahrt, M., Tailless Aircraft in Theory and Practice. AIAA education series, Washington, DC : London, England: American Institute of Aeronautics and Astronautics ; E. Arnold, 1994.

[95] Nickol, C., "Environmentally responsible aviation (era) project: Assessing progress toward simultaneous reductions in noise, fuel burn and nox," ASM 2011 Briefing, January 2011.

[96] Nickol, C., "Silent aircraft initiative concept risk assessment," Tech. Rep. NASA/TM-2008-215112, NASA Langley Research Center, Hampton, Virginia, February 2008.

[97] Nickol, C., "Hybrid wing body configuration scaling study," in 50th AIAA Aerospace Sciences Meeting including the New Horizons Forum and Aerospace Exposition, (Nashville, Tennessee), Jan. 2012.

[98] Nickol, C. and Mccullers, L., "Hybrid wing body configuration system studies," (Orlando, Florida), Jan. 2009.

[99] Nicolai, L. M. and Carichner, G. E., Fundamentals of Aircraft and Airship Design, Volume I - Aircraft Design. American Institute of Aeronautics and Astronautics, 2010.

[100] Omoragbon, A., An Integration Of A Modern Flight Control System Design Technique Into A Conceptual Design Stability And Controls Tool, AeroMech. PhD thesis, The University of Texas at Arlington, Aug. 2010.

[101] Oppenheimer, M., Doman, D., and Bolender, M., "Control allocation for over-actuated systems," in Control and Automation, 2006. MED '06. 14th Mediterranean Conference on, pp. 1 –6, June 2006.

[102] Papamoschou, D. and Mayoral, S., "Jet noise shielding for advanced hybrid wing-body configurations," in 49th AIAA Aerospace Sciences Meeting including the New Horizons Forum and Aerospace Exposition, (Orlando, Florida), Jan. 2011.

[103] Peoples, R. and Willcox, K., "A value-based mdo approach to assess business risk for commercial aircraft design," in Multidisciplinary Analysis Optimization Conferences, pp. –, American Institute of Aeronautics and Astronautics, Aug. 2004.

[104] Peoples, R. E. and Willcox, K. E., "Value-based multidisciplinary optimization for commercial aircraft design and business risk assessment," Journal of Aircraft, vol. 43, pp. 913–921, July 2006.

[105] Perez, R. E., T. Liu, H. H., and Behdinan, K., "Multidisciplinary optimization framework for control-configuration integration in aircraft conceptual design," Journal of Aircraft, vol. 43, pp. 1937–1948, Nov. 2006.

[106] Petersen, J. a. M. and Bodson, M., "Fast implementation of direct allocation with extension to coplanar controls," Journal of Guidance Control and Dynamics, vol. 25, pp. 464–473, June 2002. WOS:000175509500007.

[107] Pitera, D. M., DeHaan, M., Brown, D., Kawai, R. T., Hollowell, S., Camacho, P., Bruns, D., and Rawden, B. K., "Blended wing body concept development with open rotor engine integration," Tech. Rep. CR-2011-217303, The Boeing Company, Huntington Beach, CA, Nov. 2011.

[108] Potsdam, M., Page, M., and Liebeck, R., "Blended wing body analysis and design," (Atlanta, GA), pp. 799–805, 1997.

[109] Ramirez, C. and Argaez, M., "An\ ell _ {1} minimization algorithm for non-smooth regularization in image processing," Signal, Image and Video Processing, vol. 9, no. 2, pp. 373–386.

[110] Raney, D., Cabell, R., Sloan, A., Hautamaki, B., Barnwell, W., and Lion, S., "Wind tunnel test of an rpv with shape-change effector and sensor arrays," in Guidance, Navigation, and Control and Co-located Conferences, pp. –, American Institute of Aeronautics and Astronautics, Aug. 2004.

[111] Raymer, D., Aircraft Design: A Conceptual Approach. AIAA Education Series, American Institute of Aeronautics and Astronautics, 2006.

[112] Richardson, T. S., Beaverstock, C., Isikveren, A., Meheri, A., Badcock, K., and Ronch, A. D., "Analysis of the boeing 747-100 using CEASIOM," Progress in Aerospace Sciences, vol. 47, no. 8, pp. 660 – 673, 2011.

<ce:title>Special Issue - Modeling and Simulating Aircraft Stability and Control</ce:title> <ce:subtitle>Special Issue - Modeling and Simulating Aircraft Stability and Control</ce:subtitle>.

[113] Roman, D., Allen, J. B., and Liebeck, R. H., "Aerodynamic design challenges of the blended-wing-body subsonic transport," 2000.

[114] Roman, D., Gilmore, R., and Wakayama, S., "Aerodynamics of high-subsonic blended-wing-body configurations," in Aerospace Sciences Meetings, pp. –, American Institute of Aeronautics and Astronautics, Jan. 2003.

[115] Roskam, J., Airplane Design. No. pt. 2 in Airplane Design, DARcorporation, 1999.

[116] Roskam, J., Airplane Design. No. pt. 6 in Airplane Design, DARcorporation, 2000.

[117] Rynaski, E. G. and Weingarten, N. C., "Flight control principles for control configured vehicles," Tech. Rep. CAL-TB-3052-F-1, CORNELL AERONAUTICAL LAB INC BUFFALO NY, CORNELL AERONAUTICAL LAB INC BUFFALO NY, Jan. 1972.

[118] Sadraey, M. and Colgren, R., "A systems engineering approach to the design of control surfaces for UAVs," (Reno, Nevada), Jan. 2008.

[119] Sandlin, D. R. and Swanson, S. M., "A computer module used to calculate the horizontal control surface size of a conceptual aircraft design," Aug. 1990. The creation of a computer module used to calculate the size of the horizontal control surfaces of a conceptual aircraft design is discussed.

[120] Sargeant, M. A., Hynes, T. P., Graham, W. R., Hileman, J. I., Drela, M., and Spakovszky, Z. S., "Stability of hybrid-WingBody-Type aircraft with centerbody leading-edge carving," Journal of Aircraft, vol. 47, pp. 970–974, May 2010.

[121] Sato, S., Mody, P., Hall, D., de la Rosa Blanco, E., and Hileman, J., "Assessment of propulsion system configuration and fuel composition on hybrid wing body fuel efficiency," in Aerospace Sciences Meetings, pp. –, American Institute of Aeronautics and Astronautics, Jan. 2011.

[122] Scholz, D., Equations for a Preliminary Actuator Design, Technical Note, Deutsche Airbus, 1991.

[123] Scholz, D., "Development of a cae-tool for the design of flight control and hydraulic systems," in AeroTech '95, (Birmingham, UK), 1995.

[124] Scholz, D., "Computer aided engineering for the design of flight control and hydraulic systems," in ICAS Proccedings 1996 (20th Congress of the International Council of the Aeronautical Sciences), 1996.

[125] Schrage, D. and Mavris, D., "Recomposition: The other half of the MDO equation," in MULTIDISCIPLINARY DESIGN OPTIMIZATION: STATE OF THE ART (Alexandrov, NM and Hussaini, MY, ed.), SIAM PROCEEDINGS SERIES, (3600 UNIV CITY SCIENCE CENTER, PHILADELPHIA, PA 19104-2688), pp. 432–447, Inst Comp Appl Sci & Engn; NASA Langley Res Ctr, Multidisciplinary Optimizat Branch, SIAM, 1997. ICASE/NASA Langley Workshop on Multidisciplinary Design Optimization, HAMPTON, VA, MAR 13-16, 1995.

[126] Schutte, J. S., Jimenez, H., and Mavris, D. N., "Technology assessment of NASA environmentally responsible aviation advanced vehicle concepts," in 49th AIAA Aerospace Sciences Meeting, 2011.

[127] Simonis, J. P., Inexact Newton Methods Applied to Under-Determined Systems. PhD dissertation, Worcester Polytechnic Institute, Worcester, MA, May 2006.

[128] Sliwa, S. M., "Impact of longitudinal flying qualities upon the design of a transport with active controls," Jan. 1980. Direct constrained parameter optimization was used to optimally size a medium range transport for minimum direct operating cost.

[129] Staelens, Y., Blackwelder, R., and Page, M., "Novel pitch control effectors for a blended wing body airplane in takeoff and landing configuration," in 45th AIAA Aerospace Sciences Meeting and Exhibit, no. AIAA 2007-68, 2007.

[130] Staelens, Y., Blackwelder, R., and Page, M., "Novel pitch control effectors for a blended wing body airplane in takeoff and landing configuration," in 45th AIAA Aerospace Sciences Meeting and Exhibit, Aerospace Sciences Meetings, American Institute of Aeronautics and Astronautics, Jan. 2007.

[131] Stevens, B. and Lewis, F., Aircraft control and simulation. Wiley-interscience publication, Wiley, 1992.

[132] Sweetman, B., Inside the Stealth Bomber. Motorbooks ColorTech, Mbi Publishing Company, 1999.

[133] Thompson, K., "Notes on 'the electric control of large aeroplanes'," Aerospace and Electronic Systems Magazine, IEEE, vol. 3, pp. 19 –24, dec. 1988.

[134] Tong, M. T., Jones, S. M., Haller, W. J., and Handschuh, R. F., "Engine conceptual design studies for a hybrid wing body aircraft," Tech. Rep. TM-2009-215680, June 2009.

[135] Traverse, P., Lacaze, I., and Souyris, J., "Airbus fly-by-wire: A process towards total dependability," in ICAS 2006, 25th International Congress of the Aeronautical Sciences, 2006.

[136] Tron, X. L., "A380 flight controls overview," in Deutsche Gesellschaft Fur Luft-und Raumfahrt (DGLR), 2007.

[137] van Es, G., "Crosswind certification - how does it affect you?," Nationaal Lucht-en Ruimtevaartlaboratorium (NLR), May 2006. Report No. NLR-TP-2006-324.

[138] van Ginneken, D., Voskuijl, M., van Tooren, M., and Frediani, A., "Automated control surface design and sizing for the prandtl plane," (Orlando, Florida), Apr. 2010.

[139] Velicki, A., "Airframe development for the hybrid wing body aircraft," 2009.

[140] Vos, R. and van Dommelen, J., "A conceptual design and optimization method for blended-wing-body aircraft," in 53rd AIAA/ASME/ASCE/AHS/ASC Structures, Structural Dynamics and Materials Conference, Structures, Structural Dynamics, and Materials and Co-located Conferences, American Institute of Aeronautics and Astronautics, Apr. 2012.

[141] Voskuijl, M., La Rocca, G., and Dircken, F., "Controllability of blended wing body aircraft," ICAS 2008, 2008.

[142] WADDELL, J., "Flying the 747," in Archive Set 40, Meeting Paper Archive, American Institute of Aeronautics and Astronautics, Jan. 1963.

[143] Waggoner, E. G., "Status update on nasas integrated systems research program," 49th AIAA Aerospace Sciences Meeting, January 2011.

[144] Wakayama, S., "BLENDED-WING-BODY OPTIMIZATION PROBLEM SETUP," in 8th AIAA/USAF/NASA/ISSMO Symposium on Multidisciplinary Analysis and Optimization, (Long Beach, CA), Sept. 2000.

[145] Wakayama, S., "Multidisciplinary design optimization of the blended-wing-body," in 7TH AIAA/USAF/NASA/ISSMO Symposium on Multidisciplinary Analysis and Optimization, no. AIAA 1998-4938, American Institute of Aeronautics and Astronautics, 1998.

[146] Wakayama, S. and Kroo, I., "The challenge and promise of blended-wing-body optimization," in Archive Set 694, Meeting Paper Archive, American Institute of Aeronautics and Astronautics, 1998.

[147] Wildschek, A., "Flight dynamics and control related challenges for design of commercial blended wing body aircraft," in AIAA Guidance, Navigation, and Control Conference, SciTech 2014, no. AIAA-2014-0599, 2014.

[148] Willcox, K. and Wakayama, S., "Simultaneous optimization of a multiple-aircraft family," Journal of Aircraft, vol. 40, pp. 616–622, July 2003.

[149] Yeh, Y., "Triple-triple redundant 777 primary flight computer," in Aerospace Applications Conference, 1996. Proceedings., 1996 IEEE, vol. 1, pp. 293 –307 vol.1, feb 1996.

[150] Young, A., "The aerodynamic characteristics of flaps," Ministry of Supply, Aeronautical Research Council Reports and Memoranda, 1953. R&M. No. 2622 (10,766) Technical Report.